UNIVERSITY OF LONDON THESIS

Degree PhD Year 2007 Name of Author MASKEY, Sabin.R

AN INTEGRATED HYDRODYNAMIC AND ADSORPTION MODEL OF EXPANDED BED OPERATION: ITS DEVELOPMENT AND APPLICATION

A Thesis submitted to the University of London
for the degree of
DOCTOR OF PHILOSOPHY
by

Sabin R. Maskey
B.Sc. Agriculture (Tribhuvan University, Nepal)
M.Sc. Bioprocess Technology (Asian Institute of Technology, Thailand)

The Advanced Centre for Biochemical Engineering
Department of Biochemical Engineering
University College London
Torrington Place
London WC1E 7JE

2007

ProQuest LLC
789 East Eisenhower Parkway
P.O. Box 1346
Ann Arbor, MI 48106-1346

An integrated hydrodynamic and adsorption model of expanded bed operation: its development and application

The expanded bed adsorption (EBA) process naturally assumes a mixed bed (MB) in terms of particle size and displays particle dispersion. To date models have not accounted for this simultaneously and accurately. Moreover, there has not been any work to predict an adsorption response when the bed is in a hydrodynamic-transient state; which occurs for example while changing feedstock. A series of MB steady state hydrodynamic EBA models were developed which are increasingly close mimics of reality. This was achieved by progressively considering: a single representative equivalent particle size per axial position (MBEQD), separate particle size categories by using size-partition (MBSP) approach and inclusion of an additional component flux due to particle dispersion. Breakthrough predictions using the MB approach were more accurate compared to both that of a mono-sized bed and perfectly classified bed approaches clearly demonstrating its importance. The results of both MBEQD and MBSP were in close agreement with 40 cm bed height breakthrough experimental data. An important weakness in an existing method of including the particle dispersion was identified and a model for its more accurate representation developed.

A transient hydrodynamic EBA model was developed by integrating the mono-sized transient hydrodynamic model and adsorption model. A simulation study using this demonstrated the possibility of loading while a bed is still expanding which may afford an increase in an operational throughput.

The effects of various physical parameters on the performance of EBA were investigated using simulation. Windows of operation in relation to fluid velocity and load volume were determined which would satisfy minimum yield and throughput criteria. The model was also used to determine optimal loading time strategies in order to maximise yield and throughput. Finally a preliminary work explaining future potential developments in EBA modelling was performed.

Acknowledgements

Without the interest and support from my teacher, Prof Nigel J. Titchener-Hooker, I would not have been fortunate to do PhD here in the first place. Working under his guidance and supervision for last seven years has been one of the most valuable experiences. I am very fortunate to have his support in facing many different problems as they came along. About first time when I met him, many years ago, he told me PhD is a journey. I realised, yes it is: a long and probably not that easy one for many people. But crossing many hurdles, and finally coming to the end of the journey, or at least nearly so, has been a wonderful feeling. I am very indebted.

I would like to thank Prof Guo X. Wu (Department of Mechanical Engineering) for a useful discussion about a problem in the simulation of a transient hydrodynamic model of expanded bed. I would like to thank Dr Philip Martin and Dr Nicholas Willoughby for showing me how to set up an expanded bed experiment, and Dr Ed Varga for an adsorption experiment. I would also like to thank Dr Hu Zhang who referred to me a paper which I found very useful. And I would like to thank Spyridon Gerontas who explained to me the concept of Window of Operation lucidly.

Research is but a part of the story. Over years, I got help, support, encouragement and companionship from numerous friends. Among many at least few names would be difficult to forget. I would like to thank Narayan Nakarmi and Birendra M. Pradhan along with Sunil Gorkhali and Sudip Pradhan for being a big help. I would also like to thank Paul Griffiths, Karen Willson, Barnaby Zoro, James Myers, Helen Irvine, Sam Pickering, James Scarr, Sarah Fish, Julia Markunsen, Sundeep Thusu, Shou-Hui Ngiam and Philippa Gardner. Similarly I would like to thank Mark Emmett, Charlotte Randell, Alex Vooerhoever, Carola Gause, Tata Blancho, Emily Robin, Aristidis Askimakis, Yuiji Muira, Karen Osenton, Eamonn Horan, Rachael Pearson, Chanisa Thananuwat, Sara Carvide, Heidi Salte, James McWilliam, Krishna P. Paudel, Ajoy Bista, Pietro Colletta, Thazin Zaw Win, Christina, Kim Townsend, Silvia, Manohar Pradhan, Deepak Bajracharya, Sunita Kapali, Nabin Chitrakar, Nicolaos Gianadakis, Lorenzo and Demetris Assos. For each of these friends, I would be tempted to write several pages. But as there is not enough space in the thesis, I would like them to know that they are in my heart. I

would also like to thank Major General Andrew Ritchie for his encouragement and support for organising college activities. I am fortunate to know Evangelia Victoria Rigaki, Amy Nolen and Lorna Naomi Mudie who have been of an enormous support. I would also like to take this opportunity to thank few people who helped me in my immediate past academic life: Prof Willem F. Stevens, Prof Sudip K. Rakshit, Ernesto F. Bulayog and Mukunda P. Joshi. I am very grateful to all.

My brother, Sameer, has been the other most important person during my PhD without whose support and advice I do not know what would have happen. He helped me to keep along the track when I was going through a difficult time. I think I would not be able to express in words how grateful I am. My sister, Anju, and my father have also been of great support and encouragement. Finally, my mother: her guidance, support, love and encouragement have been one of the most critical factors in reaching here.

In the end, I would like to express my sincere gratitude to University College London and the British Government for providing me UCL Graduate School Research Scholarship and Overseas Research Studentship award respectively for this doctoral study.

CONTENTS

List of Figures

List of Tables

Nomenclature

Abbreviations:

EBA	Expanded Bed Adsorption
GR	General Rate
MB	Mixed Bed
MBEQD	Mixed Bed Equivalent Diameter
MBPD	Mixed Bed Particle Dispersion
MBSP	Mixed Bed Size Partition
MSB	Mono-sized Bed
MSBA	Mono-sized Bed Adsorption
PB	Packed Bed
PCB	Perfectly Classified Bed
PCBA	Perfectly Classified Bed Adsorption
PSD	Particle Size Distribution
SPD	Simulated Particle Dispersion
TMSB	Transient Mono-sized Bed
TMSBA	Transient Mono-sized Bed Adsorption
WO	Windows of Operation

Note:

The meanings of Greek letters and symbols used in this thesis for setting equations are explained when they first occur and when their meanings change based upon the new contexts.

1 Introduction

1.1 Expanded Bed Adsorption

One of the crucial procedures in the production of proteins for therapeutic and diagnostic use is the recovery of protein from various recombinant host organisms. The initial steps in the production process will normally be the removal of particulate materials and concentration of the desired product. To minimize the risk of proteolytic breakdown of the desired product, these initial steps need to be carried out rapidly. Overall the number of steps for this should be kept minimal to minimise the product loss. Centrifugation and/or microfiltration are the traditional techniques being employed for these initial steps. Often the degree of clarification in an industrial centrifuge is not sufficient, it often has to be supplemented with a microfiltration step to obtain a particle-free solution which can be further purified by packed bed chromatography (Hjorth, 1997). These additional operations result in a long processing time or need for comparatively large units, and the probability of more product loss. The application of expanded bed adsorption (EBA) has been found to be very promising to circumvent this problem. EBA allows the capture of proteins from particulate feedstocks without prior removal of particulates, thus enabling clarification of a cell suspension or cell homogenate and the concentration of the desired product in a single operation. Following Fig. 1.1 demonstrates the application of EBA in a typical bioprocess.

In the expanded bed, a particulate adsorbent in a column is allowed to rise by applying an upward flow from its settled state. This increases the space between the adsorbent particles, allowing cells and cell debris to pass through without blocking the bed (Fig. 1.2).

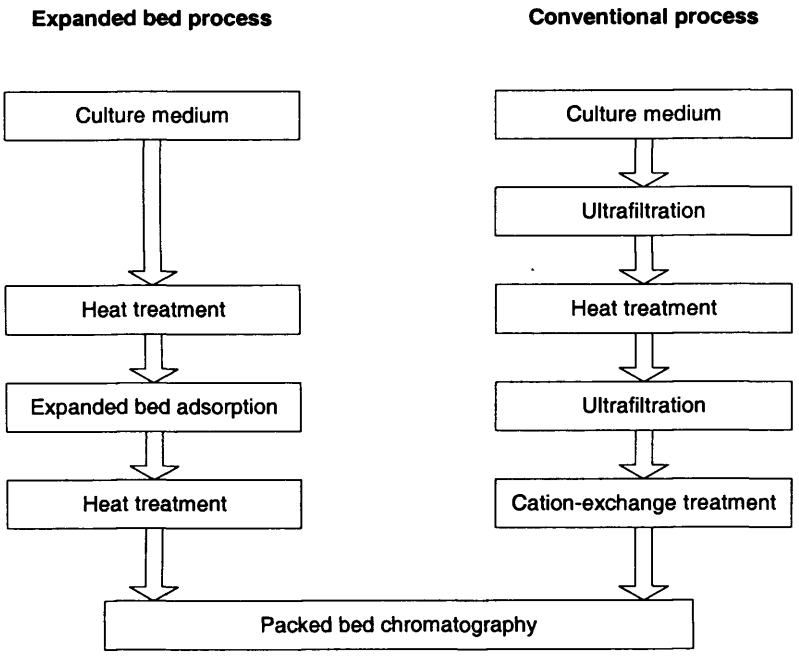

Fig. 1.1 Process schemes for the recovery of recombinant human serum albumin produced in the yeast Picia pastoris using an expanded-bed process and a conventional process (Hjorth, 1997).

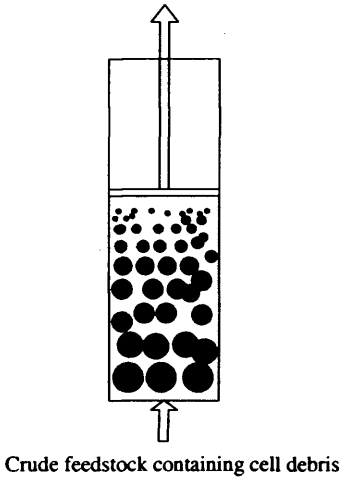

Fig. 1.2 The principle of an expanded bed. The increased and flexible space between the adsorbent particles allows cells and cell debris to pass unhindered through the bed. The arrows indicate the flow direction in the expanded bed mode. (Hjorth, 1997)

Compared with a conventional fluidized bed, one of the key characteristics of expanded bed is low back mixing, which is achieved by proper design of the adsorbent and the column. Low back mixing is a result of the formation of a segregated or stratified bed which is achieved in expanded bed mode by the particle size distribution of the

adsorbents. This results in larger adsorbent particles remaining in the lower part of the expanded bed and smaller particles in the upper part as shown in Fig. 2. Usually particle sizes ranging from 50 to 400 μm are used in the expanded bed (Hjorth, 1997). Smaller particles result in over expansion at low flow velocities while larger particles require very high flow velocities to expand the bed sufficiently. In the first case, the overall productivity of the process will be low as the void space becomes too large and solvent with load will have more probability to pass though with little interaction or adsorption to the adsorbent particles. While in the second case, protein binding is impaired due to restricted diffusion into the adsorbent particles. To operate the expanded bed at flow velocities that result in high productivity, densities in the 1.1-1.3 g/ml range are normally used.

Some of the applications of expanded bed compiled by Hjorth (1997) are given below in Table 1.1.

Table 1.1 A summary of data from selected expanded-bed adsorption processes Abbreviations: DEAE, diethyl aminoethyl; FGF fibroblast growth factor; IL-8, interleukin 8; NA, data not available; rHSA, recombinant human serum albumin; rhuNGF, recombinant human nerve growth factor; SP, sulfopropyl; ZZ-M5, synthetic IgG binding domain-malaria M5 peptide fusion protein. (Hjorth, 1997)

Feedstock	Feed vol. (l)	Product	Adsorbent ligand	Adsorbent vol. (l)	Purification factor	Yield (%)	Reference
E. coli cell suspension	8	ZZ-M5	DEAE	0.3	NA	90	Hansson et al. 1994
E. coli homogenate	26	Annexin V	DEAE	4.7	2	95	Barnfeld et al. 1994
E. coli homogenate	10	FGF-Saporin	SP	0.3	20	65	McDonald et al. 1996
E. coli periplasmic extract	180	Exotoxin	DEAE	4.7	2	79	Johansson, et al. 1996
Yeast cell suspension	2000	rHSA	SP	150	NA	87	Noda et al. 1996
Yeast cell suspension	6.4	Aprotinin	SP	0.3	3.8	76	Zurek et al. 1996
Cell culture	60	Monoclonal IgG	Protein A	0.15	30	83	Thommes et al. 1996
Cell culture	100	Monoclonal IgG	Protein A	4.7	NA	NA	Jagersten et al. 1996
Cell culture	12000	Monoclonal IgG	SP	154	NA	95	Zapata et al. 1996
Cell culture	36	Monoclonal IgG	SP	0.17	7	85	Batt et al. 1995
Cell culture	NA	rhuNGF	SP	NA	NA	95	Beck. et al. 1996
Milk	5	Lysozyme	SP	0.8	8.3	89	Noppe et al. 1996
Renatured inclusion bodies	16	IL-8	SP	0.3	3.9	100	Barnfield (Press 1997)

There are increasing large number of recent publications in expanded bed adsorption. This would signify its even wider applications. For more optimal use and the process design, accurate prediction of the system behaviour becomes important. For that purpose,

both modelling and novel techniques like extreme scale-downs (Willoughby et al., 2004) are being explored. The modelling work was seriously lacking at the outset of this thesis. Hence this thesis work was initiated to address this problem and establish a mathematical description of an expanded bed adsorption which can be used to make more accurate and reliable predictions in various operating conditions. The detail objectives of which are described in the following section.

1.2 Statement of Objectives

Expanded bed adsorption (EBA) chromatography is an important technique for the purification of macromolecules from solids-containing feedstocks. At the outset to this work there was no any integrated model which takes into account the hydrodynamic and adsorption behaviour of EBA simultaneously existed. As bed hydrodynamics are an important part of EBA, treating it as a steady state mono-sized homogeneous packed bed had been a primary source of errors in EBA predictions, thus making them unreliable to use in many contexts. This lack of an accurate model is an obstacle in its full exploitation of its possible benefits. Experiments are expensive and time consuming while modelling provides for the easy study of the system in different scenarios and under range of parameter values. This would be very useful in finding optimal operating conditions and for establishing feasibilities. Thus this work was initiated to address the problem by integrating hydrodynamic and adsorption models of expanded bed. To do this available steady state and transient models of EBA hydrodynamic and adsorption models were studied. The possible methods of their integration were devised from a simple approach to increasing levels of sophistication with the inclusion of more details so as to make their predictions more useful. The integrated models were then used to study their possible applications in a series of process contexts.

Specific objectives of this work were:

- To establish appropriate expansion relationships with which to model expanded bed behaviour.
- To establish an appropriate model or approach to describe the steady-state hydrodynamics of EBA by considering distribution of particle sizes.

- To implement available mono-sized transient EBA hydrodynamic model and to explore on improving upon it by adopting the model with distribution of particle sizes.
- To implement and establish the existing model of adsorption in packed bed chromatography for its integration with hydrodynamics in the EBA context.
- To establish a simple method of integration of a steady state hydrodynamic model of EBA and an adsorption model of a packed bed.
- To improve such an integrated model by relaxing assumptions and making them more realistic, for example dropping mono-sized assumption and considering the presence of particle size distribution (PSD) in the bed.
- To consider the variation of axial PSD in expanded bed and its effect in adsorption behaviour of EBA along with behaviour of each size classes.
- To formulate a more realistic and advanced EBA model by incorporating particle dispersion.
- To formulate a transient EBA model by integrating transient hydrodynamics and adsorption models.
- To perform sensitivity analysis of the EBA model to determine parameters which are more important to the system in terms of adsorption behaviour.
- To produce windows of operation of an EBA system in terms of yield and throughput to find out the optimal operating conditions.
- To explore different applications of transient EBA model with a view to maximising its utility.
- To recommend the possible next steps towards EBA modelling and their uses.

1.3 Organisation of the Chapters

Having introduced the rationale of this research, a general background and objectives, Chapter 2 sets out the principles and methods used in this work. A general introduction to chromatography and expanded bed and its operation are described in the first part of the chapter. Then some relevant transport equations are reviewed briefly since the modelling mass transfer is a major theme of this work. The formulated models developed in this thesis need to be simulated. Suitable numerical methods will be adopted based upon the

properties and structures of these models. The principles and methods of implementing such numerical methods are then discussed. In the last part of Chapter 2, a general framework of model development process followed in this thesis will be briefly described.

In Chapter 3 a comprehensive general rate model of chromatography is reviewed, implemented and validated. This provides the basis of the adsorption element of the EBA model. Chapters 4-8 are about formulating a series of EBA while Chapter 9 presents some of their applications. A detailed study describing expansion phenomena at steady state is given in Chapter 4. The results are validated against experimental data. A transient hydrodynamic model is implemented and validated in Chapter 5 as a first step towards formulating a transient integrated EBA model. A series of integrated models with steady state hydrodynamics is formulated and validated against experimental data in Chapter 6. And in that chapter the models are improved by inclusion of size partitions effects. An appropriate model which includes the effects of particle dispersion in EBA is developed in Chapter 7. The hydrodynamic steady state assumption of the model in Chapter 6 is subsequently relaxed and a complete model of EBA capable of predicting the transient hydrodynamic state is developed by integrating a transient hydrodynamic model with an adsorption model in Chapter 8.

A study of some of the applications of the integrated EBA model is performed in Chapter 9. Sensitivity analysis was carried out in order to determine important parameters of an EBA system in terms of adsorption behaviour. Windows of operation are determined in terms of yield and throughput to find out the optimal operating conditions. Use of a model in determining optimal loading time is also demonstrated. Some of the applications of transient EBA model are then enumerated with a view to maximising its utility.

As a preliminary work towards further development of EBA models, additional model establishment work is done. It includes establishing both steady state and transient hydrodynamic models of expanded bed which considers the existence of particle size distribution and the bed is mixed. As these are just efforts to implement the literature available models in view of using them in an EBA context, they are excluded from the main body of the thesis and included as an appendix.

In the final chapter (Chapter 10) the conclusions are drawn based on the above study in various aspects of EBA and its modelling, and recommendations made for the possible next steps towards EBA modelling and their uses.

Before explaining the details of this thesis from the next chapter, the overall process of model development followed in this thesis is described in the following section 1.4. It briefly indicates what has been done for developing an increasingly realistic and useful model in this work, why it is done and their inter-relationships. It also provides the cross-reference to the chapter and sections where their details are explained.

1.4 Flowchart of a Model Development Process

The flowchart of the model development process followed is shown in Fig. 1.3.

The sequence of steps is as follows.

1. General Rate (GR) model of adsorption in a packed bed is established. This forms the basis of adsorption modelling.
2. An appropriate expansion relation (ER) is established out of a number of relations available in literature. This provides a consistent basis to represent the expansion of a particle bed.
3. The expansion relation is based on assumption of mono-sized particles. Thus it in itself is in fact a Mono-sized Bed (MSB) model to represent steady state hydrodynamics of EBA. However, an experimental data and prediction are often found to be significantly different for the purpose of its use in bed adsorption modelling. So frequent experimental fittings of the parameters would become necessary and such a model would be termed as MSB model.
4. Distribution of particle size is considered by an initial simplifying assumption of perfect classification. Such a Perfectly Classified Bed (PCB) model to represent steady state hydrodynamics is then established.
5. However, mixed bed, the presence of different particle size in each axial position, is the reality in EBA. Thus to accommodate such a phenomenon, and tentatively predict mixing of particle sizes and expansion of the bed, an Approximate Mixed Bed (AMB) approach is developed.
6. To represent the transient hydrodynamic behaviour of an EBA, the Transient Mono-sized Bed (TMSB) model is developed.
7. The first and simplest integration of adsorption and hydrodynamics of EBA is achieved by developing a Mono-sized Bed Adsorption (MSBA) model by

integration of GR and MSB models. Here bed properties for adsorption part of the model are estimated using MSB model.

8. The consideration of particle size distribution (PSD) in EBA is at first done by developing Perfectly Classified Bed Adsorption (PCBA) model. This is achieved by integrating PCB hydrodynamic model and GR model. As before, the bed properties for an adsorption part of the model are provided by the hydrodynamic part. Such an integration approach is followed for all models in this thesis.
9. Improvement on PCBA is done by considering mixed bed. This is achieved by replacing PCB hydrodynamic model with AMB approach to describe mixed bed hydrodynamics of EBA. However, for this initial stage, though bed is considered mixed bed (MB) for hydrodynamic purpose, only one representative particle size per axial position is considered for adsorption purpose. Such a model is termed as Mixed Bed Equivalent Diameter (MBEQD) model.
10. As AMB approach still needs an improvement, a separate method by which to represent mixed bed hydrodynamics in integrated EBA models developed becomes necessary. One of the simplest ways is to directly use the experimental data related with bed properties related with hydrodynamics when available. Thus a method of using such an approach is described.
11. MBEQD model developed earlier in step 9 is simulated using experimental hydrodynamic data as explained in step 10.
12. The existence of different particle sizes in an axial position also for the adsorption part of the model is considered by adopting size partition approach in Mixed Bed Size Partition (MBSP) model. Here an EBA column is, in theory, vertically partitioned into multiple columns each having only one particle size. The net adsorption effect at any given axial position of the bed is determined by cumulative effect of each partition at that axial position.
13. As done in step 11, the MBSP model is simulated using experimental hydrodynamic data.
14. So far the effect of particle dispersion in adsorption has been ignored. Thus as a first step towards including particle dispersion effect in EBA, Mixed Bed Particle Dispersion (MBPD) model is developed by including such an effect based on Wright and Glasser (2001) approach in MBSP model.
15. As there is an important weakness in the approach followed to include particle dispersion effect in adsorption as done in MBPD model, a new more appropriate

method is developed. The model developed based on this is termed as Simulated Particle Dispersion (SPD) model.

16. Finally, to predict the adsorption behaviour of EBA when the bed is still at a hydrodynamic transient state, the Transient Mono-sized Bed Adsorption (TMSBA) model is developed by integrating GR model of adsorption and transient hydrodynamic model, TMSB.

Once models are developed, some of their applications are explored. Before beginning a model development process as mapped in the flowchart (Fig. 1.3), the principles and methods involved in such a modelling process will be described in the next chapter.

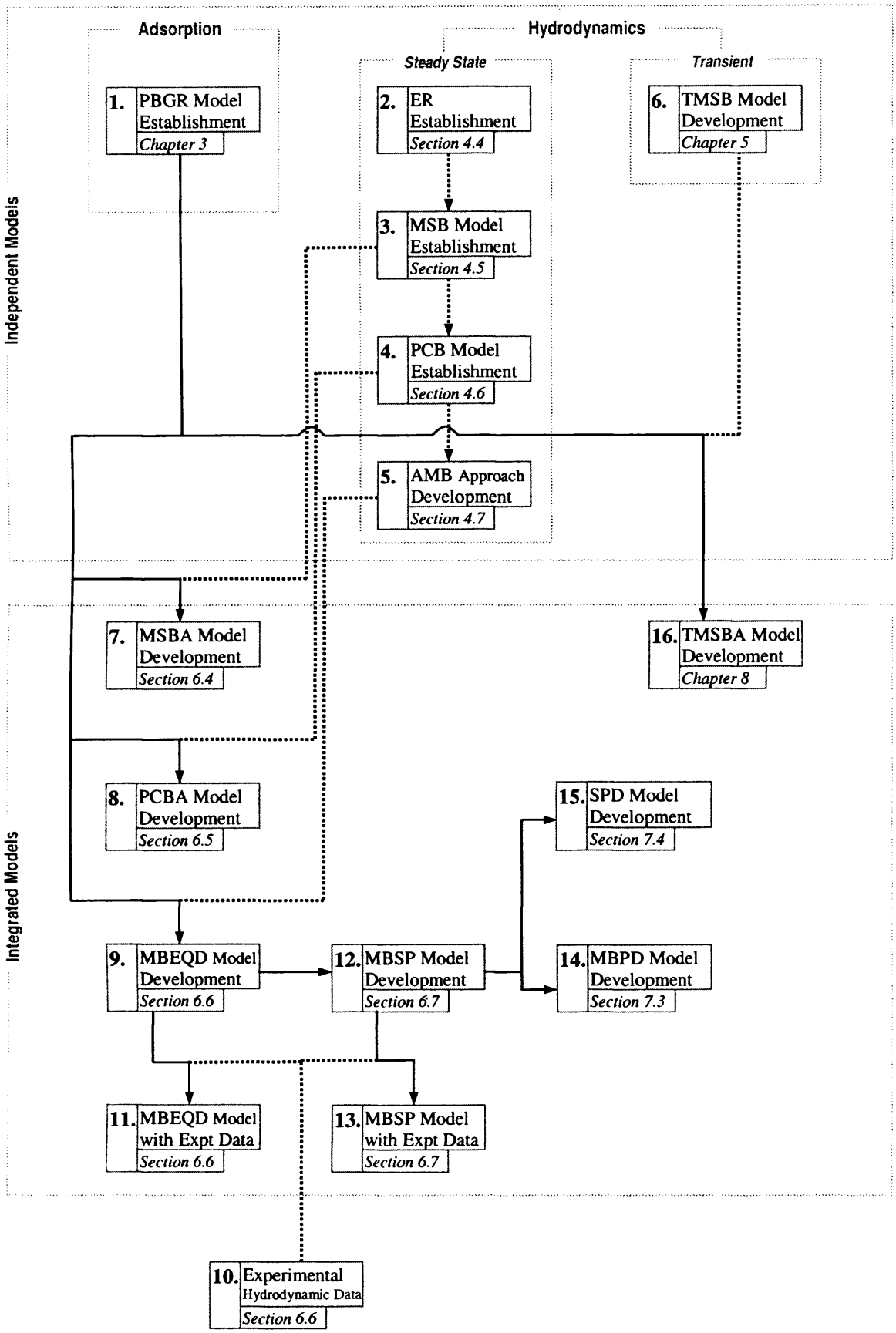

Fig. 1.3 The flowchart of a model development process.

2 Principles and Methods

2.1 Introduction

Before modelling it is important to know the essential aspects of the physical phenomena of interest. Thus in this chapter principles involved in chromatography and EBA are explained. Transport phenomenon dominates the EBA process. A brief review of some transport equations relevant to this work is first presented. This will provide the basis of modelling and also continuity from the underlying physics to models. Once the models are developed, they have to be solved or simulated. As most of the models are non-linear and complex, the analytical solutions are not possible. Thus the only possibility is numerical solutions. The second element of the chapter will present the basic numerical methods to be used. Finally how the modelling problems have been approached in this thesis has been presented in the last section.

Thus in this chapter following areas will be briefly reviewed:

- Principles of chromatography and EBA
- Relevant transport equations
- Numerical methods applied in this work
- Model development process.

2.2 Principles of Chromatography and EBA

2.2.1 Chromatography

Chromatography is a separation process whereby different chemical species are separated based upon their differential adsorptive affinity to different media or phases. The general mechanism is (Schulte and Epping, 2005; Subramanian, 1995):

- A homogeneous mixture phase consisting of chemical species to be separated is brought into contact with a new phase.
- Molecules exchanges between two phases to bring the system into thermodynamic equilibrium. The rate and quantity of exchange of chemical species between the

phases depends upon the specific thermodynamic imbalances. This can be observed as a specific partition coefficient of the chemical species between the phases in relation to the presence of other species and their concentrations.

- The phases will now have a different concentration of chemical species than that at the initial stage. The separation of phases will now result into a partial separation of chemical species.

Each chemical species will have a defined affinity to certain media or phase relative to other species. This difference in adsorptive affinity is the basis of separation. Adsorption is the accumulation of molecules on the surfaces. The process of adsorption is as follows.

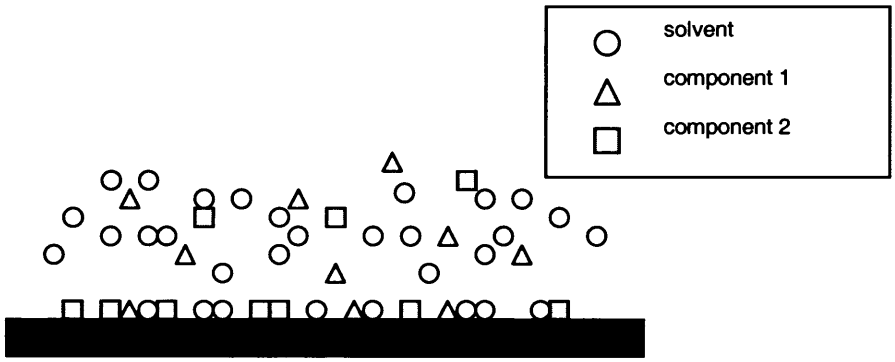

Fig. 2.1 An adsorption process. Solvent or mobile carries the components and brings in contact with stationary adsorbent phase. Components bind to the adsorbent phase to various degrees based on their mutual affinities or binding nature. In the figure, based upon the number, component 2 (□) seems to have more affinity to bind to the adsorbent phase than component 1 (△).

In an adsorption process the binding forces are formed between the molecules of one phase (fluid) to the surfaces of another phase (adsorbent) as shown in Fig. 2.1. The strength of binding depends upon the nature of binding. There are basically two different types of binding forces: physisorption (physical adsorption) and chemisorption (chemical adsorption). Physisorption is a weak binding based on van der Waals forces e.g. dipole, dispersion or induction forces. This is weaker than intramolecular binding forces of molecular species and thus the molecules will maintain their chemical identity. Chemisorption provides for strong binding and is due to valence forces similar to covalent binding. The energy involved in such a binding is strong enough to break the

intramolecular forces of adsorbed materials and adsorbent. Due to the complete reversibility requirement of a chromatographic process only adsorption based on physisorption can be used.

2.2.2 A Chromatographic Process

In a chromatographic process normally a solid (adsorbent) stationary phase is packed in a column. The other phase is a fluid. It is mobile and is composed of mixture of different chemical species. As the fluid phase passes through the stationary adsorbent phase, the chemical species in the fluid tend to become adsorbed to the adsorbent. The higher the affinity of the particular molecular species to the adsorbent, the more time they will spend in the adsorbent phase. This results in a differential migration rate for different species (Fig. 2.2). Thus at the outlet of the column the components having less affinity will elute earlier than the ones having a higher affinity. With appropriate operating conditions this can result in a complete separation of different chemical species.

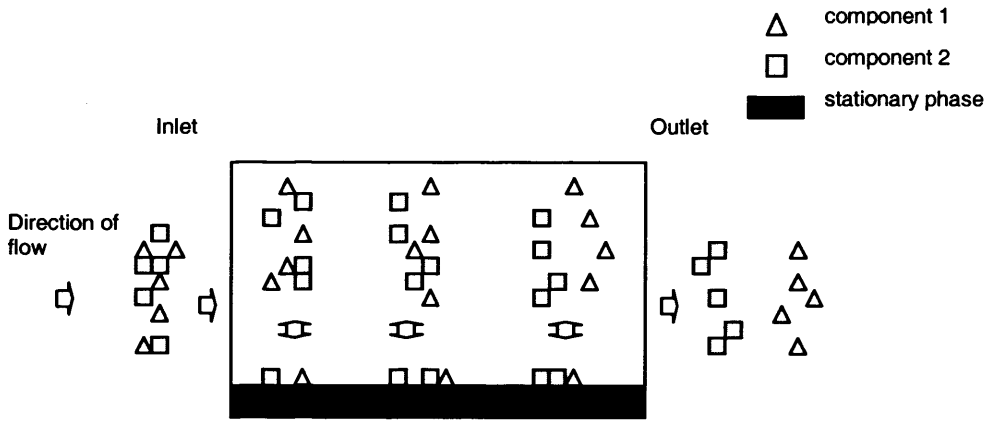

Fig. 2.2 Differential migrations of component species in a chromatographic process. Higher affinity of component 2 (□) to the adsorbent phase compared to the component 1 (Δ) will cause the slower elution of the component 2 from the column. (Fig. based on Schulte and Epping, 2005)

If the mobile fluid phase is gas, the process is called gas chromatography (GC). If the mobile phase is liquid, it is called liquid chromatography (LC). When a column is packed with small particles for higher separation efficiency in LC, it is called high performance liquid chromatography (HPLC).

2.2.3 Expanded Bed Adsorption

The adsorption behaviour in expanded bed adsorption (EBA) is the same as in normal chromatography. The only difference is the way in which the solid stationary phase is configured. Instead of a compact static packing in a column as achieved in normal chromatography, the adsorbent (solid) phase floats freely or is "expanded" using upward fluid pressure as can be seen in Fig. 2.3.

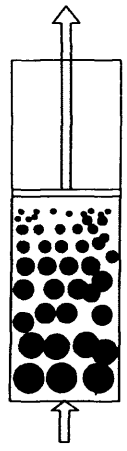

Fig. 2.3 Expanded bed adsorption

The bed stability, i.e. relative constancy in the position of the adsorbent particles, is achieved by employing a distribution of particle sizes and density. The bigger and heavier particles tend to stay at the bottom of the column while smaller and lighter particles stay at the top. A particle is subjected to many different forces: drag, gravity, buoyancy, etc. These forces in relation to its physical properties like density, size and fluid's physical properties like density and viscosity determine the expansion behaviour of the bed and a bead's relative position within the bed. This behaviour is the subject of bed hydrodynamics.

The main advantage of EBA comes from this free floating configuration of the adsorbent phase as crude feedstock containing cell debris and other solids can be fed directly into the column. This would have been impossible in a normal chromatography column as the presence of solids would clog up the column. EBA is normally operated at average bed voidage of about 0.7-0.8 (Amersham Pharmacia Biotech). As the bed voidage is large and flexible (local voidage can easily and temporarily change if need be

to adjust for large solids), the cell debris and other materials just pass through the column without clogging while the desired chemical species in the fluid are adsorbed to the adsorbent phase. Thus it obviates the need for micro-filtration or similar unit operation to remove the cell debris first.

Some basic steps of operation for preparative EBA (Fig. 2.4) are (Amersham Pharmacia Biotech):

1. Expansion
2. Equilibration
3. Loading
4. Washing
5. Elution
6. Regeneration

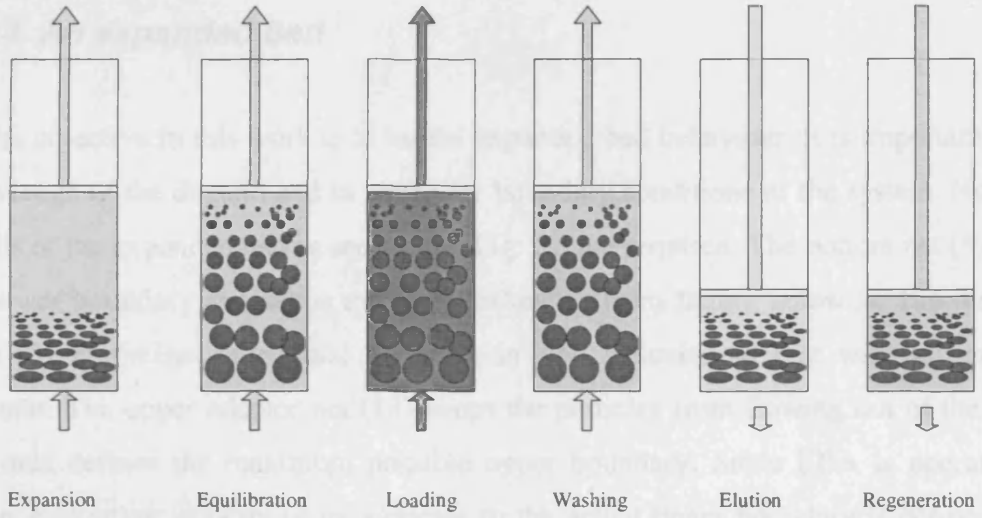

Fig. 2.4 Operation steps of expanded bed

The bed is first expanded and equilibrated using a buffer at a certain fluid velocity. The fluid velocity applied and the resulting expansion depends primarily upon matrix used besides physical properties of the fluid. In a typical operation using Streamline matrix, the bed would expand 1.7-3 times the settled bed height when fluid velocity of 100-300 cm/h is applied (Amersham Pharmacia Biotech). Once equilibrated, the feedstock is then fed into the column. As described above at this loading stage, the desired chemical species are adsorbed to the adsorbent phase while other materials pass

through. As the adsorbent becomes saturated with the component species of interest, the concentration of the component at the outlet will start to rise. When this reaches a particular point in terms of breakthrough (for example 1% or 5% of feed concentration), the loading or feeding of the feedstock is stopped as the bed does not have sufficient economic capacity to adsorb further. Then the washing step is performed whereby all molecular species of the original feed or fluid phase are washed out of the column while the component species of interest is retained adsorbed on the adsorbent. The final stage is elution. At this stage by changing the environmental conditions (pH or concentration of salt, etc.) the binding of the component species to the adsorbent is weakened and thus the species of interest are eluted from the column. In this way separation and preliminary stage purification of the species from the crude feedstock is achieved. After elution the column is regenerated by cleaning with reagents like NaOH solution and by washing with washing-buffer.

2.2.4 An expanded bed

As the objective in this work is to model expanded bed behaviour, it is important to have knowledge of the domain and in particular boundary conditions of the system. Not all the details of the expanded bed as seen in the Fig. 2.5 are required. The bottom net (5) defines the lower boundary and keeps the particles/matrix from falling below it. The distributor plate (3) minimises any radial variation in flow velocity so that will be considered constant. The upper adaptor net (13) keeps the particles from flowing out of the column and thus defines the maximum possible upper boundary. Since EBA is operated well below elutriation velocity of its particles so the actual upper boundary is defined by the maximum height that the particles can take in a given operating condition. Elutriation velocity is the fluid velocity at which upward component of a particle velocity becomes larger than the downward component which results into the exit of such particles from the bed. For a transient condition when the upper particle-bed surface is moving, it will be defined as a moving boundary.

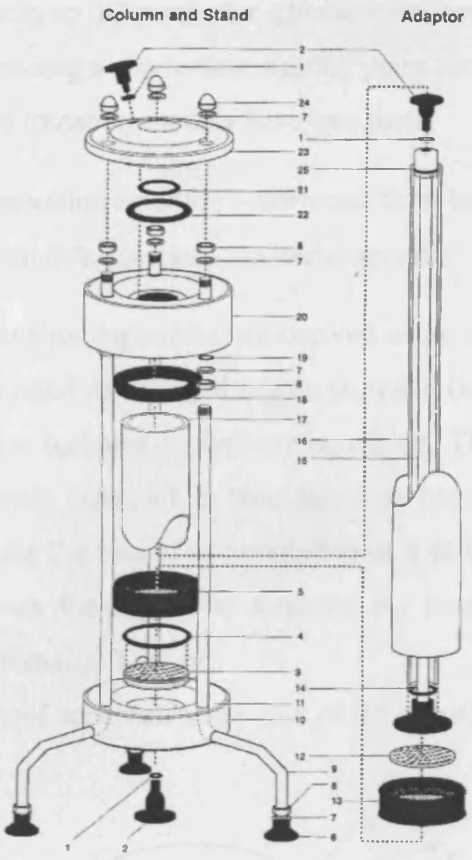

Fig. 2.5 An exploded diagram of the principal components of the 0.05m diameter STREAMLINE column (ST-50): 1,14,19,22,25 O-rings; 2 connector; 3 distributor plate, 5 bottom net; 6 stand feet; 7 washer; 8 nut; 9 stand; 10 bottom flange; 11 adaptor plate; 12 adaptor distributor plate; 13 adaptor net; 15 adaptor; 16 rod piston; 17 column tube; 18 gasket; 20 upper flange; 21 rod sealing; 23 lid, 24 domed nut (source: Willoughby, N., 2000)

General principles and properties related to an expanded bed operation have been described here. Some relevant transport equations which will form the basis of modelling an expanded bed process will be discussed in the next section.

2.3 A Brief Review of Some Relevant Transport Equations

2.3.1 Introduction

As most of the models developed in this work fall into the area of transport problems, some relevant transport equations will be reviewed here briefly. These will then be

adapted directly to the particular situations as they arise. The brief inclusion of this part is aimed at providing a convenient starting point for the modelling works here.

Typical transport models have two parts:

- Conservation equation – universal form based on first principles
- Constitutive equation – material-specific

Conservation equations are derived using the control volume concept. The control volume is defined as a closed region in space (as shown in Fig. 2.6) whose boundary is chosen to ease formulating balance equations. The size and shape of the control volume can change with time and its boundary may not correspond to physical interfaces. In the control volume the rate of accumulation of a certain quantity is equated to the net rate at which it enters the region by crossing the boundaries and the net rate at which it is generated internally. That is:

the rate of accumulation = rate of (In – Out) + rate of (Production – Consumption)

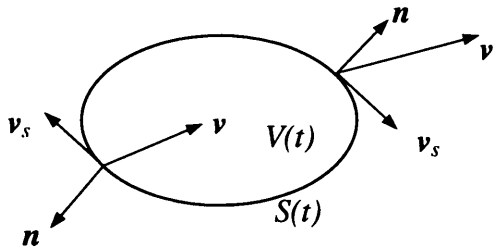

Fig. 2.6 A control volume

In this section 2.3, a general conservation equation at a point will be established, particularly in relation to the mass conservation of a component in a medium having multi-components. For the purpose, a control volume approach will be applied which will be used to generate conservation at a point. The component flux will be expanded in terms of convective and diffusive fluxes. The resulting relation will be used as the basis of modelling in other chapters. The conservation at the interface between two phases will also be established which can later be taken as the starting point to establish boundary conditions.

As described by Deen (1995) in his book, Analysis of Transport Phenomena, let u be the concentration of the quantity of interest in the control volume.

$$\frac{d}{dt}\int_{V(t)} u dV = -\int_{S(t)} \boldsymbol{F}\cdot\boldsymbol{n} dV + \int_{V(t)} R_V dV + \int_{S(t)} u\boldsymbol{v}_s \cdot \boldsymbol{n} dS \qquad (2.1)$$

where

$\boldsymbol{F}\cdot\boldsymbol{n}$ = flux of the quantity in the control volume

R_V = net rate of production of quantity internally

$u(r,t)\ dV$ = amount of quantity contained in the differential volume element dV about the point r

$\boldsymbol{v}_s \cdot \boldsymbol{n}\ dS$ = rate at which volume is swept out by element of the control volume

V refers to volume and S refers to surface area of the control volume. r is the position vector.

Liebnitz' formula for the differentiation of the volume integral yields:

$$\frac{d}{dt}\int_{V(t)} u dV = \int_{V(t)} \frac{\partial u}{\partial t} dV + \int_{S(t)} u\boldsymbol{v}_s \cdot \boldsymbol{n} dS \qquad (2.2)$$

Substituting this into Eq. (2.1)

$$\int_{V(t)} \frac{\partial u}{\partial t} dV = -\int_{S(t)} \boldsymbol{F}\cdot\boldsymbol{n} dS + \int_{V(t)} R_V dV \qquad (2.3)$$

This is a general conservation equation which requires only $u(r,t)$ be continuous within $V(t)$.

When the interior of the control volume contains a moving interface at which the concentration is discontinuous and if there is a source/sink term at the interface, it becomes: (derivation in Appendix: Eq. A.5)

$$\int_{V(t)} \frac{\partial u}{\partial t} dV + \int_{S_{I(t)}} (u_A - u_B)\boldsymbol{v}_I \cdot \boldsymbol{n}_I dS = -\int_{S(t)} \boldsymbol{F}\cdot\boldsymbol{n} dS + \int_{V(t)} R_V dV + \int_{S_{I(t)}} R_S dS \qquad (2.4)$$

where

I refers to interface between phases A and B

n_I is normal to the interface

v_I is velocity of the interface

As most of the time, the interest would be the point value of a property at a spatial position than a volumetric average value; the general conservation equation derived here will be used to derive the conservation equation at a point in the next section.

2.3.2 Conservation equation at a point:

Using Gauss' divergence theorem to the first term at right hand side (R.H.S.) of Eq. (2.3),

$$\int_{\Gamma} \boldsymbol{F} \cdot \boldsymbol{n} dS = \int_{\Omega} \nabla \cdot \boldsymbol{F} dV \tag{2.5}$$

Thus Eq.

(2.3) gives:

$$\int_{\Omega(t)} \frac{\partial u}{\partial t} dV = -\int_{\Omega(t)} \nabla \cdot \boldsymbol{F} dV + \int_{\Omega(t)} R_V dV \tag{2.6}$$

$$\int_{\Omega(t)} \left[\frac{\partial u}{\partial t} + \nabla \cdot \boldsymbol{F} - R_V \right] dV = 0 \tag{2.7}$$

Integral being equal to the product of mean value of the integrand and magnitude of region,

$$\left\langle \frac{\partial u}{\partial t} + \nabla \cdot \boldsymbol{F} - R_V \right\rangle V = 0$$

$$\frac{\partial u}{\partial t} = -\nabla \cdot \boldsymbol{F} + R_V \tag{2.8}$$

Similarly at interfaces, neglecting accumulation and transport within the interfaces: (derivation in Appendix: Eq. A.13)

$$\left[(\boldsymbol{F} - u\boldsymbol{v}_I)_B - (\boldsymbol{F} - u\boldsymbol{v}_I)_A \right] \cdot \boldsymbol{n}_I = R_S \tag{2.9}$$

where $(\boldsymbol{F} - u\boldsymbol{v}_I)$ is flux in relation to the interface, I refers to interface between phases A and B, and n_I is normal to the interface.

Having established the conservation equation at a point, both inside a domain and at an interface, the specific components of flux will be expanded in the next section.

2.3.3 Component of fluxes:

In the modelling work here the flux is basically a result of convection or diffusion. Thus,

$$\text{Total flux } F = F_{\text{convection}} + F_{\text{diffusion}} \tag{2.10}$$

$$= uv + f \tag{2.11}$$

where v = mass average velocity (of the mixture)

Thus Eq (2.8) becomes

$$\frac{\partial u}{\partial t} = -\nabla \cdot (u\boldsymbol{v} + \boldsymbol{f}) + R_V \tag{2.12}$$

$$\frac{\partial u}{\partial t} = -\nabla \cdot (u\boldsymbol{v}) + \nabla \cdot \boldsymbol{f} + R_V \tag{2.13}$$

Similarly at interfaces: (from Eq. (2.9))

$$\left[(u\boldsymbol{v} + \boldsymbol{f} - u\boldsymbol{v}_I)_B - (u\boldsymbol{v} + \boldsymbol{f} - u\boldsymbol{v}_I)_A\right] \cdot \boldsymbol{n}_I = R_S \tag{2.14}$$

$$\left[(\boldsymbol{f} + u(\boldsymbol{v} - \boldsymbol{v}_I))_B - (\boldsymbol{f} + u(\boldsymbol{v} - \boldsymbol{v}_I))_A\right] \cdot \boldsymbol{n}_I = R_S \tag{2.15}$$

For general application, u has been taken as any general quantity of interest e.g. mass, energy, etc. The conservation of the quantity would remain valid. As this thesis would focus on mass conservation, that will be established in the next section. Establishing the relation specific to mass is useful especially when the medium is incompressible which will result into an additional constraint in the system and thus simplify the model by reducing a degree of freedom.

2.3.4 Conservation of mass

Let u denotes density (ρ) of the material in the control volume.

From Eq. (2.12)

$$\frac{\partial u}{\partial t} = -\nabla \cdot (\rho \boldsymbol{v} + \boldsymbol{f}) + R_V$$

There is not net mass flow in relation to mass average velocity, v, and if there are no source and sinks:

$$\frac{\partial u}{\partial t} = -\nabla \cdot (\rho \boldsymbol{v}) = -\rho \nabla \cdot \boldsymbol{v} - \boldsymbol{v} \cdot \nabla \rho \tag{2.16}$$

For incompressible flow: ρ = constant

$$\nabla \cdot \boldsymbol{v} = 0 \tag{2.17}$$

Finally as the main focus of this thesis is modelling the conservation of a component in a multi-component medium, the general conservation equation of a component will be established in the following section which will form the basis of modelling in other chapters.

2.3.5 Conservation of a Component

As most of the time, our interest in this work is to performs a mass balance of a component or chemical species, let u_i be the concentration of component i. So u in the above equations will refer to u_i. From Eq. (2.8)

$$\dot{u} = -\nabla \cdot \boldsymbol{F} + R_V$$

Let n_i = mass flux w.r.t. fixed coordinates = F

$$\frac{\partial u_i}{\partial t} = -\nabla \cdot \boldsymbol{n}_i + R_{Vi} \tag{2.18}$$

n_i is given by:

$$\boldsymbol{n}_i = u_i \boldsymbol{v} + \boldsymbol{j}_i \tag{2.19}$$

v = mass average velocity

total mass flux = $\rho \boldsymbol{v} = \sum u_i \boldsymbol{v}$ (2.20)

j_i = mass flux w.r.t. mass average velocity (v)

= diffusive flux

For relatively dilute concentrations where one component or solvent/medium accounts for most of the mass:

$$\boldsymbol{j}_i = -D_i \nabla u_i \tag{2.21}$$

where

D_i = diffusivity of component species I in the abundant medium

$$\boldsymbol{n}_i = u_i \boldsymbol{v} - D_i \nabla u_i \tag{2.22}$$

Substituting into Eq. (2.18)

$$\frac{\partial u_i}{\partial t} = -\nabla \cdot (u_i \boldsymbol{v} - D_i \nabla u_i) + R_{Vi}$$

$$\frac{\partial u_i}{\partial t} = -\nabla \cdot (u_i \boldsymbol{v}) + \nabla \cdot (D_i \nabla u_i) + R_{Vi} \tag{2.23}$$

for constant D_i or D_i independent of space (x)

$$\frac{\partial u_i}{\partial t} = -u_i \nabla \cdot \boldsymbol{v} - \boldsymbol{v} \cdot \nabla u_i + D_i \nabla^2 u_i + R_{Vi} \tag{2.24}$$

In the material derivative form:

$$\frac{D u_i}{D t} = -u_i \nabla \cdot \boldsymbol{v} + D_i \nabla^2 u_i + R_{Vi} \tag{2.25}$$

For incompressible flow and dilute concentration of components especially when density of the components are not much different to the abundant medium in which they exist, the average density (ρ) is relatively constant (for practical purpose).

$$\nabla \cdot \boldsymbol{v} = 0$$

$$\frac{D u_i}{D t} = D_i \nabla^2 u_i + R_{Vi} \tag{2.26}$$

$$\frac{\partial u_i}{\partial t} = -\boldsymbol{v} \cdot \nabla u_i + D_i \nabla^2 u_i + R_{Vi} \qquad (2.27)$$

This general equation of continuity will be used for derivations relevant to specific situations in following chapters. The next section of this chapter will discuss the numerical methods that can be applied to solve the equations of this form.

2.4 Numerical Methods

2.4.1 Introduction

Model equations that are developed in this work are generally convective-dispersive equations which fall into the category of second order partial differential equations. Depending upon whether the problem to be solved is steady state or transient, dispersion dominant or strongly convection dominant, the resulting equations can be effectively elliptic, parabolic or hyperbolic. As most of the equation sets are nonlinear, it is not possible to solve them analytically. So a numerical solution is the only possibility for any practical applications.

At present there are lots of PDE tools available off-the-shelf. So in most of the cases, specifying the model equations or mostly graphically specifying the geometry, boundary conditions and physical properties of the domain and physics of interest is more than sufficient to solve or to simulate. This has a very huge advantage in terms of productivity. There can be two drawbacks. The first, there can be the possibility of using the tools without completely understanding its outputs and limitations. For example for a convection dominant flow, the Galerkin method would start to become inaccurate and unstable as the magnitude of fluid velocity or resulting Peclet number increases above a certain critical value. For such flow Petrov-Galerkin or other upwind schemes will have to be adopted. If the appropriate method is not applied, in spite of the physics remaining same and correct, the solution becomes incorrect. Most of such well established problems are automatically handled by available tools. However in research, new problems generate their own new requirements. So the inability to handle such problems and requirements means that in spite of developing a good and correct model, its verification can be difficult. The second problem is that the tools come with their own intrinsic limitations to make them easy to use and avoid introducing errors by users. In most of the

cases, this should not be a problem, but in some cases, this can be a limitation. In spite of explaining some of the possible drawbacks in solely relying on available tools, use of such tools to solve the kind of problems generated in this work will be important, and in fact in many involved modelling works will probably represent almost the only way to complete the works accurately and within a stipulated time.

In this work in order to keep the freedom of being able to handle an innovative and complex research problem if that arises, and as most of the model equations are one-dimensional and relatively easy to apply, appropriate numerical methods will be used. There are a number of methods that can be employed for the purposes of solution. Different methods have their own advantages and disadvantages. Finite difference is the simplest method, while the finite element method, though more involved, has its advantages in engineering applications especially when the developed methods have to be made generic so that they can handle more complicated situations and boundary conditions easily.

For this work though finite difference method alone could have solved the problem, a finite element method has been used in the adsorption part of the model so as to make it more easily amenable to multi-dimensional applications in future if desired, for example when wall effect becomes significant in very small diameter scale-down columns, etc. Orthogonal collocation has also been used for its efficiency in diffusion dominant equations which is especially important when working with multi-component models which can demand enormous computational resources. In this part of the chapter the particular methods employed within a given class of methods for a generic equation of the model are described or reviewed in sufficient depth for their use in other chapters. The generic derivations from this chapter are applied to specific situations in subsequent chapters.

Eq. (2.27), a convective-dispersive equation, is a basis equation which will be used for modelling in this thesis. For establishing generic numerical schemes which would be applicable to Eq. (2.27) and its general variations, the following generalised form of the same, Eq. (2.28), will be used in its place. The general derivations of numerical methods established in this section 2.4 can then be easily applied in specialised equations developed during the modelling process in other chapters for the purpose of simulation.

For a time (t) dependent variable u (conservation quantity of interest, e.g. a component) in domain x,

$$\frac{\partial u}{\partial t} - \nabla \cdot a_1 \nabla u + a_2 \nabla u + a_3 u = f(\boldsymbol{x},t), \qquad 0 \le x \le 1 \tag{2.28}$$

with boundary conditions:

$$x = 0: \qquad b_{11} \nabla u + b_{12} u = g_1(\boldsymbol{x},t) \tag{2.29}$$

$$x = 1: \qquad b_{21} \nabla u + b_{22} u = g_2(\boldsymbol{x},t) \tag{2.30}$$

with initial conditions:

$$t = 0: \qquad u(\boldsymbol{x},0) = u^0(\boldsymbol{x}) \tag{2.31}$$

where a_i and b_{jk} are parameters, and f and g_j are functions.

In one-dimension and simplified form, the Eqs (2.28)-(2.31) would become:

$$\frac{\partial u}{\partial t} - a_1 \frac{\partial^2 u}{\partial x^2} + a_2 \frac{\partial u}{\partial x} + a_3 u = f(x,t), \qquad 0 \le x \le 1 \tag{2.32}$$

with boundary conditions:

$$x = 0: \qquad b_{11} \frac{\partial u}{\partial x} + b_{12} u = g_1(x,t) \tag{2.33}$$

$$x = 1: \qquad b_{11} \frac{\partial u}{\partial x} + b_{12} u = g_1(x,t) \tag{2.34}$$

with initial conditions:

$$t = 0: \qquad u(x,0) = u^0(x) \tag{2.35}$$

This set of equations (2.32)-(2.35) for one-dimension [or Eqs (2.28)-(2.31) for multi-dimension] will be used to establish generic numeric schemes in this section 2.4.

Initially the finite difference method (section 2.4.2) will be described. This is used in solving the hydrodynamic models. Both the orthogonal collocation and finite element methods are based on variational principles and this will be described next (section 2.4.3). This is followed by particular methods like orthogonal collocation and Galerkin method which will be described in section 2.4.4. The finite element method (section 2.4.5), which is developed for more versatile applications, is described at the end. Numerical error, stability and convergence are all important factors, and have also been explained briefly. Many of these are active research areas. Numerous books and publications exist in the area. Most of the methods used here are standard methods and have been established and in use for several decades. So this part of the chapter judiciously and systematically chooses and elaborates the relevant and essential parts of such methods. It is hoped that this will provide a sound basis, some theoretical insights in the development and

application of such methods and make the thesis self-sufficient in terms of the capacity to handle problems arising in this work.

2.4.2 Finite Difference

2.4.2.1 Introduction

In the finite difference method, the continuous PDE problem is replaced by its corresponding difference form and the resulting discrete algebraic equations are solved to predict the state of variable (u) at a given time and spatial position.

A Taylor series expansion of a vector in terms of position vector (r) is given by (Deen, 1998):

$$\boldsymbol{u}(\boldsymbol{r}+\boldsymbol{r}')=\boldsymbol{u}(\boldsymbol{r})+\boldsymbol{r}'\cdot\nabla\boldsymbol{u}+\frac{1}{2}\boldsymbol{r}'\boldsymbol{r}':\nabla\nabla\boldsymbol{u}+\ldots \tag{2.36}$$

For a simplified form for a scalar quantity, it can be written as (Kreyszig, 1999):

$$u(x+\Delta x,y)=u(x,y)+\left.\frac{\partial u}{\partial x}\right|_{x,y}\Delta x+\left.\frac{1}{2!}\frac{\partial^2 u}{\partial x^2}\right|_{x,y}\Delta x^2+\cdots+\left.\frac{1}{n!}\frac{\partial^n u}{\partial x^n}\right|_{x,y}\Delta x^n+E(\xi) \tag{2.37}$$

where

$$E(\xi)=\left.\frac{1}{(n+1)!}\frac{\partial^{n+1}u}{\partial x^{n+1}}\right|_{\xi,y}(\Delta x)^{n+1},\qquad \xi\le\Delta x \tag{2.38}$$

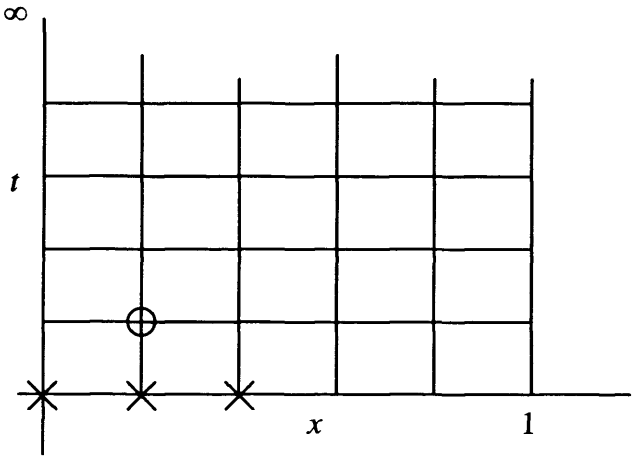

Fig. 2.7 Discretisation of domain into the grids of space (x) and time (t).

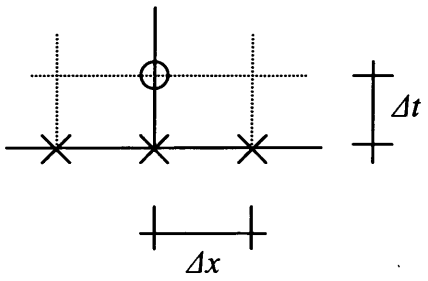

Fig. 2.8 A discretisation unit. Δx is a discrete unit of space (x) and Δt is that of time (t).

When Δx is small, higher order terms become negligible. Neglecting second and higher order terms of Eq. (2.37):

$$u(x+\Delta x,y)=u(x,y)+\left.\frac{\partial u}{\partial x}\right|_{x,y}\Delta x \qquad (+\text{ truncation error} = O(\Delta x)) \tag{2.39}$$

$$\left.\frac{\partial u}{\partial x}\right|_{x,y}=\frac{u(x+\Delta x,y)-u(x,y)}{\Delta x} \tag{2.40}$$

This is same as definition of derivatives:

$$\left.\frac{\partial u}{\partial x}\right|_{x,y}=\lim_{\Delta x\to 0}\frac{u(x+\Delta x,y)-u(x,y)}{\Delta x} \tag{2.41}$$

Similarly Taylor series can also be expanded in different direction: (backward difference)

$$u(x-\Delta x,y)=u(x,y)-\left.\frac{\partial u}{\partial x}\right|_{x,y}\Delta x+\frac{1}{2!}\left.\frac{\partial^2 u}{\partial x^2}\right|_{x,y}\Delta x^2-\cdots+\frac{1}{n!}\left.\frac{\partial^n u}{\partial x^n}\right|_{x,y}\Delta x^n-E(\xi) \tag{2.42}$$

Adding Eqs (2.37) and (2.42), and neglecting 3rd and higher order terms:

$$u(x+\Delta x,y)+u(x-\Delta x,y)=2u(x,y)+\left.\frac{\partial^2 u}{\partial x^2}\right|_{x,y}\Delta x^2 \tag{2.43}$$

(+ truncation error $O(\Delta x^2)$)

$$\left.\frac{\partial^2 u}{\partial x^2}\right|_{x,y}=\frac{u(x+\Delta x,y)-2u(x,y)+u(x-\Delta x,y)}{\Delta x^2} \tag{2.44}$$

Different variations of the differencing scheme can be followed and will result in different levels of accuracy. The first derivative Eq. (2.40) is in forward difference form and has $O(\Delta x)$ truncation error. Centered difference can be applied as used to derive 2nd derivative in Eq. (2.44). This can be done by subtracting Eq. (2.42) from Eq. (2.37) and discarding 3rd and higher order terms.

$$u(x+\Delta x,y)-u(x-\Delta x,y)=2\left.\frac{\partial u}{\partial x}\right|_{x,y}\Delta x \qquad (+O(\Delta x^2))$$

$$\left.\frac{\partial u}{\partial x}\right|_{x,y} = \frac{u(x+\Delta x, y)-u(x-\Delta x, y)}{2\Delta x} \tag{2.45}$$

This centered difference first derivative is more accurate since it only has a truncation error of $O(\Delta x^2)$.

Thus applying forward difference to time and centered difference to space, Eq. (2.32) can be discretised as:

$$\frac{u(x,t+\Delta t)-u(x,t)}{\Delta t} - a_1 \frac{u(x+\Delta x,t)-2u(x,t)+u(x-\Delta x,t)}{\Delta x^2} + a_2 \frac{u(x+\Delta x,t)-u(x-\Delta x,t)}{2\Delta x} + a_3 u(x,t) = f(x,t) \tag{2.46}$$

$$u(x,t+\Delta t) = u(x,t) + \Delta t F(u(x+\Delta x,t), u(x,t), u(x-\Delta x,t), \Delta x, a_1, a_2, a_3, f(x,t)) \tag{2.47}$$

Similarly boundary conditions, Eqs (2.33 and (2.34), can be discretised as:

$$b_{11}\frac{u(x+\Delta x,t)-u(x-\Delta x,t)}{\Delta x} + b_{12}u(x,t) = g_1(x,t) \tag{2.48}$$

$$b_{21}\frac{u(x+\Delta x,t)-u(x-\Delta x,t)}{\Delta x} + b_{22}u(x,t) = g_2(x,t) \tag{2.49}$$

Given the known values of u, its value at the next time step can be determined using Eq. (2.47) and given boundary conditions discretised in the similar form (Eqs. (2.48) and (2.49)). As initial values at t = 0 are known from initial conditions, all values can be determined by marching in time. This is first order accurate in time and second order accurate in space.

This kind of method is called an explicit method. But it has a serious limitation. For the method to converge, it has to satisfy a crucial criterion (Kreyszig, 1999):

$$\frac{\Delta t}{\Delta x^2} \leq \frac{1}{2} \tag{2.50}$$

This means that the time step should be very small compared to spatial discretisation size. This requirement can make it unfit for many practical applications. To avoid this limitation, an implicit method or one of its variants like Crank-Nicholson method or other θ-family of approximation methods have to be applied.

2.4.2.2 Time Discretisation

In θ-family approximation, the weighted average of time derivatives of dependent variable at two consecutive time steps using their linear interpolation values are used as follows (Reddy, 1986).

$$\frac{\partial u}{\partial t} = (1-\theta)\frac{\partial u}{\partial t}\bigg|_t + (1-\theta)\frac{\partial u}{\partial t}\bigg|_{t+\Delta t} \equiv (1-\theta)\dot{u}\big|_t + (1-\theta)\dot{u}\big|_{t+\Delta t} \qquad 0 \le \theta \le 1 \qquad (2.51)$$

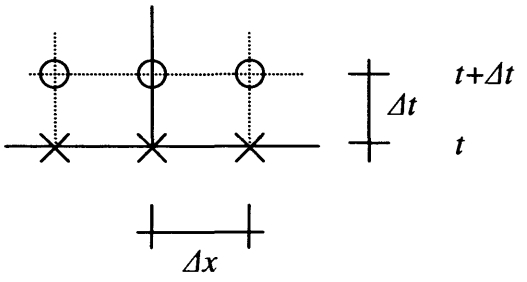

Fig. 2.9 Grid of 6 points used in θ-family approximation

Representing dot (" · ") for time derivative and apostrophe (" ' ") for a spatial derivative:

$$\dot{u} - a_1 u'' + a_2 u' + a_3 u = f(x,t) \qquad (2.52)$$

$$\dot{u} = a_1 u'' - a_2 u' - a_3 u + f(x,t) = F(u,x,t,a_i) \qquad i = 1, 2, 3 \qquad (2.53)$$

Applying weighted average approximation of $\dot{u}$ using two consecutive time steps:

$$\dot{u} = (1-\theta)\dot{u}\big|_t + \theta\dot{u}\big|_{t+\Delta t}$$

$$\dot{u} = (1-\theta)F\big|_t + \theta F\big|_{t+\Delta t} \qquad (2.54)$$

$$\frac{u(x,t+\Delta t) - u(x,t)}{\Delta t} = (1-\theta)F(u,x,t,a_i) + \theta F(u,x,t+\Delta t,a_i) \qquad (2.55)$$

Values of u (u, u', u'') in F are evaluated based on its time step, either t or $t+\Delta t$.

Cases:

$\theta = 0$: Explicit method, conditionally stable, accuracy $O(\Delta t)$

$\theta = 1/2$: Crank-Nicholson method, unconditionally stable, accuracy $O(\Delta t^2)$

$\theta = 2/3$: Galerkin method, unconditionally stable, accuracy $O(\Delta t^2)$

$\theta = 1$: Implicit method, unconditionally stable, accuracy $O(\Delta t)$

Details for the example equation, Eq. (2.32), would be:

$$\begin{aligned}
&\frac{1}{\Delta t}u(x,t+\Delta t)-\frac{1}{\Delta t}u(x,t)=(1-\theta)\frac{a_1}{\Delta x^2}\{u(x+\Delta x,t)-2u(x,t)+u(x-\Delta x,t)\}\\
&-(1-\theta)\frac{a_2}{2\Delta x}\{u(x+\Delta x,t)-u(x-\Delta x,t)\}-(1-\theta)a_3u(x,t)+(1-\theta)f(x,t)\\
&+\theta\frac{a_1}{\Delta x^2}\{u(x+\Delta x,t+\Delta t)-2u(x,t+\Delta t)+u(x-\Delta x,t+\Delta t)\}\\
&-\theta\frac{a_2}{2\Delta x}\{u(x+\Delta x,t+\Delta t)-u(x-\Delta x,t+\Delta t)\}-\theta a_3u(x,t+\Delta t)+\theta f(x,t+\Delta t)
\end{aligned} \tag{2.56}$$

Keeping all unknown or to be determined values of the new time step on the left of the equation and all known on the right result in:

$$\begin{aligned}
&\left\{-\theta\frac{a_1}{\Delta x^2}+\theta\frac{a_2}{2\Delta x}\right\}u(x+\Delta x,t+\Delta t)+\left\{\frac{1}{\Delta t}+\frac{2\theta a_1}{\Delta x^2}+\theta a_3\right\}u(x,t+\Delta t)\\
&\left\{-\theta\frac{a_1}{\Delta x^2}-\theta\frac{a_2}{2\Delta x}\right\}u(x-\Delta x,t+\Delta t)=\left\{(1-\theta)\frac{a_1}{\Delta x^2}-(1-\theta)\frac{a_2}{2\Delta x}\right\}u(x+\Delta x,t)\\
&+\left\{\frac{1}{\Delta t}-\frac{2(1-\theta)a_1}{\Delta x^2}-(1-\theta)a_3\right\}u(x,t)+\left\{(1-\theta)\frac{a_1}{\Delta x^2}+(1-\theta)\frac{a_2}{2\Delta x}\right\}u(x-\Delta x,t)\\
&+\{(1-\theta)f(x,t)+\theta f(x,t+\Delta t)\}
\end{aligned} \tag{2.57}$$

Thus resulting simultaneous equations of unknown variable (u at $t+\Delta t$) can be represented in the matrix form as:

$$\boldsymbol{A}\boldsymbol{u}^{t+\Delta t}=\boldsymbol{B}\boldsymbol{u}^{t}+\boldsymbol{f}=\boldsymbol{b} \tag{2.58}$$

$$\boldsymbol{u}^{t+\Delta t}=\boldsymbol{A}^{-1}\boldsymbol{b} \qquad \text{(after applying boundary conditions)} \tag{2.59}$$

Thus u of new time step is calculated as above from known u value of previous time step and so on.

In many situations, instead of discretising time by the method established here, it will be much easier to apply method of line technique and not to discretise time at all. Such method and its requirement will be discussed in the following section.

2.4.2.3 Method of Line

In many situations when there are readily available powerful ordinary differential equation solvers available on hand, it would be easy to apply only spatial discretisation. This will convert partial differential equations into ordinary differential equation which are easily solved by using ODE-solver software tools. Such techniques are especially useful for stiff-equations having more than one and very different time scales where more elaborate time stepping algorithms including adaptive time steps have to be employed for simulations.

Applying this method to Eq. (2.32):

$$\dot{u} = \frac{a_1}{\Delta x^2}\{u(x+\Delta x,t) - 2u(x,t) + u(x-\Delta x,t)\} + \\ -\frac{a_2}{2\Delta x}\{u(x+\Delta x,t) - u(x-\Delta x,t)\} - a_3 u(x,t) + f(x,t) \tag{2.60}$$

$$\dot{u} = F(u(x+\Delta x,t), u(x,t), u(x-\Delta x,t), \Delta x, a_1, a_2, a_3, f(x,t)) \tag{2.61}$$

The ODE is solved using available software tools after applying boundary and initial conditions. In this work while applying this method, due to the stiffness of the model equations, MATLAB ODE-solver routine ode15s will be used.

Simulation of convective-dispersive equation poses a special problem in some circumstances. Thus circumstance at which it becomes problematic and how to solve it will be discussed in the following section.

2.4.2.4 Upwind Scheme

In the convective-dispersive equation, which is the basic equation of most of the work performed here, when flow becomes convection-dominated, the discretisation adopted as in the previous section becomes unstable after exceeding a certain critical value of Peclet no (*Pe*, ratio of convection to dispersion terms). The reason for this is the fact that the use of centred difference in a convective term implicitly gives equal weighting in both the upward and downward values in order to estimate the value in the middle. But physically when convection is strong, only backward influences will really exists from the origin. Use of a forward value approach is not physically realistic. Thus backward difference or upwind scheme in terms of direction of flow instead of centred difference for convective term has to be applied. This will represent the physics more appropriately in a numerical scheme, and the method becomes stable.

Hence considering direction of flow to be from x to $x+\Delta x$, the convective term is discretised as:

$$\left.\frac{\partial u}{\partial x}\right|_{x,t} = \frac{u(x,t) - u(x-\Delta x,t)}{\Delta x} \tag{2.62}$$

With the exception of this modification all other parts of the discretisation are the same as described in the previous section.

Before going to another numerical method which is also one of the basic methods applied in this thesis, some of the important aspects which need to be considered before applying a numerical scheme will be discussed briefly in the context of finite difference.

2.4.2.5 Numerical Errors and Convergence

While applying any numerical scheme, it is important to analyse its errors and convergence. Some of the areas which need to be considered are given below. More details can be found in Anderson et al. (1984).

2.4.2.5.1 Truncation error

While representing the derivatives with its finite difference form, higher order terms from Taylor's series are truncated and thus truncation errors (TE) are automatically introduced as can be seen in Eqs (2.37), (2.39), (2.43), etc.

$$PDE = FDE + TE \tag{2.63}$$

TE is expressed in order of magnitude of discretisation units. For example:

$$TE = O(\Delta t, (\Delta x)^2)$$

Thus the resulting solution of FDE gives an approximate solution to the original PDE. Given TE is small, the solution can be acceptable. But in any marching problem (parabolic equations) and nonlinear problems (where solution has to be determined iteratively by contraction mapping), this error term can propagate during the progression of time or iteration. This makes the numerical scheme unstable. Thus to ascertain whether a particular numerical scheme or finite difference representation is acceptable, it will have to meet conditions of consistency and stability.

2.4.2.5.2 Consistency

Consistency indicates the extent to which the finite difference (FD) equations approximates the partial differential equations. The difference, as seen above, is the truncation error. For FD representation to be consistent, the TE should vanish as the mesh size is refined, i.e. as discretisation size (Δt, Δx) approaches zero.

$$\lim_{mesh \to 0} (PDE - FDE) = 0 \tag{2.64}$$

In cases where TE is $O(\Delta t/\Delta x)$, the scheme should if necessary be modified so that

$$\lim_{\Delta t,\Delta x\to 0}\frac{\Delta t}{\Delta x}=0 \tag{2.65}$$

2.4.2.5.3 Stability

A numerical scheme can be considered stable if the errors introduced into the system does not grow as the calculation proceeds. The source of errors can be anything e.g. truncation, round off, small perturbations, etc. This is particularly an important criterion for marching problems and non-linear problems where the sequence of operations is based on the value of the previous step. A stable numerical scheme restricts the propagation of errors. Von-Neumann or Fourier analysis can be performed to check stability of a numerical scheme for linear problems.

2.4.2.5.4 Convergence

Convergence means that as the mesh is refined the solution of the finite difference approaches the true solution to the PDE. Generally, consistent and stable numerical scheme is convergent.

Having established the finite difference method in section 2.4.2 which has been applied in this thesis at a number of places, the principles of one of the basic numerical methods applied this thesis will be discussed and established in the next section.

2.4.3 Variational Principles

Both orthogonal collocation and finite element method, which are used in this thesis, fall into the family of method called weighted residual method (WRM) which is at even much broader sense is termed a variational method. The variational principle is the basis of such methods. Thus in this section variational principle and WRM are briefly explained before going into particular methods in detail. The general derivations made in these sections will then be applied directly for simulation in the subsequent chapters. All the sections related to the variational methods are organised and described as follows.

Organisation of Sections: This section 2.4.3 and the rest of the sections, 2.4.4 and 2.4.5, in the numerical methods discussed in this chapter are organised as follows. Variational

formulation (section 2.4.3.1) of a given operator equation or a physical problem is described first. A number of methods can be applied to get an approximate solution of the problem thus formulated. The Rayleigh-Ritz method is one of them. Though the Galerkin method is used in this thesis, for simplicity in choosing a basis function, an approach used in the Rayleigh-Ritz method which incorporates natural boundary condition into the variation form will be applied. This enables possibility of using C^1 continuous basis function instead of C^2 continuity required otherwise. Therefore the Rayleigh-Ritz method (section 2.4.3.2) will be explained next. Using this method, the criteria for convergence and stability of a variational method (section 2.4.3.3) will be presented. Both the Galerkin method and Orthogonal Collocation (OC) method fall into a class of method called Weighted Residual Method. Thus general property and principles of such method will be described first in the section 2.4.4 before going to specific details in sections 2.4.4.1 for the Galerkin method and 2.4.4.3 for OC method. As OC is a type of collocation method, that will be described before OC in section 2.4.4.2. For possibility of using complex domains and boundary conditions, finite element method (FEM) is used in this thesis. In this method variational approximation (here the Galerkin method) is applied element-wise instead of the whole domain. Hence FEM and the procedure to apply it are described in section 2.4.5. Many of the explanations and derivations are based on Thommaset (1981), Bathe (1996), Reddy (1986), Reddy (1993), Zienkiewicz and Taylor (2000a, 2000b), and Finlayson (1972).

2.4.3.1 Variational Formulation

The Eq. (2.28) or other field equations can be represented in an abstract form as operator equation as follows.

$$Au = f \quad \text{in domain } (\Omega) \qquad Bu = g \quad \text{on boundary } (\Gamma) \tag{2.66}$$

Where A is linear or nonlinear operator from an inner product space U into another inner product space V. For Eq. (2.28)

$$A = \frac{\partial}{\partial t} - \nabla \cdot a_1 \nabla + a_2 \nabla + a_3 \qquad \text{in } \Omega \subset R^3 \tag{2.67}$$

$$f = f(x,t)$$

boundary conditions

$$B = b_1 \nabla + b_2 \qquad \text{on } \Gamma$$

$\overline{\Omega} = \Omega + \Gamma$ (closed domain)

In the classical solution $u(x,t)$ is continuous in $\overline{\Omega}$ and satisfies A and B in Ω and Γ respectively. Assuming $f \in C(\overline{\Omega})$, $u(x,t)$ should be a continuous function with partial derivatives of second order continuous, $u \in C^2(\overline{\Omega})$ and should satisfy boundary conditions B on Γ. The set of such admissible functions (D_A) is given by:

$$D_A = \{u(x,t) \in C^2(\overline{\Omega}),\ x \in \Omega \subset R^3,\ B(u) = g(x,t) \text{ on } \Gamma\} \tag{2.68}$$

Thus the solution of the problem is:

$$u \in D_A \text{ which satisfies } Au = f \tag{2.69}$$

For a simple equation (a simple operator A) and simple domain (Ω), u can be determined in closed form using several analytical methods like separation of variables, Finite Fourier Transform, etc. Different methods and different functions used within the same method yield different forms of solutions. But the value of u would remain practically the same as required. For more complex operators and domains, approximate methods will have to be applied. Variational formulation is one of them.

Here the variational method will be applied to seek an approximate solution to an example case. It can be observed that it also has an immediate physical meaning.

The general operator equation is: (from Eq. (2.66))

$Au = f$ in Ω

$Bu = g$ on Γ

For a simple one-dimension (1D) case let boundary conditions (BC) be as follows

$$u|_{\Gamma_u} = u^f \quad \text{Dirichlet BC} \tag{2.70}$$

$$\left.\frac{\partial u}{\partial x}\right|_{\Gamma_q} = 0 \quad \text{Neumann BC} \tag{2.71}$$

While A and f are as in Eq. (2.67) (but for 1D).

From Eq. (2.66):

$$Au - f = 0 \quad \text{in } \Omega \tag{2.72}$$

Thus the value of u in a given domain of x should be such that it should satisfy Eq. (2.72) (or Eq. (2.66)) and boundary conditions (at any given time).

For approximation purposes if there are n values of u chosen to be determined from n positions in the x domain, those values has to satisfy Eq. (2.72). As it is, this would result in only one equation (excluding BC) for n unknowns. For a determinate solution of

this, thus a method of setting n equations becomes important. Variational approach is one of them which is explained as follows.

Let $\delta u(x)$ be an arbitrary variation on u (or an arbitrary continuous function) with $\delta u|_{x=0} = 0$ (for a Dirichlet BC as in Eq. (2.70)). Then

$$\int_\Omega (Au - f)\delta u \, dx = 0 \tag{2.73}$$

This corresponds to the requirement that the residual, $(Au - f)$, should be orthogonal to the arbitrary variations, providing both of them are taken from same vector space. This can be represented as

$$(Au - f, \delta u) = 0 \qquad \forall \delta u \in V \tag{2.74}$$

when V is taken to be an inner product space with L_2 norm.

$(\cdot,\cdot)$ = L_2 scalar product over the domain of integration

$$(u, \delta u) = \int_\Omega u \delta u \, dx$$

Those conditions allow us to utilize theories developed in such spaces, viz. Sobolev and Hilbert spaces, for their generic application and to test and prove the existence, uniqueness and convergence of the solution.

As both u and δu are taken from the same space, their dimensions are also the same, and thus Eq. (2.73) will provide n equations for n unknowns. Therefore the unknown spatial values of u can be determined.

The expanded form of Eq. (2.73):

$$\int_\Omega \left(\frac{\partial u}{\partial t} - \frac{\partial}{\partial x}\left(a_1 \frac{\partial u}{\partial x} \right) + a_2 \frac{\partial u}{\partial x} + a_3 u - f \right) \delta u \, dx = 0 \tag{2.75}$$

Applying variational principles, δu, a variation, can be treated analogously as normal differential operator.

$$\int_\Omega \frac{\partial u}{\partial t} \delta u \, dx - \int_\Omega \frac{\partial}{\partial x}\left(a_1 \frac{\partial u}{\partial x} \right) \delta u \, dx + \int_\Omega a_2 \frac{\partial u}{\partial x} \delta u \, dx + \int_\Omega a_3 u \delta u \, dx = \int_\Omega f \delta u \, dx \tag{2.76}$$

Integrating by parts

$$\begin{aligned} &\int_\Omega \frac{\partial u}{\partial t} \delta u \, dx - \int_\Omega \frac{\partial}{\partial x}\left(a_1 \frac{\partial u}{\partial x} \delta u \right) dx + \int_\Omega a_1 \frac{\partial u}{\partial x} \frac{\partial (\delta u)}{\partial x} dx \\ &+ \int_\Omega a_2 \frac{\partial u}{\partial x} \delta u \, dx + \int_\Omega a_3 u \delta u \, dx = \int_\Omega f \delta u \, dx \end{aligned} \tag{2.77}$$

Applying Gauss' divergence theorem

$$\int_\Omega \frac{\partial u}{\partial t}\delta u\,dx - \int n\left(a_1\frac{\partial u}{\partial x}\delta u\right)dx + \int_\Omega a_1\frac{\partial u}{\partial x}\frac{\partial(\delta u)}{\partial x}dx$$
$$+ \int_\Omega a_2\frac{\partial u}{\partial x}\delta u\,dx + \int_\Omega a_3 u\delta u\,dx = \int_\Omega f\delta u\,dx$$

$$\int_\Omega \frac{\partial u}{\partial t}\delta u\,dx + \int_\Omega a_1\frac{\partial u}{\partial x}\frac{\partial(\delta u)}{\partial x}dx + \int_\Omega a_2\frac{\partial u}{\partial x}\delta u\,dx + \int_\Omega a_3 u\delta u\,dx \qquad (2.78)$$
$$= \int_\Omega f\delta u\,dx + \int nq^s\delta u\,dx$$

where

$$q^s = a_1\frac{\partial u}{\partial x}$$

We have

$$\text{Total surface: } \Gamma = \Gamma_u + \Gamma_q \quad \text{and} \quad \Gamma_u \cap \Gamma_q = 0 \qquad (2.79)$$

And,

$$\delta u = 0 \qquad \text{on } \Gamma_u \qquad (2.80)$$

Thus

$$\int_\Omega \delta u\frac{\partial u}{\partial t}dx + \int_\Omega \frac{\partial(\delta u)}{\partial x}a_1\frac{\partial u}{\partial x}dx + \int_\Omega \delta u a_2\frac{\partial u}{\partial x}dx + \int_\Omega \delta u a_3 u\,dx$$
$$= \int_\Omega \delta u f\,dx + \int \delta u q_n^s\,dx$$

(2.81)

where

$$q_n^s = \boldsymbol{n}\cdot q^s$$

(Note: Depending upon the context or the physical property represented by u, the above formulation can also be termed as derivation from principle of virtual concentration, virtual temperature or virtual work in field problems of engineering.)

The variation, $\delta u(x)$, can be represented by a test function, $v(x)$ of the same space. This will result Eq. (2.73) as:

$$\int_\Omega (Au - f)v\,dx = 0 \qquad (2.82)$$

Thus Eq. (2.81) will become:

$$\int_\Omega v\frac{\partial u}{\partial t}dx + \int_\Omega \frac{\partial v}{\partial x}a_1\frac{\partial u}{\partial x}dx + \int_\Omega v a_2\frac{\partial u}{\partial x}dx + \int_\Omega v a_3 u\,dx \qquad (2.83)$$
$$= \int_\Omega vf\,dx + \int v q_n^s\,dx$$

Thus the variational formulation of the original problem Eq. (2.28), also called a weak formulation, will be as follows:

Find u such that:

$$u(0) = u^f \qquad \text{essential BC}$$

$$a(v,u) = (v,f) \qquad \forall v \text{ such that } v(0) = 0 \tag{2.84}$$

where

$$a(v,u) = \int_\Omega v\frac{\partial u}{\partial t}dx + \int_\Omega \frac{\partial v}{\partial x}a_1\frac{\partial u}{\partial x}dx + \int_\Omega v a_2\frac{\partial u}{\partial x}dx + \int_\Omega v a_3 u\,dx$$

$$(v,f) = \int_\Omega vf\,dx + \int_\Gamma vq_n^s\,dx$$

a(v,u) is a bilinear functional and *(v,f)* is a linear functional as they are linear functions of corresponding functions in appropriate inner product space with appropriate norm.

The condition under which the above variational formulation will have a unique solution is given by the Lax-Milgram theorem (Reddy, 1986) which is as follows:

The Lax-Milgram theorem: Let H be a Hilbert space, and let $B(\cdot\,,\cdot): H\times H \to R$ be a bilinear form on $H\times H$, with following properties:

a) continuity of $B(\cdot\,,\cdot): |B(v,u)| \le M\|v\|\,\|u\| \qquad 0 < M < \infty$

b) positive definiteness of $B(\cdot\,,\cdot): |B(u,u)| \le \alpha\|v\|^2 \qquad \alpha > 0$

for all $u, v \in H$. Then for any continuous linear functional $l: H \to R$ on H, there exists a unique vector u_0 in H such that

$$B(v,u_0) = l(v) \qquad \forall v \in H \tag{2.85}$$

From Eq. 11, for integrals involved to be finite,

$$\int_\Omega v^2\,dx < +\infty$$

$$\int_\Omega \left(\frac{\partial v}{\partial x}\right)^2 dx < +\infty \tag{2.86}$$

$$\int_\Omega \left|v\frac{\partial v}{\partial x}\right| dx < +\infty$$

Therefore applying conditions based on the Lax-Milgram theorem, for a unique solution, the final problem (or the variational formulation of the original problem) is expressed as:

Find u such that:

$$a(v,u) = (v,f) \qquad \forall v \in V \tag{2.87}$$

where space V is defined as

$$V = \left[v : v \in L_2(\Omega), \nabla v \in L_2(\Omega), v\big|_{\Gamma_u} = 0 \right]$$

$L_2(\Omega)$: space of square integrable functions over the domain Ω.

$$L_2(\Omega) = \left\{ w : w \text{ is defined over } 0 \le x \le \Omega \text{ and } \int_\Omega (w)^2 \, dx = \|w\|_{L_2}^2 \le \infty \right\} \tag{2.88}$$

A method to determine approximate solution of the above formulation, the Rayleigh-Ritz method, is described next.

2.4.3.2 Rayleigh-Ritz Method

In Rayleigh-Ritz method, the basis of the solution space (separable Hilber space, H_A):

$$\phi_1, \phi_2, \ldots, \phi_N, \ldots$$

For approximation only the finite basis will be taken. If N be the number of basis taken, the approximation u_N of the solution u is:

$$u_N = \sum_{j=1}^{N} c_j \phi_j \tag{2.89}$$

As $\phi \in C_0^\infty(\Omega)$ or function with compact support, it does not satisfy the boundary conditions if they are not homogeneous. Thus for equations having non-homogeneous essential boundary condition either the equation is modified to form homogeneous BC or following form of approximation of u will have to be used to satisfy such BC.

$$u_N = \sum_{j=1}^{N} c_j \phi_j + \phi_0 \tag{2.90}$$

where c_j are unknown constants which have to be determined. ϕ_0 is chosen to satisfy essential BC.

This u_N has to satisfy the variational form of equation (2.87):

$$a(v,u) = (v,f) \tag{2.91}$$

This will result in the determination of coefficients c_i which correspond to the unique vector v_0 from the same space. In Rayleigh-Ritz method the v are taken to be the basis ϕ_j of the space.

Thus for the finite basis N:

$$a(v_N, u_N) = (v_N, f) \qquad \forall v_N \in V \tag{2.92}$$

$$a\left(\phi_i, \sum_{j=1}^{N} c_j \phi_j + \phi_0\right) = (\phi_i, f) \qquad i = 1,2,\ldots,N \tag{2.93}$$

These N equations will determine the values of N unknown c_j which thus gives the approximate solution u_N. The existence and uniqueness of the solution is guaranteed for a linear case by Lax-Milgram theorem as given in the previous section providing the space defined by the basis ϕ_i satisfies the required properties which means it is a separable Hilbert space with L_2 norms. The properties which arbitrary ϕ_i has to satisfy are:

1. $\{\phi_i\} \subset H_A$
2. $\phi_1, \phi_2, \ldots, \phi_N$ are linearly independent for any N.
3. $\{\phi_i\}$ is complete in H_A.

For bilinear a, the summation and constants c_j can be taken outside the operator:

$$\sum_{j=1}^{N} a(\phi_i, \phi_j) c_j + a(\phi_i, \phi_0) = (\phi_i, f)$$

$$\sum_{j=1}^{N} a(\phi_i, \phi_j) c_j = (\phi_i, f) - a(\phi_i, \phi_0) \tag{2.94}$$

$$\boldsymbol{Bc} = \boldsymbol{F} \tag{2.95}$$

$$\boldsymbol{c} = \boldsymbol{B}^{-1}\boldsymbol{F} \tag{2.96}$$

This gives the approximate solution (u_N) of the problem. The convergence and stability of the solution is an important aspect and therefore described briefly in the following section.

2.4.3.3 Convergence and Stability

Some of the important concepts to be derived for numerical solutions are convergence, stability and conditioning of equations. They are as follows.

2.4.3.3.1 Convergence

As seen above u is approximated as:

$$u_N = \sum_{j=1}^{N} c_j \phi_j \tag{2.97}$$

when $N \rightarrow \infty$

$$u = \sum_{j=1}^{\infty} c_j \phi_j \tag{2.98}$$

By applying Gram-Schmidt orthogonalisation procedure, it can be represented in a resulting set of orthonormal basis $\hat{\phi}_j$ or a Fourier series as:

$$u = \sum_{j=1}^{\infty} c_j \hat{\phi}_j \tag{2.99}$$

It has been proved for φ_j space as used in the previous section

$$\lim_{N \to \infty} u_N = u \qquad \text{in } H_A \tag{2.100}$$

i.e. $$|u_m - u_n| < \varepsilon \qquad \forall m, n > N \tag{2.101}$$

The solution u converges to the true solution as N increases.

2.4.3.3.2 Stability

As seen above increase in N will converge u to its true solution providing all computations are done exactly. But during computation only finite word length can be used which will automatically introduce some numerical errors. So increase in N can increase in such numerical errors. In some conditions such numerical errors can propagate and can make the solution unstable. In the following Eqs. (2.102)-(2.103), $\Delta \boldsymbol{B}, \Delta \boldsymbol{c}$ and $\Delta \boldsymbol{F}$ are numerical errors introduced during the computation.

$$\boldsymbol{B}\boldsymbol{c} = \boldsymbol{F} \tag{2.102}$$

$$(\boldsymbol{B} + \Delta \boldsymbol{B})(\boldsymbol{c} + \Delta \boldsymbol{c}) = (\boldsymbol{F} + \Delta \boldsymbol{F}) \tag{2.103}$$

In Ritz approximation for the solution to numerically stable, it has to satisfy following stability criterion:

$$\|\Delta \boldsymbol{c}\| \leq \beta \|\Delta \boldsymbol{B}\| + \gamma \|\Delta \boldsymbol{F}\| \tag{2.104}$$

where α, β, γ are independent of N.

$$\|\Delta \boldsymbol{B}\| \leq \alpha \tag{2.105}$$

$\|\cdot\|$ Euclidian norm

2.4.3.3.3 Conditioning of the equations

Among the different sources of numerical error, round-off error is important error. It can become significant under particular situations. So it is important to know when such

situations may occur and to remedy it. Round-off errors introduced during the solution of an equation system is proportional to the condition number of its coefficient matrix. In the above case, for a positive definite matrix (B), condition number is given by:

$$K(\boldsymbol{B}) = \frac{\lambda_N^{(N)}}{\lambda_1^{((N))}} \tag{2.106}$$

where

$\lambda_1^{(N)}$ = smallest eigenvalue of matrix B

$\lambda_N^{(N)}$ = largest eigenvalue of matrix B

For well conditioning of the system $K(B)$ remains bounded as N increases.

i.e. $\alpha < K(\boldsymbol{B}) < \beta$ (2.107)

where

$\beta > \alpha > 0$ and $\alpha, \beta \neq f(N)$

As described in the section organisation part of the section 2.4.3, the weighted residual method is described next before going into details of Galerkin and OC methods which are the main variational methods applied in this thesis.

2.4.4 Weighted Residual Method

The main principle of weighted residual method (WRM) is: if a vector is orthogonal to all basis in a given inner product space, its value is zero. So the function value of u which makes the residual, $Au-f$, orthogonal to all the basis in the same space is the solution as it means it satisfies the given operator equation or residual is zero. The basis function can be of different type but should cover all. As this basis can be considered as weights whose inner product with residual result into zero, the method is called weighted residual method. In more detail the approach is as follows.

Let H be a separable Hilbert space with S its dense subspace.

If for some $u \in H$

$$(u,v) = 0 \qquad \forall v \in S \Rightarrow u = 0 \quad \text{in } H \tag{2.108}$$

If ψ_j is basis of S,

$$(u,\psi_j) = 0 \quad \forall j \quad \Rightarrow u = 0 \text{ in } H \tag{2.109}$$

A given operator equation

$$Au = f \qquad \text{in } \Omega \tag{2.110}$$

where domain of A is D_A: $D_A \subset H \rightarrow H$

D_A consists of elements or functions which satisfy both differential equations (A) and associated appropriate homogeneous boundary conditions.

Thus if $u \in D_A \subset H$ is such that

$$\left(Au - f, \psi_j\right) = 0 \quad \forall j \quad \Rightarrow Au - f = 0 \text{ in } H \tag{2.111}$$

where ψ_j is basis in H.

u can be represented by any basis and not necessarily by ψ_j

$$u = \sum_{j=1}^{\infty} c_j \phi_j \tag{2.112}$$

Taking a finite N basis for an approximate solution

$$u_N = \sum_{j=1}^{N} c_j \phi_j \tag{2.113}$$

This gives,

$$\left(Au_N - f, \psi_j\right) = 0 \quad j = 1,2,\ldots,N \tag{2.114}$$

For a linear operator A:

$$\sum_{j=1}^{N} \left(A\phi_i, \psi_j\right) c_j = \left(f, \psi_j\right) \qquad j = 1,2,\ldots,N \tag{2.115}$$

$$\boldsymbol{Bc} = \boldsymbol{F} \tag{2.116}$$

Because of the requirement that $\phi_i \subset D_A$, ϕ_i need be $2m$ times differentiable if A is differential order of $2m$, and must satisfy the boundary conditions.

According to the types of basis ψ_j (or weighed function) used, there are different kinds of weighted residual methods. For a general case, $\phi_i \neq \psi_j$, and is known as Petrov-Galerkin method. Some of the different types are:

- Galerkin method
- Collocation method
- Petrov-Galerkin method
- Subdomain method
- Least Square method

The first two will be used in this work and will be explained briefly. For higher Peclet no flow which is highly dominated by convection, the basis might have to be modified. For

example an exponential upwinding scheme would be necessary for stability of the numerical solution in such flow simulations. Thus a Petrov-Galerkin method could be necessary.

2.4.4.1 The Galerkin Method

When basis of S or H, ψ_j, is also used as a basis to represent u, ϕ_i, it is known as Galerkin method.

$$u_N = \sum_{j=1}^{N} c_j \psi_j \tag{2.117}$$

and $$\left(Au_N - f, \psi_j\right) = 0 \quad \forall j \tag{2.118}$$

For a linear operator A

$$\sum_{j=1}^{N} \left(A\psi_i, \psi_j\right) c_j = \left(f, \psi_j\right) \qquad j = 1,2,\ldots,N \tag{2.119}$$

For a linear positive definite operator A when natural boundary conditions are incorporated within the formulation by transferring a one differentiation to the basis function, ψ_j, this is equivalent to Ritz formulation as described in the previous section. In such a case ψ_j can be m order differentiable for a differential operator of $2m$ as in Ritz formulation. This is a huge benefit in terms of choosing simple ψ_j. If the natural boundary conditions could not have been incorporated, they will have to be satisfied by the trial function or basis ψ_j and a higher order function like Hermite cubic polynomial will have to be employed.

Before explaining and making derivations to apply orthogonal collocation method, the generic collocation method will be described first and establish its major principles as follows.

2.4.4.2 Collocation Method

In the collocation method Dirac delta function is used as the basis (ψ_j) or weighting function.

$$\psi_j(x) = \delta(\boldsymbol{x} - \boldsymbol{x}_j) \tag{2.120}$$

This has the property that

$$\int_{\Omega} \psi_j (Au - f)\, dx = (Au - f)\big|_{x_j} \tag{2.121}$$

Thus

$$(Au_N - f, \psi_j) = 0$$

$$(Au_N - f)\big|_{x_j} = 0 \qquad j = 1,2,\ldots,N \tag{2.122}$$

For a linear operator A:

$$\sum_{i=1}^{N} A[\phi_i(x_j)]c_i = f(x_j) \qquad j = 1,2,\ldots,N \tag{2.123}$$

$$\boldsymbol{Bc} = \boldsymbol{F} \tag{2.124}$$

The principle of collocation method is to determine parameters c_i used to approximate $u_N = \sum_{i=1}^{N} c_i \phi_i$ by forcing the residual $Au - f$ to vanish as N selected points x_j ($j = 1,2,\ldots,N$) in the domain. As N increases, the point where u exactly satisfies the operator equation increases, and thus the solution is expected to converge. To avoid ill-conditioning, the collocation points should be evenly spaced.

After establishing basic principle of collocation method here, orthogonal collocation method will be explained and important derivations, for their direct applications, will be made in the next section.

2.4.4.3 Orthogonal Collocation

The explanation here is based on that of Finlayson (1972). In higher order approximations the choice of method or weighing function in WRM is not important. The choice will thus be based on ease of computation. If the collocation method is applied the position of collocation points would not become important either. Improvements in the method can be achieved when the collocation points are chosen to be roots of a set of orthogonal polynomial trial functions which satisfy the equation and the boundary conditions. The resulting solution is more reliable even for low order approximations.

As in collocation method, in general, for a linear operator A, the solution is given by Eq. (2.123):

$$\sum_{i=1}^{N} A[\phi_i(x_j)]c_i = f(x_j) \qquad j = 1,2,\ldots,N \tag{2.125}$$

where

$$u \approx u_N = \sum_{i=1}^{N} c_i \phi_i$$

$$\boldsymbol{Bc} = \boldsymbol{F} \tag{2.126}$$

As x_j is determinate (being roots of polynomials), $A[\phi_i(\boldsymbol{x}_j)]$ or B is also determinate. So the computation of the unknown nodal values c_i becomes straightforward. Some standard general trial functions, x_j values are available in the literature along with matrix equivalents of some operators (gradient, Laplacian). So their use for general problems becomes almost routine. An example case including the construction of a trial function for a 1D case which is relevant to this work is shown here.

A trial function: with a requirement of satisfying a boundary condition, a solution can be expressed as:

$$u(x) = \phi_0(x) + \sum_{i=1}^{N} c_i \phi_i(x) \tag{2.127}$$

where

$$\left(\phi_i, \phi_j\right)_w = \delta_{ij} \qquad \text{(Orthogonal basis with respect to } w\text{)}$$

A common form of basis can be a polynomial:

$$\phi_m(x) = P_m(x) = \sum_{i=0}^{m} a_i x^i \tag{2.128}$$

Polynomial coefficients, a_i, can be defined by requiring the successive polynomials to be orthogonal to all polynomials of order less than m_i w.r.t. some weighting function $w(x) \geq 0$:

$$\int_a^b w(x) P_n(x) P_m(x)\, dx = 0 \qquad n = 0,1,\ldots,m-1 \tag{2.129}$$

For example when a = -1, b = 1, w =1 and $P_0(x) = 1$, $P_1(x) = a_0 + a_1 x$ is given by:

$$\int_{-1}^{1} (a_0 + a_1 x)\, dx = 0 \tag{2.130}$$

This gives $a_0 = 0$ and a_1 arbitrary. Choosing $a_1 = 1$ gives $P_1(x) = 1$.

Similarly $P_2(x) = a_0 + a_1 x + a_2 x^2$ will be determined by:

$$\int_{-1}^{1} 1 \cdot P_2(x)\, dx = 0 \qquad \text{and} \qquad \int_{-1}^{1} x \cdot P_2(x)\, dx = 0 \tag{2.131}$$

The resulting set is called Legendre polynomial.

Table 2.1 Roots of Legendre polynomial (Finlayson, 1972)

Legendre polynomial	Roots
$P_0 = 1$	
$P_1 = x$	$x_j = 0$
$P_2 = 1 - 3x^2$	$x_j = \pm 1/\sqrt{3} = \pm 0.577$

These m roots of polynomials $P_m(x)$ can serve as the collocation points in the interval of $a \le x \le b$.

Polynomials can be constructed with additional convenient properties. When solution is sought on the domain $0 \le x \le 1$ and it is required to be symmetric about x=0, it can be expanded in terms of powers of x^2. Along with satisfying the Dirichlet boundary condition, a possible trial function can be:

$$u_N(x) = \phi_0(x) + \sum_{i=1}^{N} c_i \phi_i(x) \tag{2.132}$$

where

$$\phi_i = (1 - x^2) P_{i-1}(x^2)$$

and N = number of interior collocation points.

The polynomials are determined by the orthogonality condition like:

$$\int_0^1 w(x^2) P_j(x^2) P_i(x^2) x^{a-1}\, dx = k_{(i)} \delta_{ij} \qquad j = 1,2,\ldots,i-1 \tag{2.133}$$

where

a = 1, 2, 3 for planar, cylindrical or spherical geometries

For ease in computation, Eq. (2.132) can be written in the form of

$$u_N(x) = \sum_{i=1}^{N+1} d_i x^{2i-2} \tag{2.134}$$

where

x = 1 for $(N+1)^{th}$ collocation point.

Taking gradient and Laplacian of it and evaluating them at collocation points (as given by roots of the used orthogonal polynomial) results in:

$$u(x_j) = \sum_{i=1}^{N+1} x_j^{2i-2} d_i \tag{2.135}$$

$$\nabla u\big|_{x_j} = \frac{du}{dx}\bigg|_{x_j} = \sum_{i=1}^{N+1} \frac{dx^{2i-2}}{dx}\bigg|_{x_j} d_i \tag{2.136}$$

$$\nabla^2 u\big|_{x_j} = \sum_{i=1}^{N+1} \nabla^2 (x^{2i-2})\big|_{x_j} d_i \tag{2.137}$$

In the matrix form:

$$\boldsymbol{u} = \boldsymbol{Qd} \tag{2.138}$$

$$\nabla \boldsymbol{u} = \boldsymbol{Cd} \tag{2.139}$$

$$\nabla^2 \boldsymbol{u} = \boldsymbol{Dd} \tag{2.140}$$

Solving for d:

$$\boldsymbol{d} = \boldsymbol{Q}^{-1}\boldsymbol{u} \tag{2.141}$$

Using the value of d in the gradient and Laplacian of u, results in:

$$\nabla \boldsymbol{u} = \boldsymbol{CQ}^{-1}\boldsymbol{u} \equiv \boldsymbol{Au} \tag{2.142}$$

$$\nabla^2 \boldsymbol{u} = \boldsymbol{DQ}^{-1}\boldsymbol{u} \equiv \boldsymbol{Bu} \tag{2.143}$$

Thus derivatives here are expressed as value of the function u at collocation points.

Quadrature formulae may be used to evaluate integrals as follows:

$$\int_0^1 f(x^2) x^{a-1}\, dx = \sum_{j=1}^{N+1} w_j f(x_j) \tag{2.144}$$

For $f_i = x^{2i-2}$, weight (w_i) is given by

$$\int_0^1 x^{2i-2} x^{a-1}\, dx = \sum_{j=1}^{N+1} w_j x_j^{2i-2} \tag{2.145}$$

$$\text{L.H.S.} = \frac{1}{2i-2+a} \equiv f_i \tag{2.146}$$

$$\text{R.H.S.} = \boldsymbol{wQ} \tag{2.147}$$

Thus

$$\boldsymbol{wQ} = \boldsymbol{f} \tag{2.148}$$

$$\boldsymbol{w} = \boldsymbol{fQ}^{-1} \tag{2.149}$$

Thus in this method, the operator equation and its boundary conditions are discretised using appropriate orthogonal polynomial as shown above. This results into an equivalent matrix form or a simultaneous equation set on unknown nodal values.

Some computed value for such matrices for some standard conditions for certain number of collocation points using general orthogonal polynomial are given in Finlayson (1972). The finite element method, which will be applied in conjunction with the orthogonal collocation method to simulate adsorption parts of the models developed in this thesis, will be discussed and established in the following section.

2.4.5 Finite Element Method

When the geometry is complex or there is discontinuity in material properties or forcing term, finding an approximate function (or trial function) which satisfies the whole domain becomes difficult in a normal variational method. To overcome this problem, such a complex domain is divided into geometrically simple subdomains which permit systematic construction of simple approximation functions to apply variational methods in each. These subdomains are called finite elements. Algebraic polynomials derived from using an interpolation theory are used for approximation functions. The undetermined parameters represent the value of u at nodes of the approximating functions including essential boundary conditions. Due to continuity requirements, values at shared boundaries of adjacent elements are naturally considered as same for all such elements. The assembly of all elements gives the whole domain. Applying domain boundary conditions, will result in N equations for N unknown parameters. This is a finite element method (FEM) and is especially suitable for automated computer procedures.

The basic procedure of applying FEM is:

- mesh generation or division of whole domain into simple parts/elements
- derivation of approximating functions
- variational approximation of the operator equation
- assembly of elements
- imposition of boundary conditions
- solution of equation
- post-processing: further computation of other dependent quantities if required.

2.4.5.1 Mesh Generation

The whole domain (Ω) of problem is divided into small parts (Ω^e) with simple geometries.

$$\overline{\Omega} = \Omega \cup \Gamma \tag{2.150}$$

$$\overline{\Omega} \approx \overline{\Omega}_h = \bigcup_{e=1}^{N} \overline{\Omega}^e \tag{2.151}$$

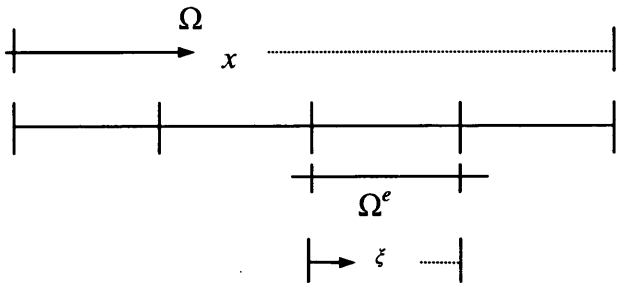

Fig. 2.10 Mesh generation

2.4.5.2 Derivation of approximation function

Appropriate interpolation functions are used as approximation functions because of their simplicity, ease of computation and relative ease in studying convergence and other theoretical aspects.

$$u^e \approx u_h^e = \sum_{i=1}^{n} u_i^e \psi_i^e \tag{2.152}$$

(This is similar to $u = \sum_{i=1}^{n} c_i \phi_i$ in previous section but its domain is just an element, $\overline{\Omega}^e$.)

For example for 1D element of length h:

For a linear element (or a linear function u_h^e)

$$\psi^e = \left[\left(1 - \frac{\xi}{h}\right) \quad \frac{\xi}{h} \right], \qquad 0 \le \xi \le h \tag{2.153}$$

For a quadratic element (or a quadratic function u_h^e)

$$\psi^e = \left[\left(1 - \frac{2\xi}{h}\right)\left(1 - \frac{\xi}{h}\right) \quad \frac{4\xi}{h}\left(1 - \frac{\xi}{h}\right) \quad -\frac{\xi}{h}\left(1 - \frac{2\xi}{h}\right) \right], \; 0 \le \xi \le h \tag{2.154}$$

u^e has to satisfy continuity requirement between adjacent elements.

$$u^e \in P_1(\Omega^e) \subset H \tag{2.155}$$

2.4.5.3 Variational approximation

The operator equation is approximated by its variational or weak form for each element using one of the methods discussed in the previous section. The Weighted Residual Method is more versatile but the variational method based on the Rayleigh-Ritz method is more useful if it can be applied as it allows a lesser degree of continuity requirement in approximation function (ψ^e) (e.g. C^1 compared to C^2 required for differential operator A of second order) due to incorporation of the natural boundary condition within the variational form. This makes solution easier.

Thus

$$\left(Au^e - f, \psi_j^e\right) = 0, \qquad j = 1,2,\ldots,n \tag{2.156}$$

For a linear operator A:

$$\sum_{i=1}^{n}\left(A\psi_i^e, \psi_j^e\right)u_i^e = \left(f, \psi_j^e\right), \qquad j = 1,2,\ldots,n \tag{2.157}$$

or in the form of Eq. (2.84)

$$a^e\left(v^e, u^e\right) = \left(v^e, f^e\right) \tag{2.158}$$

From Eq. (2.157)

$$\sum_{i=1}^{n} a\left(\psi_j^e, \psi_i^e\right)u_i^e = \left(\psi_j^e, f^e\right), \qquad j = 1,2,\ldots,n \tag{2.159}$$

$$\left[K^e\right]\left\{u^e\right\} = \left\{F^e\right\} \tag{2.160}$$

where

$k_{ji}^e = a\left(\psi_j^e, \psi_i^e\right)$ (in solid mechanics – stiffness matrix)

$F_j^e\left(\psi_j^e, f^e\right)$ (in solid mechanics – forcing vector)

As ψ_j^e are algebraic polynomials, K^e and F^e can be numerically evaluated but as F^e contains inter-element fluxes, Eq. (2.160) can not be solved at elemental level. Boundary conditions are available only for a full (or global) domain.

2.4.5.4 Assembly of elements

As seen above the whole problem domain is divided into elemental parts. The connectivity of elements is established by requiring all the nodal values of the elements

are same for the nodes common to adjacent elements. Thus a global interpolation can be defined covering all assembled elements and their nodal values as follows. It will be linearly independent, continuous and within compact support.

$$u \approx u_h = \sum_{J=1}^{N} U_J \Phi_J \tag{2.161}$$

As shown below Φ_i is defined by disjoint local function $\psi_2^{i-1}(x)$ and $\psi_1^i(x)$.

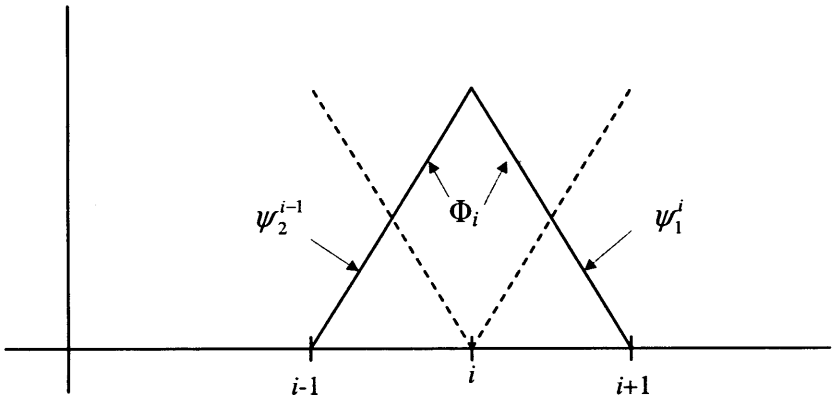

Fig. 2.11 A global coordinate for element assembly

The space spanned by the linearly independent set $\{\Phi_J\}_{J=1}^N$ is called a finite element space, and can be denoted as $S^h(\Omega_h)$.

2.4.5.5 Imposition of Boundary Conditions

After assembly, the global boundary conditions are applied which can be either essential or natural boundary conditions. If natural boundary conditions are incorporated within the variation form, it may appear as inter-element flux (P^e). The sum of this secondary degree of freedom at the element boundary is know if the nodal u value (i.e. primary degree of freedom) is not known. For example if there is no nodal source, $P_2^e + P_1^e = 0$. This information will be applied in assembly (to compute F^e) before solution.

2.4.5.6 Solution of Equation

$$[K]\{U\} = \{F\} \tag{2.162}$$

$$\{U\} = [K]^{-1}\{F\} \tag{2.163}$$

Any direct or indirect method can be employed to solve the resulting simultaneous equation systems. For transient problems the time discretisation will have to be applied using Wilson θ-family approximation (section 2.4.2.2). If a powerful ODE-solver available, it can be directly employed as in method of line solution.

2.4.5.7 Post-processing

If secondary variables are also of interest, they can also be computed by the interpolation using the same basis function (ψ^e) which was used for an approximate solution of the variational form of the elements.

With this, the basis equations of the modelling along with the generic derivations of all the numerical methods applied in this thesis have been established. The next section will briefly describe the systematic approach followed for modelling in this thesis.

2.5 Model Development Process

In general the model development process has been performed and presented in a tentative standard format. Usually models have been developed stage-wise from simple independent units to increasingly complex and more realistic models and their integration when applicable. For each model, an introduction is presented at first along with literature review. Once established the objective, reason, past work and scope, the model development is performed. Each model comes with a number of essential parameters. The methods employed in estimating such parameters are described next. The simulation of the model is then done by applying appropriate numerical methods. Convergence analysis is done when required. The simulation results are then collected by using the data from the experimental system of interest. The interpretation of the results in relation to the experimental data, the significance of the model and further developments are then discussed and conclusions drawn in the final section.

2.6 Summary

This chapter explains the principles and methods applied in analysing the problems, formulating the models and simulating their results in this thesis. Specifically principles of chromatography and EBA have been described. Some relevant transport equations have been reviewed which will be a basis of modelling in this work. Out of the large number of numerical methods available, some important ones which were relevant and more appropriate for the simulation of models developed in this work have been reviewed and presented systematically. Derivations were also done for relevant generic sets of equations here so when such equations were encountered during the later part of this work, their solutions could be used directly. This avoids repeated derivation every time such situations arise. Finally a systematic method applied to approach modelling problems has been described. Prepared with these tools and methods, the modelling of EBA was attempted from the next chapter onwards.

3 Chromatography Modelling

3.1 Introduction

From a modelling perspective expanded bed adsorption (EBA) is essentially treated like any general liquid chromatography problem apart from the existence of axial variations in particle size and voidage which arise as a result of EBA hydrodynamics. Thus in its simplest form if such variation is neglected and a steady state hydrodynamic bed is considered, EBA becomes equivalent to a normal liquid chromatography packed bed. Besides, even when such variations are considered, the basic adsorption of any component along the bed is still represented by the same model as used in a liquid chromatography. Thus in this chapter a comprehensive model of a liquid chromatography is established which will provide the basis for modelling EBA in the subsequent chapters.

The specific objectives of this chapter are to:

- establish a comprehensive model of liquid chromatography
- simulate it using an appropriate numerical method
- validate the model and its method of implementation against literature data.

3.2 Literature Review

Chromatography has been modelled with different approaches and with various degrees of complexity. A quite comprehensive summary of which can be found in monographs by Guiochon et al. (1994), Michel et al. (2005), a review by Spieker et al. (1998), etc. Over decades the chromatography model seems to have matured and reached the stage where it covers most of the essential aspects of the phenomena. Models now produce results which are fairly accurate for many applications. However new materials to separate bring with them new challenges along with their different thermodynamic and physical properties. So the research for better chromatography models continues. From the mass balance perspective, the phenomenon that occurs within a general chromatography can be fairly well captured by a structure which in the literature is termed the general rate model. This is also one the most comprehensive models available (Michel et al., 2005).

Thus in this chapter a comprehensive general rate model as developed by Gu (1995) and Spieker et al. (1998) is established. The reason for deriving the model equations here from first principles is in order to adapt and modify them as necessary when the EBA model is developed in subsequent chapters.

3.3 The Model

A Mass balance of a chemical species or component in a chromatography column can be analysed as follows. The chemical species to be separated enter the column at the inlet (Fig. 3.1). Part of it is carried along the column by convective transfer and some portion is diffused into the interstitial space while part diffuses inside the pore space of the chromatography matrix or particles (Fig. 3.2).

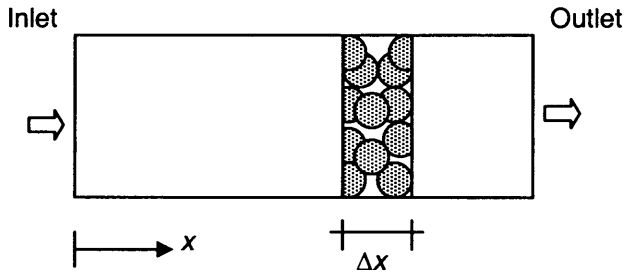

Fig. 3.1 A differential volume in a chromatography column. A Component of interest mixed with other components or chemical species in bulk liquid phase will enter at inlet, pass through the column where adsorption takes place and comes out of outlet with the liquid phase which are not adsorbed inside the column.

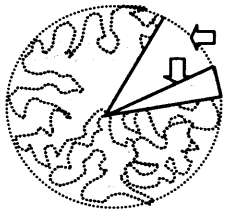

Fig. 3.2 A diffusion of component species inside a chromatography matrix particle.

Inside such particles the chemical species is distributed between the pore liquid phase and adsorption phase or particle surface. Such partitioning is a result of thermodynamic equilibrium which can be observed via an adsorption isotherm. The chemical species

passes through each differential volume as shown in Fig. 3.1 subject to all these situations and finally exits from the column outlet.

Following assumptions are taken for the modelling.

- Mass transfer of a chemical species is considered to be in 3 phases: bulk liquid phase, pore liquid phase and adsorbent phase.
- Mass transfer in the bulk phase is due to convection and dispersion.
- Chemical species transfer from the bulk liquid phase to the particle is governed by film mass transfer.
- Mass is transported in the pore liquid phase of the particle only by diffusion.
- Adsorption equilibrium is considered to be instantaneous on the pore surface of the particles in comparison to mass transfer rates, especially diffusion, which occurs inside the particle.
- For simplification only one axial dimension is used to describe the bulk phase and due to the symmetry of a spherical particle only one radial dimension is considered for the particle phase.
- Mass concentrations of different chemical component species are considered to be very low compared to the carrier solvent/medium. The weighted average density (ρ) of the liquid phase including all component species is considered to be constant.

The mass balance of a component i in each phases are derived as follows.

3.3.1 Bulk phase

Applying a mass balance for a chemical species in a differential volume element (Fig. 3.3) of a column, from Eq. (2.27)

$$\frac{\partial u_i}{\partial t} = -\boldsymbol{v} \cdot \nabla u_i + \nabla \cdot D_i \nabla u_i + R_{Vi} \qquad (3.1)$$

where

v = mass average velocity

and $\nabla \cdot \boldsymbol{v} = 0$ as ρ = constant

Source/sink term (R_{Vi}) is the rate at which the chemical species is transferred into the particle phase from the bulk liquid phase. It is given by:

$$R_{Vi} = -w\boldsymbol{n}_{fi} \qquad (3.2)$$

n_{fi} = film mass flux of a component species i

w = outer surface area per unit volume of adsorbent particle

Considering v as a superficial (mass average) velocity and ε_B be bulk phase porosity inside the column.

$$v = \frac{\text{volumetric flow rate}}{\text{cross - sectional area of the column}} \tag{3.3}$$

Only ε_B is available for bulk phase mass transport. Thus

$$\varepsilon_B \frac{\partial u_i}{\partial t} = -\varepsilon_B \boldsymbol{v} \cdot \nabla u_i + \varepsilon_B \nabla \cdot D_i \nabla u_i + R_{Vi} \tag{3.4}$$

where R_{Vi} is taken to be in relation to total volume of differential element, as sink term is related to the total differential volume element (including counter part of ε_B). This can be visualized as follows:

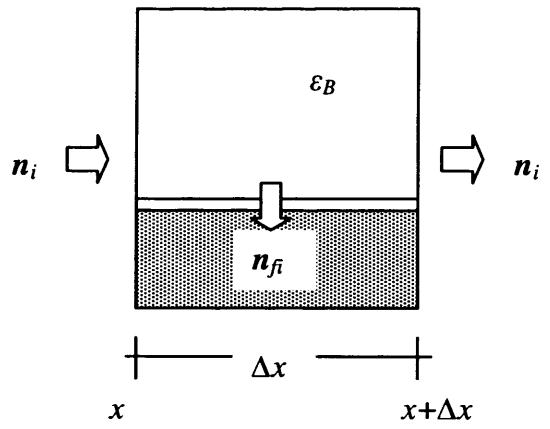

Fig. 3.3 Differential volume element of a chromatography column

n_{fi} can be adequately represented by film mass transfer mechanism in the stationary liquid film surrounding the adsorbent which the chemical species has to pass through to get transported from the bulk liquid phase to the pore liquid phase. It is given by:

$$\boldsymbol{n}_{fi} = k_{fi}(u_i - u_{pi}\big|_{r=R}) \tag{3.5}$$

where

k_{fi} = film mass transfer coefficient

u_{pi} = concentration of chemical species in pore phase immediately next to film or its outer boundary

Representing the concentration of a chemical species in the bulk liquid phase as u_{Bi} and E as the dispersion coefficient of the bulk liquid in the column, the bulk phase mass balance for the component i becomes:

$$\varepsilon_B \frac{\partial u_{Bi}}{\partial t} = -\varepsilon_B \boldsymbol{v} \cdot \nabla u_{Bi} + \varepsilon_B \nabla \cdot E \nabla u_{Bi} - w \boldsymbol{n}_{fi} \tag{3.6}$$

E will be relatively constant for all components as in the bulk phase the diffusion of component species is dominated by bulk dispersion of average fluid element. Considering E to be independent of spatial position:

$$\frac{\partial u_{Bi}}{\partial t} = -\boldsymbol{v} \cdot \nabla u_{Bi} + E \nabla^2 u_{Bi} - \frac{w}{\varepsilon_B} k_{fi} (u_{Bi} - u_{pi}|_{r=R}) \tag{3.7}$$

The Eq. (3.7) describes the mass balance of a component in bulk phase.

Boundary conditions for bulk phase ($t \geq 0$) are derived as follows.

At inlet ($x = 0$) :

From Eq. (2.15), mass balance at interface:

$$[(\boldsymbol{j}_i + u_{Bi}(\boldsymbol{v} - \boldsymbol{v}_I))_{x=0} - (\boldsymbol{j}_i + u_{Bi}(\boldsymbol{v} - \boldsymbol{v}_I))_{in}] \cdot \boldsymbol{n}_I = R_{Si} \tag{3.8}$$

Boundary interface being stationary, $v_I = 0$, $n_I = 1$ and no surface source ($R_{Si} = 0$)

$$(\boldsymbol{j}_i + u_{Bi}\boldsymbol{v})_{x=0} = (\boldsymbol{j}_i + u_{Bi}\boldsymbol{v})_{in} \tag{3.9}$$

where equivalent phase B is at $(x = 0)^+$ - in-column

equivalent phase A is at "*in*" or $(x = 0)^-$ - out-column

There is only convective flux in the incoming flux at the inlet interface while both convection and dispersion flux exist in outgoing flux at the inlet interface.

$$(\boldsymbol{j}_i + u_{Bi}\boldsymbol{v})_0 = (u_{Bi}\boldsymbol{v})_{in}$$

$$\boldsymbol{j}_i = -E \nabla u_{Bi} \qquad \text{from Eq. (2.21) with } E \text{ replacing } D_i$$

$$\boldsymbol{v}(u_{Bi}|_{in} - u_{Bi}|_0) + E \nabla u_{Bi}|_0 = 0 \tag{3.10}$$

At oulet ($x = L$):

$$\nabla u_{Bi}|_{x=L} = 0 \tag{3.11}$$

3.3.2 Particle phase

Applying the mass balance to a differential volume element of particle phase (Fig. 3.4), from Eq. (2.27)

$$\frac{\partial u_{Pi}}{\partial t} = -\boldsymbol{v}_P \cdot \nabla u_{Pi} + \nabla \cdot (D_i \nabla u_{Pi}) + R_{Vi} \tag{3.12}$$

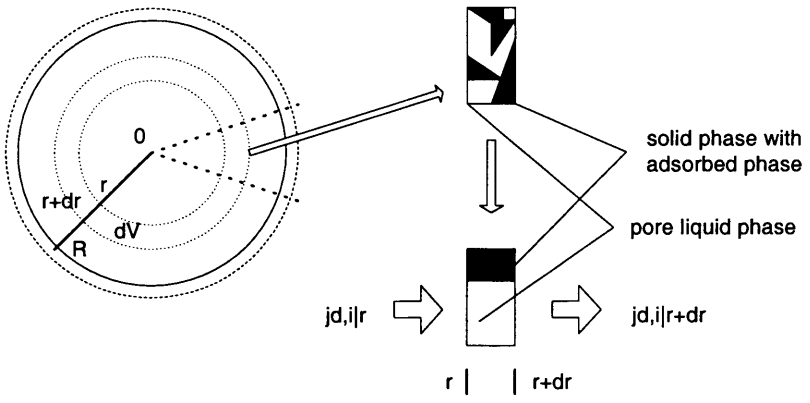

Fig. 3.4 Differential volume element of a particle. (Figure based on Spieker et al., 1998)

Inside the pore phase the only flux is due to diffusion as the convective flux is negligible. There is no source/sink considered. The above relationship would be valid if there is no adsorption. If there is adsorption where the rate is slow and it is in the time scale of diffusion, it can be incorporated as a separate term. Since, however the adsorption phenomena that are being studied in chromatography are considered instantaneous in relation to the diffusion, it is expressed in the accumulation term. The component in the pore liquid phase is instantaneously distributed between the pore liquid phase and the adsorption phase (i.e. proximate surface of solid phase) to maintain thermodynamic equilibrium.

Let u_{ki} be the total mass of component species distributed between the pore liquid phase and the adsorbent phase.

$$u_{Ki} = \varepsilon_P u_{Pi} + (1-\varepsilon_P) u_{Ai} \tag{3.13}$$

where ε_P is the pore space in the particle phase and u_{Pi} and u_{Ai} are the concentration of component in the pore liquid phase and adsorbent phase respectively.

The mass balance of Eq. (3.12) becomes:

$$\frac{\partial u_{Ki}}{\partial t} = \varepsilon_P \nabla \cdot (D_i \nabla u_{Pi}) \tag{3.14}$$

Only the ε_P part of the differential volume is available for diffusive flux while u_{Ki} is related to the total differential volume element.

As the diffusivity of component i (D_i) is independent of spatial position:

$$\frac{\partial u_{Ki}}{\partial t} = \varepsilon_P D_i \nabla^2 u_{Pi} \tag{3.15}$$

The instantaneous equilibrium partition of u_{Pi} into u_{Pi} and u_{Ai} is represented by the adsorption isotherm:

$$f_j(u_{A1},\ldots,u_{AN},u_{P1},\ldots,u_{PN}) = 0 \qquad j = 1,2,\ldots,N \tag{3.16}$$

where N = no. of component species present or considered of relevance

Boundary conditions of the particle phase (for $t \geq 0$) are derived as follows.

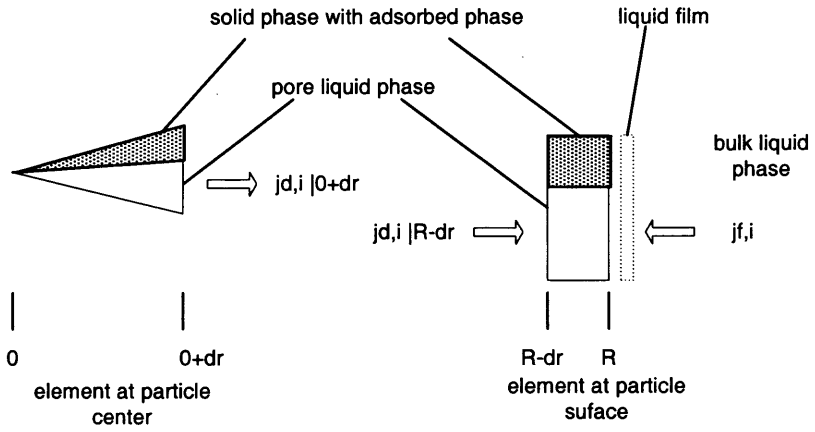

Fig. 3.5 Differential volume elements at particle centre and particle surface. (Figure based on Spieker et al., 1998)

At the particle centre, $r = 0$ (Fig. 3.5), due to radial symmetry in a spherical particle, there will not be any diffusive mass flux.

$$\boldsymbol{j}_{di}\big|_0 = -\varepsilon_P D_i \nabla u_{Pi}\big|_0 = 0$$

$$\nabla u_{Pi}\big|_0 = 0 \tag{3.17}$$

At the particle surface, $r = R$, the molecular species transfers from bulk liquid phase into the pore liquid phase of particle through stationary film around the particle. This can be modelled as a convective boundary condition where component specific rate is characterised by a mass transfer coefficient (k_{ci}). Such flux is given by:

$$\boldsymbol{j}_{fi} = k_{fi}(u_{Bi} - u_{Pi}\big|_R) \tag{3.18}$$

Applying mass balance at the interface or particle surface (using eq. A.13)

$$\left[(\boldsymbol{F}_i - u_{Pi}\boldsymbol{v}_I)_P - (\boldsymbol{F}_i - u_{Pi}\boldsymbol{v}_I)_B\right]\cdot \boldsymbol{n}_I = R_{Si}$$

$$\boldsymbol{F}_{iP} = -\boldsymbol{F}_{iB}$$

$$\boldsymbol{j}_{di} = -\boldsymbol{j}_{fi} \qquad \text{(Orientation of } r \text{ is taken as a positive direction)}$$

$$\varepsilon_P D_i \nabla u_{Pi}\big|_0 = k_{fi}(u_{Bi} - u_{Pi}\big|_R) \tag{3.19}$$

The initial conditions ($t = 0$) of the system are given by:

For $0 \le r \le R$ and $0 \le x \le L$

$$u_{Bi}\big|_{t=0} = u_{Bi}^0 \tag{3.20}$$

$$u_{Pi}\big|_{t=0} = u_{Pi}^0 \tag{3.21}$$

$$u_{Ai}\big|_{t=0} = u_{Ai}^0 \tag{3.22}$$

The developed model is summarised in the following section.

3.3.3 The model summary

The summary of the chromatography model is as given below.

$$\frac{\partial u_{Bi}}{\partial t} = -\boldsymbol{v} \cdot \nabla u_{Bi} + E\nabla^2 u_{Bi} - \frac{w}{\varepsilon_B} k_{fi}(u_{Bi} - u_{pi}\big|_{r=R}) \tag{3.23}$$

$$\frac{\partial u_{Ki}}{\partial t} = \varepsilon_P D_i \nabla^2 u_{Pi} \tag{3.24}$$

$$u_{Ki} = \varepsilon_P u_{Pi} + (1 - \varepsilon_P) u_{Ai} \tag{3.25}$$

$$f_j(u_{A1}, \ldots, u_{AN}, u_{P1}, \ldots, u_{PN}) = 0 \qquad j = 1,2,\ldots,N \tag{3.26}$$

With boundary conditions:

u_{Bi}: $$v(u_{Bi}\big|_{in} - u_{Bi}\big|_0) + E\nabla u_{Bi}\big|_0 = 0 \tag{3.27}$$

$$\nabla u_{Bi}\big|_{x=L} = 0 \tag{3.28}$$

u_{Pi}: $$\nabla u_{Pi}\big|_0 = 0 \tag{3.29}$$

$$\varepsilon_P D_i \nabla u_{Pi}\big|_0 = k_{fi}(u_{Bi} - u_{Pi}\big|_R) \tag{3.30}$$

With initial conditions: ($t = 0$)

$$u_{Bi}\big|_{t=0} = u_{Bi}^0, \qquad u_{Pi}\big|_{t=0} = u_{Pi}^0, \qquad u_{Ai}\big|_{t=0} = u_{Ai}^0 \tag{3.31}$$

In normal chromatography, use only of the axial dimension of the column is sufficient to capture most of its essential behaviour. If two or three dimensional analysis is sought, relevant additional boundary conditions can be included in the system. Similarly due to radial symmetry of spherical particle (shape and homogeneity of

structure is reasonably valid for practical purposes), only the radial dimension is used to describe the particle phase. The model is simplified to 1-axial dimension and 1-radial dimension, and used from this point onwards in this thesis.

Thus the 1D-axial (z) and 1D-radial (r) model of adsorption becomes:

$$\frac{\partial u_{Bi}}{\partial t} = -v\frac{\partial u_{Bi}}{\partial z} + E\frac{\partial^2 u_{Bi}}{\partial z^2} - \frac{w}{\varepsilon_B}k_{fi}(u_{Bi} - u_{pi}\big|_{r=R}) \tag{3.32}$$

$$\frac{\partial u_{Ki}}{\partial t} = \varepsilon_P \frac{D_i}{r^2}\frac{\partial}{\partial r}\left(r^2 \frac{\partial u_{Pi}}{\partial r}\right) \tag{3.33}$$

$$u_{Ki} = \varepsilon_P u_{Pi} + (1-\varepsilon_P)u_{Ai} \tag{3.34}$$

With boundary conditions:

$$u_{Bi}: \quad v(u_{Bi}\big|_{in} - u_{Bi}\big|_0) + E\frac{\partial u_{Bi}}{\partial z}\bigg|_0 = 0 \tag{3.35}$$

$$\frac{\partial u_{Bi}}{\partial z}\bigg|_{z=L} = 0 \tag{3.36}$$

$$u_{Pi}: \quad \frac{\partial u_{Pi}}{\partial r}\bigg|_0 = 0 \tag{3.37}$$

$$\varepsilon_P D_i \frac{\partial u_{Pi}}{\partial r}\bigg|_R = k_{fi}(u_{Bi} - u_{Pi}\big|_R) \tag{3.38}$$

With initial conditions: ($t = 0$)

$$u_{Bi}\big|_{t=0} = u_{Bi}^0, \qquad u_{Pi}\big|_{t=0} = u_{Pi}^0, \qquad u_{Ai}\big|_{t=0} = u_{Ai}^0 \tag{3.39}$$

The isotherm relation is given by

$$f_j(u_{A1},\ldots,u_{AN},u_{P1},\ldots,u_{PN}) = 0 \qquad j = 1,2,\ldots,N \tag{3.40}$$

For components showing a multi-component competitive Langmuir isotherm behaviour the following relation can be used to describe an equilibrium relation Eq. (3.3.32) between component concentration at pore liquid phase and adsorbent or solid phase.

$$u_{Ai} = \frac{b_{0i}u_{Pi}}{1 + \sum_{j=1}^{N} b_j u_{Pj}} \tag{3.41}$$

Before simulation, this model is normalised in the following section.

3.4 Normalisation of the adsorption model

The direct use of the above model for simulation is adequate. Normalisation or non-dimensionalisation helps reduce number of variables and parameters and ease in solution. Thus the above chromatography model has been normalised as follows.

Normalising the adsorption model by using following dimensionless variables:

$$\tilde{u}_{Bi} = \frac{u_{Bi}}{u_{0i}}, \qquad \tilde{u}_{Pi} = \frac{u_{Pi}}{u_{0i}}, \qquad \tilde{u}_{Ai} = \frac{u_{Ai}}{u_{0i}} \tag{3.42}$$

where u_{0i} is defined as: $u_{0i} = \max\{u_{Bi-feed}(\tau)\} \quad -\infty < \tau + \infty$ (3.43)

$$\tau = \frac{vt}{L}, \qquad \tilde{z} = \frac{z}{L}, \qquad \tilde{r} = \frac{r}{R} \tag{3.44}$$

This gives

$$\frac{\partial \tau}{\partial t} = \frac{v}{L}, \qquad \frac{\partial \tilde{z}}{\partial z} = \frac{1}{L}, \qquad \frac{\partial \tilde{r}}{\partial r} = \frac{1}{R} \tag{3.45}$$

Now

$$u_{Bi}(z,t) \rightarrow u_{Bi}(\tilde{z},\tau) \tag{3.46}$$

$$u_{Pi}(z,r,t) \rightarrow u_{Pi}(\tilde{z},\tilde{r},\tau) \tag{3.47}$$

Partial derivatives w.r.t. $\tilde{z}$:

$$\frac{\partial u_{Bi}(z,t)}{\partial z} = \frac{\partial u_{Bi}(\tilde{z},t)}{\partial \tilde{z}}\frac{d\tilde{z}}{dz} + \frac{\partial u_{Bi}(\tilde{z},t)}{\partial t}\frac{dt}{dz} = \frac{1}{L}\frac{\partial u_{Bi}(\tilde{z},t)}{\partial \tilde{z}} \tag{3.48}$$

$$\frac{\partial^2 u_{Bi}(z,t)}{\partial z^2} = \frac{\partial}{\partial z}\left(\frac{1}{L}\frac{\partial u_{Bi}(\tilde{z},t)}{\partial \tilde{z}}\right) = \frac{1}{L}\frac{\partial}{\partial \tilde{z}}\left(\frac{\partial u_{Bi}(\tilde{z},t)}{\partial \tilde{z}}\right)\frac{d\tilde{z}}{dz} = \frac{1}{L^2}\frac{\partial^2 u_{Bi}(\tilde{z},t)}{\partial \tilde{z}^2} \tag{3.49}$$

$$\frac{\partial u_{Bi}(z,t)}{\partial t} = \frac{\partial u_{Bi}(\tilde{z},t)}{\partial \tilde{z}}\frac{d\tilde{z}}{dt} + \frac{\partial u_{Bi}(\tilde{z},t)}{\partial t}\frac{dt}{dt} = \frac{\partial u_{Bi}(\tilde{z},t)}{\partial t} \tag{3.50}$$

Transformation for τ:

$$\frac{\partial u_{Bi}(\tilde{z},t)}{\partial \tilde{z}} = \frac{\partial u_{Bi}(\tilde{z},\tau)}{\partial \tilde{z}}\frac{d\tilde{z}}{d\tilde{z}} + \frac{\partial u_{Bi}(\tilde{z},\tau)}{\partial \tau}\frac{d\tau}{dz} = \frac{\partial u_{Bi}(\tilde{z},\tau)}{\partial \tilde{z}} \tag{3.51}$$

$$\frac{\partial^2 u_{Bi}(\tilde{z},t)}{\partial \tilde{z}^2} = \frac{\partial}{\partial \tilde{z}}\left(\frac{\partial u_{Bi}(\tilde{z},\tau)}{\partial \tilde{z}}\right) = \frac{\partial^2 u_{Bi}(\tilde{z},\tau)}{\partial \tilde{z}^2} \tag{3.52}$$

$$\frac{\partial u_{Bi}(\tilde{z},t)}{\partial t} = \frac{\partial u_{Bi}(\tilde{z},\tau)}{\partial \tilde{z}}\frac{d\tilde{z}}{dt} + \frac{\partial u_{Bi}(\tilde{z},\tau)}{\partial \tau}\frac{d\tau}{dt} = \frac{v}{L}\frac{\partial u_{Bi}(\tilde{z},\tau)}{\partial \tau} \tag{3.53}$$

Final transformed variables:

$$\frac{\partial u_{Bi}(z,t)}{\partial z} = \frac{1}{L}\frac{\partial u_{Bi}(\tilde{z},\tau)}{\partial \tilde{z}} = \frac{u_{0i}}{L}\frac{\partial \tilde{u}_{Bi}(\tilde{z},\tau)}{\partial \tilde{z}} \tag{3.54}$$

$$\frac{\partial^2 u_{Bi}(z,t)}{\partial z^2} = \frac{1}{L^2}\frac{\partial^2 u_{Bi}(\tilde{z},\tau)}{\partial \tilde{z}^2} = \frac{u_{0i}}{L^2}\frac{\partial^2 \tilde{u}_{Bi}(\tilde{z},\tau)}{\partial \tilde{z}^2} \tag{3.55}$$

$$\frac{\partial u_{Bi}(z,t)}{\partial t} = \frac{v}{L}\frac{\partial u_{Bi}(\tilde{z},\tau)}{\partial \tau} = \frac{v}{L}u_{0i}\frac{\partial \tilde{u}_{Bi}(\tilde{z},\tau)}{\partial \tau} \tag{3.56}$$

Similarly for particle phase:

$$\frac{\partial u_{Pi}(z,r,t)}{\partial r} = \frac{u_{0i}}{R}\frac{\partial \tilde{u}_{Pi}(\tilde{z},\tilde{r},\tau)}{\partial \tilde{r}} \tag{3.57}$$

$$\frac{\partial^2 u_{Pi}(z,r,t)}{\partial r^2} = \frac{u_{0i}}{R^2}\frac{\partial^2 \tilde{u}_{Pi}(\tilde{z},\tilde{r},\tau)}{\partial \tilde{r}^2} \tag{3.58}$$

$$\frac{\partial u_{Pi}(z,r,t)}{\partial \tau} = \frac{v}{L}u_{0i}\frac{\partial \tilde{u}_{Pi}(\tilde{z},\tilde{r},\tau)}{\partial \tau} \tag{3.59}$$

$$\frac{\partial u_{Ai}(z,r,t)}{\partial \tau} = \frac{v}{L}u_{0i}\frac{\partial \tilde{u}_{Ai}(\tilde{z},\tilde{r},\tau)}{\partial \tau}, \tag{3.60}$$

$$\frac{\partial u_{Ki}(z,r,t)}{\partial \tau} = \frac{v}{L}u_{0i}\frac{\partial \tilde{u}_{Ki}(\tilde{z},\tilde{r},\tau)}{\partial \tau} \tag{3.61}$$

Thus substituting the original variable in the equations by the transformed variables and dropping the over-tilde (˜) for notational ease of the transformed variables yields:

For bulk phase:

$$u_{0i}\frac{v}{L}\frac{\partial u_{Bi}}{\partial \tau} = -v\frac{u_{0i}}{L}\frac{\partial u_{Bi}}{\partial z} + E\frac{u_{0i}}{L^2}\frac{\partial^2 u_{Bi}}{\partial z^2} - \frac{w}{\varepsilon_B}k_{fi}u_{0i}(u_{Bi} - u_{pi}\big|_{r=R}) \tag{3.62}$$

$$\frac{\partial u_{Bi}}{\partial \tau} = -\frac{\partial u_{Bi}}{\partial z} + \frac{E}{Lv}\frac{\partial^2 u_{Bi}}{\partial z^2} - \frac{w}{\varepsilon_B}k_{fi}\frac{L}{v}(u_{Bi} - u_{pi}\big|_{r=R})$$

Thus

$$\frac{\partial u_{Bi}}{\partial \tau} = -\frac{\partial u_{Bi}}{\partial z} + \frac{1}{Pe_L}\frac{\partial^2 u_{Bi}}{\partial z^2} - \xi(u_{Bi} - u_{pi}\big|_{r=1}) \tag{3.63}$$

where,

$$Pe_L = \frac{vL}{E} \tag{3.64}$$

$$w = \frac{(1-\varepsilon_B)4\pi R^2}{\frac{4}{3}\pi R^3} = \frac{3(1-\varepsilon_B)}{R} \tag{3.65}$$

$$\xi = \frac{w}{\varepsilon_B}k_{fi}\frac{L}{v} = \frac{3(1-\varepsilon_B)}{R}\frac{k_{fi}}{\varepsilon_B}\frac{L}{v} \tag{3.66}$$

For particle phase:

$$u_{0i}\frac{v}{L}\frac{\partial u_{Ki}}{\partial \tau}=\varepsilon_P D_i\left(\frac{2}{rR}\frac{u_{0i}}{R}\frac{\partial u_{Pi}}{\partial r}+\frac{u_{0i}}{R^2}\frac{\partial^2 u_{Pi}}{\partial r^2}\right) \tag{3.67}$$

$$\frac{\partial u_{Ki}}{\partial \tau}=\varepsilon_P D_i\frac{L}{v}\frac{1}{R^2}\left(\frac{2}{r}\frac{\partial u_{Pi}}{\partial r}+\frac{\partial^2 u_{Pi}}{\partial r^2}\right)=\eta_i\left(\frac{2}{r}\frac{\partial u_{Pi}}{\partial r}+\frac{\partial^2 u_{Pi}}{\partial r^2}\right)$$

$$\frac{\partial u_{Ki}}{\partial \tau}=\eta_i\frac{1}{r^2}\frac{\partial}{\partial r}\left(r^2\frac{\partial u_{Pi}}{\partial r}\right) \tag{3.68}$$

where $$\eta_i=\frac{\varepsilon_P D_i}{R^2}\frac{L}{v} \tag{3.69}$$

Similarly boundary conditions would become:

For bulk phase:

at z=0:

$$vu_{0i}(u_{Bi}|_{in}-u_{Bi}|_0)+E\frac{u_{0i}}{L}\left.\frac{\partial u_{Bi}}{\partial z}\right|_0=0 \tag{3.70}$$

$$\frac{vL}{E}(u_{Bi}|_{in}-u_{Bi}|_0)+\left.\frac{\partial u_{Bi}}{\partial z}\right|_0=0$$

$$\left.\frac{\partial u_{Bi}}{\partial z}\right|_0+Pe_L(u_{Bi}|_{in}-u_{Bi}|_0)=0 \tag{3.71}$$

at z=1:

$$\frac{u_{0i}}{L}\left.\frac{\partial u_{Bi}}{\partial z}\right|_{z=1}=0 \qquad \left.\frac{\partial u_{Bi}}{\partial z}\right|_{z=1}=0 \tag{3.72}$$

For particle phase:

at r=0:

$$u_{0i}\left.\frac{\partial u_{Pi}}{\partial r}\right|_0=0 \qquad \left.\frac{\partial u_{Pi}}{\partial r}\right|_0=0 \tag{3.73}$$

at r=1:

$$\varepsilon_P D_i\frac{u_{0i}}{R}\left.\frac{\partial u_{Pi}}{\partial r}\right|_{r=1}=k_{fi}u_{0i}(u_{Bi}-u_{Pi}|_{r=1}) \tag{3.74}$$

$$\left.\frac{\partial u_{Pi}}{\partial r}\right|_{r=1}=k_{fi}\frac{R}{\varepsilon_P D_i}(u_{Bi}-u_{Pi}|_{r=1})$$

$$\left.\frac{\partial u_{Pi}}{\partial r}\right|_{r=1}=Bi_i(u_{Bi}-u_{Pi}|_{r=1}) \tag{3.75}$$

where

$$Bi_i = k_{fi}\frac{R}{\varepsilon_P D_i} \tag{3.76}$$

This gives ξ as:

$$\xi = \frac{Rk_{fi}}{\varepsilon_P D_i}\frac{\varepsilon_P D_i}{R^2}\frac{L}{v}\frac{3(1-\varepsilon_B)}{\varepsilon_B} = Bi_i\eta_i\frac{3(1-\varepsilon_B)}{\varepsilon_B} \tag{3.77}$$

Initial conditions will transform into:

$$u_{0i}u_{Bi}\big|_{t=0} = u_{Bi}^0 \Rightarrow u_{Bi}\big|_{t=0} = \frac{u_{Bi}^0}{u_{0i}} = \tilde{u}_{Bi}^0 \tag{3.78}$$

Dropping the over-tilde from the initial condition as before for notational ease, but keeping the new meaning

$$u_{Bi}\big|_{t=0} = u_{Bi}^0 \tag{3.79}$$

Applying similar transformations for particle phase and adsorption phase initial conditions,

$$u_{Pi}\big|_{t=0} = u_{Pi}^0, \qquad u_{Ai}\big|_{t=0} = u_{Ai}^0, \qquad u_{Ki}\big|_{t=0} = u_{Ki}^0 \tag{3.80}$$

Transformation of an isotherm using dimensionless variables

The multi-component Langmuir isotherm of Eq. (3.117) when transformed using dimensionless variables yields: (as before over-tilde is dropped for notational ease)

$$u_{0i}u_{Ai} = \frac{b_{0i}u_{0i}u_{Pi}}{1+\sum_{j=1}^{N} b_j u_{0i}u_{Pj}} \tag{3.81}$$

$$u_{Ai} = \frac{b_{0i}u_{Pi}}{1+\sum_{j=1}^{N} b_j u_{0i}u_{Pj}} \tag{3.82}$$

As the model comprises a relatively large set of equations, which will be referenced in this thesis repeatedly in various chapters, a summary of this is presented below.

$$\frac{\partial u_{Bi}}{\partial \tau} = -\frac{\partial u_{Bi}}{\partial z} + \frac{1}{Pe_L}\frac{\partial^2 u_{Bi}}{\partial z^2} - \xi(u_{Bi} - u_{pi}\big|_{r=1}) \tag{3.83}$$

$$\frac{\partial u_{Ki}}{\partial \tau} = \eta_i \frac{1}{r^2}\frac{\partial}{\partial r}\left(r^2\frac{\partial u_{Pi}}{\partial r}\right) \tag{3.84}$$

$$u_{Ki} = \varepsilon_P u_{Pi} + (1-\varepsilon_P)u_{Ai} \tag{3.85}$$

With boundary conditions:

u_{Bi}: $$\left.\frac{\partial u_{Bi}}{\partial z}\right|_0 + Pe_L(u_{Bi}|_{in} - u_{Bi}|_0) = 0 \tag{3.86}$$

$$\left.\frac{\partial u_{Bi}}{\partial z}\right|_{z=1} = 0 \tag{3.87}$$

u_{Pi}: $$\left.\frac{\partial u_{Pi}}{\partial r}\right|_0 = 0 \tag{3.88}$$

$$\left.\frac{\partial u_{Pi}}{\partial r}\right|_{r=1} = Bi_i(u_{Bi} - u_{Pi}|_{r=1}) \tag{3.89}$$

With initial conditions:

$$u_{Bi}|_{t=0} = u_{Bi}^0, \qquad u_{Pi}|_{t=0} = u_{Pi}^0, \qquad u_{Ai}|_{t=0} = u_{Ai}^0, \qquad u_{Ki}|_{t=0} = u_{Ki}^0 \tag{3.90}$$

Isotherm relation:

$$f_j(u_{A1},\ldots,u_{AN},u_{P1},\ldots,u_{PN}) = 0 \qquad j = 1,2,\ldots,N \tag{3.91}$$

or for a multi-component competitive Langmuir:

$$u_{Ai} = \frac{b_{0i}u_{Pi}}{1 + \sum_{j=1}^{N} b_j u_{0i} u_{Pj}} \tag{3.92}$$

Feed concentration:

$$u_{0i} = \max\{u_{Bi-feed}(\tau)\} \qquad -\infty < \tau + \infty \tag{3.93}$$

Constants of the system:

$$Pe_L = \frac{vL}{E} \tag{3.94}$$

$$\xi = Bi_i\eta_i\frac{3(1-\varepsilon_B)}{\varepsilon_B} \tag{3.95}$$

$$\eta_i = \frac{\varepsilon_P D_i}{R^2}\frac{L}{v} \tag{3.96}$$

$$Bi_i = k_{fi}\frac{R}{\varepsilon_P D_i} \tag{3.97}$$

There are several parameters used in this model. To be able to solve or simulate the model, determining the values of those parameters becomes important. Hence, methods of estimating the values of such parameters are explained in the following section.

3.5 Parameters Estimation

There are number of parameters involved in the chromatography model. These parameters are specific to the materials and flow (operating conditions). Parameters employed in the model include: bulk fluid phase dispersion (E), diffusivity of a component species (D), film mass transfer coefficient of a component species (k_f), isotherm parameters and axial dispersion coefficient of particle phase. Some of these have to be determined experimentally. Whenever possible in this thesis, appropriate literature-available correlations were employed to estimate their values. Some theoretical approaches are available from which to estimate the values of some of the parameters. However they have limitations on their valid range and operating conditions.

The following sections detail the approaches applied in this thesis to estimate the values of these parameters. The same approach will be applied throughout this work unless otherwise specifically mentioned. There are a number of methods and correlations available in the literature for some of the parameters. Here only one which seems to be fairly generic and robust is used for each case.

3.5.1 Bulk liquid phase dispersion coefficient (E)

The dispersion of the bulk fluid is difficult to measure experimentally. In dimensionless form, it is used to calculate the Peclet number (Pe_L).

$$Pe_L = \frac{vL}{E} \tag{3.98}$$

where

v = superficial fluid velocity

L = length of a column

E = dispersion coefficient

In this work Pe_L is directly estimated by correlation given by Chung and Wen (1968):

$$\mathrm{Re} = \frac{d_P v \rho_f}{\mu} \qquad \text{(Reynolds no)} \tag{3.99}$$

where

d_P = diameter of adsorption particle

ρ_f = fluid density

μ = fluid viscosity

$$Pe_L = \frac{L}{d_P \varepsilon_B}\left(0.2 + 0.011\mathrm{Re}^{0.48}\right) \qquad 10^{-3} < \mathrm{Re} < 10^{3} \qquad (3.100)$$

where

ε_B = bulk voidage or porosity

3.5.2 Diffusion coefficient of component species (D)

The diffusivity of a component species is estimated based on the procedure as outlined in the paper by Li et al. (1998). For systems having adsorbent particle pore diameters sufficiently larger than the diameter of solute component, the molecular diffusivity (D_m) as such is used in the calculation as there will not be a size-related entry barrier. When the diameters are closer, the entry barrier effect becomes important and an effective diffusivity has to be calculated. This is especially true for size exclusion systems.

As given by Deen (1998), the molecular diffusivity (D_m) of a spherical molecule can be given by Stokes-Einstein equation:

$$D_m = \frac{\kappa T}{6\pi\mu r_m} \qquad (3.101)$$

where

κ = Boltzmann constant = $1.38*10^{-23}$ J/K

T = absolute temperature (°K)

μ = viscosity of solvent

r_m = radius of solute molecule

The radius of the solute molecule can be estimated from its specific volume (V_s) and molecular weight (Mw) assuming it is spherical:

$$r_m = \left(\frac{3MwV_s}{4\pi N_A}\right)^{1/3} \qquad (3.102)$$

where

N_A = Avogardo's number = $6.0221367*10^{23}$ molecules/mole

For proteins the V_s value lies in a narrow range of 0.728~0.751. So using average value of 0.7384, r_m is given by

$$r_m(A°) = 0.66(Mw)^{1/3} \qquad (3.103)$$

But as a protein is normally in solution and is in hydrated form, there is an increase in size. The hydrodynamic radius is assumed to be proportion to $(Mw)^{1/3}$.

$$r_m = a_r (Mw)^{1/3} \tag{3.104}$$

where

a_r = proportionality constant

Substituting this into Eq. (3.5.4):

$$D_m = \frac{\kappa T}{6\pi\mu a_r} \frac{1}{(Mw)^{1/3}} = \frac{C}{(Mw)^{1/3}} \qquad (m^2/s) \tag{3.105}$$

Using Eq. (3.105), Polson (1950) performed an experimental investigation for a number of organic substances including proteins like BSA, myoglobulin, haemoglobulin and determined their C values. This was found to be in average $2.74*10^{-9}$ sm^{-2} little variations when the molecular weight of the organic substances exceeds 1000 (Li, 1998). Thus molecular diffusivity (D_m) is estimated as:

$$D_m (m^2/s) = \frac{2.74*10^{-9}}{(Mw)^{1/3}} \tag{3.106}$$

When the diameter of the solute component comes closer to that of the pore diameter as in the case of gel filtration, the diffusivity has to be corrected as an effective diffusivity (D_e) taking into account the resulting entry barrier. This is given by:

$$D_e = \frac{D_m}{\tau_{tor}} \left(1 - 2.104\lambda + 2.09\lambda^3 - 0.95\lambda^5\right) \tag{3.107}$$

where

τ_{tor} = pore tortuosity

$$\lambda = \frac{\text{solute molecular diameter}}{\text{pore diameter}} \tag{3.108}$$

The pore diameter can be approximated by the upper size exclusion limit. λ can be estimated by:

$$\lambda = \lambda_0 \left(\frac{\text{MW of solute molecule}}{\text{MW of upper size exclusion limit}} \right)^{1/3} \tag{3.109}$$

where λ_0 is found to be 0.35 by Stegeman et al. (1991) implying that when the solute diameter reaches 35% of the pore diameter, the entry of solute inside the pore becomes negligible. Pore tortuosity (τ_{tor}) has to be estimated experimentally. For example: Li et al. (1998) found τ_{tor} to be 2 for Bio-Rad P60 gel.

3.5.3 Film mass transfer coefficient of a component species (k_f)

There are a number of correlations available to estimate k_f. Wilson and Geankoplis (1966) developed the following correlation in terms of Sherwood number (*Sh*) and Reynolds number (*Re*) for small *Re* flow.

$$k_f = \frac{ShD_m}{d_P} \qquad \text{(m/s)} \tag{3.110}$$

where

d_P = diameter of (adsorbent) particle

D_m = molecular diffusivity of solute component

$$Sh = \frac{1.09}{\varepsilon_B}(\mathrm{Re}\,Sc)^{1/3} = \frac{1.37}{\varepsilon_B}\left(v\frac{d_P}{2}\frac{1}{D_m}\right)^{1/3} \qquad 0.0015 \le Re \le 5.5 \tag{3.111}$$

where

ε_B = bulk voidage

$$Sc = \frac{\mu}{D_m\rho_f} = \text{Schmidt's number} \tag{3.112}$$

μ = viscosity of fluid

ρ_f = density of fluid

$$\mathrm{Re} = \frac{d_P v\rho_f}{\mu} = \text{Reynolds number} \tag{3.113}$$

Another correlation to estimate *Sh* number, developed by Wright and Li (Andreas, 1998), which seems to be also widely used is given below for reference purpose only.

$$Sh = 2 + 1.45(1-\varepsilon_B)\mathrm{Re}^{1/2}\,Sc^{1/3} \tag{3.114}$$

Wilson and Geankoplis' correlation (Eq. (3.111)) described earlier will be used in this thesis instead of Wright and Li's correlation (Eq. (3.114)) as done by Li et al. (1998). This will make the estimation method consistent with the approach of Li et al. which was also used for estimating diffusivity earlier.

3.5.4 Isotherm parameters

The proportion or partition of a component species between the adsorbent phase and fluid or solvent is given by isotherm parameters. In the time scale of molecular diffusivity of a

component, it is almost instantaneous. Hence, an instantaneous equilibrium partition can be fairly assumed for most cases.

Parameters are usually estimated from batch experimental data. The objective is to estimate the parameter values which best fit the given set of data and which satisfies certain theoretical expectations. Based upon the type of adsorption system used an appropriate empirical/semi-empirical isotherm model is chosen. A range of isotherm models exists:

1. Langmuir isotherm

$$C_{Ai} = \frac{QC_{Pi}}{k_d + C_{Pi}} \tag{3.115}$$

parameters: Q, K_d

2. Langmuir isotherm for transient condition

$$\frac{\partial C_{Ai}}{\partial t} = k_1 C_{Pi}(Q - C_{Ai}) - k_2 C_{Ai} \tag{3.116}$$

parameters: Q, dissociation constant (k_d)

$$k_d = \frac{k_1}{k_2}$$

3. Competitive Langmuir isotherm for multi-component systems

$$C_{Ai} = \frac{b_{0i} C_{Pi}}{1 + \sum_{j=1}^{N} b_j C_{0i} C_{Pj}} \tag{3.117}$$

parameters: b_0, b_j $(j=1,2, \ldots, N)$

4. Langmuir-Freundlich

$$C_{Ai} = bC_{Pi}^{m} \tag{3.118}$$

parameters: b, m

In this work, a competitive Langmuir isotherm will bed used as instaneous equilibrium is assumed and this will automatically result into a simple Langmuir isotherm when mono-component system is investigated. This will also be used for simulation in other chapters for Lysozyme-Streamline-SP system as done by Bruce and Chase (2001) and Wright and Glaser (2001). In those cases of Lysozyme-Streamline-SP system assumption of an instaneous equilibrium was also found to be valid which was demonstrated by Wright (2000) using a transient experimental study.

3.6 Simulation

The normalised chromatography model [Eqs. (3.83)-(3.97)] is simulated using an Orthogonal Collocation-Finite Element Method (OCFE). This is the method of choice in the literature (Gu, 1995; Lazo, 1999) as it provides a stable solution of multi-component chromatography models without requiring a large extent of discretisation. The bulk phase is discretised using finite element method in section 3.6.1. And the particle phase is discretised using orthogonal collocation for its efficiency in diffusion dominant equations in section 3.6.2. The resulting system of ordinary differential equations (ODE) was solved using Matlab's ODE-solver. The algorithm employed for the purpose is described in section 3.6.3.

3.6.1 Discretisation of bulk phase

Applying the Galerkin method (section 2.4.4.1) based finite element method (section 2.4.5) to discretise Eq. (3.83) and incorporating the natural boundary conditions by transferring one differential order from variable to trial function as in the Ritz method (section 2.4.3.2), we obtain:

$$A_i u_{Bi} - f_i = 0 \tag{3.119}$$

where

$$A_i = \frac{\partial}{\partial \tau} - \frac{1}{Pe_L}\frac{\partial^2}{\partial z^2} + \frac{\partial}{\partial z} + \xi_i$$

$$f_i = \xi_i u_{pi}\Big|_{r=1}$$

Approximating u_{Bi} by u_{Bin}, a quadratic element or approximation function

$$u^e_{Bin} = \sum_{j=1}^{3} u^e_{Bij}\psi^e_j \tag{3.120}$$

Applying Galerkin method (based on Eq. (2.118)):

$$\left(A_i u^e_{Bi} - f_i, \psi^e_k\right) = 0 \qquad \text{for } k = 1, 2, 3 \tag{3.121}$$

This gives

$$\int_{\Omega^e} \psi^e_k \left\{ \frac{\partial u^e_{Bi}}{\partial \tau} - \frac{1}{Pe_L}\frac{\partial^2 u^e_{Bi}}{\partial z^2} + \frac{\partial u^e_{Bi}}{\partial z} + \xi_i u^e_{Bi} - \xi_i u^e_{Pi}\Big|_{r=1} \right\} dz = 0 \tag{3.122}$$

Reducing one differential order of second derivative term by transferring to the basis function using integration by parts:

$$\int_{\Omega^e} \psi_k^e \frac{\partial u_{Bi}^e}{\partial \tau} dz - \int_{\Omega^e} \frac{\partial}{\partial z}\left(\psi_k^e \frac{1}{Pe_L} \frac{\partial u_{Bi}^e}{\partial z} \right) dz + \int_{\Omega^e} \frac{\partial \psi_k^e}{\partial z} \frac{1}{Pe_L} \frac{\partial u_{Bi}^e}{\partial z} dz + \int_{\Omega^e} \psi_k^e \frac{\partial u_{Bi}^e}{\partial z} dz + \int_{\Omega^e} \psi_k^e \xi_i u_{Bi}^e \, dz - \int_{\Omega^e} \psi_k^e \xi_i u_{Pi}^e \Big|_{r=1} dz = 0 \tag{3.123}$$

Applying Gauss' divergence theorem

$$\int_{\Omega^e} \psi_k^e \frac{\partial u_{Bi}^e}{\partial \tau} dz - \int_{\Gamma^e} \boldsymbol{n}\left(\psi_k^e \frac{1}{Pe_L} \frac{\partial u_{Bi}^e}{\partial z} \right) dS + \int_{\Omega^e} \frac{\partial \psi_k^e}{\partial z} \frac{1}{Pe_L} \frac{\partial u_{Bi}^e}{\partial z} dz + \int_{\Omega^e} \psi_k^e \frac{\partial u_{Bi}^e}{\partial z} dz + \int_{\Omega^e} \psi_k^e \xi_i u_{Bi}^e \, dz - \int_{\Omega^e} \psi_k^e \xi_i u_{Pi}^e \Big|_{r=1} dz = 0 \tag{3.124}$$

Integrating from z_1 and z_2 of an element

$$\int_{z_1}^{z_2} \psi_k^e \frac{\partial u_{Bi}^e}{\partial \tau} dz + \int_{z_1}^{z_2} \frac{\partial \psi_k^e}{\partial z} \frac{1}{Pe_L} \frac{\partial u_{Bi}^e}{\partial z} dz + \int_{z_1}^{z_2} \psi_k^e \frac{\partial u_{Bi}^e}{\partial z} dz + \int_{z_1}^{z_2} \psi_k^e \xi_i u_{Bi}^e \, dz = \int_{z_1}^{z_2} \psi_k^e \xi_i u_{Pi}^e \Big|_{r=1} dz + \left(\psi_k^e \frac{1}{Pe_L} \frac{\partial u_{Bi}^e}{\partial z} \right) \Bigg|_{z_1}^{z_2} \tag{3.125}$$

Substituting the value of the approximating function

$$\sum_{j=1}^{3} \frac{\partial u_{Bij}^e}{\partial \tau} \int_{z_1}^{z_2} \psi_k^e \psi_j^e \, dz + \sum_{j=1}^{3} u_{Bij}^e \int_{z_1}^{z_2} \frac{1}{Pe_L} \frac{\partial \psi_k^e}{\partial z} \frac{\partial \psi_j^e}{\partial z} dz + \sum_{j=1}^{3} u_{Bij}^e \int_{z_1}^{z_2} \psi_k^e \frac{\partial \psi_j^e}{\partial z} dz + \sum_{j=1}^{3} u_{Bij}^e \int_{z_1}^{z_2} \xi_i \psi_k^e \psi_j^e \, dz = \int_{z_1}^{z_2} \xi_i \psi_k^e u_{pi}^e \Big|_{r=1} dz + \left(\frac{1}{Pe_L} \psi_k^e \frac{\partial u_{Bij}^e}{\partial z} \right) \Bigg|_{z_1}^{z_2} \tag{3.126}$$

In matrix form for a component i:

$$\boldsymbol{M}_i^e \dot{\boldsymbol{u}}_{Bi} + \boldsymbol{K}_i^e \boldsymbol{u}_{Bi} = \boldsymbol{F}_i^e \tag{3.127}$$

where

$$\boldsymbol{M}_i^e = \int_{z_1}^{z_2} \psi_k^e \psi_j^e \, dz \tag{3.128}$$

$$\boldsymbol{K}_i^e = \int_{z_1}^{z_2} \frac{1}{Pe_L} \frac{\partial \psi_k^e}{\partial z} \frac{\partial \psi_j^e}{\partial z} dz + \int_{z_1}^{z_2} \psi_k^e \frac{\partial \psi_j^e}{\partial z} dz + \int_{z_1}^{z_2} \xi_i \psi_k^e \psi_j^e \, dz \tag{3.129}$$

$$\boldsymbol{F}_i^e = \int_{z_1}^{z_2} \xi_i \psi_k^e u_{pi}^e \Big|_{r=1} dz + \boldsymbol{q}_i^e \tag{3.130}$$

$$\boldsymbol{q}_i^e = \left(\frac{1}{Pe_L} \psi_k^e \frac{\partial u_{Bij}^e}{\partial z} \right) \Bigg|_{z_1}^{z_2} \tag{3.131}$$

Each matrix $\boldsymbol{M}_i^e, \boldsymbol{K}_i^e, \boldsymbol{F}_i^e$ is evaluated element-wise and component-wise. During global assembly (as described in section 2.4.5.4-2.4.5.6), the outflux $\boldsymbol{q}_i^e$ from one element cancels out the influx $\boldsymbol{q}_i^e$ into the following elements. Incoming $\boldsymbol{q}_i^e$ at the first element and outgoing $\boldsymbol{q}_i^e$ at the last element are given by the natural boundary conditions (Eqs (3.86)-(3.87)). That is:

$$\boldsymbol{q}_i^e\big|_{z=0} = u_{Bi}\big|_{in} - u_{Bi}\big|_{z=0} \tag{3.132}$$

$$\boldsymbol{q}_i^e\big|_{z=1} = 0 \tag{3.133}$$

3.6.2 Discretisation of Particle Phase

As the particle phase (Eq. (3.84)) is diffusion dominated, orthogonal collocation as described in chapter 2.4.3.3 is applied for its discretisation due to its computational efficiency.

$$\frac{\partial u_{Ki}}{\partial \tau} = \eta_i \nabla^2 u_{Pi} \tag{3.134}$$

where

$$u_{Ki} = \varepsilon_P u_{Pi} + (1-\varepsilon_P) u_{Ai} = f(u_{Pi})$$

$$\frac{\partial f(u_{Pi})}{\partial \tau} = \eta_i \nabla^2 u_{Pi} \tag{3.135}$$

Applying orthogonal collocation (Eq. (2.143)) on Eq. (3.135):

$$\frac{\partial f(\boldsymbol{u}_{Pi})}{\partial \tau} = \eta_i \boldsymbol{B}\boldsymbol{u}_{Pi} \tag{3.136}$$

$$\frac{\partial f(\boldsymbol{u}_{Pi})}{\partial \boldsymbol{u}_{Pi}} \frac{\partial \boldsymbol{u}_{Pi}}{\partial \tau} = \eta_i \boldsymbol{B}\boldsymbol{u}_{Pi} \tag{3.137}$$

In matrix form:

$$\boldsymbol{M}_{Pi}\dot{\boldsymbol{u}}_{Pi} = \eta_i \boldsymbol{B}\boldsymbol{u}_{Pi} \tag{3.138}$$

where

$$\boldsymbol{M}_{Pi} = \frac{\partial f(\boldsymbol{u}_{Pi})}{\partial \boldsymbol{u}_{Pi}}$$

In the case of multi-components, $i \geq 1$, u_P will be represented by a series of radial u_{Pi}. The mass matrix, M_P will represent the interaction between components as given by the isotherm relation.

$$\boldsymbol{M}_P\dot{\boldsymbol{u}}_P = \eta \boldsymbol{B}\boldsymbol{u}_P \tag{3.139}$$

where B and η are adjusted in relation to multi-component u_P vector.

The boundary conditions (Eqs. (3.88)-(3.89)) are also discretised in the similar way.

At $r = 0$:

$$\nabla u_{Pi}\big|_{r=0} = 0 \tag{3.140}$$

At $r = 1$:

$$\nabla u_{Pi}\big|_{r=1} = Bi_i(u_{Bi} - u_{Pi}\big|_{r=1}) \tag{3.141}$$

Applying orthogonal collocation (Eq. (2.142)) on Eq. (3.141):

$$\boldsymbol{A}\boldsymbol{u}_{Pi}\big|_{r=1} = Bi_i(u_{Bi} - u_{Pi}\big|_{r=1}) \tag{3.142}$$

$$\sum_{j=1}^{N+1} A_{N+1,j}u_{Pj,i} = Bi_i(u_{Bi} - u_{PN+1,i}) \tag{3.143}$$

$$\sum_{j=1}^{N} A_{N+1,j}u_{Pj,i} + A_{N+1,N+1}u_{PN+1,i} = Bi_i u_{Bi} - Bi_i u_{PN+1,i} \tag{3.144}$$

$$A_{N+1,N+1}u_{PN+1,i} + Bi_i u_{PN+1,i} = Bi_i u_{Bi} - \sum_{j=1}^{N} A_{N+1,j}u_{Pj,i} \tag{3.145}$$

$$u_{PN+1,i} = \frac{Bi_i u_{Bi} - \sum_{j=1}^{N} A_{N+1,j}u_{Pj,i}}{A_{N+1,N+1} + Bi_i} \tag{3.146}$$

The discretised equations of bulk phase and particle phase along with their boundary conditions result into a system of ordindary differential equation which was solved simultaneously using a stiff ODE solver, ode15s, routine of MATLAB. The following algorithm was employed.

3.6.3 Algorithm

The computational method for the above simulation is structured as follows.

Pre-processor:

- parameter specification
- equipment, operation, computational
- mesh parameters and mesh generation
- system parameters
- general, element-specific, components

Processor:

- preliminary computation
- element specific parameter values
- element matrices and vector computation
- computation of element matrices (bulk phase)
- computation of matrices resulting from OC (particle phase)
- global assembly of elements
- computation of model parameter values
- particle boundary effect update
- solution of ODE by ODE-solver (*time progression*) ($\boldsymbol{M}\dot{\boldsymbol{y}} = f(\boldsymbol{y})$)
- for $t = 0 : T$
    - evaluation of time derivative function ($f = dy/dt$)
    - update data structure matrices from solution vectors
    - for $i = 1 : Nc$ (*component specific computation*)
    - evaluation of boundary node of particle phase
    - imposing boundary conditions in the bulk phase
    - evaluating time derivative function of bulk phase
    - evaluating time derivative function of particle phase
    - update solution vector from the data structure with updated elements.
    - evaluation of mass matrix (M)
    - retrieve particle phase data from solution vector
    - evaluate particle phase mass matrix (Jacobian) for each particle node along the bulk phase nodes
    - assemble particle phase mass matrix
    - assemble the system mass matrix (combining bulk phase and particle phase mass matrix)
    - compute value or state of y (solution vector) at this new time step (using ODE-solver)

Post processor:

- visualisation and further processing of the output/result set

The results of the simulations and their discussion are as follows.

3.7 Results and Discussion

To test the validity of the model and its implementation simulations were performed using parameter values as given in the literature and outputs were compared with the literature data. Data from Gu (1995) was used to test the model as given below. As derived parameter values, for example *pe*, *Bi*, η, etc., were readily available in the literature along with their associated results, in this part of the work, deriving them from primary variables like v, μ, ρ, etc was not done. Instead such derived parameters were directly used to get the simulation results and compared with the literature results.

Here two tests were done. The first is based upon single component breakthrough for frontal chromatography and the second is multi-component breakthrough result for a pulse injection.

1. System 1: single component

Following system parameters and variables are used from Gu (1995, p. 29) for a mono-component simulation for frontal operation.

$Pe = 200$, $\eta_i = 2$, $Bi_i = 10$, $b_0 = 8$, $b_1 = 7$, $u_{0i} = 0.2$,

$\varepsilon_B = 0.4$, $\varepsilon_P = 0.4$

The simulated result compared with the published data is shown in Fig. 3.6.

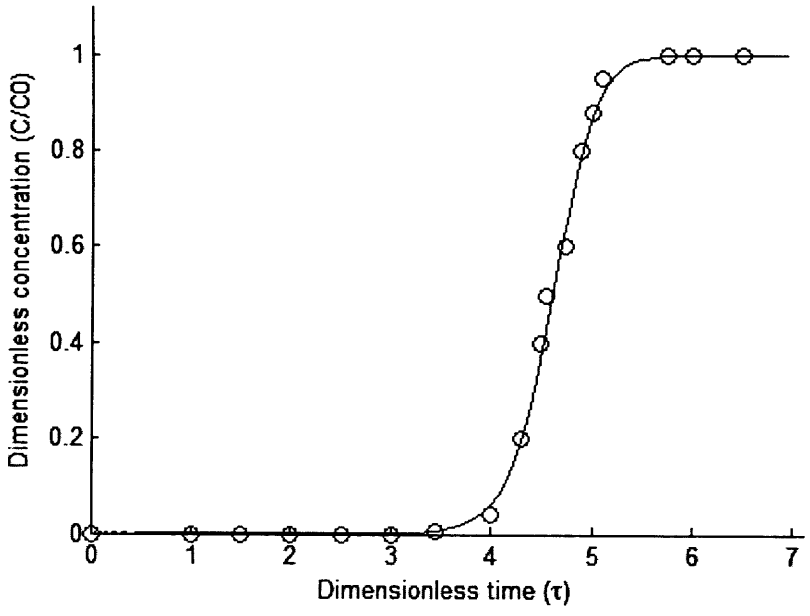

Fig. 3.6 A breakthrough curve: a comparison of simulated result with literature published data (Gu, 1995). —, simulation result; o, literature published data

The result simulation result matched with the published data very well. Similarly, a second test of multi-component simulation using pulse injection was performed as follows.

2. System 2: multi-component

Following system parameters and variables are used from Gu (1995, p. 29) for a multi-component simulation with pulse injection.

Component 1: $Pe = 50$, $\eta_i = 10$, $Bi_i = 4$, $b_0 = 4$, $b_1 = 3.5$, $u_{0i} = 0.2$

Component 1: $Pe = 50$, $\eta_i = 10$, $Bi_i = 4$, $b_0 = 8$, $b_1 = 7$, $u_{0i} = 0.2$

$\varepsilon_B = 0.4$, $\varepsilon_P = 0.4$

Dimensionless sample loading time (τ_{inj}) = 0.2

The simulated result compared with the published data is shown in Fig. 3.7.

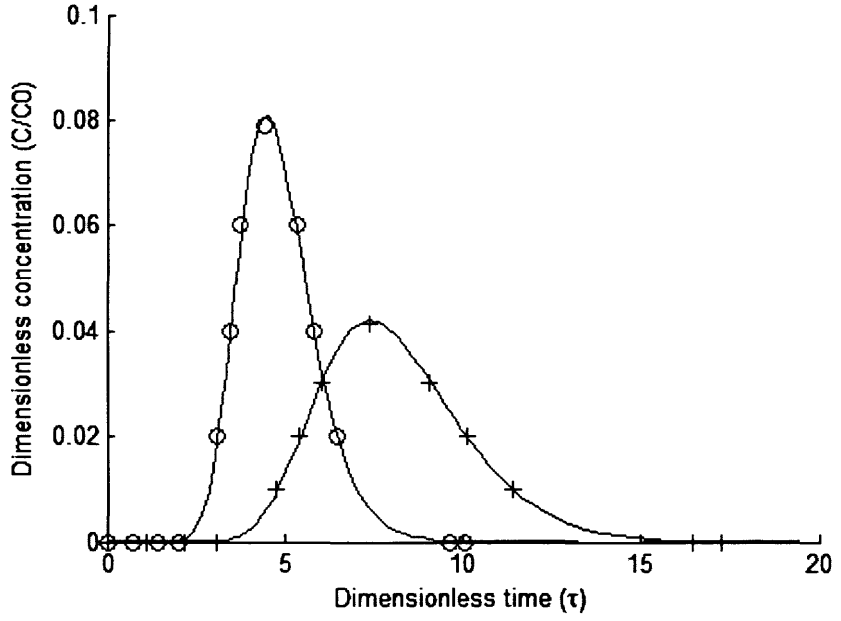

Fig. 3.7 A chromatogram of pulse injection (2 components): a comparison with literature published model (Gu, 1995) and simulation result. —, simulation results, ○, literature published data for component 1, + literature published data for component 2

The simulated result almost exactly matched the published data for pulse injection multi-component chromatography. As observed above in both cases, since the simulation results and the published data/results matched very well, it can be concluded that the model and its implementation (code) is correct and valid for the general purpose as relevant to this work.

3.8 Conclusion

This completes the general chromatography modelling and its validation work. It was found that the model and its implementation are accurate. This will provide a basis for modelling adsorption part of an EBA model, and also its verification in the other parts of this thesis. Now, before attempting to develop a complete integrated model of EBA, hydrodynamic aspects of expanded bed will be investigated in detail and appropriate models will be established in the chapters 4 and 5 for steady state and transient state respectively.

4 Steady State EBA Hydrodynamics

4.1 Introduction

Modelling of an expanded bed can be separated into two relatively independent parts: distribution of matrix particles in a column and adsorption by such almost stationary particles behaving as an ordinary chromatography system. The second part has been essentially dealt with in the previous chapter. The first part will be dealt here as expanded bed adsorption (EBA) hydrodynamics. Deriving a hydrodynamic model of EBA from first principles is challenging. Here a semi-empirical model/correlation is sought to describe this phenomena for practical applications.

The expansion and configuration of particles in the bed at a given fluid velocity is the subject matter of EBA hydrodynamics. When fluid is passed through a settled bed, the particles will be subjected to upward drag along the direction of fluid flow while gravity will try to bring it down. Besides these, the particles will be subject to other forces like buoyancy, inter-particle interactions, etc. The net effect of these forces in relation to particle properties like size, density, etc. will cause the particles to lift and stabilize at certain unique axial positions of the bed. Once the bed reaches its equilibrium or steady state, the axial position of a particular particle category will remain constant. There will still be dispersion of particles but the net change in concentration of a particle category in a given axial position will be null. Similarly if there is a change in the fluid velocity, the bed will further expand or compact based upon whether the velocity is raised or reduced and the particles will settle into new axial positions. The study of the response of EBA systems in terms of its steady state values at a given fluid velocity is considered here as steady state EBA hydrodynamics. The model to predict the steady state response of EBA will be established in this chapter. The response of the bed when the fluid velocity is changed before it reaches to steady state will be considered as the basis of a transient EBA hydrodynamic model and will be studied in the next chapter.

In formulating a complete EBA model, it is necessary to know the composition of the bed in terms of voidage and particle sizes and their concentration if there is a particle size distribution (PSD). EBA hydrodynamics will provide the information on such bed composition. In many cases, EBA is operated after it reaches to its hydrodynamic equilibrium value, that is, the bed composition will not change further or such changes are

negligibly small. For such purposes, the model to represent the steady state EBA hydrodynamics becomes important. This part of the work will try to formulate and establish such a model.

4.2 Literature Review

One of the earliest works to predict expansion in a liquid fluidised bed was that by Richardson and Zaki (1954). It is a semi-empirical method and establishes a relationship between the superficial bed fluid velocity and bed voidage in a mono-sized homogeneous bed. The parameter in the relationship, also termed the Richardson-Zaki correlation parameter (n), is estimated by a correlation based on Reynold's number (Re) with respect to particle terminal velocity (v_t). Al-Dibouni and Garside (1979) used a different correlation to estimate the parameter n though still based on Re. Anspach et al. (1999), Fenneteak et al. (2003), Yun et al. (2003), etc. used a Galileo number (Ga) based correlation to estimated the parameter n. As such correlations are based on mono-sized bed, they do not accurately represent EBA as there is in reality a distribution of particle sizes. So frequently experimental fitting of the parameter n along with even effective average terminal velocity (v_t) has been employed as done by Thelen and Ramirez (1997) for accuracy.

The work of Kennedy and Bretton (1966) is one of the earliest in the area of liquid fluidised beds which considers the existence of more than one particle categories (based on size and density). They considered two particle size categories and predicted their segregation and mixing due to dispersion. The segregation is due to differences in the upward particle velocity. The particle velocity is represented by the Richardson-Zaki correlation as a function of voidage. Al-Dibouni and Garside (1979) developed a model where an arbitrary particle size distribution is considered. The model was simplified by assuming the bed to be perfectly classified, i.e. no particle dispersion, and thus termed perfectly classified bed (PCB). Here also the particle velocity is estimated by the Richardson-Zaki correlation or the expansion relationship. Yun et al. (2004) implemented this PCB approach for EBA.

In this context, it seems pertinent to enumerate what some of the important weaknesses in the current models are and where the effort should be so as to lay a background for this work. They are as follows.

- Even after half a century, there is no good theoretical model which can replace the semi-empirical Richardson-Zaki correlation.
- The Richardson-Zaki correlation is based on mono-sized bed in a certain interval of operational conditions. EBA has a PSD and the correlation does not accurately predict the expansion.
- Though PCB is an improvement over mono-sized bed because it considers PSD, since the reality is a mixed bed, there still exists error. The magnitude of this error can be high especially when there is a wide variation in the particle size as small particles exist which will have tendency to expand disproportionately.
- The mixed bed model of Kennedy and Bretton (1966), considered PSD, would be a better approach to apply in EBA to predict its steady state hydrodynamics. But it has not been implemented for EBA yet.

4.3 Plan and Objectives

The main objective of this chapter is to establish or formulate a steady state EBA hydrodynamic model. The Richardson-Zaki correlation is the main basis used for representing bed expansion and has at its heart the Richardson-Zaki correlation parameter (n). There are a number of correlations available to estimate the value of n. The first objective is to establish an expansion relationship based using a correlation which can produce consistently accurate prediction of bed expansion.

Bed expansion correlations are developed for mono-sized beds. However in practice EBA intrinsically displays particle size distribution, and such models naturally can not accurately represent EBA expansion. So as a first step towards the model which considers particle size distribution, perfectly classified bed (PCB) model developed by Al-Dibouni and Garside (1976) for a liquid fluidised bed will be implemented in the EBA context. It simplifies the system by assuming the bed to be perfectly classified. But this is far from a reality. There exists mixing or distribution of particle size categories at any given axial position. So as to accommodate this reality and make the model more accurate, a semi-empirical approximate mixed bed approach will be developed and its usefulness in representing bed expansion will be tested. Based upon the findings, conclusions will be drawn for representing the steady state EBA hydrodynamics.

Specific objectives of this chapter are as follows (in relation to steady state EBA hydrodynamics).

- establish an appropriate expansion relationship
- implement a perfectly classified bed (PCB) model in EBA
- develop an approximate mixed bed approach to represent expanded bed behaviour.

4.4 Establishment of Expansion relationship

4.4.1 Introduction

As has been mentioned above the Richardson-Zaki correlation is the main basis used for representing bed expansion. There are a number of correlations available to estimate the value of the parameter n which lies at the core of this correlation. The best way to express the expansion relationship which produces consistently accurate predictions of bed expansion will be established here. It can be either with the use of a particular correlation or if required even fitting from a given data set.

4.4.2 Method

For the purpose of selecting the most appropriate approach, two of the widely used correlations will be presented briefly. A range of experimental data (bed height data with respect to given flow rates and operating conditions) have collected from the literature. The prediction from those expansion relations along with experimental fitting will be used against the data set to establish which is more robust and accurate for general use. This will be based on both the accuracy of the prediction and its variance in different experimental sets.

4.4.3 Tested Expansion Relationship

During expansion, the particulate phase is subjected to different forces mainly: gravity, buoyancy, drag by fluid and inter-particle interactions. A bed expands uniformly and stays at an equilibrium height corresponding to the superficial fluid velocity when this is

greater than the minimum fluidisation velocity of the particles. The bed porosity and distribution of particle will remain uniform for mono-size particles.

The Richardson and Zaki (1954) developed the following semi-empirical correlation to describe the expansion in relation to superficial fluid velocity.

$$\frac{v_0}{v_t} = \varepsilon_B^n \tag{4.1}$$

where

v_0 = superficial fluid velocity

v_t = terminal velocity of particle

ε_B = bed porosity

n = correlation parameter (or Richardson-Zaki parameter)

Eq. (4.1) is the expansion relationship used for describing expansion in most of the liquid fluidised bed models. This establishes the relationship between the superficial fluid velocity and the resulting bed voidage. Different methods employ a range of approaches for estimating the parameter n and will be explained next.

i. Reynolds number based correlation

Richardson and Zaki (1954) proposed the correlation parameter, n, was a function of Reynolds number (Re_t) and d_P/D (particle diameter/column diameter).

For $Re_t < 0.2$ (viscous flow, inertial force negligible)

$$n = 4.65 + 19.5\frac{d_P}{D} \tag{4.2}$$

For $0.2 < Re_t < 1$

$$n = \left(4.35 + 17.5\frac{d_P}{D}\right)\mathrm{Re}_t^{-0.03} \tag{4.3}$$

For $1 < Re_t < 200$

$$n = \left(4.45 + 18\frac{d_P}{D}\right)\mathrm{Re}_t^{-0.1} \tag{4.4}$$

where

$$\mathrm{Re}_t = \frac{\rho_f v_t d_P}{\mu} \tag{4.5}$$

$$v_t = \frac{d_P^2 g(\rho_s - \rho_f)}{18\mu} \tag{4.6}$$

where

ρ_f = fluid density

d_P = particle diameter

μ = fluid viscosity

g = acceleration due to gravity

ρ_s = particle density

ii. Galileo number based correlation

The following general correlation based on the use of Galileo number, *Ga,* has been used by Anspach et al. (1999), Fenneteak et al. (2003) and Yun et al. (2003) to estimate the value of parameter *n*:

$$\frac{5.1 - n}{n - 2.4} = 0.01 Ga^{0.67} \tag{4.7}$$

where the Galileo number (*Ga*) is given by

$$Ga = \frac{d_P^3 g(\rho_s - \rho_f)\rho_f}{\mu^2} \tag{4.8}$$

iii. Experimental fitting approach

Often the prediction afforded using the correlation-estimated Richardson-Zaki parameter (*n*) is not accurate enough in EBA. One of the reasons for these inaccuracies is because the correlations are developed based on mono-size particles and do not accurately represent the EBA system where wide distribution of particle sizes is crucial for bed stability. The mixing of different size species makes the observed expanded height values different from predicted. When such a difference becomes large and significant, it becomes necessary to use the experimental fitting. Especially in relation to predicting adsorption response of the bed, 10% error in bed height estimation results into a huge error. Hence for better accuracy, an alternative is for both *n* and terminal velocity (v_t) to be fitted simultaneously using the experimental data set at different flow rates in the Eq. (4.1) as done by Thelen and Ramirez (1997). Once determined these parameters are then used to predict the bed expansion or voidage for any flow rates within the range of data.

Parameters n and v_t were determined by fitting the experimental data as slope and f(intercept) from:

$$\ln v_0 = \ln v_t + n \ln \varepsilon_B \tag{4.9}$$

4.4.4 Results and Discussion

For the comparative study of the 3 approaches noted above the following dataset (Table 4.1) was used. It consisted of literature published equilibrium bed height results with respect to applied fluid velocity under a set of given experimental conditions.

Table 4.1 Data set used in the analysis

Data set	Reference	EBA column		Fluid velocity (v0) cm/s	Settled bed height (h0) cm	Equilibrium bed height (h) cm
		Matrix (Streamline)	Diameter mm			
1	Thelen and Ramirez (1997)	DEAE	50	0.017	20.5	22.5
				0.021	20.5	24.2
				0.030	20.5	28.3
				0.038	20.5	32.1
				0.047	20.5	36.1
2	Bruce and Chase (2001)	SP	50	0.051	21.2	42
3	Tong et al.	Quartz	26	0.050	10.0	20
				0.128	10.0	30
				0.078	10.0	25
				0.024	10.0	15
4	Yun et al. (2004)	SP	50	0.056	18.5	36.5
				0.077	18.0	42
				0.090	18.0	47

Estimation of bed heights were made for all data sets using both *Re* based and *Ga* based correlations and a relative error in terms of the root mean square (RMS) percent error were calculated as given in Table 4.2.

Table 4.2 Correlation error as a root mean square (RMS) percentage observed when different methods are applied to each data set.

Data sets	No of data points per set	Correlation Error (RMS%)	
		Re-based	Ga-based
1	5	8.6	7.7
2	1	18	11.9
3	4	9.8	8.8
4	3	11	4.1
Model average		11.8	8.1

The bed height estimated by the *Ga* based correlation was found to be slightly better than when using *Re* based correlations. The former had about an 8% error and the latter 12% on average. When both v_t and n were fitted, the approach produced more accurate estimate as can be seen for Ramirez data in the following Fig. 4.1.

Based on the above result *Ga* based method was found to be more accurate than *Re* based method. However average 8% error can still be significant error when using this to estimate bed height and voidage for predicting adsorption response. In such cases, more accurate method might be required. This can be achieved by experimental fitting approach as observed in Fig. 4.1. When such an approach is employed both v_t and n are fitted using experimental data. The natural v_t (intrinsic v_t of a particle when there is no inter-particle interferences) has to be ignored in preference for an effective v_t as given by the experimental data. The fact that the natural v_t is not used, means one important physical meaning is lost. Since two parameters are fitted, the result is close to the experimental data, but its valid range is narrow and rapidly loses its predictive power when experimental conditions are changed. The correlation remains useful to predict the expansion within the flow rate interval under which the parameter values were estimated and providing the other experimental conditions is kept constant.

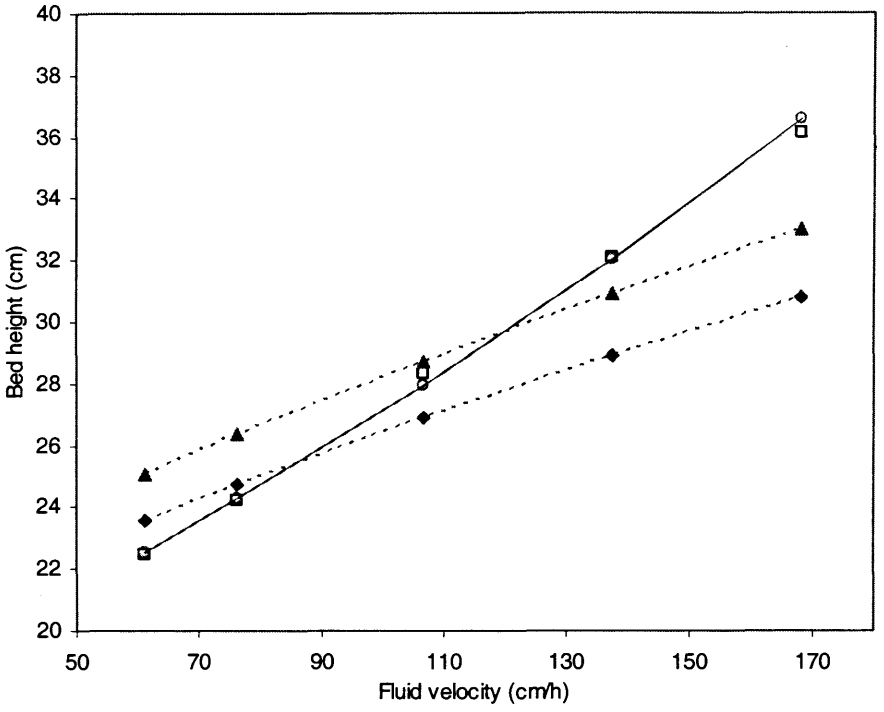

Fig. 4.1 Bed height estimated for Thelen and Ramirez (1997) data set at different fluid velocities. ♦, using *Re* based correlation; ▲, using *Ga* based correlation; ○, using parameter fitting for both v_t and n; □, experimental data.

4.4.5 Conclusion

In the situation where experimental data is not available, *Ga* based method seems to be the method of choice to predict the bed expansion using the Richardson-Zaki correlation. If there is adequate experimental data and the prediction has to be made within the interval of the data set or just near its boundary, parameter fitting from available data would be better for accuracy, but suffers from the lack of general applicability.

The expansion relationship established in this section will be the basis for describing bed expansion in this thesis. Though these relationship themselves are based on mono-sized bed assumption, the next section is included to specify clearly what it means when mono-sized bed model is the model which used to describe hydrodynamics of EBA.

4.5 Mono-sized Bed Model

In this simplest form, the bed is assumed to be mono-sized and the Richardson-Zaki correlation is used to predict bed expansion. Based upon the findings of section 4.4, Galileo number (*Ga*) based correlation will be used to estimate the parameter n as shown below.

$$\frac{v_0}{v_t} = \varepsilon_B^n \tag{4.10}$$

where $n = f(Ga)$ as given by (4.7) and (4.8).

When experimental data is available and much accurate prediction of bed expansion is necessary, experimental fitting approach will be applied. One possible improvement over experimental fitting approach described earlier can be that instead of totally discarding both v_t and n, it could be advantageous to add two modifying variables (a_1 and a_2) as shown below.

$$\frac{v_0}{v_t} = a_1 \varepsilon_B^{a_2 n} \tag{4.11}$$

where $n = f(Ga)$ as given by (4.7) and (4.8).

a_1 and a_2 = fitted values based on experimental data

Though this is effectively same as the experimental fitting described in section 4.4, by keeping natural v_t and *Ga* based n means that it will at least partially retain the effect of physical properties of the system. Once the parameters a_1 and a_2 are determined using a set of v_0 for a range of possible operating conditions, they can be considered relatively constant. Whereas slight variations in the expansion due to slight changes in physical properties might be able to manifest through the natural v_t and *Ga* based n used. However, this is just a hypothesis, and has not been verified in this work.

Hydrodynamics of expanded bed assuming mono-sized bed has been established here. This can be a huge assumption especially while predicting adsorption response. So when mono-size bed assumption is relaxed, one of the simplest approaches to include particle size distribution in the model is by assuming the bed to be perfectly classified. The next section will investigate such an approach in the context of EBA.

4.6 PCB Model

4.6.1 Introduction

The first step towards incorporating particle size distribution (PSD) in a model of expanded bed behaviour is by using the Perfectly Classified Bed (PCB) approach. This approach was developed by Al-Dibouni and Garside (1979) for liquid fluidized beds. In the expansion of a particulate system having particle size distribution (PSD) the bed is considered to be perfectly classified or segregated into strata based upon particle size as shown in Fig. 4.2. Each stratum contains particles of only one size.

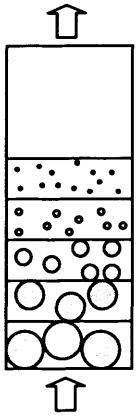

Fig. 4.2 A perfectly classified bed showing segregation of particles based upon their size when the bed is expanded (according to the Al-Dibouni and Garside, 1979).

In an expanded bed particles do not perfectly classify. Instead in reality a mixed bed with many particle sizes co-existing in an axial position is generated. Another limitation of the PCB approach is especially when there is wide size distribution with a large amount of small particles, the error in estimation can be high as small particles tend to expand to a greater degree. The approach was implemented for EBA by Yun et al. (2004). One of the reasons for its re-implementation here is for using it to develop an integrated EBA model whose hydrodynamic part will be defined by a PCB approach.

4.6.2 Model Development

The expansion of each column segment as shown in Fig. 4.2 with respect to superficial fluid velocity (v_0) is determined by its representative particle size. The relationship

developed for mono-size particles, as in the previous section 4.5, will be used for each segment to predict the segment expansion. The cumulative of all segments then gives the total bed height, and the voidage profile.

The PCB model in his thesis is established as follows. Let volumetric particle size distribution be represented by a normal distribution $N(\overline{R},\sigma)$ with mean particle size radius $\overline{R}$ and std. deviation σ. It is assumed that the distribution of particle sizes in EBA can be considered approximately normal as has been done by Yun et al. (2004). Considering a constant density (ρ_s) for all particle size sp., the cumulative mass distribution is given by,

$$M = \int N(\overline{R},\sigma)\rho_s dR \tag{4.12}$$

$$\frac{dM}{dR} = \rho_s \frac{d}{dR}\int N(\overline{R},\sigma)dR = \rho_s N(\overline{R},\sigma) \tag{4.13}$$

$$m = \frac{dM}{dR} = \rho_s N(\overline{R},\sigma) \tag{4.14}$$

Assuming a perfectly classified bed (PCB), a particular particle size (R) will correspond to particular axial position (z) with one to one mapping as shown in Fig. 4.3.

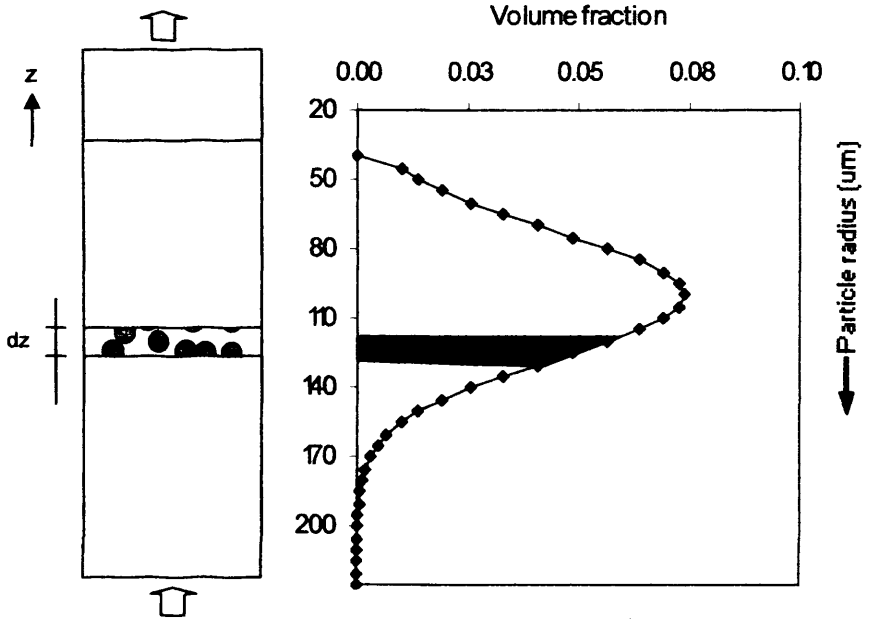

Fig. 4.3 PCB and particle size correspondence: Bed is perfectly classified and particle size decrease as height increases. The volume of each size categories is fixed and given by volume fraction covered by the radius interval. In the column that volume will occupy space along the vertical axis and its thickness will be given by dz.

After bed expansion, if particle size R to $R+\Delta R$ is contained exactly between z to $z+\Delta z$ then:

$$\text{Mass fraction contained} = \frac{\Delta M}{\Delta R}\Delta R = \text{vol fraction*density} = \Delta z A\left(1-\varepsilon\big|_z\right)\rho_s \quad (4.15)$$

(where Δz is fraction of total equilibrium bed height)

$$m\,dR = \rho_s A(1-\varepsilon)dz \quad (4.16)$$

Integrating the mass fraction in PSD covered by an interval of radius (ΔR) to evaluate the total mass fraction contained within it, will be equivalent to an integration along the bed axis in a corresponding axial interval (Δz).

$$\int_{\Delta R}\frac{m}{\rho_s A(1-\varepsilon)}dR = \int_{\Delta z} dz \quad (4.17)$$

Substituting the value of m from Eq. (4.15) and evaluating the integral,

$$\frac{1}{\rho_s A}\int_{\Delta R}\frac{\rho_s N(\bar{R},\sigma)}{(1-\varepsilon)}dR = \Delta z \quad (4.18)$$

As demonstrated by Hassan et al. (2005) density of particle can be reasonably considered constant for all particle sizes for hydrodynamic purpose, it can be taken out of integral and will be cancelled out.

$$\frac{1}{A}\int_{\Delta R}\frac{N(\bar{R},\sigma)}{(1-\varepsilon)}dR = \Delta z \quad (4.19)$$

For a discrete value of size class or segments, each segment can be considered to expand as a mono-sized bed. Thus the resulting expansion or ε is given by v_0 and R of the segment as if mono-sized. Appropriate models as in section 4.5 can be used to represent it. If Ga based correlation is used:

$$v_0 = v_t\varepsilon^n \quad (4.20)$$

where n is given by (4.7) and (4.8). This means

$$n = f(Ga) = f_1(R)$$
$$v_t = f_2(R)$$

From Eq. (4.20),

$$\varepsilon = \left(\frac{v_0}{v_t}\right)^{1/n} \quad (4.21)$$

Eq. (4.19) along with Eq. (4.21) gives the location of a particular size category in an expanded bed or vice versa. The largest or heaviest particle lies at the bottom and the

smallest or lightest particle lies at the top (assuming constant particle density, ρ_s). The top surface of the smallest particle gives the bed height or expansion at a given v_0.

4.6.3 Result and Discussion

Using the data set 1, 2 and 4 in Table 4.1, expanded bed heights were estimated using both PCB and Mono-sized bed approaches. The results can be observed below in Fig. 4.4.

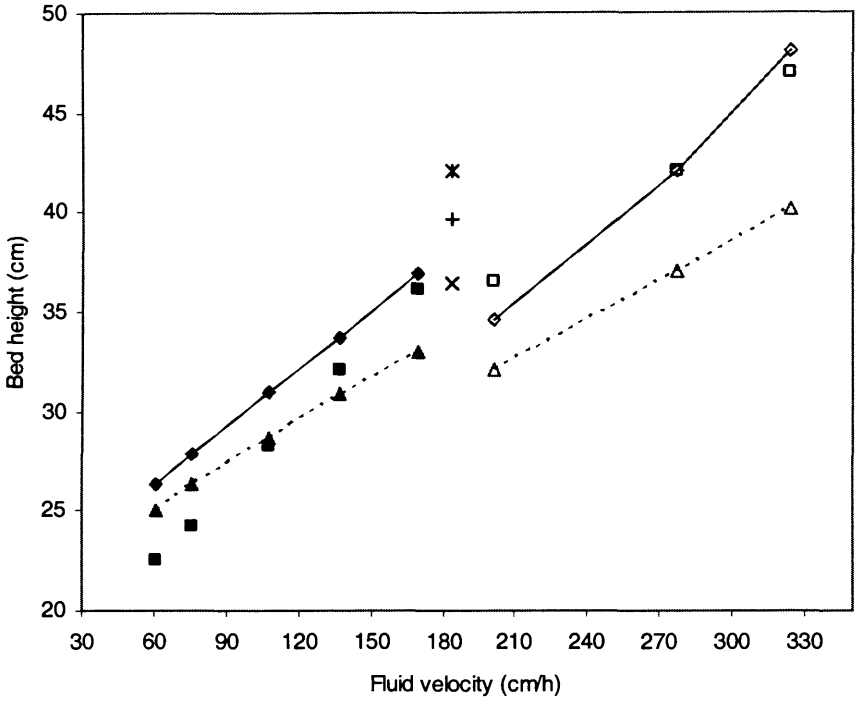

Fig. 4.4 Bed heights at different fluid velocities estimated using Perfectly classified bed (PCB) model and Mono-sized bed (MSB) model for 3 different experimental data sets: Thelen and Ramirez, 1997 (TR); Bruce and Chase , 2001 (BC); Yun et a., 2004 (YU). ♦, PCB estimate for TR; ▲, MSB estimate for TR; ■, experimental data of TR; +, PCB estimate for BC; x, MSB estimate for BC; *, experimental data of BC; ◊, PCB estimate for YU; △, MSB estimate for YU; □, experimental data of YU.

The PCB approach was found to be more accurate for datasets 2 and 4. For one case (dataset 1), the PCB model may be slightly better than mono-sized bed approach but not significantly. Most importantly the PCB approach considers distribution of particle sizes and also provides a better estimate of axial variation of voidage which is especially important when making an integrated model to predict the adsorption response as a function of axial positions. The PCB approach is superior to that of a simple mono-sized

bed. Improvements with PCB method by considering the existence of a distribution of particle sizes in any axial position by mixed bed approach will be explored next.

4.7 Approximate Mixed Bed Approach to Represent Expanded Bed Behaviour

4.7.1 Introduction

In the perfectly classified bed (PCB) model the bed is considered to be segregated based on particle sizes and the amount of each size range or stratum is known. The expansion of each size-specific stratum at a given flow rate causes bed expansion and results in a full expanded bed height. In a mixed bed model, the existence of different particle sizes at each axial position or strata is taken into account (Fig. 4.5). For a given flow rate, it is assumed that the bed expands such that there exists a characteristic PSD and voidage at each axial position. In this part of the work, an approximate method to estimate mixed bed expansion was developed and was tested for its effectiveness in representing expanded bed.

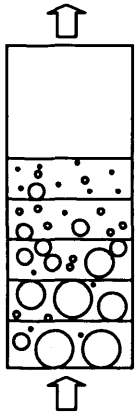

Fig. 4.5 A mixed bed displaying the existence of particles of different sizes at any axial position when the bed is expanded.

Willoughby et al. (2000) demonstrated that axial variation of voidage in EBA is function of fluid velocity and also published the axial particle size distribution (PSD) for a fluid velocity. Bruce and Chase (2001) and Yun et al. (2004) also published axial PSD in expanded bed at different experimental settings. It is envisaged that, given an

experimental setting, axial variation of PSD and voidage in EBA can be described by an empirical model as a function of fluid velocity. Clearly such an approximate approach based on experimental data will have a limited predictive capacity, but can still be useful for practical applications by representing the PSD along the bed axis. The main objective in this thesis was to model expand bed adsorption, and by keeping the hydrodynamic part independent of adsorption part, the final model can easily make use of any better hydrodynamic description as and when it is available; replacing the original approach.

The mixing of particle size species is due to the natural propensity to reach an equilibrium in relation to the segregation velocity and diffusion at a given superficial velocity as described by Kennedy-Bretton (1966). However in this black-box approach, the mixing propensity of a particle size species is taken as a function of the applied v_0 and particle size provided all other parameters are kept constant. This is a fundamental weakness in the approach. In spite of this weakness, the advantage of using this approach is that it gives one single parameter or a function to represent the axial PSD variations in an expanded bed.

4.7.2 Method

It is envisaged that mixed bed expansion can be approximated by the combined effect of two separable steps, which are as follows:

1. Particle size composition or mixing specific to axial position in the bed
2. Expansion of each axial segment

4.7.2.1 Particle size composition

Bed mixing is determined by the propensity of the bed to deviate from perfect classification based on particle sizes as is assumed in the PCB model earlier. The magnitude of this can be represented by the standard deviation, σ_{mi} (mixing sigma), for each particle size species *i*. If $\sigma_{mi} = 0$ (for all *i*), perfect segregation of sizes exists. This σ_m can be considered to be dependent on fluid velocity (v_0), particle sizes (R_i), amount and PSD of the bulk matrix and other physical properties of fluid and flow. It is assumed that for a given system, keeping important influencing parameters constant, the effect on it due to control variables like v_0 can be estimated at least by using prior experimental data.

The particle size composition of a bed is determined by first segregating the bed into different size specific strata and then mixing of sizes in different strata as a result of σ_m. The mixing is considered to be as a result of migration of a particle species to domain or strata of other size species. This will redefine the strata in terms of its composition and thickness.

The mixing parameter specific to a particle size category, σ_{mi}, is estimated empirically as observed in steady-state expansion. Though there can be skewness, for a simplified modelling approach, it is assumed such deviations make little effect on the overall size composition and distribution and so will be neglected. For a more accurate representation, a skewed distribution like the Generalized Exponentially Modified Gaussian distribution with additional parameters can be applied. For this work only one parameter σ_{mi} is assumed to be adequate.

From whatever initial size composition it starts, at steady state it is considered to always reach and stabilise in a particular composition specific to the experimental conditions. There will be a limited level of continuous dispersive particle movement across strata but their net effect will be null for equilibrium to exist.

The mixing parameter σ_{mi} is taken as based on the spread along the bed axis which will imply the spread along the layers originally of other particle size categories. Due to mixing each original size-specific segment is changed along with its composition. These are determined by net transfer of mass or particles from different original segments. The particle size specific mixing parameter, σ_{mi}, is approximated by a simple correlation like:

$$\sigma_{mi} = a_0 + a_1 R_i + a_2 R_i^{\,2} \tag{4.22}$$

where a_0, a_1 and a_2 are parameters fitted from experimental data, and are considered to be function of v_0.

$$(a_0, a_1, a_2) = f(v_0) \tag{4.23}$$

4.7.2.2 Expansion of each segment

Once the segment composition and thickness of the resulting mass/volume fractions have been determined as explained above, the characteristic equivalent particle size or radius of each segment is then determined by using a weighted mass or volume average particle radius. As particle density can be considered fairly constant, the mass average or volume average are equivalent. This segment specific characteristic radius is then used to estimate

the expansion using relationship such as those developed for mono-sized particles as in PCB model described in section 4.6.

Equivalent particle size or radius of segment j (R_j) is given by:

$$R_j = \sum_i \phi_i R_i \qquad (4.24)$$

where ϕ_i = mass/volume fraction of particle size species i (radius R_i)

This approach is applied using following algorithm.

4.7.3 Algorithm

The algorithm employed was based upon a number of assumptions. First, due to narrow difference between representative particle sizes of segments which is already averaged based on volume fractions, the bulk porosity when settled is assumed to be fairly equal. (In the case, where more accurate bulk porosity data is available for different size species based on experimental data or correlations, such insight can be used to provide for a more accurate result.)

The algorithm then proceeds as follows:

- Bed segmentation and estimation of mass average particle size
    - Settled bed as in PCB
    - Division of bed into N equal segments or volume fractions
    - Estimation of mass/volume average particle size representing each segment
- Specification of size specific mixing parameter value (σ_{mi}) – using function or prior data from experimental fitting
- Determination of new segment composition after mixing
    - Mass repositioning of each representative size species along bed axis due to σ_{mi}
    - Determination of new size composition or PSD for each segment, its thickness and estimation of representative mass average particle size
- Expansion of each segment based on Richardson-Zaki correlation as in PCB model using representative particle size to give total bed expansion behaviour.

This provides the bed expansion, axial voidage profile and size compositions in each axial segment. However to implement this, the procedure needs particle size specific

mixing parameter (σ_{mi}). When experimental data on axial PSD for a set of fluid velocity is available, this can be estimated by fitting as follows. (Further simplification can be done by assuming σ_{mi} be relatively constant in a range of flow rate used in EBA.)

The method of estimating mixing parameter (σ_i) by fitting:

- Choose σ_i or its associated parameters $(a_0, a_1, a_2) = f(v_0)$
- Apply mixing and expansion as above
- Determine axial PSD at specified location of the bed
- Determine error of estimate

$$\text{Error} = \sum_{\text{number of axial positions}} \sum_{i} \left(\phi_i|_{estimated} - \phi_i|_{observed}\right)^2 \qquad (4.25)$$

  where ϕ_i is volume fraction of size species i
- Find σ_{mi} or its associated parameters which minimise the error as given above in Eq. (4.25).

Using this method, bed expansion, axial particle size distribution and voidage profile was estimated. The results are as follows.

4.7.4 Results and Discussion

At first, in section 4.7.4.1, mixing parameter (σ_{mi}) values were estimated using Willoughby et al. (2000) experimental data set of 200 cm/h fluid velocity. These values were then applied to predict axial PSD at different bed heights and axial voidage profile for the same dataset. After this, in section 4.7.4.2, assuming the σ_{mi} constant and that the value applicable in a similar operation conditions in terms of fluid, flow and particle physical properties, the method was then applied to predict the bed expansion in different experimental set ups as described in Table 3.3.1.

4.7.4.1 Estimation of mixing parameter from experimental PSD data

In order to apply a simplified mixed bed approach, the mixing parameter (σ_{mi}) specific to each particular particle species i is required. This can be determined using the experimental data of axial PSD at different axial position using the method as described

in section 4.7.3. Here Willoughby et al. (2000) experimental data was used to estimate such parameter in Streamline Phenyl 50 column operated at 200 cm/h fluid velocity. The PSD of the bulk matrix was considered as: 200 μm mean particle diameter, 50 μm standard deviation and 70-500 μm range. It is expected that the value estimated for this would also act as rough guideline for the expected values in other similar EBA matrices and operating conditions. This value is always bracketed in between two extremes:

$\sigma_{mi} = 0$: no mixing as in PCB or

$\sigma_{mi} \rightarrow \infty$: completely mixed resulting in almost mono-size bed behaviour. Infinity is a relative term. In the present context of mixing sigma value 3-4 times the magnitude of bulk PSD sigma can be considered to be approaching to infinity.

For comparison and estimation the experimental axial PSD data was normalised. Here five size categories of equal mass/volume (density being considered constant) were used to cover the whole range. It can be any number, but at the present limitations and simplifying assumptions of the method for example use of same bed voidage for all used size categories. Too high a number of categories can introduce errors while the use of very few categories will not adequately represent the PSD. The use of five categories was found to be optimal in the present context. Using different mixing parameter (σ_{mi}) value axial PSD was determined which was compared with experimental data to find out best σ_{mi} which minimises the difference between estimated and observed as described in section 4.7.3.

As shown in the Fig. 4.6, the mean σ_m value (corresponding to the mean particle size) was found be to be about 40 μm. It was assumed that σ_m varies linearly with slope of 0.5 to the variation in particle size. And σ_m was considered higher for the lower particle sizes. However for a simple approximation such size specific variation does not necessarily need to be considered and in which cases σ_m can be considered constant for all particle sizes.

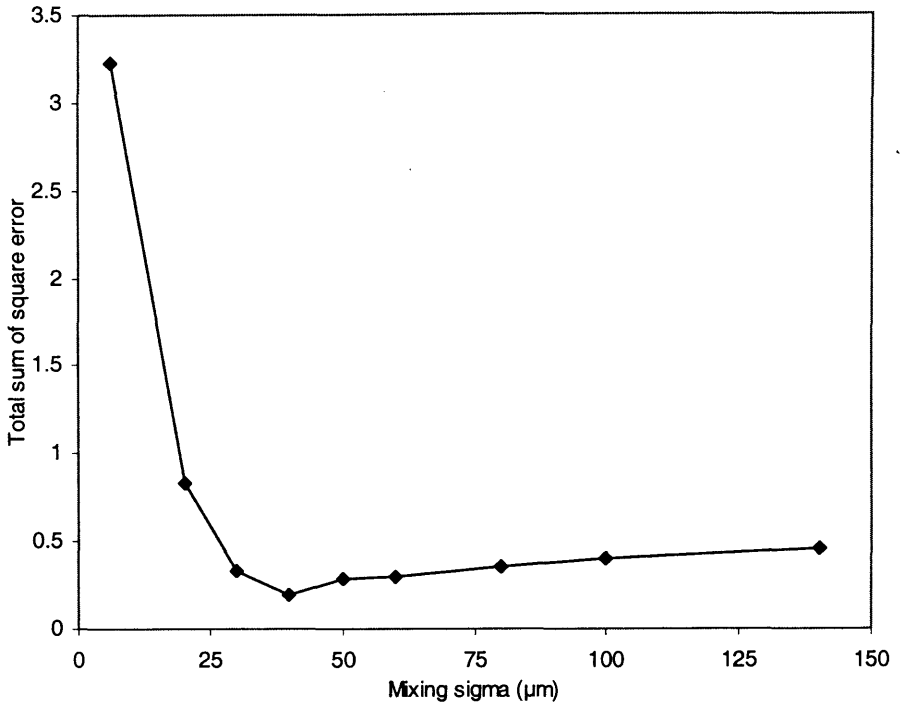

Fig. 4.6 Estimation of mean mixing sigma (σ_m) parameter value which minimises total sum of square error (SSE) of simulated axial particle size distribution (PSD) with respect to experimental axial PSD data at 200 cm/h fluid velocity (Willoughby et al., 2000). In the figure σ_m value of about 40 is found to produce the least total SSE and thus the best estimate to represent axial PSD of a mixed bed.

The comparison of estimated axial PSD at different axial positions using mean mixing sigma parameter of 40 μm to the experimental data is shown in Fig. 4.7 and Fig. 4.8. Though there are conspicuous differences, in general, they seem to compare reasonably well for a practical purpose. The correlation coefficient between simulated prediction and experimental data was found to be 0.83. Hence, although this method needs further refinement for more accurate predictions, it seems possible to use this for an approximate estimate of mixed bed state and its resulting bed expansion in an expanded bed.

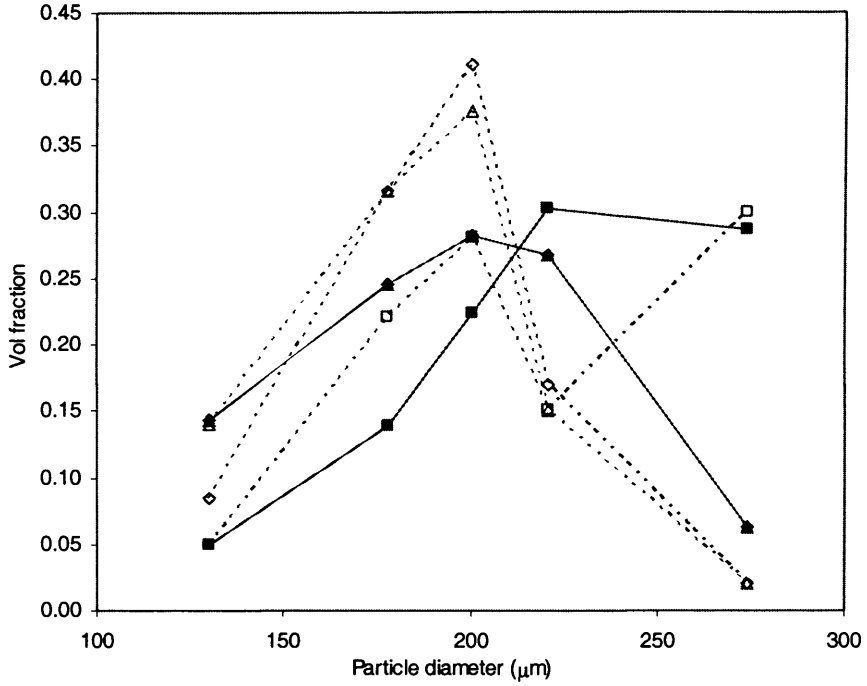

Fig. 4.7 Comparison of an axial particle size distribution (PSD) at 200 cm/h fluid velocity estimated using Approximate mixed bed (AMB) approach with mixing sigma (σ) of 40 to the experimental data of Willoughby et al. (EX) at different bed heights. ■, 5 cm AMB; ♦, 10 cm AMB; ▲, 15 cm AMB; □, 5 cm EX; ◊, 10 cm EX; △, 15 cm EX.

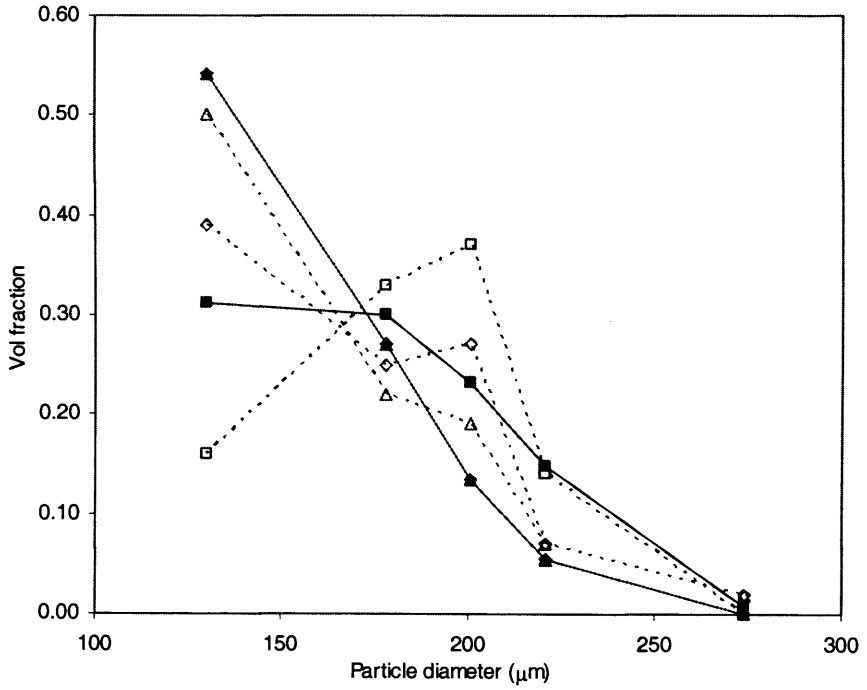

Fig. 4.8 Comparison of an axial particle size distribution (PSD) at 200 cm/h fluid velocity estimated using Approximate mixed bed (AMB) approach with mixing sigma (σ) of 40 to the experimental data of Willoughby et al. (EX) at different bed heights. ■, 20 cm AMB; ♦, 25 cm AMB; ▲, 30 cm AMB; □, 20 cm EX; ◊, 25 cm EX; △, 30 cm EX.

When PSD are available for wide range of fluid velocity, such data can be used to estimate mixing sigma (σ_m) as a function of fluid velocity by the method as has been described in sections 4.7.2 and 4.7.3. Here only one fluid velocity data at 200 cm/h was used which estimated mean σ_m of 40 μm. Assuming the relatively no variation in σ_m when fluid velocity is changed within a small range, approximate mixed bed (AMB) approach was applied to estimate bed heights in the next section.

4.7.4.2 Bed Height Estimation

Bed height was estimated for different experimental sets with different fluid velocities and by employing range of predictive methods and the result compared with experimental data. Bed heights were predicted using mono-sized bed, PCB and AMB approaches. The results are shown in the figure below (Fig. 4.21).

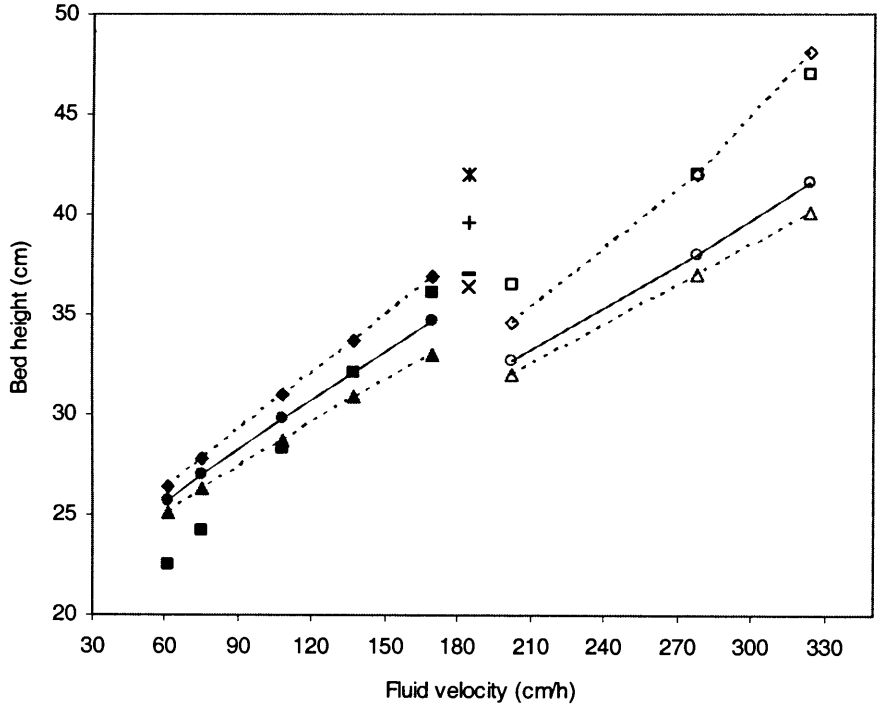

Fig. 4.9 Bed heights at different fluid velocities estimated using Approximate mixed bed (AMB) approach, Perfectly classified bed (PCB) model and Mono-sized bed (MSB) model for 3 different experimental data sets: Thelen and Ramirez, 1997 (TR); Bruce and Chase , 2001 (BC); Yun et a., 2004 (YU). •, AMB estimate for TR; ♦, PCB estimate for TR; ▲, MSB estimate for TR; ■, experimental data of TR; –, AMB estimate for BC; +, PCB estimate for BC; x, MSB estimate for BC; *, experimental data of BC; ○, AMB estimate for YU; ◊, PCB estimate for YU; △, MSB estimate for YU; □, experimental data of YU.

For estimation purposes using mixed bed approach, mean mixing sigma value of 40 μm was used. To accommodate for variations in the mixing sigma value with respect to particle size, the mixing sigma was approximated by a linear function with mean as above and a slope of 0.5 with respect to particle size. Apart from these for mixed bed, the results were primarily produced without using fitted parameters. The natural terminal velocity (Eq. (4.6)) was used and the Richardson-Zaki parameter (n) was estimated using the Ga based correlation (Eqs. (4.7)-(4.8)).

The assumption of mixed bed (MB) approach did not improve results over that of perfectly classified bed (PCB) approach for the data set used in this study. Estimates by the MB approach were within about 10-15% of experimental values and slightly better than mono-sized bed approach. This result was as expected since the mixed bed approach lies in between that of the mono-sized and PCB approaches which naturally are the boundary conditions of mixed bed with complete-mixing and no-mixing.

Whereas the mono-size is a crude approximation, the PCB approach provides an improved approximation and also provides some estimate on the variation of particle size and voidage along the bed axis. But besides such estimates being a crude guide, it has one important limitation. As flow rate increases, the segment of small sized particle will have a tendency to expand greater degree. Especially if the particle size distribution is wide, this can cause a problem in the simulation. The particle velocity of small particles is likely to rise almost to the elutriation velocity and raise the bed height significantly. The mixed bed approach improves the model in many ways. Due to the averaging nature in each segment not only does it stabilise or avoids such overexpansion problems but also more accurately estimates the axial voidage variations. Even of more significance is that it provides an estimate for axial PSD at any given axial position. These advantages come at the cost of having to provide a mixing sigma parameter value which is a further experimental investment.

4.7.5 Conclusion

The development of an approximate mixed bed approach was attempted and tested for its suitability in representing EBA. The approach seems to hold promise but requires further refinement. Use of an optimal discretisation or size categories to represent PSD, gave a resulting axial PSD close to the experimental data, and with the estimated bed height lying in between that produced by PCB and mono-sized bed approaches. Because in

reality the bed is mixed, the axial PSD and voidage variation estimated by the mixed bed approach can be expected to be more accurate than those estimated using PCB. Compared to the PCB assuming the mixed bed approach also provides stability in the simulation of bed expansion but comes at the cost of providing an additional parameter i.e. mixing sigma (σ_m).

The need to use an optimal number of discretisation or size categories is an important limitation of the approach at its current state. This is due to the use of a simplified method and the code at present. Further work to correct the current weakness of this approximate mixed bed approach is necessary and recommended. Besides, it is also recommended to determine the σ_m as a function of fluid velocity by using experimental data from a range of fluid velocity. This will make the approach more robust and useful for more accurate predictive applications.

4.8 Conclusion

The Richardson-Zaki correlation is a widely used method to estimate bed expansion in a liquid fluidised bed including EBA. The estimation of the Richardson-Zaki correlation parameter (n) using a Galileo number (Ga) based correlation seems to be slightly better than the adoption of a Reynolds number (Re) based correlation for expanded beds with an error in the order of 10%. The existence of particle size distribution (PSD) in real EBA system is probably the root cause of this error since all correlations have been developed based on the assumption of mono-sized bed. When such an error becomes too significant, for example for adsorption purposes, parameter fitting using experimental data may be necessary.

The perfectly classified bed is a better approach than mono-sized bed approach when particle size distribution (PSD) and variation of axial voidage have to be considered. PCB produces better results than assuming a mono-sized bed for estimation of bed height for the representative data set used in the study.

The development of an approximate mixed bed approach was attempted and tested for its suitability in representing EBA. The approach seems to hold promise but requires further refinement. Use of an optimal discretisation or size categories to represent PSD, gave a resulting axial PSD close to the experimental data, and with the estimated bed

height lying in between that produced by PCB and mono-sized bed approaches. Because in reality the bed is mixed, the axial PSD and voidage variation estimated by the mixed bed approach can be expected to be more accurate than those estimated using PCB. Further work to correct for the current weaknesses of this approximate mixed bed approach are necessary and recommended.

The next chapter will study representing the transient hydrodynamic response of EBA which will be crucial for developing an integrated EBA model with transient hydrodynamics.

5 Transient EBA Hydrodynamics

5.1 Introduction

In the previous chapter, the approach to predict bed expansion and axial particle size distribution at steady state was established. There are however a number of situations in which knowledge of the dynamic response of a bed in relation to a given change in the system, for example changes in fluid velocity or fluid properties, will be desirable. With this in mind this chapter will study and establish the possible model needed to predict the transient hydrodynamic response of an expanded bed (EBA).

Some of the possible reasons for the need of such transient models can be as follows.

- While loading in EBA, the physical properties (density, viscosity, etc.) of the fluid change. This will cause the bed to adopt a new equilibrium based upon these parameters. Until the bed assumes this new equilibrium stage, it will be in hydrodynamic transient mode which will affect the adsorption behaviour of the column.
- Even when the bed has equilibrated to a constant bed height axial particle dispersion continues. The net change in particle concentration at any axial position remains constant at steady state but it affects the adsorption response of the bed. Thus consideration of such axial particle dispersion becomes important. Depending upon the system of study the axial particle dispersion coefficient can vary. In some it can be small and neglected; while in others it can be significant. The most rapid adsorption changes take place in the lower part of the bed, the effect of such axial particle dispersion is especially critical in this part of the bed or when the bed height used is small. Thus estimating the axial particle dispersion coefficient becomes important. A correlation developed for fluidized beds has frequently been used in literature (Van der Meer et al., 1984). Depending upon the contexts in which it is to be applied this approach may be adequate. However if it is necessary to verify it or to improve the accuracy, another independent method would be required. One such method is to estimate the axial particle dispersion

from experimental data. Transient EBA hydrodynamic model can be used for such purposes even when mono-sized bed is considered.

- During EBA operation it is necessary to know how much time it will take for a bed to reach hydrodynamic equilibrium for a given system so that appropriate control action can be taken in a given process sequence. For example this would be especially valuable for increasing throughput and maintaining product quality. A transient hydrodynamic model would be useful for such purposes.
- As will be discussed in Chapter 9, an integrated EBA adsorption model linked with a transient hydrodynamic model can have many uses e.g. for gradient change in flow velocity for bed stability, operation in hydrodynamic transient bed mode for possibility of maximizing bed productivity, etc. Development and proving of a transient hydrodynamic model is the first step toward building such models.

In this chapter a simple mono-sized transient hydrodynamic model of expanded bed behaviour will be established. Literature available models will be adopted when possible, and improved or adapted if and when required.

5.2 Literature Review

There are not many work related to modelling of transient hydrodynamics of expanded bed. Transient model of expanded bed is generally represented by a general mass balance model of particle phase as of Eq. (2.16) with no source term. The critical part in the model is the velocity of the particle phase. As done by Kennedy-Bretton (1966) and shown in appendix A.3.3, this is estimated based on the inclination of the particle phase concentration to go towards an equilibrium as observed in steady state value as of mono-sized bed, i.e. using a Richardson-Zaki correlation. When the particle size distribution (PSD) is considered to exist, the bed will be segregated and mixed based on the relative strength of the convective and dispersive terms of each size species. Large, heavy particles have a lower upward particle velocity compared to that of small and lighter particles. So small particles move up and large particles tend to stay towards the bottom of the bed. However the dispersion of each size species will result into a partially mixed bed with a degree of segregation. Asif et al. demonstrated this approach in modelling liquid fluidized bed of coal particles in their 1994 paper. There was a subsequent paper by

Kaufmann et al. from the same research group in 1995. Thelen and Ramirez (1997) used the approach but for a simplified system of mono-sized bed.

5.3 Plan and Objective

With the aim of developing an integrated EBA model capable of predicting adsorption response while the bed is at transient hydrodynamic state later, in this chapter, a simple transient hydrodynamic model of expanded bed as developed by Thelen and Ramirez (1997) by assuming only mono-sized bed will be established. The specific objectives are:

- to establish mono-sized bed transient hydrodynamic model of EBA
- to verify the model using experimental data.

5.4 Model Development

The first stage in the development of a mono-sized bed model was to construct a mass balance of a differential volume element of an expanded bed is done here at first. This neglects the existence of particle size distribution (PSD) and assumes the bed to comprise of only mono-sized beads. As in the steady state models discussed in the previous chapter, the following additional assumptions were taken.

- Assuming the validity of self-diffusion of small particles (<300 μm diameter) for practical purpose as shown by Brotz (1952), Fick's Law can be applied to model dispersion in expanded bed as demonstrated by Kennedy and Bretton.
- Only one axial dimension will be taken as Willoughby et al. (2000) has demonstrated that there is no or limited radial variation in particle phase concentration
- Bed is stable.
- Convective flux is the result of particle movement to bring the local solid phase concentration to equilibrium w.r.t. applied superficial velocity. It is assumed that the flux can be represented by the Richardson-Zaki correlation as developed for a mono-sized bed in spite of having a PSD. Irrespective of the particular composition of size, only the total solid phase concentration is considered to be factor which is important for the equilibrium state. Moreover as the bed is

assumed to be mono-sized, the Richardson-Zaki correlation could be directly used.

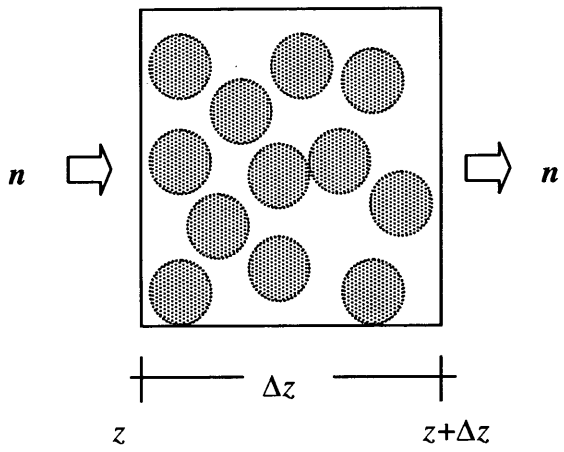

Fig. 5.1 A differential volume element of a column

From Eq. (2.18), a mass balance of particles in a differential volume element of a column (Fig. 5.1), as there is no source term, yields:

$$\frac{\partial \rho_s}{\partial t} + \nabla \cdot \boldsymbol{n}_s = 0 \tag{5.1}$$

where ρ_s is concentration of particle (s) and n_s mass flux which is given by

$$\boldsymbol{n}_s = -\rho E \nabla w_s + \rho_s v_s \tag{5.2}$$

where ρ is bulk density, E_s dispersion coefficient of particle size species s, w_s is mass fraction and v_s is velocity of particle w.r.t. to bed (that is Eularian).

Voidage (ε) is given by

$$\varepsilon = 1 - c \tag{5.3}$$

And bulk density is given by

$$\rho = c\bar{\rho}_s + \varepsilon \rho_f \tag{5.4}$$

where ρ_f is density of fluid.

$$\rho = c\bar{\rho}_s + (1-c)\rho_f$$

$$\rho = (\bar{\rho}_s - \rho_f)c - \rho_f \tag{5.5}$$

From Eq. (5.1) and (5.2)

$$\frac{\partial \rho_s}{\partial t} - \nabla \cdot (\rho E \nabla w_s) + \nabla \cdot (\rho_s v_s) = 0 \tag{5.6}$$

Taking only one axial dimension (z),

$$\frac{\partial \rho_s}{\partial t} - \frac{d}{dz}(\rho E \nabla w_s) + \frac{d}{dz}(\rho_s v_s) = 0 \tag{5.7}$$

Representing fractional volumetric concentration of particle phase by c:

$$\rho_s = \frac{\text{particle mass}}{\Delta \text{ volume}} = \text{particle mass fraction} \frac{\text{total mass}}{\Delta \text{ volume}} = w_s \rho \tag{5.8}$$

where Δ volume is the volume of a differential element.

$$\rho_s = \frac{\text{particle mass}}{\text{particle volume}} \frac{\text{particle volume}}{\Delta \text{ volume}} \tag{5.9}$$
$$= \text{particle density} * \text{particle volume fraction} = \bar{\rho}_s c$$

Thus,

$$w_s \rho = \bar{\rho}_s c \tag{5.10}$$

where $\bar{\rho}_s$ is density of particle.

$$w_s = \frac{\bar{\rho}_s}{\rho} c \tag{5.11}$$

Substituting the value of w_i into ∇w_s,

$$\frac{\partial w_s}{\partial z} = \bar{\rho}_s \frac{\partial}{\partial z}\left(\frac{c}{\rho}\right) = \frac{\bar{\rho}_s}{\rho^2}\left(\rho \frac{\partial c}{\partial z} - c \frac{\partial \rho}{\partial z}\right) \tag{5.12}$$

Substituting the value of w_i and ∇w_i into Eq. (5.7),

$$\bar{\rho}_s \frac{\partial c}{\partial t} - \frac{\partial}{\partial z}\left[E_s \rho \frac{\bar{\rho}_s}{\rho^2}\left(\rho \frac{\partial c}{\partial z} - c \frac{\partial \rho}{\partial z}\right)\right] + \bar{\rho}_s \frac{\partial}{\partial z}(c v_s) = 0$$

$$\frac{\partial c}{\partial t} - \frac{\partial}{\partial z}\left[E_s\left(\frac{\partial c}{\partial z} - \frac{c}{\rho}\frac{\partial \rho}{\partial z}\right)\right] + \frac{\partial}{\partial z}(c v_s) = 0$$

$$\frac{\partial c}{\partial t} - E_s \frac{\partial^2 c}{\partial z^2} + E_s \frac{\partial}{\partial z}\left(\frac{c}{\rho}\frac{\partial \rho}{\partial z}\right) + v_s \frac{\partial c}{\partial z} + c \frac{\partial v_s}{\partial z} = 0 \tag{5.13}$$

The above equation represents the transient hydrodynamic model of an expanded bed when the bed is considered to be made up of homogenous mono-sized beads. This can be simplified as follows.

Simplification of the term: $\frac{\partial}{\partial z}\left(\frac{c}{\rho}\frac{\partial \rho}{\partial z}\right)$

$$\frac{\partial}{\partial z}\left(\frac{c}{\rho}\frac{\partial \rho}{\partial z}\right) = \frac{\partial \rho}{\partial z}\frac{\partial}{\partial z}\left(\frac{c}{\rho}\right) + \frac{c}{\rho}\frac{\partial^2 \rho}{\partial z^2} \tag{5.14}$$

$$= \frac{\partial \rho}{\partial z}\left(\rho \frac{\partial c}{\partial z} - c \frac{\partial \rho}{\partial z}\right)\frac{1}{\rho^2} + \frac{c}{\rho}\frac{\partial^2 \rho}{\partial z^2}$$

$$= \frac{1}{\rho}\frac{\partial \rho}{\partial z}\frac{\partial c}{\partial z} - \frac{c}{\rho^2}\left(\frac{\partial \rho}{\partial z}\right)^2 + \frac{c}{\rho}\frac{\partial^2 \rho}{\partial z^2} \tag{5.15}$$

Substituting the value of ρ, from Eq. (5.5),

$$E\frac{\partial}{\partial z}\left(\frac{c}{\rho}\frac{\partial \rho}{\partial z}\right) = -E\frac{1}{(\rho_s-\rho_f)c+\rho_f}(\rho_s-\rho_f)\left(\frac{\partial c}{\partial z}\right)^2 - E\frac{c}{((\rho_s-\rho_f)c+\rho_f)^2}(\rho_s-\rho_f)^2\left(\frac{\partial c}{\partial z}\right)^2 + E\frac{c}{(\rho_s-\rho_f)c+\rho_f}(\rho_{sj}-\rho_f)\frac{\partial^2 c}{\partial z^2} \tag{5.16}$$

By order of magnitude analysis using experimental data from normal operating condition, shows that this term is about $O(0.05\text{-}0.1)$, and thus may be neglected. Thus Eq. (5.13) becomes:

$$\frac{\partial c}{\partial t} = E\frac{\partial^2 c}{\partial z^2} - v_s\frac{\partial c}{\partial z} - c\frac{\partial v_s}{\partial z} \tag{5.17}$$

The Eq. (5.17) is same as that of Thelen and Ramirez (1997). The crucial part of this is determining particle velocity (v_s). For that the same approach as used by Kennedy-Bretton (1966) has been used as given below.

Particle velocity (v_s): The particle size species velocity (v_s) is determined as follows. The particle interstitial relative velocity with respect to fluid (v_{rs}), as a result of expansion of the bed to reach equilibrium as given by Richardson-Zaki (RZ) correlation, is given by:

$$v_{rs} = v_f - v_s = \frac{v_t \varepsilon^n}{\varepsilon} = v_t \varepsilon^{n-1} \tag{5.18}$$

where v_t is terminal velocity of particle, n is its RZ correlation parameter and ε is the voidage at that axial position z. Fluid velocity (v_f) is given by:

$$v_f = v_0 + cv_{rs} \tag{5.19}$$

$$v_f = v_0 + cv_t\varepsilon^{n-1} \tag{5.20}$$

From eq. (5.18)

$$v_s = v_f - v_t\varepsilon^{n-1} \tag{5.21}$$

Substituting the value of v_f

$$v_s = v_0 + cv_t\varepsilon^{n-1} - v_t\varepsilon^{n-1} \tag{5.22}$$

$$v_s = v_0 - (1-c)v_t\varepsilon^{n-1}$$

$$v_s = v_0 - v_t(1-c)^n \tag{5.23}$$

Thus substituting the value of v_s in Eq. (5.17):

$$\frac{\partial c}{\partial t} = E\frac{\partial^2 c}{\partial z^2} - \left(v_0 - v_t(1-c)^n\right)\frac{\partial c}{\partial z} - c\frac{\partial\left(v_0 - v_t(1-c)^n\right)}{\partial z} \tag{5.24}$$

$$\frac{\partial c}{\partial t} = E\frac{\partial^2 c}{\partial z^2} - \left(v_0 - v_t(1-c)^n\right)\frac{\partial c}{\partial z} - ncv_t(1-c)^{n-1}\frac{\partial c}{\partial z}$$

$$\frac{\partial c}{\partial t} = E\frac{\partial^2 c}{\partial z^2} - \left(\left(v_0 - v_t(1-c)^n\right) + ncv_t(1-c)^{n-1}\right)\frac{\partial c}{\partial z} \tag{5.25}$$

This is a non-linear partial differential equation. If the upper surface of the solid phase is considered as an upper boundary by applying conservation of total solid phase in the domain as a constraint, the problem becomes a moving boundary problem with a non-stationary upper boundary. To make it easier to solve numerically, this moving boundary value problem is converted to stationary two point boundary value problem with variable coefficient by spatial variable transformation as follows:

$$\lambda = \frac{z}{h(t)} \qquad \text{height with respect to maximum height} \tag{5.26}$$

$$\frac{d\lambda}{dz} = \frac{1}{h(t)} \tag{5.27}$$

Partial derivatives w.r.t. new variable λ:

$$\frac{\partial c(z,t)}{\partial z} = \frac{\partial c(\lambda,t)}{\partial t}\frac{dt}{dz} + \frac{\partial c(\lambda,t)}{\partial \lambda}\frac{d\lambda}{dz} = \frac{1}{h(t)}\frac{\partial c(\lambda,t)}{\partial \lambda} \tag{5.28}$$

$$\frac{\partial^2 c(z,t)}{\partial z^2} = \frac{1}{h(t)}\left(\frac{\partial}{\partial t}\left(\frac{\partial c(\lambda,t)}{\partial \lambda}\right)\frac{dt}{dz} + \frac{\partial}{\partial \lambda}\left(\frac{\partial c(\lambda,t)}{\partial \lambda}\right)\frac{d\lambda}{dz}\right) = \frac{1}{h^2(t)}\frac{\partial^2 c(\lambda,t)}{\partial \lambda^2} \tag{5.29}$$

$$\frac{\partial c(z,t)}{\partial t} = \frac{\partial c(\lambda,t)}{\partial t}\frac{dt}{dt} + \frac{\partial c(\lambda,t)}{\partial \lambda}\frac{d\lambda}{dt} = \frac{\partial c(\lambda,t)}{\partial t} - \frac{\lambda}{h(t)}\frac{dh(t)}{dt}\frac{\partial c(\lambda,t)}{\partial \lambda} \tag{5.30}$$

Also transformation for dimensionless time:

$$\tau = \frac{tv_0}{L} \tag{5.31}$$

$$\frac{d\tau}{dt} = \frac{v_0}{L} \tag{5.32}$$

$$\frac{\partial c(\lambda,t)}{\partial \lambda} = \frac{\partial c(\lambda,\tau)}{\partial \tau}\frac{d}{d\lambda} + \frac{\partial c(\lambda,\tau)}{\partial \lambda}\frac{d\lambda}{d\lambda} = \frac{\partial c(\lambda,\tau)}{\partial \lambda} \tag{5.33}$$

$$\frac{\partial^2 c(\lambda,t)}{\partial \lambda^2} = \frac{\partial^2 c(\lambda,\tau)}{\partial \lambda^2} \tag{5.34}$$

$$\frac{\partial c(\lambda,t)}{\partial t} = \frac{\partial c(\lambda,\tau)}{\partial \tau}\frac{d\tau}{dt} + \frac{\partial c(\lambda,)}{\partial \lambda}\frac{d\lambda}{dt} = \frac{v_0}{L}\frac{\partial c(\lambda,\tau)}{\partial \tau} - \frac{\lambda}{h(t)}\frac{dh(t)}{dt}\frac{\partial c(\lambda,\tau)}{\partial \lambda} \tag{5.35}$$

Final transformed variables:

$$\frac{\partial c(z,t)}{\partial z} = \frac{1}{h(t)}\frac{\partial c(\lambda,\tau)}{\partial \lambda} \tag{5.36}$$

$$\frac{\partial^2 c(z,t)}{\partial z^2} = \frac{1}{h^2(t)}\frac{\partial^2 c(\lambda,\tau)}{\partial \lambda^2} \tag{5.37}$$

$$\frac{\partial c(z,t)}{\partial t} = \left(\frac{v_0}{L}\frac{\partial c(\lambda,\tau)}{\partial \tau} - \frac{\lambda}{h(t)}\frac{dh(t)}{dt}\frac{\partial c(\lambda,\tau)}{\partial \lambda}\right) - \frac{\lambda}{h(t)}\frac{dh(t)}{dt}\frac{\partial c(\lambda,\tau)}{\partial \lambda}$$

$$= \frac{v_0}{L}\frac{\partial c(\lambda,\tau)}{\partial \tau} - 2\frac{\lambda}{h(t)}\frac{dh(t)}{dt}\frac{\partial c(\lambda,\tau)}{\partial \lambda} \tag{5.38}$$

Thus:

$$\frac{\partial c}{\partial t} = E\frac{\partial^2 c}{\partial z^2} - \left(\left(v_0 - v_t(1-c)^n\right) + ncv_t(1-c)^{n-1}\right)\frac{\partial c}{\partial z} \tag{5.39}$$

$$\frac{v_0}{L}\frac{\partial c}{\partial \tau} - 2\frac{\lambda}{h(t)}\frac{dh(t)}{dt}\frac{\partial c}{\partial \lambda} = E\frac{1}{h^2(t)}\frac{\partial^2 c}{\partial \lambda^2}$$
$$- \left(\left(v_0 - v_t(1-c)^n\right) + ncv_t(1-c)^{n-1}\right)\frac{1}{h(t)}\frac{\partial c}{\partial \lambda}$$

$$\frac{\partial c}{\partial \tau} = E\frac{1}{h^2(t)}\frac{L}{v_0}\frac{L}{L}\frac{\partial^2 c}{\partial \lambda^2}$$
$$- \left(\left(\left(v_0 - v_t(1-c)^n\right) + ncv_t(1-c)^{n-1}\right)\frac{1}{h(t)}\frac{L}{v_0} - 2\frac{\lambda}{h(t)}\frac{dh(t)}{dt}\frac{L}{v_0}\right)\frac{\partial c}{\partial \lambda} \tag{5.40}$$

Using following modified Peclet number (Pe) as a model parameter,

$$Pe = \frac{v_0 L}{E} \tag{5.41}$$

Let,

$$\gamma = \frac{L}{h(t)} \tag{5.42}$$

$$U = \frac{ncv_t(1-c)^{n-1} + v_0 - v_t(1-c)^n}{v_0} \tag{5.43}$$

$$W = \frac{dh(t)/dt}{v_0} \tag{5.44}$$

Substituting values,

$$\frac{\partial c}{\partial \tau} = \frac{\gamma^2}{Pe}\frac{\partial^2 c}{\partial \lambda^2} - (\gamma U - 2\lambda W\gamma)\frac{\partial c}{\partial \lambda} \tag{5.45}$$

$$\frac{\partial c}{\partial \tau} + \gamma(U - 2\lambda W)\frac{\partial c}{\partial \lambda} - \frac{\gamma^2}{Pe}\frac{\partial^2 c}{\partial \lambda^2} = 0 \tag{5.46}$$

The initial and boundary conditions of the system are as follows.

Initial conditions:

$$c_{New} = \frac{c_{Settled} h_{Settled}}{h_{New}} \tag{5.47}$$

Boundary conditions:

As the superficial fluid velocity is far below the elutriation velocity, the total solid phase or particle mass is conserved and remains constant in the column. If the domain is considered to be from the bottom to the upper surface of the solid phase, the size or volume of domain is changing with time but total mass within it is contained and constant as given below (Thelen and Ramirez, 1997).

$$\int_{\Omega(t)} (\overline{\rho}_s c) dV = m \tag{5.48}$$

Taking a time differential and expanding Eq. (5.48) utilizing extended Liebnitz' formula:

$$\frac{\partial}{\partial t}\int_{\Omega(t)} (\overline{\rho}_s c) dV = \int_{\Omega(t)} \overline{\rho}_s \frac{\partial c}{\partial t} dV + \int_{\Gamma(t)} \overline{\rho}_s c(\boldsymbol{v}_{surf} \cdot \boldsymbol{n}) dS = 0 \tag{5.49}$$

where

v_{surf} = velocity of boundary surface

n = unit outward pointing normal (as confined to axial direction only: = ± z)

Rewriting the mass balance as an integral over the surrounding volume:

$$\int_{\Omega(t)} \left(\frac{\partial \rho_s c}{\partial t} + \nabla \cdot \boldsymbol{N}_s \right) dV = \int_{\Omega(t)} \overline{\rho}_s \frac{\partial c}{\partial t} dV + \int_{\Omega(t)} (\nabla \cdot \boldsymbol{N}_s) dV = 0 \tag{5.50}$$

From the divergence theorem of Gauss:

$$\int_{\Omega(t)} (\nabla \cdot \boldsymbol{N}_s) dV = \int_{\Gamma(t)} (\boldsymbol{N}_s \cdot \boldsymbol{n}) dS \tag{5.51}$$

Thus,

$$\int_{\Gamma(t)} (\boldsymbol{N}_s \cdot \boldsymbol{n}) dS = \int_{\Gamma(t)} \overline{\rho}_s c (\boldsymbol{v}_{surf} \cdot \boldsymbol{n}) dS \tag{5.52}$$

$$\boldsymbol{N}_s \cdot \boldsymbol{n} = \overline{\rho}_s c (\boldsymbol{v}_{surf} \cdot \boldsymbol{n}) \tag{5.53}$$

The flux expression then becomes:

$$\boldsymbol{N}_s = \left(-E \frac{\partial (c\overline{\rho}_s)}{\partial \lambda} + vc\overline{\rho}_s \right) z \tag{5.54}$$

(z : unit normal vector along z axis)

1. At the bottom of the column: λ=0 (n = -z)

$$v_{surf} = 0 \tag{5.55}$$

$$\left(-E \frac{\partial (c\overline{\rho}_s)}{\partial \lambda} + vc\overline{\rho}_s \right) z \cdot (-z) = \overline{\rho}_s c (\boldsymbol{v}_{surf} \cdot (-z)) \tag{5.56}$$

$$E\overline{\rho}_s \frac{1}{h(t)} \frac{\partial c}{\partial \lambda} - c\overline{\rho}_s (v_0 - v_t (1-c)^n) = 0$$

$$\frac{\partial c}{\partial \lambda} = (v_0 - v_t (1-c)^n) c \frac{h(t)}{E} \frac{Lv_0}{Lv_0}$$

$$\frac{\partial c}{\partial \lambda} = \frac{Pe}{\gamma} \left(1 - \frac{v_0}{v_t} (1-c)^n \right) c \tag{5.57}$$

2. At the top of the column: λ=1 (n = z)

$$v_{surf} = dh(t)/dt \tag{5.58}$$

$$\left(-E \frac{\partial (c\overline{\rho}_s)}{\partial \lambda} + vc\overline{\rho}_s \right) z \cdot (z) = \overline{\rho}_s \phi_s \left(\frac{dh(t)}{dt} z \cdot z \right) \tag{5.59}$$

$$-E\overline{\rho}_s \frac{1}{h(t)} \frac{\partial c}{\partial \lambda} + c\overline{\rho}_s \left(v_0 - v_t (1-c)^n \right) = \overline{\rho}_s c \frac{dh(t)}{dt}$$

$$\frac{\partial c}{\partial \lambda} = \left(c(v_0 - v_t (1-c)^n) - c \frac{dh(t)}{dt} \right) \frac{h(t)}{E}$$

$$\frac{\partial c}{\partial \lambda} = \left((v_0 - v_t (1-c)^n) - \frac{dh(t)}{dt} \right) \frac{h(t)}{E} c \frac{Lv_0}{Lv_0}$$

$$\frac{\partial c}{\partial \lambda} = \frac{Pe}{\gamma} \left(1 - \frac{v_0}{v_t} (1-c)^n - W \right) c \tag{5.60}$$

Thus the model of transient hydrodynamics of expanded bed is given by Eq. (5.46) with initial conditions, Eq. (5.47), and boundary conditions, Eqs. (5.57) and (5.60). It was found that there was difficulty in implementing this model. Thus for a unique and stable

solution, some additional assumptions on the boundary conditions were taken. It is possible that this can make the solution slightly different from what it should have been. But such difference will be small and contained, and null when its reaches to an equilibrium level or steady state. Besides the difference introduced by such assumption can be reduced by increasing the number of discretisation.

Additional boundary conditions assumptions:

The assumptions and their subsequent results are as follows.

1. At $\lambda = 0$: Immediately after expansion starts, c at the bottom surface will try to equilibrate with the new v_0. Considering that the effect of convection is considerably higher than dispersion, we may assume that c at $\lambda = 0$ immediately adopts the new c value which makes the velocity of the particle (v) zero with respect to the new v_0, and remains at that value throughout. From Eq. (5.57), the c at the bottom surface will then be given by:

$$v_0 - v_t(1-c)^n = 0 \tag{5.61}$$

2. At $\lambda = 1$: As the bed height is moving, the compression or expansion of c (that is change in c) at that upper surface is significantly lower compared than that in other parts of the bed, so $dc/d\lambda$ at that upper moving surface may be effectively assumed to be zero. The boundary equation, Eq. (5.60), at that surface derived from mass conservation can thus be used to determine the surface velocity. The surface velocity is thus given by:

$$\frac{dh}{dt} = v_0 - v_t(1-c)^n \tag{5.62}$$

Thus the final model for a transient hydrodynamics of expanded bed is given by Eq. (5.46) with initial conditions Eq. (5.47), boundary conditions Eqs. (5.61)-(5.62), and constants of the system, Eqs (5.41)-(5.44). In the next section, the method employed to estimate parameters of the model will be explained. That will be followed by simulation.

5.5 Parameter Estimation

In chromatography modelling (Section 3.5), it is required to estimate several parameters. In line with this need the hydrodynamic model derived above needs the estimation of one parameter, particle dispersion coefficient. The method applied to estimate it is described below.

5.5.1 Particle Dispersion Coefficient

Van der Meer et al. (1984) developed a correlation to estimate the particle dispersion coefficient in a fluidized bed. It is given by:

$$E = 0.04 v_0^{1.8} * 10^4 \quad \text{cm}^2/\text{s} \tag{5.63}$$

where v_0 = superficial velocity (cm/s)

This has been used for EBA model to estimate particle dispersion [Wright and Glasser (2001), Tong et al. (2002), Chen et al. (2003), Li and Rodrigues (2004), Yun et al. (2005) and Li et al. (2005)]. Though it has been widely used, it appears that most of these papers have taken for granted in terms of the hydrodynamics the validity of the correlation and there has not been another independent method to verify it. It should also be noted that this correlation does not provide estimation of particle dispersion for specific particle size categories when particle size distribution is considered. So in this work, when required, the particle dispersion coefficient will be fitted based upon experimental data developed with transient hydrodynamics.

5.5.2 Richardson-Zaki Correlation Parameter

As discussed in model development section, the Richardson-Zaki correlation parameter (n) is required to determine the particle size species velocity (v_s) as given in Eq. (5.18). This can be determined using a Galileo number (Ga) based correlation as discussed in the previous chapter on EBA steady state hydrodynamics. Often however the final bed height prediction based on such correlations differs by 10-15% or more from the observed experimental result. In these cases both n and the observed terminal velocity v_t are required to be fitted in order to match the experimental data. Once estimated those values should remain valid within the interval of the set of fluid velocities used for the purpose.

5.6 Simulation

The transient model (Eq. (5.46) and associated equations) was discretised using the method of line principle (section 2.4.2.3) to result in an ODE system which was solved using an ODE-solver within MATLAB. A centred finite difference as described in section 2.4.2 was used to achieve spatial discretisation and an upwind scheme (section 2.4.2.4) was followed to accommodate for the convective term. The difference scheme employed is as follows.

$$\frac{\partial c}{\partial \tau} = -\gamma(U - 2\lambda W)\frac{u(\lambda,\tau) - u(\lambda - \Delta\lambda,\tau)}{\Delta\lambda} + \frac{\gamma^2}{Pe}\frac{c(\lambda + \Delta\lambda,\tau) - 2c(\lambda,\tau) + c(\lambda - \Delta\lambda,\tau)}{\Delta\lambda^2} \tag{5.64}$$

Thus resulting ordinary differential equation system Eq. (5.64), after applying boundary conditions (Eqs. (5.61)-(5.62)) and initial condition (Eq. (5.47)), is solved using ODE-solver of MATLAB. The results are as follows.

5.7 Results and Discussion

Using the above model for a mono-sized transient bed, the simulation was performed using the Thelen and Ramirez (1997) data set and transient bed experimental data obtained in this work. Thelen and Ramirez used Streamline DEAE for expansion in 50 mm diameter column. The bed was assumed to be mono-sized with mean particle diameter was 200 μm. The average particle density was considered to be 1.2 g/cm^3. Twenty percent aqueous ethanol solution was used for expansion whose density and viscosity were taken to be 0.98 g/cm^3 and 0.01 g/cm.s. Settled bed voidage was 0.4. The experimental set up and parameter values for the experiment performed in this work were also same except that the column diameter was 25 mm instead of 50 mm.

In the case of the steady state model, without fitting the Richardson Zaki correlation coefficient, the results were about 10% away from the Ramirez data set (Fig. 5.2) and in the case of experimental data set more than 25% out (Fig. 5.3). About 10% margin of error for *Ga*-based correlation appears to be common based upon the analysis in section

4.4. But much larger difference in prediction for experimental data of this work is probably due to the old matrix used for the study. Due to many uses and long storage, its physical properties might have changed such that it resulted in much higher expansion than that would have been expected. Thus model fitting approach (as discussed in section 4.4) was used to fit both effective terminal velocity (v_t) and Richardson-Zaki correlation parameter (n). For Thelen and Ramirez data 0.139 cm/s v_t and 2.663 n were used. Similarly for the experiment in this work 0.136 cm/s v_t and 4.323 n were used. An axial particle dispersion coefficient was fitted to adjust for the rate of bed expansion for each data set examined in this work.

The simulation results obtained for the mono-sized bed approach using fitted parameters of v_t and n matched very well with both the literature data of Thelen and Ramirez and the experimental data obtained in this work as shown below in Fig. 5.2 and Fig. 5.3. The modification in the boundary conditions from those adopted by Thelen and Ramirez model appears to be valid. It is observed that this slightly modified model actually gives more accurate result than those results published in the literature.

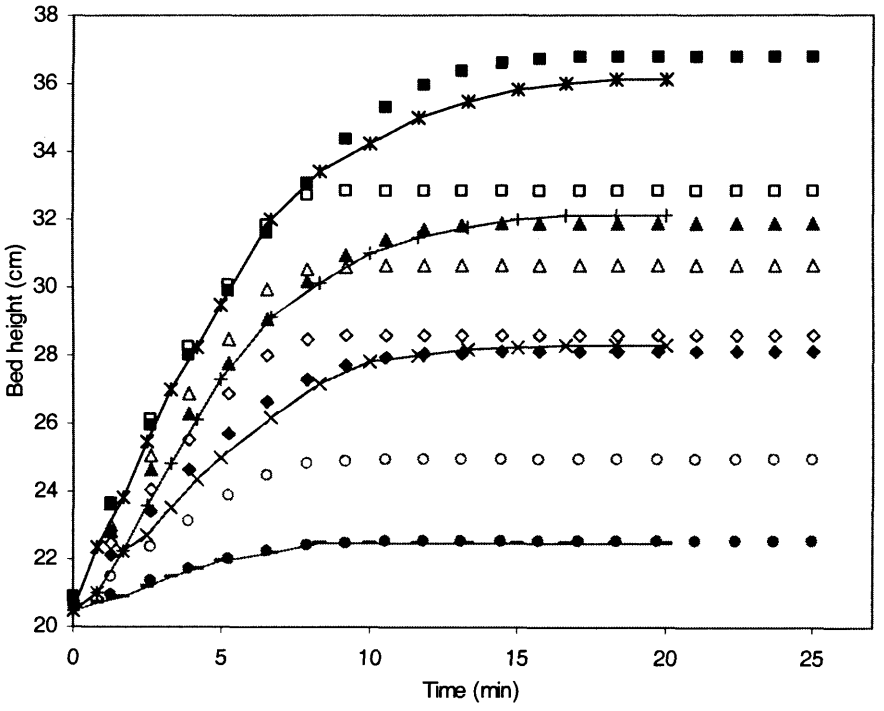

Fig. 5.2 Transient bed heights predicted using Transient mono-sized bed hydrodynamic model for a data set of Thelen and Ramirez (1997) at different fluid velocities. Three sets of results are shown. Parameters (n and v_t) are fitted in the first set (PF). Parameters are not fitted in the second set (NF). Final set is experimental data (EX). ■, 169 cm/h PF; ▲, 137 cm/h PF; ♦, 108 cm/h PF; ●, 61 cm/h PF; □, 169 cm/h NF; △, 137 cm/h NF; ◊, 108 cm/h NF; ○, 61 cm/h NF; *, 169 cm/h EX; +, 137 cm/h EX; x, 108 cm/h EX; –, 61 cm/h EX.

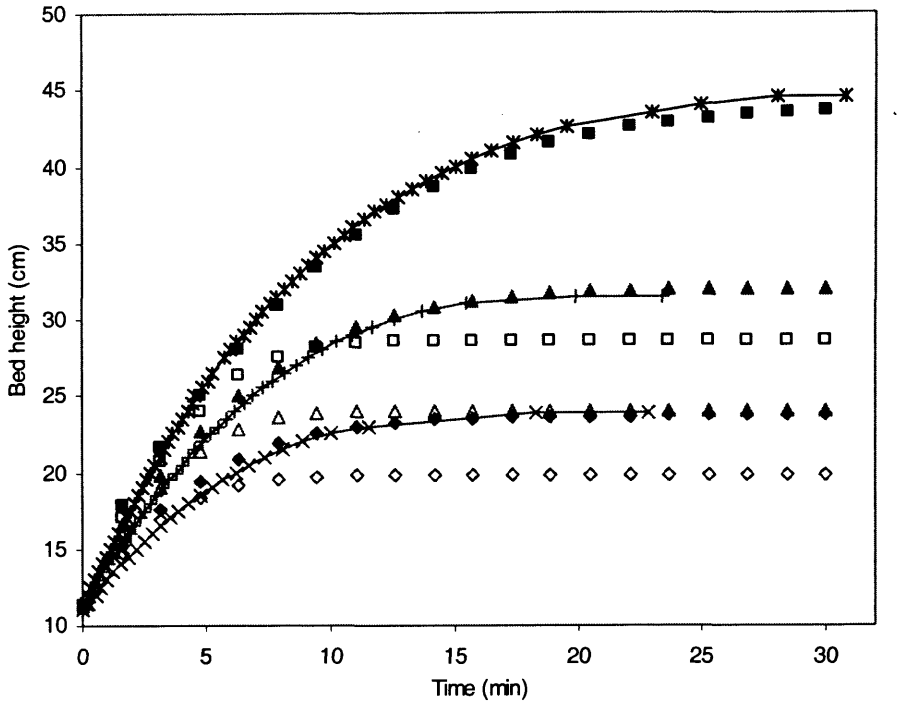

Fig. 5.3 Transient bed heights predicted using Transient mono-sized bed hydrodynamic model for a data set produced in this thesis at different fluid velocities. Three sets of results are shown. Parameters (n and v_t) are fitted in the first set (PF). Parameters are not fitted in the second set (NF). Final set is experimental data (EX). ■, 241 cm/h PF; ▲, 180 cm/h PF; ♦, 108 cm/h PF; □, 241 cm/h NF; △, 180 cm/h NF; ◊, 108 cm/h NF; *, 241 cm/h EX; +, 180 cm/h EX; x, 108 cm/h EX.

The results showed that depending upon the particular process situation, parameter fitting can be important when a mono-sized bed approach is followed. It may be possible to obviate or to minimise the need for parameter fitting by improvement in the modelling by consideration of the effect that particle size distribution (PSD) has on expansion.

5.8 Conclusion

The assumption of a mono-sized bed model accurately predicts the bed height of an expanded bed when the Richardson-Zaki correlation parameters along with particle dispersion coefficient are fitted. As correlations are available for both of those parameters, it is in principle possible to simulate without fitting any parameters and depending upon the system, the result may be close to the experimental data. In some

cases however, the error can be too large to be of any practical use and parameter fitting can become necessary. The approach to use can be decided based upon the closeness of prediction based on the correlation to the steady state result.

There is one additional weakness in the mono-sized bed modelling approach. In reality there is a large particle size distribution, and a big axial variation in voidage which is particularly important to account for when representing the bed's adsorption behaviour. The models developed so far would not able to represent such axial variations and their subsequent effect on adsorption when integrated with an adsorption model. Besides, such a mono-sized bed model will not be adequate when any axial variation of particle size distribution requires to be accounted for. In order to achieve such a capability a general transient hydrodynamic model will have to be developed which will be able to accommodate for the existence of PSD and their axial variations. Such a model will be able to predict the overall impact that this will have on the EBA behaviour. Thus this is recommended as a future work. A preliminary work in that direction has been carried on and included in an appendix.

Mono-sized bed transient hydrodynamic model established in this chapter will be used to formulate an integrated transient hydrodynamic EBA model in chapter 8. Before that, an integrated EBA model with steady state hydrodynamics will be developed in the next chapter

6 Integrated Model: Steady State Hydrodynamics

6.1 Introduction

The hydrodynamic aspects of any model to simulate Expanded Bed Adsorption (EBA) rely upon an ability to predict the bed expansion and the rate of movement. Such models are based upon fluid velocity and particle size distributions and have been described and developed in earlier [Chapters 4 and 5]. However, the most important objective from an industrial point of view is the adsorption behaviour. Adsorption models to predict the response of a packed bed chromatography are well established, but this is not the case for EBA. In spite of importance of EBA as a key downstream tool in protein purification, there is a lack of accurate comprehensive models, which take into account its unique nature and are able to predict its behaviour. There were very few papers available which dealt with EBA modelling at the outset to this thesis. Over the intervening years there are number of EBA adsorption modelling papers have been published and which bear on the work of this doctorate. The details of the key contributions are reviewed in the following section. It is however clear that the models developed and available to date are still far from providing an accurate representation of EBA. Some of the important aspects of EBA like the appropriate integration of bed hydrodynamics and adsorption, the existence of mixed bed, the accurate representation of particle dispersion, use of multi-component models, etc. are still lacking. This thesis sets out to fill major part of this gap and to make a more comprehensive and accurate integrated model of EBA.

6.2 Literature Review

Work by Draeger and Chase (1990), Wiblin et al. (1995) are among the earliest in EBA modelling where each adopted packed bed chromatography model. Wiblin et al. used BIOSEP Simulus (AEA Technology, Didcot, UK), a software package to simulate packed bed adsorption process to predict adsorption of α-amylase onto Streamline DEAE. Such models consider the bed to be mono-sized and of a uniform voidage along the bed axis.

The assumption of a homogeneous bed with constant bed voidage and particle size along the axis is far from reality. So a second major improvement was to assume the bed

was composed of a few different beds or segments in series such that each segment has its own physical properties like bed voidage and particle size, that are assumed constant within each segment. This is a much better approach than the former and captures some of the fundamental properties of EBA. Towards using this approach, Bruce and Chase (2002) divided the bed into 3 discrete segments or zones for simulation purposes. Average voidage, particle sized distribution, axial liquid dispersion for each segments were experimentally determined. Other parameters were fitted from experimental data. As done by Wiblin et al., they also used BIOSEP Simulus software to simulate, each segment (or in the case of a uniform bed the whole bed) as a set of packed bed each with its specific parameter values. They demonstrated that the inclusion of such axial variation in bed properties improved the accuracy of the model prediction. Lysozyme-Streamline SP and Bovine serum albumin (BSA)-Streamline DEAE were used as the model systems.

An improvement in this is instead of applying a few discrete segments the bed is considered perfectly classified bed (PCB) so the bed properties are allowed to vary more uniformly as given by PCB hydrodynamic models. Wistrand and Lacki (2002) developed this approach and demonstrated its effect in the prediction of EBA performance. Yun et al. (2005) also adopted this approach for the integration of PCB hydrodynamics and adsorption to formulate an EBA model and tested it against BSA-Streamline DEAE and lysozyme-Streamline SP model systems.

EBA models have also become more realistic by the representation of the distribution of particle sizes and the variation of axial bed voidage. In all cases to this point however particle dispersion was ignored. Although the bed was considered as a homogeneous mono-sized, Wright and Glasser (2001) were able to develop a model by introducing the effect of particle dispersion.Using the model they predicted the lysozyme adsorption in Streamline SP and S-HyperD LS resin and found the result to be in close agreement with the experimental data. This model was adopted by Tong et al. (2002) to predict the lysozyme breakthroughs in EBA using a specialised dense adsorbent CB-NFBA (a customised Nd-Fe-B alloy-densified agrose gel modified with Cibacron Blue 3GA). Similarly Chen et al. (2003) used the model to simulate EBA for the adsorption of BSA to DEAE Spherodex M (BioSepra) where a yeast cell suspension was used as feedstock. Both of them found that the model predictions were in good agreement with the experimental data.

Li et al (2004) followed the model developed by Wright and Glasser but improved upon it by considering 3-discrete segments of the bed based upon particle size as done by

Bruce and Chase (2002) and its associated voidage instead of taking one single homogenous bed. Experimental data were used to define bed properties in those segments instead of getting them from hydrodynamic model. They validated the model using a lysozyme-Streamline SP breakthrough data set of Bruce and Chase (2001, 2002). Li et al. (2005) in their second paper on EBA modelling, used the same model but instead of using 3 discrete segments, developed an empirical interpolation function to estimate particle size and voidage along the bed axis based on experimental data. They successfully tested the model on adsorption of BSA in both Streamline DEAE (first generation adsorbent with low density base matrix, wide particle size distribution (PSD) and ligand sensitive to ionic strength and salt concentration) and Streamline direct CST I (second generation adsorbent with high density base matrix, narrow PSD and ligand not sensitive to ionic strength and salt concentration). The limitation of these approaches is the bed properties are specified using an experimental data. So not only the existence of such experimental data is a pre-requisite but also the inability to predict when fluid velocity is changed. Furthermore, the approach of including the particle dispersion effect in the model has an important weakness, which will be discussed in Chapter 7.

Representing the bed as a PCB instead of homogenous mono-sized is an important step in improving EBA modelling. Another important step to achieve an even more realistic representation is by consideration of mixed bed (MB) instead of PCB. The natural reality of the expanded bed is the existence of mixed particle sizes in any axial location. This moderates the difference in mean particle size and voidage along the bed axis. PCB model will estimate a much wider difference than is true in reality. The MB approach will naturally solve this problem and will make the estimation of bed properties along the bed axis more accurate. At the start of this thesis, little work has been published in the area of EBA adsorption modelling. Over time, this has changed. Hence, to reflect this, developing a mixed bed approach to EBA modelling, keeping track of differences in adsorption state in different particle size categories, has been taken as one of the major themes of this thesis. A similar approach was eventually developed by Kaczmarski and Bellot (2005). They used experimental data to define the bed properties. Using a few data points of the mean particle size variation along the bed axis, they interpolated the mean of PSD along the bed axis. Assuming the standard deviation of the distribution to be constant along the axis, the volume fraction of size categories was computed to represent the bed as a mixed bed. Although PSD was considered, bed voidage was considered constant throughout the bed. These values are then used to calculate parameters for

adsorption model. Consideration of mixed bed is an important contribution of this paper and it would represent as one additional milestone in EBA modelling. However, the assumption of constant bed voidage throughout the bed in spite of considering PSD is an important weakness in this approach especially as bed voidage is a critical parameter. In addition, as the bed properties are interpolated from experimental data, this model can not handle change in operating conditions like fluid velocity, fluid and particle properties, etc.

Hence formulating a complete integrated model of EBA, which would solve the problems and weaknesses existing in the currently available models, is seen as important. The next section of this thesis describes the objectives and approach for making such a model.

6.3 Plan and Objectives

In this work the EBA model will be gradually improved. Here hydrodynamics is considered to be at steady state equilibrium so resulting in an EBA model which is treated as being similar to a packed bed but with relevant parameters (Pe_i, ξ_i, η_i, Bi_i) as functions of axial position (z). Such parameters are determined using an independent hydrodynamic model based on the Richardson-Zaki correlation. The following five stages were identified for modelling progressively from a simplified approximation of the system to a more realistic physics.

1. Mono-sized bed adsorption model (MSBA)
2. Perfectly classified bed adsorption model (PCBA)
3. Mixed bed model – equivalent diameter approach (MBEQD)
4. Mixed bed size partition model (MBSP)
5. Mixed bed particle dispersion model (MBPD)

At first, the steady state PCB hydrodynamic model will be integrated with an adsorption model. This way the parameters at the different axial position of the bed required for the adsorption part of the model will be determined by the hydrodynamic element of the model. Consideration of the axial particle size distribution in the bed using a mixed bed approach will be another major improvement. This will bring the EBA model closer to reality. In the beginning, the mixed bed is used just to determine the hydrodynamic parts of the model and a simple equivalent diameter based on axial PSD is

used for the adsorption part. Later the distribution of particle sizes at a given axial position is explicitly considered also in the adsorption part of the model by applying size partitions. This means evaluating adsorption in different particle size ranges at each axial position. Further improvement can be done by incorporating particle dispersion into the model for each size species. However, the inclusion of particle dispersion effect in EBA model will not be performed in this part of the work and will be attempted in the next chapter.

The objectives of this chapter are:

- To integrate adsorption and steady state hydrodynamic parts of an EBA model so as to represent a complete EBA system
- To compare the quality of the representation of EBA using different modelling approaches.

6.4 Mono-sized Bed Model

6.4.1 Introduction

The mono-sized bed model is the simplest EBA model where the bed is considered to be homogeneous and mono-sized. Both particle size and bed voidage will remain constant throughout the bed. The bed voidage and total bed height will be given by the hydrodynamic part of the model as described in section 4.5. Such estimated values can be used in a chromatography model as described in section 3.4 to predict the EBA adsorption response. Though this is a simple approach, it provides a rapid means by which to use existing packed bed models or software tools to make EBA predictions. This approach with minor variations was used by Bruce and Chase (2001) to predict the EBA response using BIOSEP Simulus software developed for packed bed chromatography. As the first step towards EBA modelling this approach has been implemented here.

6.4.2 Model development

The bed is considered a homogeneous mono-size, so it will look like a packed bed. The bed expansion and its properties are given Eq. (4.10) along with Eqs (4.7) and (4.8) as

described in chapter 4.5. When predicted bed height does not match with the real height, as discussed in section 4.5, the parameters will have to be fitted using Eq. (4.11).

Application of this system of equations will give constant bed voidage throughout the bed. As both particle size and bed voidage will be constant, the adsorption part of the model will be same as that of packed model described in section 3.4 and given by set of equations (3.83)-(3.97).

6.4.3 Parameters Estimation

There are 3 main parameters: liquid dispersivity (E_i), component species diffusivity (D_i), film mass transfer coefficient (K_{fi}) and 2 isotherm parameters used in the adsorption part of the model. Isotherm parameters were used as published by Bruce and Chase (2001). They are normally determined from batch experimental data. The remaining 3 parameters were estimated based on correlations as described in the chromatography modelling chapter (section 3.5).

For the hydrodynamic part, the Richardson-Zaki correlation parameter was determined using *Ga* based correlation but natural terminal velocity was modified using a fitting parameter to match the observed final bed height.

6.4.4 Simulation

Since a mono-sized bed model is essentially the same as a normal packed bed chromatography model, its discretisation and simulation can be performed as described in section 3.5 using FEM for the bulk phase and Orthogonal Collocation for the particle phase. The resulting ODE systems were solved using MATLAB's stiff ODE-solver. The hydrodynamic part, which remains independent, has its values determined as described in the section 4.5. For simulation 12 elements for bulk phase were used, 2 internal orthogonal collocation points for the particle phase and single component were used. These computational parameters gave converging results.

Convergence Analysis

Computational validation of the simulation result, was done using different element numbers. As discretisation becomes smaller or the number of elements increased results a

smoother and more accurate. Use of 12 elements was found to be sufficient for the convergence of the result as shown in Fig. 6.1. Beyond this as element number increased the solution converged. The converged solution was close to the experimental data.

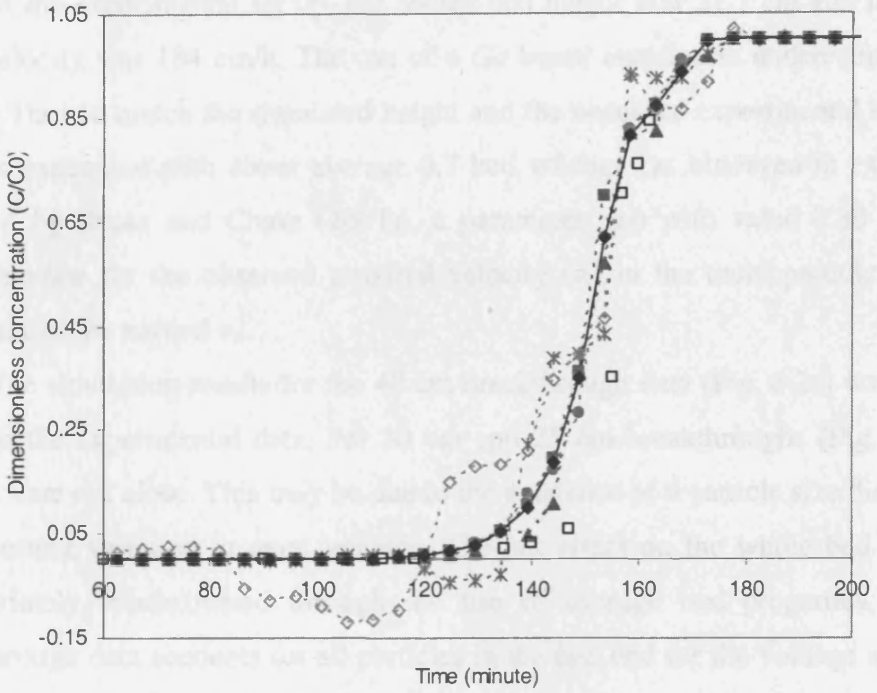

Fig. 6.1 Convergence analysis of breakthrough curves at 40 cm bed height using Mono-sized bed adsorption model. *en* is number of elements used in the simulation. ◊, 2 *en*; *, 4 *en*; ▲, 8 *en*; ●, 12 *en*; ■, 25 *en*; ♦, 50 *en*; □, experimental data.

6.4.5 Results and Discussion

Simulations were performed for the Lysozyme-Streamline SP data set of Bruce and Chase (2001) to predict the breakthrough at 10 cm, 25 cm and 40 cm axial positions of the bed. Particles size distribution (PSD) of the Streamline SP matrix was taken to be of 192 μm mean and 51 μm std. deviation as estimated by Bruce and Chase (2001). The range of particle size was taken to be 90-450 μm as estimated by Yun et al. (2004). These are slightly different from the manufacturer specified 200 μm average particle diameter and 100-300 μm range. For the mono-sized bed model, an average particle size of 192 μm was used to represent the whole bed. The density of particle was considered to be 1.184 g/cm^3 as by Yun et a. (2004) which was close to the manufacturer's specification of 1.2 g/cm^3. Fluid density and viscosity of the sample in phosphate buffer were taken to be 0.99

g/cm^3 and 0.102 gm/cm.s respectively. Coulson (1991) estimated the voidage in a packed bed for different diameter spherical particles to be in the range of 0.395-0.415. Based on it the settled bed voidage was taken as 0.4. Particle pore voidage was taken to be 0.35 as described by Li et al. (2004).

In the experimental set up, the settled bed height was 21.2 cm and the superficial fluid velocity was 184 cm/h. The use of a *Ga* based correlation underestimated the bed height. Thus to match the simulated height and the observed experimental bed height for 2 times expansion with about average 0.7 bed voidage (as observed in experiment and reported by Bruce and Chase (2001)), a parameter (a_1) with value 0.80 was fitted to accommodate for the observed terminal velocity (v_t) in the multi-particle environment compared to the natural v_t.

The simulation results for the 40 cm breakthrough data (Fig. 6.2a) was found to be close to the experimental data. For 10 cm and 25 cm breakthroughs (Fig. 6.2 b,c), the results were not close. This may be due to the existence of a particle size distribution and the resulting variation in axial voidage. The net effect on the whole bed can be more appropriately approximated through the use of average bed properties. The 40 cm breakthrough data accounts for all particles in the bed and for the voidage along the bed. On the other hand, breakthrough data at 10 cm and 25 cm consider only part of the bed. The bed being partially classified, it follow then that the average particle size is larger and the voidage smaller at lower parts of the bed. In such cases the use of average properties to represent them, means the particle size and voidage assumed is larger in simulation than it is in reality. Thus, breakthrough comes earlier than for the real experimental data. To correct these problems, instead of assuming mono-size, the existence of particle size distribution (PSD) will be considered in the next section.

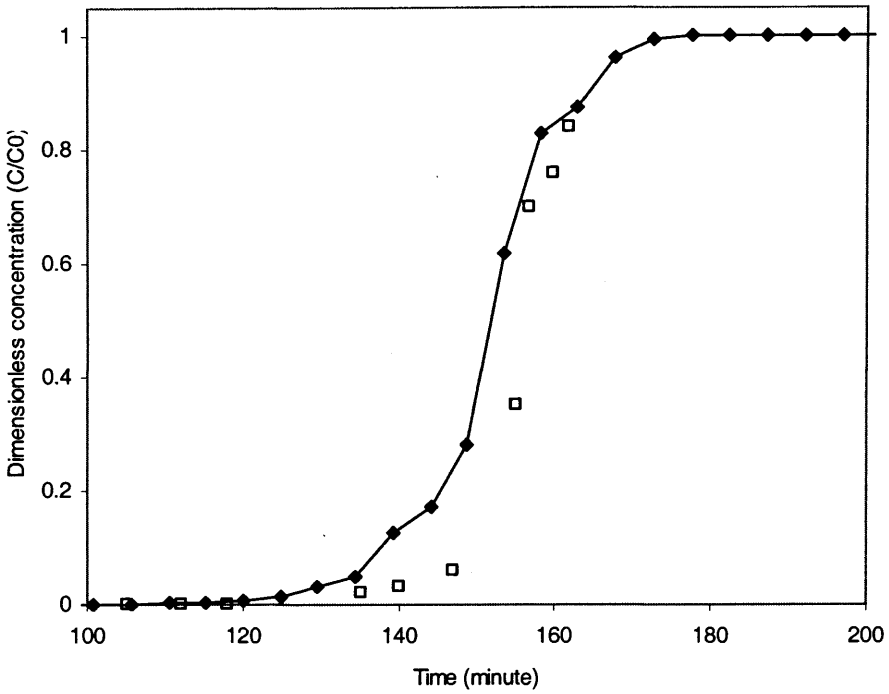
Dimensionless concentration (C/C0)
1
0.8
0.6
0.4
0.2
0
100
120
140
160
180
200
Time (minute)

(a)

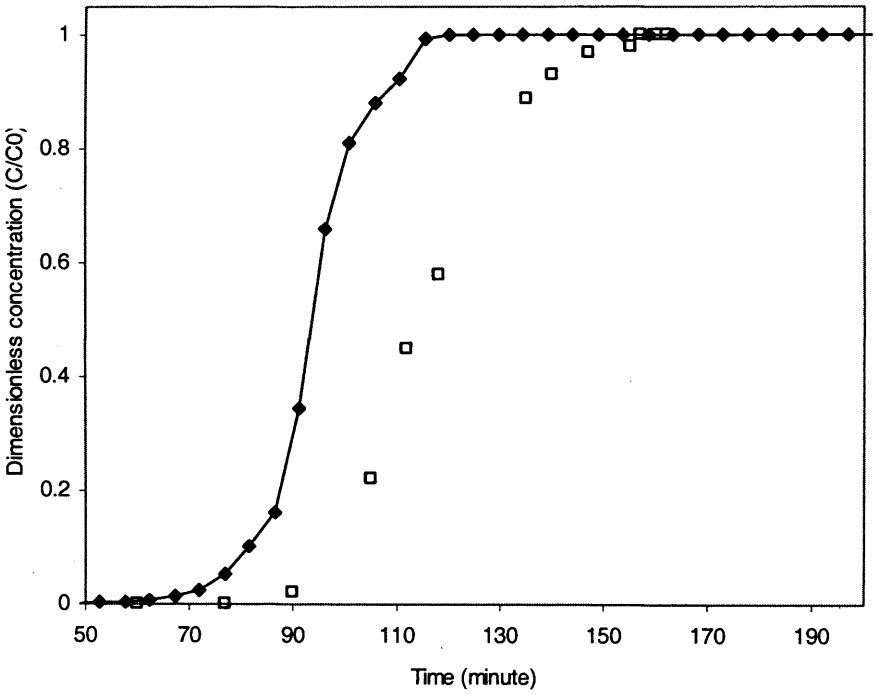
Dimensionless concentration (C/C0)
1
0.8
0.6
0.4
0.2
0
50
70
90
110
130
150
170
190
Time (minute)

(b)

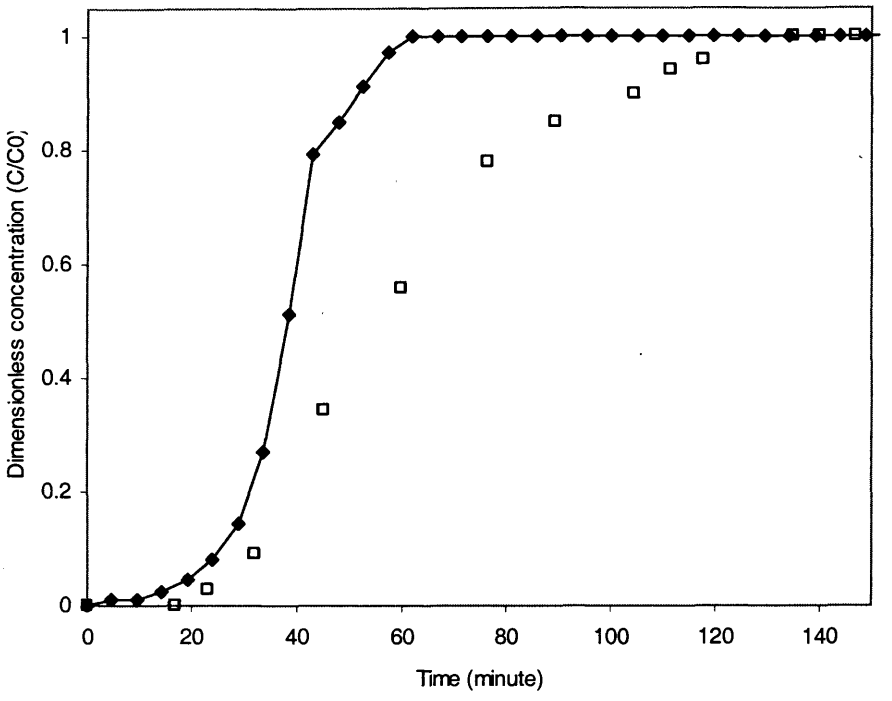

(c)

Fig. 6.2 A breakthrough curve simulated by a Mono-size bed model at bed height (a) 40 cm, (b) 25 cm and (c) 10 cm. Experimental data set is from Bruce and Chase (2001). ♦, simulation; □, experimental data.

In spite of the fact that mono-sized bed model did not represent the concentration profile along the bed axis well due to the neglect of PSD and resulting axial variation in bed voidage, it does represent successfully the aggregate-average effect of the bed as a whole reasonably. Therefore, despite its simplicity, it seems possible to use it to make a crude estimate of EBA behaviour. This is especially useful as existing packed bed modelling software tool can be employed for the purpose.

6.5 Perfectly Classified Bed Model

6.5.1 Introduction

There exists a particle size distribution (PSD) in EBA, which the mono-sized bed model does not account for. One of the simplest ways to include the distribution of particle size is by assuming the bed to be perfectly classified. Here each class or category of particle size will form a segment one above another, the largest being at the bottom. The

expansion and voidage of each segment will be given by a perfectly classified bed (PCB) hydrodynamic model. The adsorption at each segment will be the same as in packed bed chromatography using average bed-segment properties: mean segment particle size and voidage. As this PCB model accounts for the distribution of particle sizes and its classification along the bed axis based on size and continuous axial change in voidage, it represents the EBA more accurately and thus its predictions are of more significance and can be expected to be more accurate. Wistrand and Lacki (2002) developed this approach and demonstrated its effect in the prediction of EBA performance using Streamline DEAE column. Yun et al. (2005) also adopted this approach for the integration of PCB hydrodynamics. This approach of EBA modelling is developed and implemented here as an intermediary step to develop more advanced mixed bed model in the next section.

6.5.2 Model Development

Compared to the mono-sized bed explained earlier, the model will be improved by consideration of the changes of physical properties of the bed including particle size and voidage as given by the PCB hydrodynamic model. The nature of integration though will remain essentially the same.

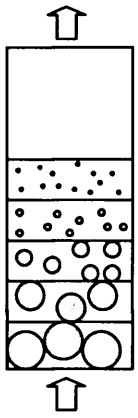

Fig. 6.3 A perfectly classified bed adsorption showing stratification of particles based on their size. The adsorption at each layer is given by cumulative adsorption of all particles in that layer.

The bed is considered to be completely segregated based on particle sizes (Fig. 4.2) as in the hydrodynamic PCB model discussed in Chapter 4. This is integrated with an

adsorption model of chromatography discussed in Chapter 3 as shown in the flow chart below (Fig. 6.4).

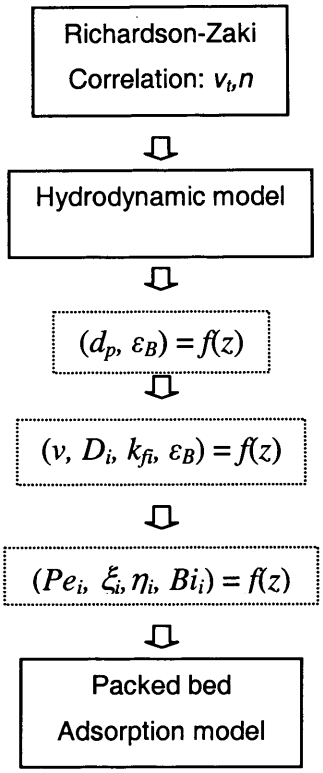

Fig. 6.4 Flowchart of integration of hydrodynamic and adsorption parts of EBA model

Using the PCB model the bed is divided into series of segments. Each segment is considered to be of homogeneous bed properties. Thus in totality the system will look like different packed bed columns in series. The hydrodynamic model is independent of the adsorption part. The only purpose of the hydrodynamic model is to estimate the parameter values at different axial positions in the bed. These parameters are then used in the adsorption part of the model to represent a complete EBA system. In the case where experimental data of axial d_p and ε_B are available, these can also be directly used especially to check the validity of the model or for achieving a more accurate simulation result. The automatic estimation of such parameters by use of a hydrodynamic model without need of experimental data is a key benefit of using in integrated EBA model.

Thus the hydrodynamics is represented by set of equations (4.19), (4.20), (4.6)-(4.8) of PCB hydrodynamic model as described in chapter 4.6.2. As in earlier section, if predicted bed height differs from the real height significantly, as discussed in chapter 4.5,

the parameters will have to be fitted using Eq. (4.11). In such a case, the fitted parameters, a_1, a_2, will be assumed constant irrespective of particle sizes.

The above hydrodynamic part will gives bed voidage and particle size as a function bed height. These are then used to calculate parameters for each segment which will be taken as a segment of a packed bed. Similar to previous section of mono-sized bed model, the bed is represented by packed model described in section 3.4 and given by set of equations (3.83)-(3.97) but with axial variation in parameters and bed properties.

6.5.3 Parameters Estimation

The parameters (E_i, D_i, K_{fi}, b_{0i} and b_{1i}) for the adsorption part of the model and the method for their estimation in PCB model are the same as in the mono-sized bed model described earlier. For the hydrodynamic part, the Richardson-Zaki correlation parameter was determined using Ga based correlation. If required, fitting parameters could be employed to match the final bed height.

6.5.4 Simulation

As in the previous section for the mono-sized bed model, the discretisation and simulation were performed as described in section 3.6 using FEM for bulk phase and Orthogonal Collocation for particle phase. The resulting ODE systems were solved using MATLAB's stiff ODE-solver. The hydrodynamic part was kept as an independent part, and their values were determined as described in the section 4.6. Particle size and bed voidage data as a function of axial position in the bed estimated from hydrodynamic part of the model were used to interpolate such values at the middle node of elements. The parameters computed based on such values were taken as constant within that element to make the computation simpler and faster though at the loss of some accuracy. Providing the finer discretisation using a large number of elements, such a loss in accuracy will be minimal and contained especially as the bed properties are continuous functions with no sharp gradients. For simulations 12 elements were used for the bulk phase, 2 internal orthogonal collocation points were used for the particle phase, 1 component species was assumed and 40 particle size categories were used. These computational parameters gave converging results.

Convergence Analysis

To achieve computational validation of the simulation results, a convergence analysis was performed using different element numbers. As the level of discretisation became smaller or the number of elements was increased, so the result became smoother and accurate. Use of 12 elements was found to be sufficient for the convergence of the result as shown in the Fig. 6.5. As element number is increased, the solution converged. The converged solution was also broadly close to the experimental data.

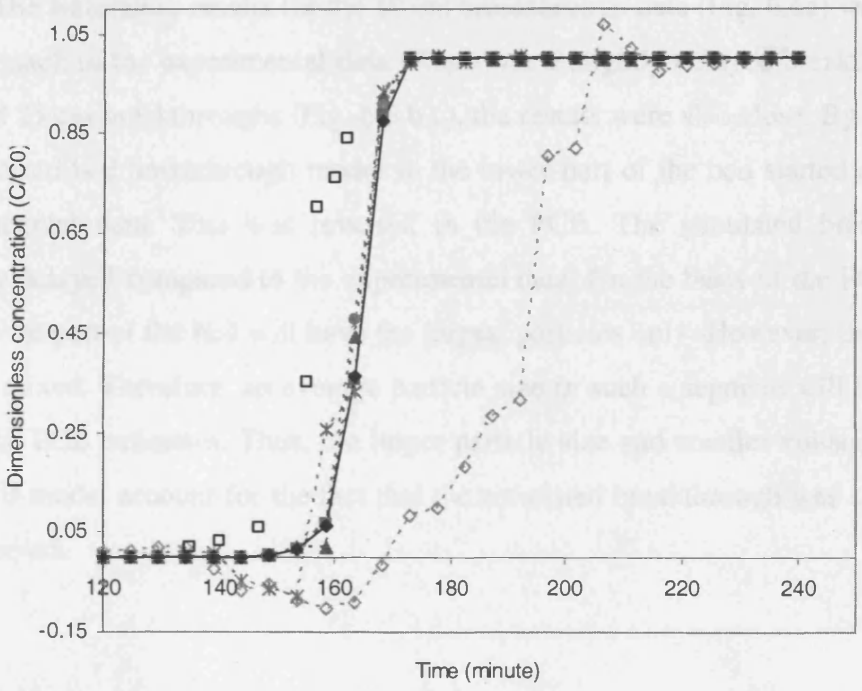

Fig. 6.5 Convergence analysis of breakthrough curves at 40 cm bed height using Perfectly classified bed adsorption model. *en* is number of elements used in the simulation. ◊, 2 *en*; *, 4 *en*; ▲, 8 *en*; ●, 12 *en*; ■, 25 *en*; ♦, 50 *en*; □, experimental data.

6.5.5 Results and Discussion

The Lysozyme-Streamline SP data set of Bruce and Chase (2001), as used and discussed in the previous mono-sized bed model (section 6.4), was used to predict the breakthrough at 10 cm, 25 cm and 40 cm axial positions of the bed. Particles size distribution (PSD) of the Streamline SP matrix was considered to be of 192 μm mean and 51 μm std. deviation

with range of 90-450 μm as described in previous section (6.4.5). This PSD value was used in the hydrodynamic part of the model.

In the experimental set up, the settled bed height was 21.2 cm and the superficial fluid velocity was 184 cm/h. While using PCB model, the use of *Ga* based correlation slightly underestimated the bed height. Thus to match the simulated cumulative height of all size classes and the observed experimental bed height for 2 times expansion with an average 0.7 bed voidage (as observed in experiment and reported by Bruce and Chase (2001)), a parameter (a_1) with value 0.95 was fitted to accommodate for the observed terminal velocity (v_t) for each particle size category.

The simulation results for the 40 cm breakthrough data (Fig. 6.6a) were found to be a fair match to the experimental data. There was a slightly delayed breakthrough. For 10 cm and 25 cm breakthroughs (Fig. 6.6 b,c), the results were also close. By contrast, in the mono-sized bed breakthrough model in the lower part of the bed started earlier than the experimental data. This was reversed in the PCB. The simulated breakthrough was slightly delayed compared to the experimental data. On the basis of the PCB hypothesis, the lowest part of the bed will have the largest particles only. However, the real bed is in reality mixed. Therefore, an average particle size in such a segment will be smaller than what the PCB estimates. Thus, the larger particle size and smaller voidage estimated by the PCB model account for the fact that the simulated breakthrough was slightly delayed as observed.

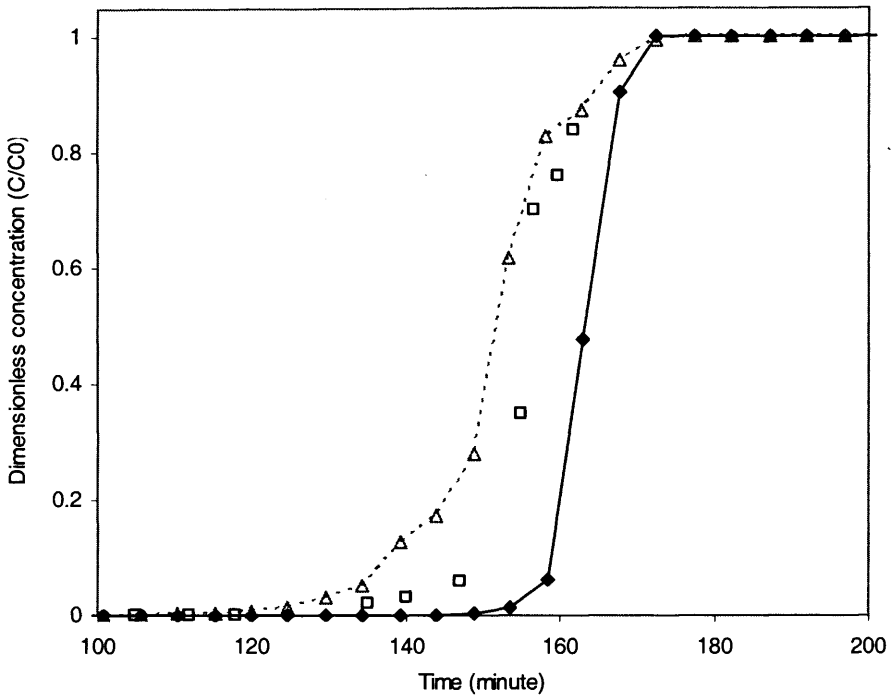
Dimensionless concentration (C/C0)
1
0.8
0.6
0.4
0.2
0
100
120
140
160
180
200
Time (minute)

(a)

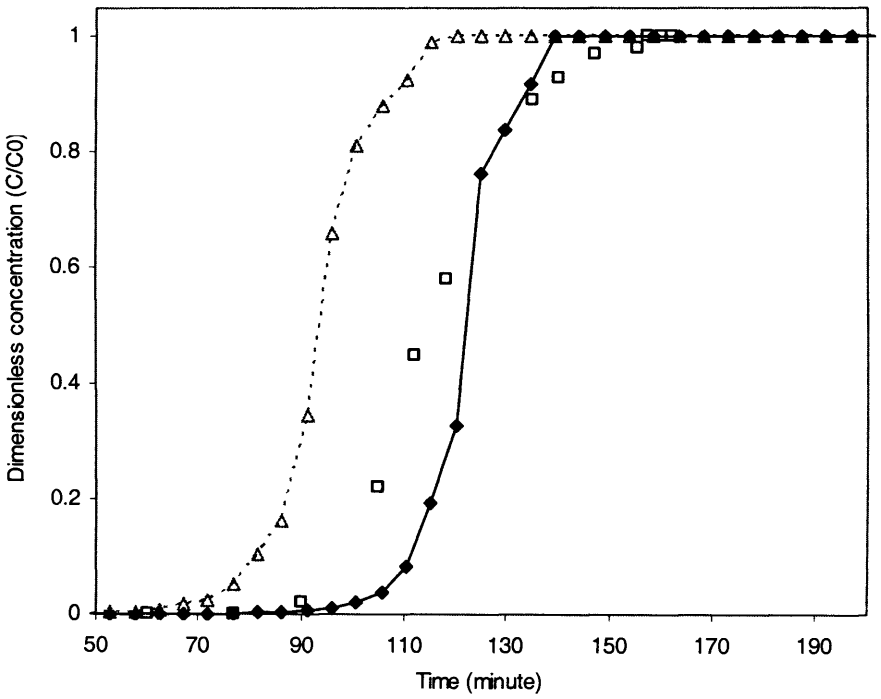
Dimensionless concentration (C/C0)
1
0.8
0.6
0.4
0.2
0
50
70
90
110
130
150
170
190
Time (minute)

(b)

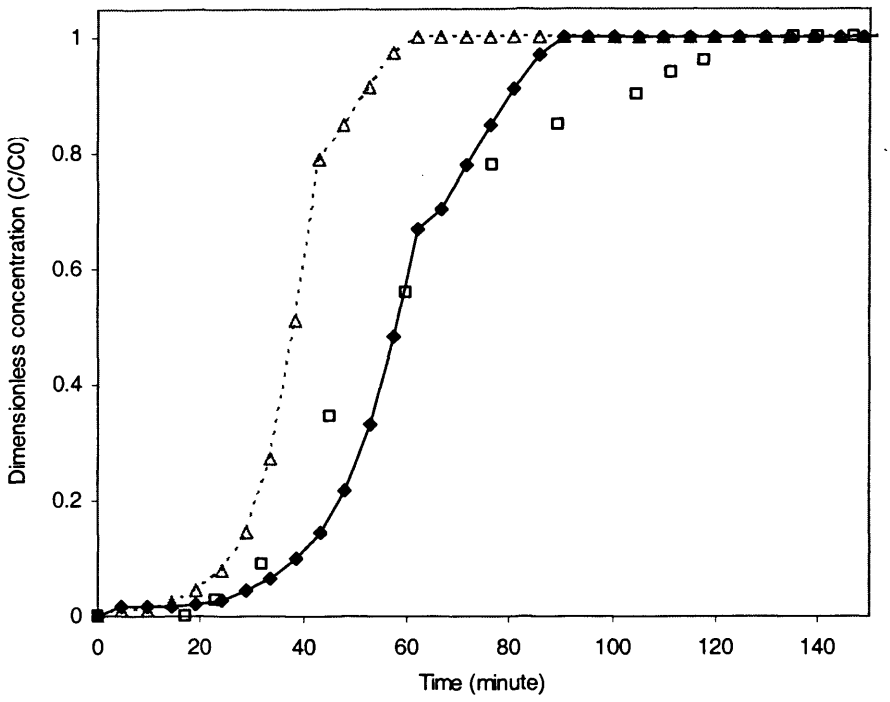

(c)

Fig. 6.6 Breakthrough curves at (a) 40 cm (b) 25 cm and (c) 10 cm bed heights as simulated by perfectly classified bed and mono-size bed models. ♦, perfectly classified bed model simulation; Δ, mono-sized bed model simulation; □, experimental data.

The PCB model predictions were found to be slightly better than the mono-sized bed model and especially so for the lower parts of the bed. The mono-sized bed and PCB model are two extremes of reality. The real bed being mixed lies in between them. This is clearly demonstrated by the fact that the experimental data lies in between the simulation results of the mono-sized bed and PCB models at all axial positions. In general, at 40 cm (about the end of the bed), the breakthrough curve of mono-sized bed and PCB was expected to be similar, as both will represent the aggregate effect of the whole bed. However, delayed breakthrough for the PCB model even at 40 cm indicated that the axial variation of particle size and voidage is still important in controlling the computed results at the bed outlet.

The data set of Bruce and Chase (2001), has also been simulated by Yun et al. (2004) using a similar perfectly classified bed modelling approach. Their prediction was also close to the experimental data but could not capture the slow rate of rise of component concentration before it reaches to its saturation or maximum value at the lower parts of the bed.

The result obtained in this thesis demonstrates that the consideration of an existence of particle size distribution and resulting variation of axial bed voidage are crucially important. To represent the bed more accurately by considering the existence of different particle size at all axial positions a mixed bed model will be developed in the next section.

6.6 Mixed Bed Equivalent Diameter Model

6.6.1 Introduction

The perfectly classified bed (PCB) model accounts for the distribution of particle size, but fails to consider the existence of different sized particles at any axial positions. However, a mixed bed (MB), i.e. various degree of mixing of different particle sizes at all axial positions, is a reality. Due to mixing the extremities of particle size and bed voidage, as projected by the PCB model are avoided. Inclusion of mixing in the model will make the representation of a bed and its adsorption response more in line with reality and thus improve the accuracy of its predictions.

At the outset of this thesis work, no expanded bed adsorption (EBA) model which takes into account the mixed bed to predict an adsorption response existed. Developing such a model became a key objective of the doctorate. In this approach, though bed is considered as a mixed bed for hydrodynamic purposes, for adsorption, only one equivalent particle size, which represents the distribution of size at that axial location, was used. This makes the model simple and represents a first pragmatic step towards a more involved mixed bed model of EBA. In spite of its simplicity, it captures some essential aspects of expanded bed. Recently Kaczmarski and Bellot (2005) proposed a more involved mixed bed model that is similar to the MB-size partition model developed in the next section. Here a simple mixed bed model based on an equivalent diameter approach will be developed and validated using available experimental data.

6.6.2 Model Development

Model development was similar to the PCB model as described earlier in section 6.5.2. The hydrodynamic part and the adsorption part of the model were integrated as described

in Fig. 6.4. The only difference was the hydrodynamic part of the model. Instead of assuming a PCB model, a mixed bed approach was followed so that the existence of a PSD at any axial position is considered. The equivalent diameter of representative particle size of the segment was calculated based on the mass/volume average (with assumption of constant density).

Equivalent diameter at axial position j (d_{pj}):

$$d_{pj} = \frac{\sum_i \phi_{ij} d_{pj}}{\sum_i \phi_{ij}} \tag{6.1}$$

where ϕ_{ij} = mass (or volume) fraction of particle size sp. (d_{pi}) at axial position j. (Density is considered constant.)

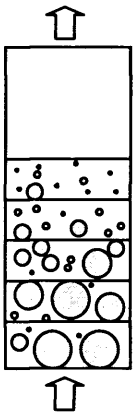

Fig. 6.7 A mixed bed adsorption showing co-existence of particles of different sizes at each axial position. The adsorption at each layer is given by cumulative adsorption of all particles in that layer.

As in previous section, the bed is again considered as a series of packed bed or segment with its parameters given by d_p and ε_B of each segments. It is important to note at this point that two independent approaches were employed to compute the bed properties, especially axial PSD and voidage:

i. Approximate mixed bed approach
ii. Interpolation using experimental data

The use of two different approaches will help in independent validations of the integrated model developed. The descriptions of these approaches are as follows.

i. Approximate mixed bed approach

In this hydrodynamic mixed bed approach, the fractions of different particle size species along with bed voidage at a given location of the bed is determined by mixing parameter, σ_m, of particle size species with respect to an applied flow rate (v_0) . The detail of such an approach has been explained in detail in section 4.7.

ii. Interpolation using experimental data

When experimental data on EBA bed properties – axial particle size distribution ($PSD|_z$) and voidage ($\varepsilon_B|_z$), are available, they can be used in the model for simulation. This will obviate the need of a hydrodynamic model whose function otherwise would have been to estimate such values. In a normal experimental setting, when point estimates of the particle size distribution (PSD) at few axial positions are available, one simple approach to estimate PSD at other required axial position is to compute mean and standard deviation of the distribution by separately interpolating them using a polynomial function. The combination of estimated mean and standard deviation at a given axial location will then define its PSD. PSD estimate can be used to estimate properties of each size category or partitions at a given axial position.

Relatively few assumptions need to be taken for this approach to be valid. It is assumed that the PSD is normally distributed. From the experimental data of Bruce and Chase (2001), Yun et al. (2004), this seems to be approximately valid for the operating conditions used for the simulation in this work. It was also observed that the variation of mean particle size and standard deviation along the bed axis is continuous and monotonic. Therefore, it is assumed that separate interpolation of mean and standard deviation to estimate PSD at a given axial position is a viable approach.

However, often only interval estimate of voidage are available as determined by blue dextran and acetone based experiments in Streamline columns. In such cases, such interval estimates will have to be first converted to the point estimates, after which normal interpolation can be applied. Alternatively, a correlation of bed voidage as a function of bed height (z) has to be developed using the interval data. A method of developing such a correlation is as follows.

Let bed voidage (ε_B) in an EBA be defined by a polynomial function with the assumption of monotonic continuity of voidage with respect to bed height (z), a cubic function is considered to be enough as given in the following equation.

$$f(\varepsilon_B) = \frac{\varepsilon_B}{\bar{\varepsilon}_B} = a_0 + a_1 z + a_2 z^2 + a_3 z^3 \tag{6.2}$$

where

z = normalised axial position with respect to total bed height (H) = (*Height/H*)

$\bar{\varepsilon}_B$ = average bed voidage

Integrating Eq. (6.2) along axis (z),

$$\int f(\varepsilon_B)\, dz = a_0 z + \frac{a_1}{2} z^2 + \frac{a_2}{3} z^3 + \frac{a_3}{4} z^4 = F(\varepsilon_B) \tag{6.3}$$

An interval-average bed voidage ($\tilde{\varepsilon}_B$) is given by

$$\tilde{\varepsilon}_B\Big|_{z_1}^{z_2} = \frac{\int_{z_1}^{z_2} f(\varepsilon_B)\, dz}{\int_{z_1}^{z_2} dz} = \frac{1}{(z_2 - z_1)} \int_{z_1}^{z_2} f(\varepsilon_B)\, dz = \frac{F(\varepsilon_B)}{(z_2 - z_1)} \tag{6.4}$$

$$F(\varepsilon_B) = \tilde{\varepsilon}_B\Big|_{z_1}^{z_2} (z_2 - z_1) \tag{6.5}$$

Data on an interval-average voidage, $\tilde{\varepsilon}_B\Big|_{z_1}^{z_2}$, are available for different axial positions (z). This gives $F(\varepsilon_B)$ as a function of z. This data can then be used to estimate parameters (a_0, a_1, ...) of Eq. (6.3) by fitting or least square estimation. Thus parameters of ε_B correlation (Eq. (6.2)) are determined. Such correlation can be used to estimate the bed voidage at required axial positions with the bed, operating under same experimental condition.

Once axial PSD and bed voidage are determined, the model parameter values at given axial positions can be estimated. Thus before simulation using this model, the methods employed to estimate the parameters of the model are described in the following section.

6.6.3 Parameters Estimation

The parameters (E_i, D_i, K_{fi}, b_{0i} and b_{1i}) for the adsorption part of the model and their estimation in mixed bed model are same as in mono-sized bed model described earlier. For the hydrodynamic part, the Richardson-Zaki correlation parameter was determined

using *Ga* based correlation but the natural terminal velocity was modified using a fitting parameter to match the observed final bed height. For the mixed bed model the mean mixing sigma (σ_m) value of 40 and σ_m slope (the linear variation of σ_m w.r.t. particle size) of 0.5 was used assuming conditions did not to vary significantly from those used by Willoughby (2000).

While using an experimental data approach, the mixed bed PSD was interpolated from the experimental data. The following relation was used for estimation.

$$\frac{R}{\overline{R}} = 1.333 - 0.8819z + 0.2778z^2 \tag{6.6}$$

$$\frac{\sigma}{\overline{\sigma}} = 0.9935 - 0.3922z + 0.2092z^2 \tag{6.7}$$

where z is normalised axial position with respect to total bed height (H), R and σ are particle radius and its standard deviation at axial position z. Similarly $\overline{R}$ and $\overline{\sigma}$ are mean particle radius and mean standard deviation of the bulk matrix. The bed voidage correlation estimated from the experimental data was:

$$\frac{\varepsilon_B}{\overline{\varepsilon}_B} = 0.6411 + 0.72z \tag{6.8}$$

With these parameter values, the simulation of the model is performed in the next section.

6.6.4 Simulation

As in the previous section for the mono-sized bed and PCB models, discretisation and simulation were performed as described in section 3.6 using FEM for the bulk phase and Orthogonal Collocation for the particle phase. The resulting ODE systems were solved using MATLAB's stiff ODE-solver. The hydrodynamic part was kept as an independent part, and their values were determined as described in section 4.7. Particle size and bed voidage as a function of axial position in the bed estimated from the hydrodynamic part of the model were used to interpolate such values at the middle node of elements. The parameters computed based on such values were taken as constant within that element to make the computation simpler and faster though at the loss of some accuracy. Providing a finer level of discretisation using large number of elements, will minimise any loss in accuracy which will be contained especially as such bed properties are continuous functions with no sharp gradients. For simulations 12 elements for the bulk phase, 2

internal orthogonal collocation points for the particle phase, 1 component and 5 particle size categories were used. These computational parameters gave converging results.

Convergence Analysis

The computational validation of the simulation result via convergence analysis was performed using different numbers of elements. As discretisation becomes smaller or the number of elements increased the result became smoother and more accurate. Use of 12 elements was found to be sufficient to achieve accuracy of the result as shown in Fig. 6.8. As the element number increased so the solution converged. The converged solution is also close to the experimental data.

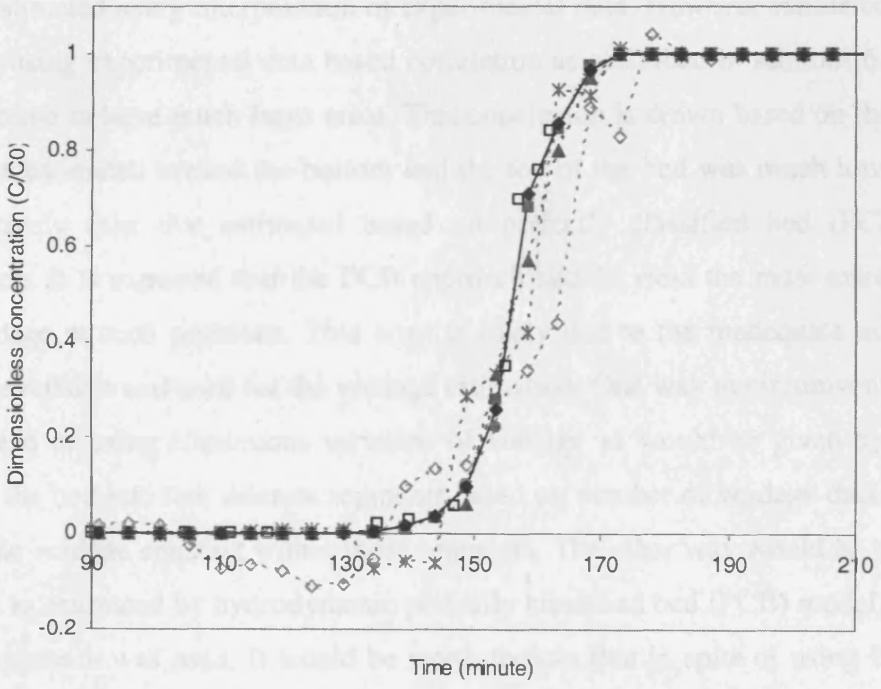

Fig. 6.8 Convergence analysis of breakthrough curves at 40 cm bed height using Mixed bed equivalent diameter model. *en* is number of elements used in the simulation. ◊, 2 *en*; *, 4 *en*; ▲, 8 *en*; ●, 12 *en*; ■, 25 *en*; ♦, 50 *en*; □, experimental data.

6.6.5 Results and Discussion

The lysozyme-Streamline SP data set of Bruce and Chase (2001), as used and discussed in the previous mono-sized bed and PCB models, was used to predict the breakthrough at

10 cm, 25 cm and 40 cm axial positions of the bed. As described earlier two independent approaches were employed to estimate the hydrodynamic bed properties.

In using mixing approach to define mixed bed hydrodynamics, a mixed bed mean mixing sigma value of 40 μm and slope (with respect to particle size) of 0.5 were used based on similar experiment data available from Willoughby et al. (2000). As in the mono-sized bed model described earlier, use of the *Ga*-based correlation underestimated the bed height, and hence a parameter (a_1 in Eq. (4.11)) with value 0.80 was fitted to accommodate for the observed terminal velocity (v_t) in the multi-particle environment. (Parameter a_2 was kept at unity for it to have no effect.) That matched the simulated height and the observed experimental bed height for 2 times expansion with an average 0.7 bed voidage (as observed in experiment and reported by Bruce and Chase (2001)).

While using the experimental data approach, the particle size and its distribution were estimated using interpolation of experimental data. However estimated bed voidage profile using experimental data based correlation as described in sections 6.6.2 and 6.6.3 were found to have much large error. This conclusion is drawn based on the fact that the voidage estimated toward the bottom and the top of the bed was much lower and higher respectively than that estimated based on perfectly classified bed (PCB) modelling approach. It is expected that the PCB approach should yield the most extreme estimates of voidage at such positions. This error is likely due to the inadequate number of data points available and used for the voidage estimation. One way to circumvent this problem is instead of using continuous variation of voidage as would be given by correlations, divide the bed into few discrete segments based on number of voidage data available and keep the voidage constant within those segments. The other way would be to use voidage profile as estimated by hydrodynamic perfectly classified bed (PCB) model. In this work, PCB approach was used. It would be worth to note that in spite of using PCB approach for bed voidage estimation, bed is still considered mixed bed and PSD at each axial position were determined using experimental data as described earlier.

The simulation results for the 40 cm breakthrough data (Fig. 6.9a) was found to almost exactly match with the experimental data when a mixed bed model was used. For 10 cm and 25 cm breakthroughs (Fig. 6.9 b,c), the results were not as accurate as for 40 cm breakthroughs but matched very close at least for the first half (40-50%) of the breakthrough curves. The mixed bed model was found be better for prediction compared to both mono-sized bed and perfectly classified bed (PCB) models. The only drawback is the need for an additional parameter, the mixing sigma. Since the bed is naturally always

in a mixed state, any approximate value will always give a better result than either mono-sized bed or PCB models which represent the boundary for the MB results. The bracketing of predictions using mixed bed assumptions in between those predictions based upon the mono-sized bed and PCB models was clearly visible at all three axial positions investigated.

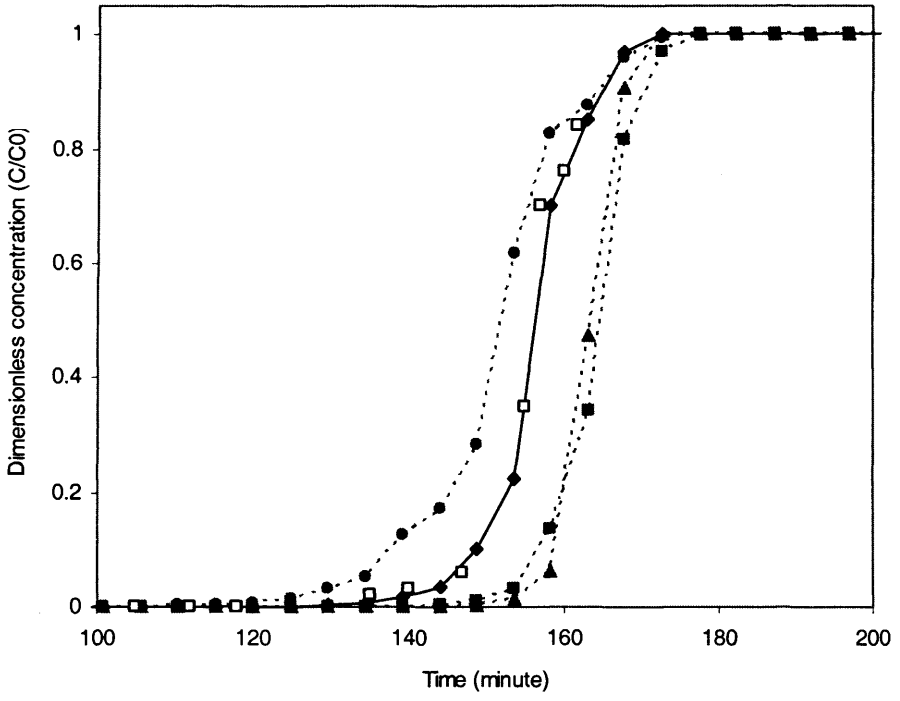

(a)

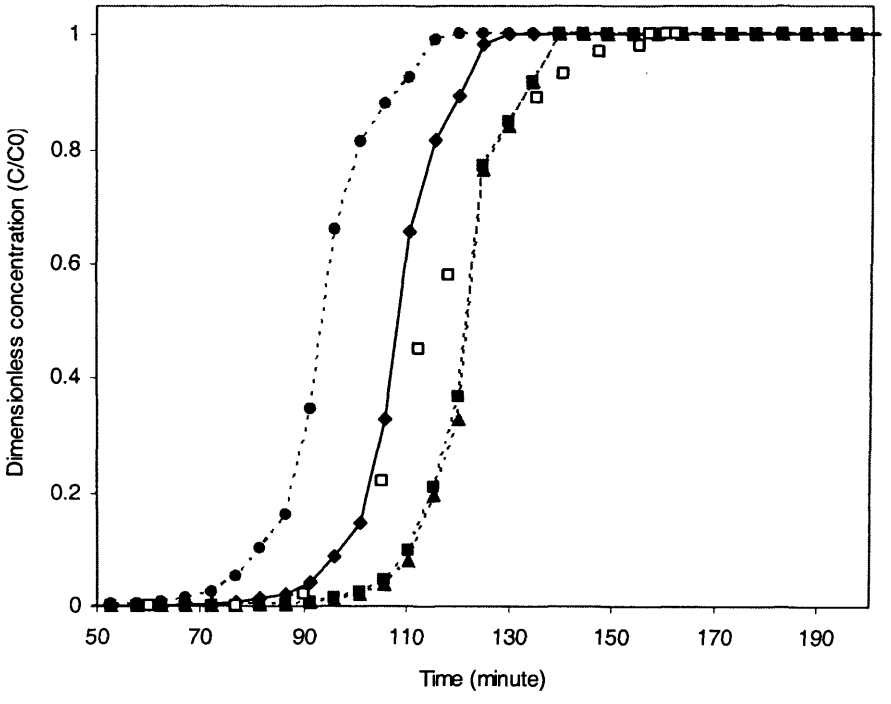

(b)

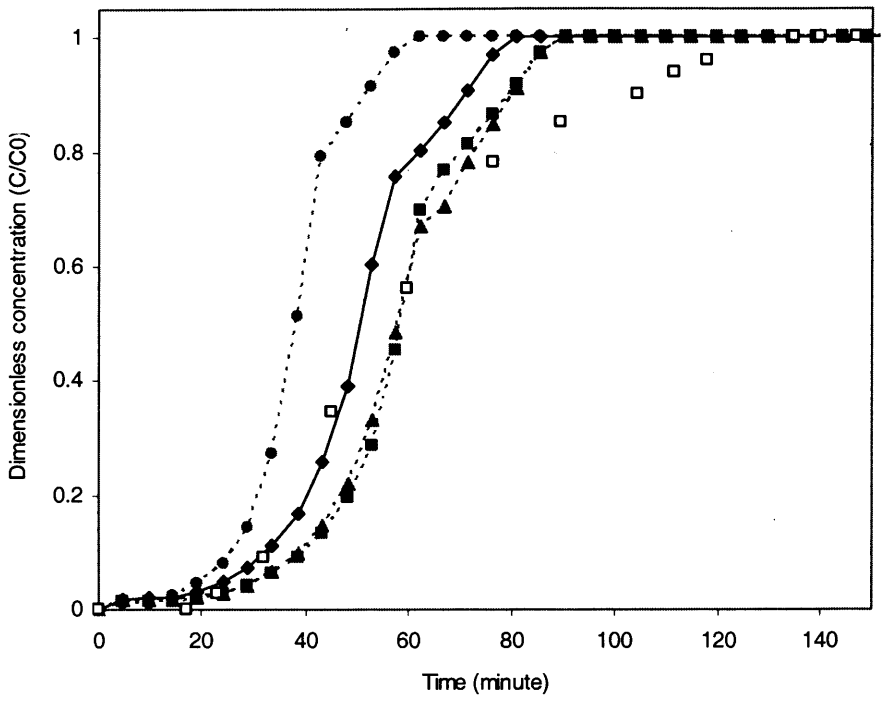

(c)

Fig. 6.9 Breakthrough curves at (a) 40 cm (b) 25 cm and (c) 10 cm bed heights as simulated by Mixed bed equivalent diameter (MBEQD) model, MBEQD model using experimental data for axial particle size distribution (MBEQD-ex), Perfectly classified bed adsorption (PCBA) model and Mono-sized bed adsorption (MSBA) Model. ♦, MBEQD; ■, MBEQD-ex; ▲, PCBA; ●, MSBA; □, experimental data.

In the lower regime of the bed, for example at 10 cm, the particle size is large. Thus, the rate of breakthrough will be slower due to large particle sizes having longer diffusion paths in the particle phase. The PCB result also reflects this phenomenon as the average size of particles in the lower segment in that model is much larger compared to the mixed bed approximation while result of mono-size would naturally become worse as the difference between particle size used in the simulation and the particle size that actually existed becoming significantly different. This can be clearly seen in the above simulation and experimental result. Another reason for such slow rate of breakthrough is likely be due to particle dispersion.

The simulation results of the mixed bed model using experimental data approach, i.e. using experimental data interpolation for PSD and PCB approach from voidage estimation, was very close to the breakthrough prediction using earlier PCB model (section 6.5) for all three axial position as can be seen in Fig. 6.9 a-c. However, it was not that close to the experimental data as compared to the mixed bed model whose

hydrodynamics was determined using mixing approach as described earlier. This was due to the realistic axial variation of voidage estimated in the latter approach compared to that estimated using the PCB approach.

Thus, it is concluded that a mixed bed model provides the best modelling approach to be used for representing EBA among the three modelling approaches described thus far. From the results observed here, it can also be concluded that inclusion of mixing, or defining the bed to be mixed, is important for accurate EBA prediction. Adoption of one equivalent diameter used for the adsorption part of the model appears to be valid representation. This is likely be due to preservation of mass balance of particle phase, whether this was represented by the cumulative fractions of different particles or their weighted average. An important limitation is, although this model provides accurate breakthrough prediction at the bed outlet, it is not able to provide the response of individual size categories. For applications where such information is desired for example, when studying size specific adsorption response to design matrices of optimal physical properties, this model would not be adequate. Hence, use of an equivalent diameter assumption will be relaxed in the next modelling stage, and all size categories will be simultaneously considered at each axial position also in the adsorption part of the model.

6.7 Mixed Bed Size Partition Model

6.7.1 Introduction

Further improvements from the modelling approach adopted in the previous mixed bed model – equivalent diameter approach (section 6.6) may be achieved by taking into account the existence of particle size distribution at each axial position of the bed even for the adsorption part of the model instead of using one representative particle size per segment. This makes the representation of the bed even closer to reality and such a model can be expected to be more accurate and robust. The most important benefit of this approach would be additional information about the system, e.g. the adsorption behaviour to particular size specific particles along the bed axis, etc. Such information can be useful when designing novel matrices for improving bed performance, devising new ways of operating EBA to maximise bed productivity, etc. A similar approach has also been

developed by Kaczmarski and Bellot (2005). They used experimental data to interpolate the mean particle size at different axial positions and assumed the standard deviation of the size distribution to be constant at all axial positions. This provided the size partition proportion for the adsorption part of the model. Furthermore, they assumed constant voidage across the bed. In this part of the work, a mixed bed model with size partition will be developed and verified. As in the previous mixed bed models, the hydrodynamic part will be represented by two independent approaches: mixing method as described in section 4.7 and experimental data.

6.7.2 Model Development

In this approach, each axial segment is further partitioned into sections of different particle size. The size or volume fraction of each such partition was given by the mixed bed hydrodynamic model. However, for expansion purposes and thus to determine an average bed voidage of each segment, a representative particle diameter was used. The partition approach can be seen as in the following figures.

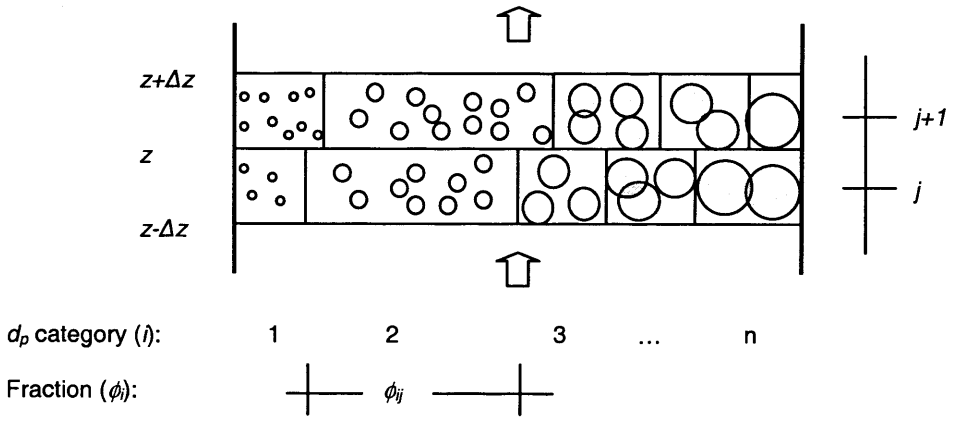

Fig. 6.10 A method of size partition in an axial segment. Each partition (i) consists of particles of only one size or diameter (d_p category). The proportion of such a partition (i) in an axial segment (j) is denoted by fraction ϕ_{ij}. The ϕ_{ij} varies based on both partition and axial position.

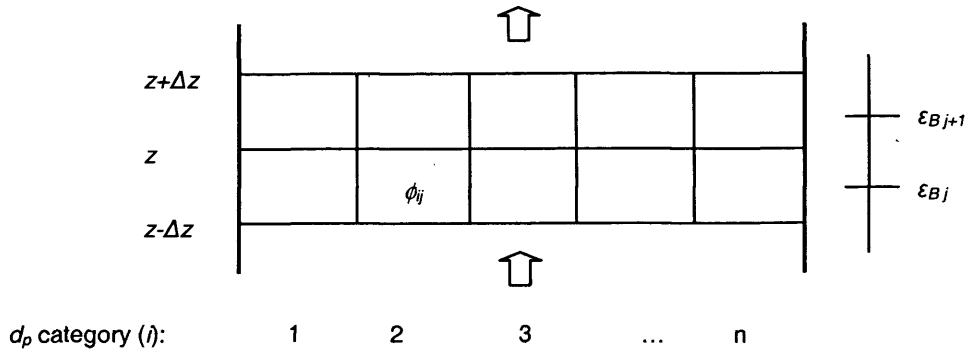

Fig. 6.11 A simplified figure of Fig. 6.10. Partitions are represented as parallel columns of specific particle size category. As before, the ϕ_{ij} varies based on both partition and axial position. Bed voidage (ε_{Bj}) at each axial segment (j) will be constant within that segment irrespective of the partition (i).

As shown in Fig. 6.10 and Fig. 6.11, the resulting system will resemble a set of parallel packed bed columns of different particle sizes while there exists an axial variation of bed voidage in each. The net effect at any segment will be given by weighted sum of each partition.

$$\text{Aggregate effect at a segment} = \sum_i \phi_i \left(\text{Effect due to partition}\right)_i \qquad (6.9)$$

The hydrodynamic part of the model will remain the same as described in previous sections. The adsorption part of the model had to be modified to accommodate the changes as given below.

The mass balance for the concentration of chemical component sp. i is given by (from Eq. (3.4)):

$$\varepsilon_B \frac{\partial u_i}{\partial t} = -\varepsilon_B \boldsymbol{v} \cdot \nabla u_i + \varepsilon_B \nabla \cdot D_i \nabla u_i + R_{Vi} \qquad (6.10)$$

When multiple partitions are considered, the sink term (R_{Vi}) is the sum of the effects of each partition at an axial position (z). This is given by:

$$R_{Vi} = -\sum_m w_m \boldsymbol{n}_{fim} \qquad (6.11)$$

where

n_{fim} = film mass flux of a component i in size partition m

w_m = outer surface area per unit volume of adsorbent particle in size partition m

Similar to the approach taken in Chapter 3, the film mass flux in each partition is given by

$$\boldsymbol{n}_{fim} = k_{fim}(u_i - u_{pim}\big|_{r=R}) \qquad (6.12)$$

where

k_{fim} = film mass transfer coefficient of a component i in size partition m

u_{pim} = concentration of component i in pore phase immediately next to the film or its outer boundary in size partition m

And w_m is given by

$$w_m = \frac{3(1-\varepsilon_B)}{R_m}\phi_m \tag{6.13}$$

where

ϕ_m = volume fraction of particles representing size partition m

The sum of the particle or solid fractions is unity.

$$\sum_m \phi_m = 1 \tag{6.14}$$

Substituting the value of R_{vi} in Eq. (6.10),

$$\frac{\partial u_{Bi}}{\partial t} = -\boldsymbol{v}\cdot\nabla u_{Bi} + E\nabla^2 u_{Bi} - \sum_m \frac{w_m}{\varepsilon_B} k_{fim}(u_{Bi} - u_{pim}\big|_{r=R}) \tag{6.15}$$

Taking only one significant dimension z,

$$\frac{\partial u_{Bi}}{\partial t} = -v\frac{\partial u_{Bi}}{\partial z} + E\frac{\partial^2 u_{Bi}}{\partial z^2} - \sum_m \frac{w_m}{\varepsilon_B} k_{fim}(u_{Bi} - u_{pim}\big|_{r=R}) \tag{6.16}$$

Making this equation dimensionless as in section 3.4, yields

$$\frac{\partial u_{Bi}}{\partial \tau} = -\frac{\partial u_{Bi}}{\partial z} + \frac{1}{Pe_L}\frac{\partial^2 u_{Bi}}{\partial z^2} - \sum_m \phi_m \xi_{im}(u_{Bi} - u_{pim}\big|_{r=1}) \tag{6.17}$$

Where ξ_{im} is analogous to ξ_i in the previous models of adsorption, but specific to the size partition m. The detail of this is given below at the end of this section.

Similarly, the changes in other parts of the model to account for the partition (m) are as follows. As the mass balance is done within a particle, it will remain the same as before. The only difference is the reference of particle to denote its origin to the particular size category or the partition. Thus, it yields:

$$\frac{\partial u_{Kim}}{\partial \tau} = \eta_{im}\frac{1}{r^2}\frac{\partial}{\partial r}\left(r^2\frac{\partial u_{Pim}}{\partial r}\right) \tag{6.18}$$

$$u_{Kim} = \varepsilon_{Pm}u_{Pim} + (1-\varepsilon_{Pm})u_{Aim} \tag{6.19}$$

With boundary conditions:

$$u_{Bi}: \quad \frac{\partial u_B}{\partial z}\bigg|_0 + Pe_L(u_B|_{in} - u_B|_0) = 0 \tag{6.20}$$

$$\left.\frac{\partial u_B}{\partial z}\right|_{z=1} = 0 \tag{6.21}$$

u_{Pim}: $$\left.\frac{\partial u_{Pim}}{\partial r}\right|_{0} = 0 \tag{6.22}$$

$$\left.\frac{\partial u_{Pim}}{\partial r}\right|_{r=1} = Bi_{im}(u_{Bi} - u_{Pim}|_{r=1}) \tag{6.23}$$

With initial conditions:

$$u_{Bi}|_{t=0} = u^0_{Bi}, \qquad u_{Pim}|_{t=0} = u^0_{Pim}, \quad u_{Aim}|_{t=0} = u^0_{Aim}, \quad u_{Kim}|_{t=0} = u^0_{Kim} \tag{6.24}$$

Isotherm relation:

$$f_k(u_{A1},\ldots,u_{AN},u_{P1},\ldots,u_{PN})|_m = 0 \qquad k = 1,2,\ldots,N \qquad \forall j \tag{6.25}$$

or for a multi-component competitive Langmuir:

$$u_{Aim} = \frac{b_{0i}u_{Pim}}{1+\sum_{k=1}^{N} b_k u_{0i} u_{Pkm}} \tag{6.26}$$

Feed concentration:

$$u_{0i} = \max\{u_{Bi-feed}(\tau)\} \qquad -\infty < \tau + \infty \tag{6.27}$$

Constants of the system:

$$Pe_L = \frac{vL}{E}, \qquad \xi_{im} = Bi_{im}\eta_{im}\frac{3(1-\varepsilon_B)}{\varepsilon_B}, \tag{6.28}$$

$$\eta_{im} = \frac{\varepsilon_{Pm}D_i}{R_m^2}\frac{L}{v}, \qquad Bi_{im} = k_{fim}\frac{R_m}{\varepsilon_{Pm}D_i}$$

Bed properties: As in the previous section 6.6, following both independent approaches were implemented for determining bed properties.

i. Approximate mixed bed approach for hydrodynamics as proposed in section 4.7
ii. Interpolation using experimental data

Details of such implementation are the same as in the relevant sections.

6.7.3 Parameters Estimation

The parameters (E_i, D_i, Kf_i, b_{0i} and b_{1i}) for adsorption part of the model and their estimation in mixed bed model are the same as in mono-sized bed model described

earlier. For the hydrodynamic part, the Richardson-Zaki correlation parameter was determined using a *Ga*-based correlation but the natural terminal velocity was modified using a fitting parameter to match the observed final bed height. For the mixed bed model a mean mixing sigma (σ_m) value of 40 and σ_m slope (the linear variation of σ_m w.r.t. particle size) of 0.5 were used assuming these do not to vary much from similar operating conditions as used by Willoughby (2000). While using experimental data approach, the mixed bed PSD and voidage were interpolated from the experimental data.

6.7.4 Simulation

The above equations were discretised using FEM for bulk phase and Orthogonal Collocation for particle phase. The basis of which is same as described in section 3.6. The resulting ODE systems were solved using Matlab's stiff ODE-solver. As this is a different equation set than as in section 3.6, the details of the finite element formulation are described here. The discretisation of particle phase remained essentially the same. As in the previous sections the hydrodynamic part remains independent with values determined as described in the *Ga*-based relation in section 4.4 and section 4.5 if fitting is required. The details of the bulk phase discretisation were as follows.

As in section 3.6, by applying the Galerkin method (section 2.4.4.1) based finite element method (section 2.4.5) to discretise Eq. (6.17) and incorporating nature boundary condition by transferring one differential order from variable to trial function as in the Ritz method (section 2.4.3.2):

$$A_i u_{Bi} - f_i = 0 \tag{6.29}$$

where

$$A_i = \frac{\partial}{\partial \tau} - \frac{1}{Pe_L}\frac{\partial^2}{\partial z^2} + \frac{\partial}{\partial z} + \sum_m \phi_m \xi_{im} \tag{6.30}$$

$$f_i = \sum_m \phi_m \xi_{im} u_{pim}\Big|_{r=1} \tag{6.31}$$

Approximating u_{Bi} by u_{Bin}, a quadratic element or approximation function which is given by

$$u^e_{Bin} = \sum_{j=1}^{3} u^e_{Bij} \psi^e_j \tag{6.32}$$

Applying the Galerkin method (based on Eq. 2.4.82) yields:

$$\left(A_i u^e_{Bi} - f_i, \psi^e_k\right) = 0 \qquad \text{for } k = 1, 2, 3 \tag{6.33}$$

This gives

$$\int_{\Omega^e} \psi^e_k \left\{ \frac{\partial u^e_{Bi}}{\partial \tau} - \frac{1}{Pe_L} \frac{\partial^2 u^e_{Bi}}{\partial z^2} + \frac{\partial u^e_{Bi}}{\partial z} + \sum_m \phi_m \xi_{im} u^e_{Bi} - \sum_m \phi_m \xi_{im} u^e_{Pim}\Big|_{r=1} \right\} dz = 0 \tag{6.34}$$

Reducing one differential order of second derivative term by transferring to the basis function using integration by parts:

$$\begin{aligned} &\int_{\Omega^e} \psi^e_k \frac{\partial u^e_{Bi}}{\partial \tau} dz - \int_{\Omega^e} \frac{\partial}{\partial z}\left(\psi^e_k \frac{1}{Pe_L} \frac{\partial u^e_{Bi}}{\partial z} \right) dz + \int_{\Omega^e} \frac{\partial \psi^e_k}{\partial z} \frac{1}{Pe_L} \frac{\partial u^e_{Bi}}{\partial z} dz \\ &+ \int_{\Omega^e} \psi^e_k \frac{\partial u^e_{Bi}}{\partial z} dz + \int_{\Omega^e} \psi^e_k \sum_m \phi_m \xi_{im} u^e_{Bi}\, dz - \int_{\Omega^e} \psi^e_k \sum_m \phi_m \xi_{im} u^e_{Pim}\Big|_{r=1} dz = 0 \end{aligned} \tag{6.35}$$

Applying Gauss' divergence theorem

$$\begin{aligned} &\int_{\Omega^e} \psi^e_k \frac{\partial u^e_{Bi}}{\partial \tau} dz - \int_{\Gamma^e} \boldsymbol{n}\left(\psi^e_k \frac{1}{Pe_L} \frac{\partial u^e_{Bi}}{\partial z} \right) dS + \int_{\Omega^e} \frac{\partial \psi^e_k}{\partial z} \frac{1}{Pe_L} \frac{\partial u^e_{Bi}}{\partial z} dz \\ &+ \int_{\Omega^e} \psi^e_k \frac{\partial u^e_{Bi}}{\partial z} dz + \int_{\Omega^e} \psi^e_k \sum_m \phi_m \xi_{im} u^e_{Bi}\, dz - \int_{\Omega^e} \psi^e_k \sum_m \phi_m \xi_{im} u^e_{Pim}\Big|_{r=1} dz = 0 \end{aligned} \tag{6.36}$$

Integrating from z_1 and z_2 of an element

$$\begin{aligned} &\int_{z_1}^{z_2} \psi^e_k \frac{\partial u^e_{Bi}}{\partial \tau} dz + \int_{z_1}^{z_2} \frac{\partial \psi^e_k}{\partial z} \frac{1}{Pe_L} \frac{\partial u^e_{Bi}}{\partial z} dz + \int_{z_1}^{z_2} \psi^e_k \frac{\partial u^e_{Bi}}{\partial z} dz \\ &+ \int_{z_1}^{z_2} \psi^e_k \sum_m \phi_m \xi_{im} u^e_{Bi}\, dz = \int_{z_1}^{z_2} \psi^e_k \sum_m \phi_m \xi_{im} u^e_{Pim}\Big|_{r=1} dz + \left(\psi^e_k \frac{1}{Pe_L} \frac{\partial u^e_{Bi}}{\partial z} \right)\Bigg|_{z_1}^{z_2} \end{aligned} \tag{6.37}$$

Substituting the value of the approximating function

$$\begin{aligned} &\sum_{j=1}^{3} \frac{\partial u^e_{Bij}}{\partial \tau} \int_{z_1}^{z_2} \psi^e_k \psi^e_j\, dz + \sum_{j=1}^{3} u^e_{Bij} \int_{z_1}^{z_2} \frac{1}{Pe_L} \frac{\partial \psi^e_k}{\partial z} \frac{\partial \psi^e_j}{\partial z} dz + \sum_{j=1}^{3} u^e_{Bij} \int_{z_1}^{z_2} \psi^e_k \frac{\partial \psi^e_j}{\partial z} dz \\ &+ \sum_{j=1}^{3} u^e_{Bij} \int_{z_1}^{z_2} \sum_m \phi_m \xi_{im} \psi^e_k \psi^e_j\, dz = \int_{z_1}^{z_2} \sum_m \phi_m \xi_{im} \psi^e_k u^e_{Pim}\Big|_{r=1} dz + \left(\frac{1}{Pe_L} \psi^e_k \frac{\partial u^e_{Bij}}{\partial z} \right)\Bigg|_{z_1}^{z_2} \end{aligned} \tag{6.38}$$

In matrix form for a component i:

$$\boldsymbol{M}^e_i \dot{\boldsymbol{u}}_{Bi} + \boldsymbol{K}^e_i \boldsymbol{u}_{Bi} = \boldsymbol{F}^e_i \tag{6.39}$$

where

$$\boldsymbol{M}^e_i = \int_{z_1}^{z_2} \psi^e_k \psi^e_j\, dz \tag{6.40}$$

$$\boldsymbol{K}^e_i = \int_{z_1}^{z_2} \frac{1}{Pe_L} \frac{\partial \psi^e_k}{\partial z} \frac{\partial \psi^e_j}{\partial z} dz + \int_{z_1}^{z_2} \psi^e_k \frac{\partial \psi^e_j}{\partial z} dz + \int_{z_1}^{z_2} \sum_m \phi_m \xi_{im} \psi^e_k \psi^e_j\, dz \tag{6.41}$$

$$\boldsymbol{F}_i^e = \int_{z_1}^{z_2} \sum_m \phi_m \xi_{im} \psi_k^e u_{Pim}^e \Big|_{r=1} dz + \boldsymbol{q}_i^e \tag{6.42}$$

$$\boldsymbol{q}_i^e = \left(\frac{1}{Pe_L} \psi_k^e \frac{\partial u_{Bij}^e}{\partial z} \right) \Bigg|_{z_1}^{z_2} \tag{6.43}$$

Each matrix $\boldsymbol{M}_i^e, \boldsymbol{K}_i^e, \boldsymbol{F}_i^e$ is evaluated element-wise and component-wise. During global assembly (as described in section 2.4.5.4-2.4.5.6), the outflux $\boldsymbol{q}_i^e$ from one element cancels out the influx $\boldsymbol{q}_i^e$ into the following elements. The incoming flux $\boldsymbol{q}_i^e$ at the first element and outgoing $\boldsymbol{q}_i^e$ at the last element are given by the natural boundary conditions (Eq. (6.20)-(6.21)). That is:

$$\boldsymbol{q}_i^e \Big|_{z=0} = u_{Bi}\Big|_{in} - u_{Bi}\Big|_{z=0} \tag{6.44}$$

$$\boldsymbol{q}_i^e \Big|_{z=1} = 0 \tag{6.45}$$

As in Eq. (3.134), applying orthogonal collocation to Eq. (6.17) and its associated boundary conditions, following discretised form will result in a representation equivalent to Eq. (3.138) for each size partition *m*. As each partition is independent of each other for the particle phase, the derivation of the discretised equation is the same as given in section 3.6.

$$\boldsymbol{M}_{Pim} \dot{\boldsymbol{u}}_{Pim} = \eta_{im} \boldsymbol{B} \boldsymbol{u}_{Pim} \tag{6.46}$$

where

$$\boldsymbol{M}_{Pim} = \frac{\partial f(\boldsymbol{u}_{Pim})}{\partial \boldsymbol{u}_{Pim}} \tag{6.47}$$

And u_{Pim} is a vector representing the concentration of component *i* at collocation nodes of a particle in partition *m*.

The boundary conditions of particle phase are given by,

At $r = 0$: $\quad \nabla u_{Pim}\Big|_{r=0} = 0 \tag{6.48}$

At $r = 1$: $\quad u_{PN+1,im} = \dfrac{Bi_{im} u_{Bi} - \sum_{j=1}^{N} A_{N+1,j} u_{Pj,im}}{A_{N+1,N+1} + Bi_{im}} \tag{6.49}$

Matlab's ODE-solver was used to solve these discretised equations. For simulation 10 elements were used for bulk phase, 2 internal orthogonal collocation points for particle phase, 1 component species was assumed and 5 particle size categories were used. These computational parameters gave converging results.

Convergence Analysis

For the purpose of computational validation of the simulation results, a convergence analysis was performed using different element numbers. As discretisation becomes smaller or the number of elements increased the result became smoother and accurate. Use of 10 elements was found to be sufficient for the convergence of the result as shown in the Fig. 6.12. The converged solution was also closer to the experimental data.

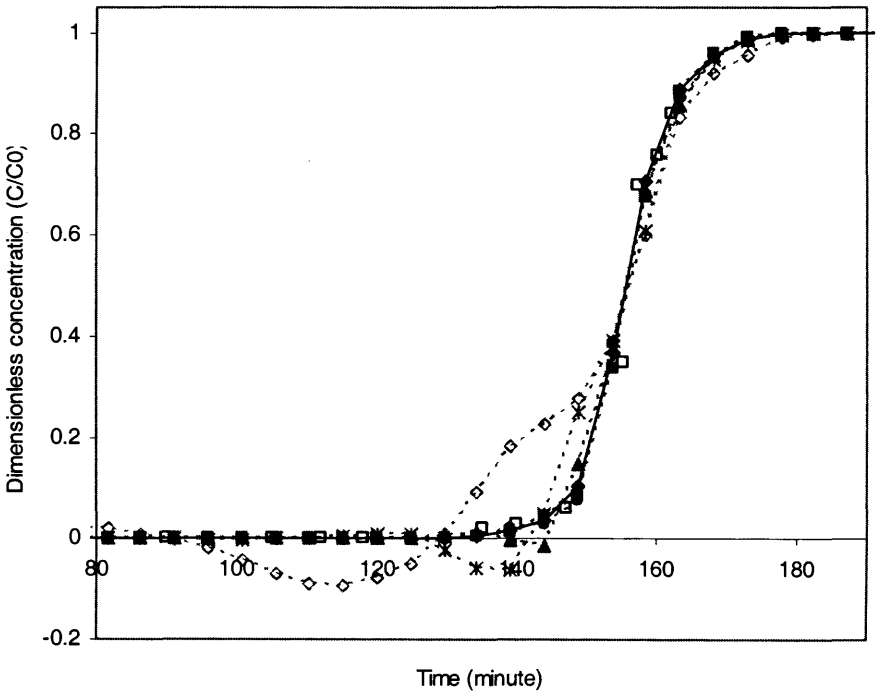

Fig. 6.12 Convergence analysis of breakthrough curves at 40 cm bed height using Mixed bed size partition model. *en* is number of elements used in the simulation. ◊, 2 *en*; *, 4 *en*; ▲, 8 *en*; ●, 12 *en*; ■, 25 *en*; ♦, 50 *en*; □, experimental data.

6.7.5 Results and Discussion

As in the previous section 6.6.5, simulations were performed for the Lysozyme-Streamline SP data set of Bruce and Chase (2001) using the Mixed bed size partition model as described above to predict the breakthrough at 10 cm, 25 cm and 40 cm axial positions of the bed. (All dataset and associated parameter values were as described in section 6.6.)

The mixed bed-size partition model prediction of breakthrough was found to match very closely to the MB-equivalent diameter approach predictions at both 40 cm and 25 cm axial positions (Fig. 6.13 a,b). There was slight difference at 10 cm (Fig. 6.13c). In terms of overall accuracy this model, did not improve the predictions compared to those under the MB-equivalent diameter approach. However, it provides additional information of the system like adsorption behaviour specific to particular particle size categories without additional input.

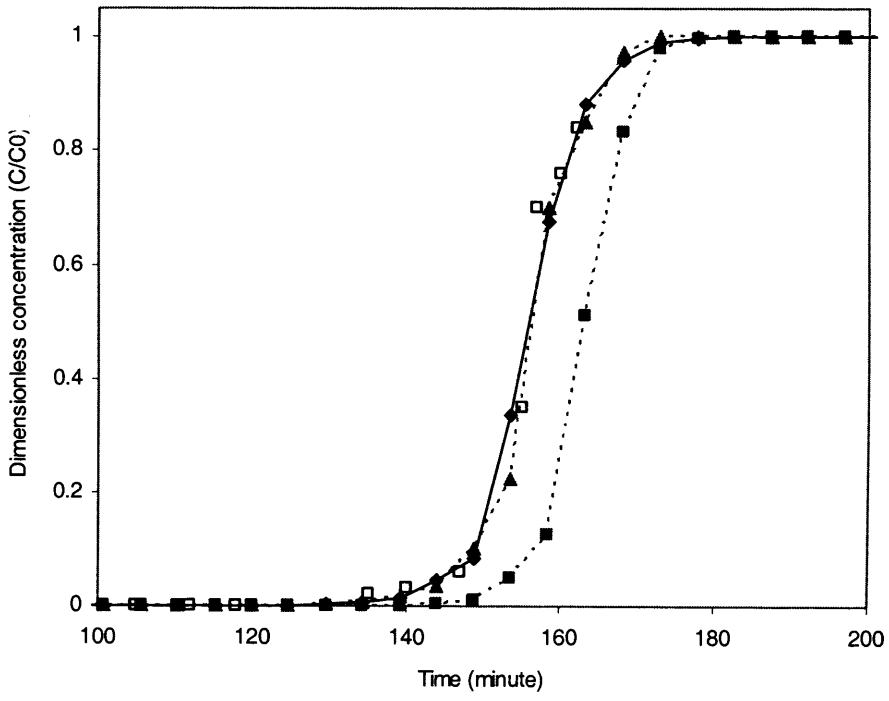

(a)

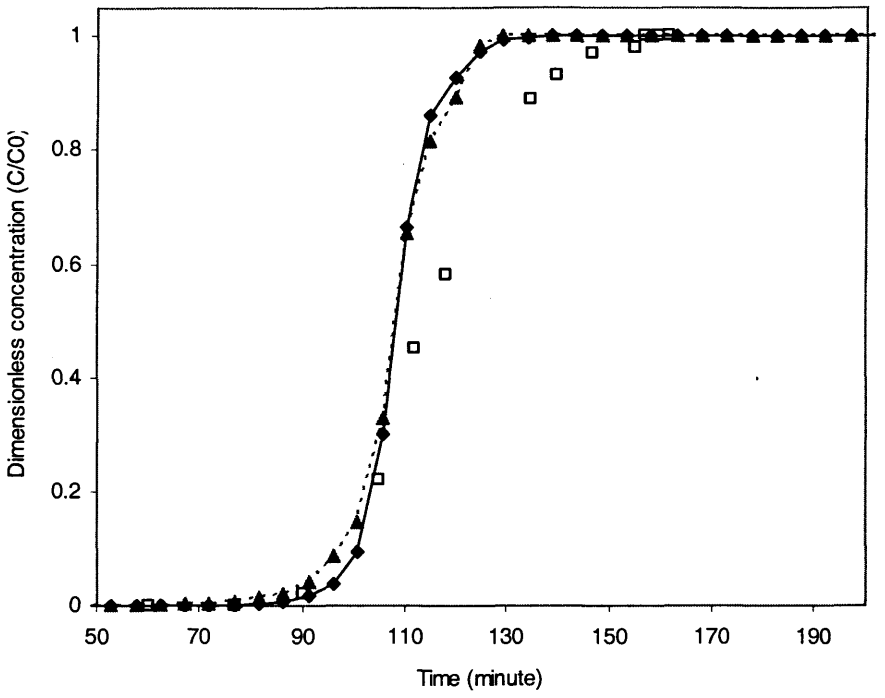

(b)

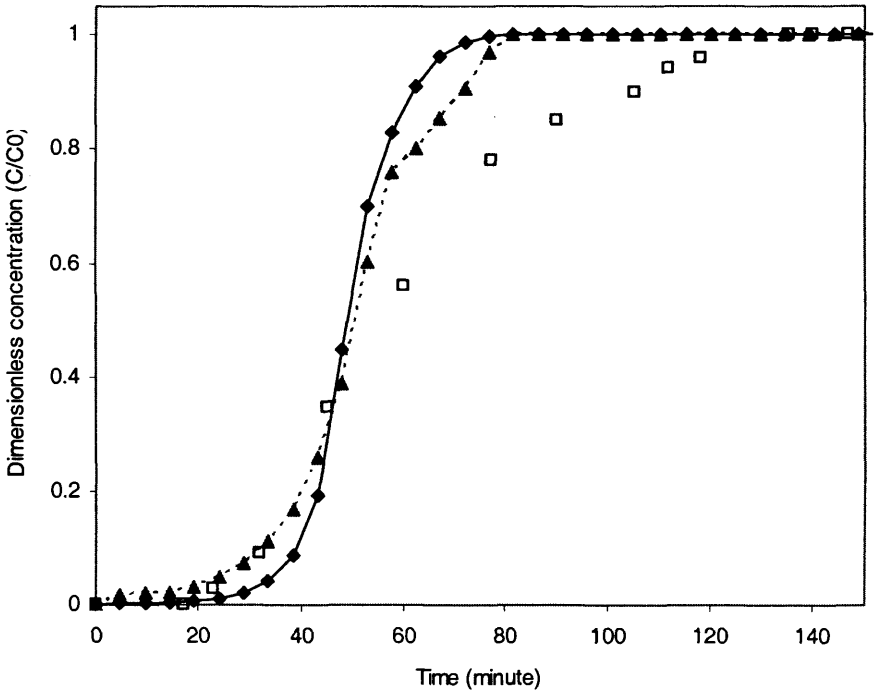

(c)

Fig. 6.13 Breakthrough curves at (a) 40 cm (b) 25 cm and (c) 10 cm bed heights as simulated by Mixed bed size partition (MBSP) model, MBSP model with experimental data for bed properties (MBSP-ex) and mixed bed model equivalent diameter (MBEQD) model. ♦, MBSP; ■, MBSP-ex; ▲, MBEQD; □, experimental data.

Predictions were more accurate compared to those of the mono-sized bed or PCB model. When experimental data was used for particle size distribution and PCB based axial voidage variation, as in the previous model, the resulting breakthrough at 40 cm was delayed and close to that produced by the PCB model. So here again use of accurate estimate of voidage variation seemed to be an important factor. Kaczmarski and Bellot (2005) developed a similar model as described here. The main difference is they used interpolation from an experimental data for an axial variation of mean particle size and assumed constant voidage across the bed. The variance of PSD was also assumed constant. As has been mentioned earlier, bed voidage is a critical parameter, so its constant assumption is an important limitation in their approach especially when concentration at other parts of the bed apart from bed outlet is desired. In addition, as the bed properties are interpolated from experimental data, their model can not handle change in operating conditions like fluid velocity, fluid and particle properties, etc. Use of hydrodynamic model to estimate bed properties solved both of those limitations in the MB-SP model developed here.

There are two major drawbacks to the model developed here. The first is it takes far more computational time than the previous mixed bed model. Even for 10 elements, 2 internal collocation points and 5 size partitions, it took about an hour to simulate for a mono-component system in a 1.7 GHz Pentium 4 processor with 500 MB RAM. When much finer levels of discretisation and more size categories are required, it will take a lot more time making it unsuitable for real-time applications like model-based controls. In such cases MB-equivalent diameter approach is recommended whenever feasible as the accuracy of the model are essentially same. The second weakness of the model is as this is based on mixed bed hydrodynamic model, it inherits all the limitations and weaknesses of the same. As explained in section 4.7, the approximate mixed bed hydrodynamic approach needs further improvement in the method to enable it to simulate accurately for more than 5 particle size categories. This is an important limitation of this approach at present. For the 5 size categories used here it predicted axial PSD variation in line with the experimental observations. Most importantly, what has been established in this part of the work is a method or model to simulate adsorption in an expanded bed when insight of an axial variations of particle size distribution and voidage are available. Those values can come from either experimental data, which has also been demonstrated here, or from an independent hydrodynamic model. Here an approximate mixed bed hydrodynamic modelling approach was used.

One additional limitation of the MB-size partition model and other previous models is that particle dispersion has been assumed negligible. In reality dispersion exists, but the magnitude of it may be sufficiently small to have no significant effect on the overall adsorption response of the bed. The slow rise of breakthrough curve in the lower part of the bed indicates that dispersion effects are more pronounced in that part of the bed and current model developed so far has not been able to capture this. Thus in the next chapter attempt will be made to develop an EBA model which will include the effect of particle dispersion.

6.8 Conclusion

In this part of work, an integrated EBA model was developed which takes into account the steady state hydrodynamics to predict adsorption response. Mono-sized bed (MSB) and PCB models were implemented. Mixed bed model was developed using equivalent diameter approach (MB-EQD). The result was found to match very close to the experimental data for breakthrough at 40 cm bed height. A mixed bed size partition (MB-SP) model was developed to be able predict particle size specific adsorption response. The result was also found to match almost exactly to the MB-EQD model and thus very close to the experimental data. Both MB-EQD and MB-SP models were also implemented using interpolated experimental data on bed properties for an applied operating condition instead of hydrodynamic model. The result was also close to the experimental data but less accurate compared to the result when hydrodynamic model was employed. This was because of paucity of experimental data points available and thus the representation of the bed using it had been crude. Nevertheless, it demonstrated the validity of the model developed. Mixed bed models, both MB-EQD and MB-SP, were found to be more accurate than MSB and PCB, and in fact, their result lied in between those two, as it should have been. Both MB-EQD and MB-SP are useful models and can be used based upon the needs. If short simulation time is important for example for use in real time control of the process, MB-EQD will be suitable. On the other hand, more detail information of the system like particle size specific adsorption response of EBA is desired MB-SP would be necessary. In the next chapter, further improvement in the model will be attempted by incorporating particle dispersion.

7 Integrated Model: Steady State Hydrodynamics with Particle Dispersion

7.1 Introduction

An integrated model with steady state hydrodynamics was developed in the previous chapter. For simplification, effect of particle dispersion in adsorption response was neglected. However, although bed is operated at steady state hydrodynamics, continuous particle dispersion along the bed exists. It is more like a random motion of particles with a net aggregate effect on hydrodynamics null. Since adsorption is in transient mode, it will bring about changes in adsorption behaviour of the system. Depending upon the system, the magnitude of particle dispersion can vary. The significance of this effect also can vary based upon the objective. For example, if the objective is to know the changes in concentration of a component within the lower parts of the bed, its significance will be higher than compared to that at the end of the bed, especially in the early parts of an operation. This is due to the effect of dispersion in reducing the sharp gradient of concentration which otherwise would have existed. Thus including particle dispersion in the model is an important step and ensures that the model offers a more accurate representation of reality. The current state of EBA model with particle dispersion has already been described in literature review section of chapter 6. As an EBA model that considers the existence of both a mixed bed and particle dispersion does not exist, developing such a model, which is more realistic physics, is the objective of this part of the thesis.

7.2 Plan and Objectives

Further improvement in mixed bed size partition (MB-SP) model developed in the previous chapter is done by incorporating particle dispersion into the model for each size species. At first Wright and Glasser (2001) approach will be employed. Due to an important weakness in that approach as explained in the next section, a new particle dispersion model will be also be developed which accurately represent the system.

The objectives of this chapter are:

- to develop a mixed bed EBA model with particle dispersion using Wright and Glasser (2001) approach
- to develop an approach to correctly include the effect of particle dispersion in an EBA model.

7.3 Mixed Bed-Particle Dispersion Model

7.3.1 Introduction

Wright and Glasser (2001) first introduced the effect of particle dispersion in the EBA model. For simplification they assumed the bed to be homogeneous mono-sized. They added one additional variable – an average concentration of component in an aggregate particle phase (u_{qi}) at that axial position. The aggregate particle phase includes both the particle pore phase (u_P) and adsorbent phase (u_A). Particle dispersion and transfer of a component from the bulk liquid phase into the particle bring about the changes in u_{qi}. This aggregate particle phase concentration is then used to update changes in concentration of a component inside a particle or at its radial nodes through boundary conditions. This model has been adopted by Tong et al. (2002), Chen et al. (2003), Li et al. (2004) and Li et al. (2005). They found the simulated results close to the breakthrough experimental data. The particle dispersion directly affects the whole particle and thus simultaneously brings about changes in component concentration at each particle radial nodes at both particle pore phase (u_{Pi}) and adsorbent phase (u_{Ai}). Thus, this approach of using average concentration of particle as an aggregate particle phase (u_{qi}) and implementing its effect through boundary condition does not seem to represent the physics accurately. The agreement of simulation to the experimental data can be due to the relatively small value of particle dispersion coefficient estimated and used. That will automatically cause the effect of particle dispersion in the system to be small. Using sensitivity analysis, Wright and Glasser (2001) reported that the effect of particle dispersion in the system as observed in the breakthrough of a component was small and not significant compared to other variables like superficial fluid velocity and particle radius.

To remove the weakness in the existing model, a new and better approach to include particle dispersion in the EBA model is proposed in the next section. Before

going to that stage, Wright and Glasser's approach of including the effect of particle dispersion in EBA model was adapted in the context of the multi-particle size bed model and implemented. Consideration of the existence of a distribution of particle sizes through adoption of size partition approach in the mixed bed has not been attempted before.

7.3.2 Model Development

Dispersion was considered just within particle size category or partition (Fig. 7.1). Hence the net proportion of particle size categories at each node z remain constant throughout the operation.

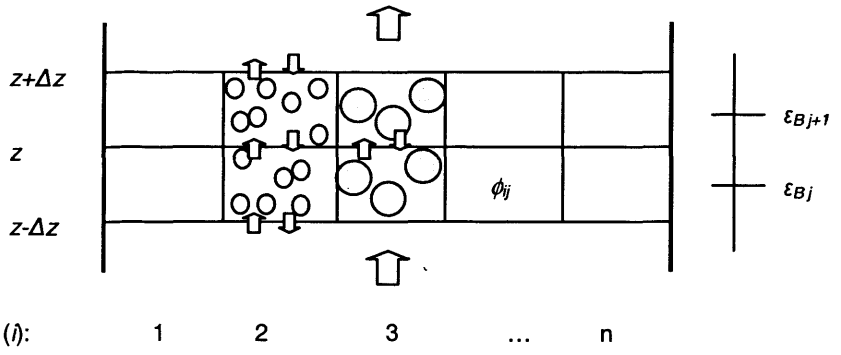

Fig. 7.1 Particle dispersion at each partition. Figure shows the equal transfer of particles between upper and lower cells of each size partition with null net transfer. The result of all particle sizes in that the axial node determines voidage.

As in the mixed bed size partition (MBSP) model of the previous chapter, the properties of a mixed bed (MB) are given by the hydrodynamic part of the model. This can be by either using an appropriate hydrodynamic model or directly using and interpolating experimental data. Here both approaches were implemented.

The adsorption part of the model is also similar to MBSP model. A mass balance of a component in both bulk liquid phase (Eq. (6.17)) and particle phase (Eq. (6.18)) are same as in MB-SP model. The difference is a mass balance of the additional variable, the concentration of component in aggregate particle phase (u_{qi}), and its use in the update of particle phase (u_{Pi}) through the outer boundary of a particle. The derivation is as follows.

As in the MBSP model, the mass balance for the concentration of component i is given by (in a discrete form of partitions):

In *bulk liquid phase*:

$$\frac{\partial u_{Bi}}{\partial t} = -\frac{\partial u_{Bi}}{\partial z} + \frac{1}{Pe_L}\frac{\partial^2 u_{Bi}}{\partial z^2} - \sum_m \phi_m \xi_{im}(u_{Bi} - u_{pim}\big|_{r=1}) \tag{7.1}$$

where ϕ_m is fraction of partition size species or partition m.

Similarly in *particle phase* of the partition (m):

$$\frac{\partial u_{Kim}}{\partial \tau} = \eta_{im}\frac{1}{r^2}\frac{\partial}{\partial r}\left(r^2\frac{\partial u_{Pim}}{\partial r}\right) \tag{7.2}$$

$$u_{Kim} = \varepsilon_{Pm}u_{Pim} + (1-\varepsilon_{Pm})u_{Aim} \tag{7.3}$$

With boundary conditions for bulk phase:

$$u_{Bi}: \quad \frac{\partial u_B}{\partial z}\bigg|_0 + Pe_L(u_B|_{in} - u_B|_0) = 0 \tag{7.4}$$

$$\frac{\partial u_B}{\partial z}\bigg|_{z=1} = 0 \tag{7.5}$$

With initial conditions:

$$u_{Pim}|_{t=0} = u^0_{Pim}, \quad u_{Aim}|_{t=0} = u^0_{Aim}, \quad u_{Kim}|_{t=0} = u^0_{Kim} \tag{7.6}$$

Feed concentration:

$$u_{0i} = \max\{u_{Bi-feed}(\tau)\} \quad -\infty < \tau + \infty \tag{7.7}$$

Isotherm relation:

$$f_k(u_{A1},\ldots,u_{AN},u_{P1},\ldots,u_{PN})\big|_m = 0 \qquad k = 1,2,\ldots,N \qquad \forall j \tag{7.8}$$

or for a multi-component competitive Langmuir:

$$u_{Aim} = \frac{b_{0i}u_{Pim}}{1+\sum_{k=1}^{N} b_k u_{0i}u_{Pkm}} \tag{7.9}$$

Constants of the system:

$$Pe_L = \frac{vL}{E}, \qquad \xi_{im} = Bi_{im}\eta_{im}\frac{3(1-\varepsilon_B)}{\varepsilon_B}, \tag{7.10}$$

$$\eta_{im} = \frac{\varepsilon_{Pm}D_i}{R_m^2}\frac{L}{v}, \qquad Bi_{im} = k_{fim}\frac{R_m}{\varepsilon_{Pm}D_i}$$

The outer boundary condition of particle phase will be based on the aggregate phase. So the mass balance of a component in the aggregate phase will be derived first and its effect on the particle phase through the boundary will also be set.

Aggregate particle phase:

Let u_{qim} be an average concentration of component i in the aggregate particle phase at size partition m. Applying a mass balance for a component specific aggregate phase (u_{qi}) in a differential volume of partition m (Fig. 7.2), from Eq. (2.27),

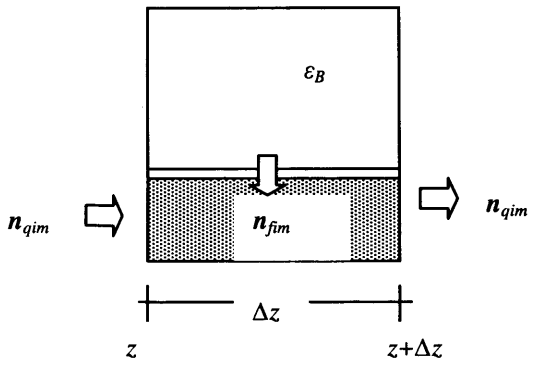

Fig. 7.2 Mass balance of a component specific aggregate phase (u_{qi}) in a differential volume of partition m

$$(1-\varepsilon_B)\frac{\partial u_{qim}}{\partial t} = -\boldsymbol{v}_m \cdot \nabla u_{qim} + \nabla \cdot E_{Pm} \nabla u_{qim} + R_{Vim} \tag{7.11}$$

As particle movement is only due to dispersion (because of hydrodynamic equilibrium state), particle velocity at partition m (v_m) is zero. Taking only one significant dimension z,

$$(1-\varepsilon_B)\frac{\partial u_{qim}}{\partial t} = E_{Pm}\frac{\partial^2 u_{qim}}{\partial z^2} + w_m n_{fim} \tag{7.12}$$

where E_{Pm} is particle dispersion coefficient of particle size partition m. The source term (R_{Vim}) is given by flux (n_{fim}) due to mass transfer from bulk phase to particle phase. w_m is surface area per unit volume of partition m. As in MB-SP model, n_{fim} is given by,

$$n_{fim} = k_{fi}(u_{Bi} - u_{Pim}|_{r=1}) \tag{7.13}$$

and $$w_m = \frac{3}{R}(1-\varepsilon_B)\phi_m \tag{7.14}$$

Substituting these values into Eq. (7.12),

$$\frac{\partial u_{qim}}{\partial t} = \frac{E_{Pm}}{(1-\varepsilon_B)}\frac{\partial^2 u_{qim}}{\partial z^2} + \phi_m \frac{3}{R} k_{fi}(u_{Bi} - u_{Pim}|_{r=1}) \tag{7.15}$$

When $\phi_m = 1$, i.e. single size partition, Eq. (7.15) becomes same as Wright and Glasser's derivation for u_{qi}.

Normalising the Eq. (7.15) as rest of the other equations as done in chapter 3.4 on the same basis:

$$\tilde{u}_{qim} = \frac{u_{qim}}{u_{0i}}, \qquad \tilde{u}_{Pim} = \frac{u_{Pim}}{u_{0i}} \tag{7.16}$$

Dimensionless variables for time τ and for axial height $\tilde{z}$ are defined as before:

$$\tau = \frac{vt}{L}, \qquad \tilde{z} = \frac{z}{L} \tag{7.17}$$

Which gives,

$$\frac{\partial \tau}{\partial t} = \frac{v}{L}, \qquad \frac{\partial \tilde{z}}{\partial z} = \frac{1}{L} \tag{7.18}$$

Applying them to transform terms into dimensionless forms (as explained in chapter 3.4):

$$\frac{\partial u_{qim}(z,t)}{\partial z} = \frac{u_{0i}}{L}\frac{\partial \tilde{u}_{qim}(\tilde{z},\tau)}{\partial \tilde{z}} \tag{7.19}$$

$$\frac{\partial^2 u_{qim}(z,t)}{\partial z^2} = \frac{u_{0i}}{L^2}\frac{\partial^2 \tilde{u}_{qim}(\tilde{z},\tau)}{\partial \tilde{z}^2} \tag{7.20}$$

$$\frac{\partial u_{qim}(z,t)}{\partial t} = \frac{v}{L}u_{0i}\frac{\partial \tilde{u}_{qim}(\tilde{z},\tau)}{\partial \tau} \tag{7.21}$$

Substituting the terms using Eqs (7.16),(7.20) and (7.21) into Eq. (7.15),

$$\frac{v}{L}u_{0i}\frac{\partial \tilde{u}_{qim}}{\partial \tau} = \frac{E_{Pm}}{(1-\varepsilon_B)}\frac{1}{L^2}\frac{\partial^2 \tilde{u}_{qim}}{\partial z^2} + \phi_m \frac{3}{R}k_{fi}u_{0i}(\tilde{u}_{Bi} - \tilde{u}_{Pim}|_{r=1}) \tag{7.22}$$

As done in chapter 3.4, dropping the over-tilde (~) for notational ease but keeping the meaning of the transformed variables yields,

$$\frac{\partial u_{qim}}{\partial \tau} = \frac{E_{Pm}}{(1-\varepsilon_B)}\frac{1}{Lv}\frac{\partial^2 u_{qim}}{\partial z^2} + \phi_m \frac{3}{R}k_{fi}\frac{L}{v}(u_{Bi} - u_{Pim}|_{r=1}) \tag{7.23}$$

Thus the mass balance of component i in the aggregate phase is given by,

$$\frac{\partial u_{qim}}{\partial \tau} = \frac{1}{(1-\varepsilon_B)}\frac{1}{Pe_P}\frac{\partial^2 u_{qim}}{\partial z^2} + \phi_m \frac{\varepsilon_B}{(1-\varepsilon_B)}\xi_i(u_{Bi} - u_{Pim}|_{r=1}) \tag{7.24}$$

where

$$Pe_P = \frac{vL}{E_P} \tag{7.25}$$

And boundary conditions for u_{qim} in a normalised form:

$$\left.\frac{\partial u_{qim}}{\partial z}\right|_{z=0} = 0 \tag{7.26}$$

and $$\left.\frac{\partial u_{qim}}{\partial z}\right|_{z=1} = 0$$

The initial condition is given by:

$$u_{qim}\big|_{t=0} = 0 \tag{7.27}$$

The outer boundary condition of the particle phase of size partition m can then be updated using Wright and Glasser's approach.

Boundary conditions of particle phase:

Due to radial symmetry at the centre of the particle, the boundary condition is given by,

$$\left.\frac{\partial u_{Pim}}{\partial r}\right|_{0} = 0 \tag{7.28}$$

Where as at the outer boundary, applying Wright and Glasser's approach of including an additional flux due to particle dispersion:

$$\frac{3}{R}\varepsilon_P D_i \left.\frac{\partial u_{Pim}}{\partial r}\right|_{R} = \frac{E_{Pm}}{(1-\varepsilon_B)}\frac{\partial^2 u_{qim}}{\partial z^2} + \frac{3}{R}k_{fim}(u_{Bi} - u_{Pim}|_R) \tag{7.29}$$

Normalising at before:

$$\tilde{u}_B = \frac{u_{Bi}}{u_{0i}}, \qquad \tilde{r} = \frac{r}{R} \tag{7.30}$$

Which gives,

$$\frac{\partial \tilde{r}}{\partial r} = \frac{1}{R} \tag{7.31}$$

$$\frac{\partial u_{Pim}(r,t)}{\partial r} = \frac{u_{0i}}{R}\frac{\partial \tilde{u}_{Pim}(\tilde{r},\tau)}{\partial \tilde{r}} \tag{7.32}$$

Substituting these into Eq. (7.29)

$$\frac{3}{R}\varepsilon_P D_i \frac{u_{0i}}{R}\left.\frac{\partial \tilde{u}_{Pim}}{\partial r}\right|_{r=1} = \frac{E_{Pm}}{(1-\varepsilon_B)}\frac{u_{0i}}{L^2}\frac{\partial^2 \tilde{u}_{qim}}{\partial z^2} + \frac{3}{R}k_{fim}u_{0i}(\tilde{u}_{Bi} - \tilde{u}_{Pim}|_{r=1}) \tag{7.33}$$

As before, dropping the over-tilde (˜) for notational ease but keeping the meaning of the transformed variables yields,

$$\left.\frac{\partial u_{Pim}}{\partial r}\right|_{r=1} = \frac{E_{Pm}}{(1-\varepsilon_B)}\frac{1}{L^2}\frac{R^2}{3\varepsilon_P D_i}\frac{\partial^2 u_{qim}}{\partial z^2} + \frac{Rk_{fim}}{\varepsilon_P D_i}(u_{Bi} - u_{Pim}|_{r=1}) \tag{7.34}$$

$$\left.\frac{\partial u_{Pim}}{\partial r}\right|_{r=1} = \gamma_{im}\frac{\partial^2 u_{qim}}{\partial z^2} + Bi_{im}(u_{Bi} - u_{Pim}|_{r=1}) \tag{7.35}$$

where

$$\gamma_{im} = \frac{R^2}{3L^2}\frac{1}{(1-\varepsilon_B)\varepsilon_P}\frac{E_{Pm}}{D_i} \tag{7.36}$$

Thus mass balance of component *i* in bulk fluid phase, particle phase and aggregate phase and their associated initial and boundary conditions as derived above, equations: (7.1)-(7.10), (7.24)-(7.28), (7.35)-(7.36), describes the EBA system.

7.3.3 Parameter Estimation

The parameters for this model and simulation are same as in previous sections. The additional parameter axial particle dispersion coefficient (E_p) has been estimated using correlation of Van Deer Meer et al. (1984) by Wright and Glasser (2001), Tong et al. (2002), Chen et al. (2003), Li et al. (2004), Yun et al. (2005) and Li et al. (2005) and given by:

$$E_p = 0.04\, v^{1.8} \quad \text{m}^2/\text{s} \tag{7.37}$$

Here E_p 0.008 cm^2/s has been used as estimated from transient bed height model fitting. The above correlation gives similar value 0.0047 cm^2/s (as given in Li et al., 2004). In the EBA adsorption system, this value seems be small and does not seem to have significant contribution in the adsorption behaviour of EBA as observed below.

7.3.4 Simulation

Discretisation of the bulk and particle phases was done as before. The average aggregate particle phase (u_{qim}) was discretised using finite difference as follows.

$$\left.\frac{\partial u_{qim}}{\partial t}\right|_z = \frac{1}{(1-\varepsilon_B)}\frac{1}{Pe_m}\frac{\left(u_{qim}|_{z+\Delta z} - 2u_{qim}|_z + u_{qim}|_{z-\Delta z}\right)}{\Delta z^2} + \phi_m\frac{\varepsilon_B}{(1-\varepsilon_B)}\xi_{im}\left(u_{Bi} - u_{Pim}|_{r=1}\right)\Big|_z \tag{7.38}$$

And boundary conditions of u_{qim}:

At $z = 0$: $$u_{qim}\big|_{z-\Delta z} = u_{qim}\big|_{z+\Delta z} \tag{7.39}$$

and at $z = 1$: $$u_{qim}\big|_{z+\Delta z} = u_{qim}\big|_{z-\Delta z} \tag{7.40}$$

And, $\frac{\partial^2 u_{qim}}{\partial z^2}$ part of particle boundary condition is discretised as follows

$$\frac{\partial^2 u_{qim}}{\partial z^2} = \frac{\left(u_{qim}\big|_{z+\Delta z} - 2u_{qim}\big|_{z} + u_{qim}\big|_{z-\Delta z}\right)}{\Delta z^2} \tag{7.41}$$

The rest of the discretisation was the same as described in previous sections for MB-SP model. The resulting system of ordinary differential equations was solved using Matlab's ODE-solver. For simulation 10 elements for bulk phase, 2 internal orthogonal collocation points for particle phase, 1 component species and 5 particle size categories were used. These computational parameters gave converging results.

Convergence Analysis

To achieve computational validation of the simulation results, a convergence analysis was done using different element numbers. As discretisation becomes smaller or the number of elements increased the result became smoother and accurate. Use of 10 elements was taken to be sufficient for the convergence of the result as shown in the Fig. 7.3. As can be seen below, as element number is increased the solution converged. The converged solution was close to the experimental data.

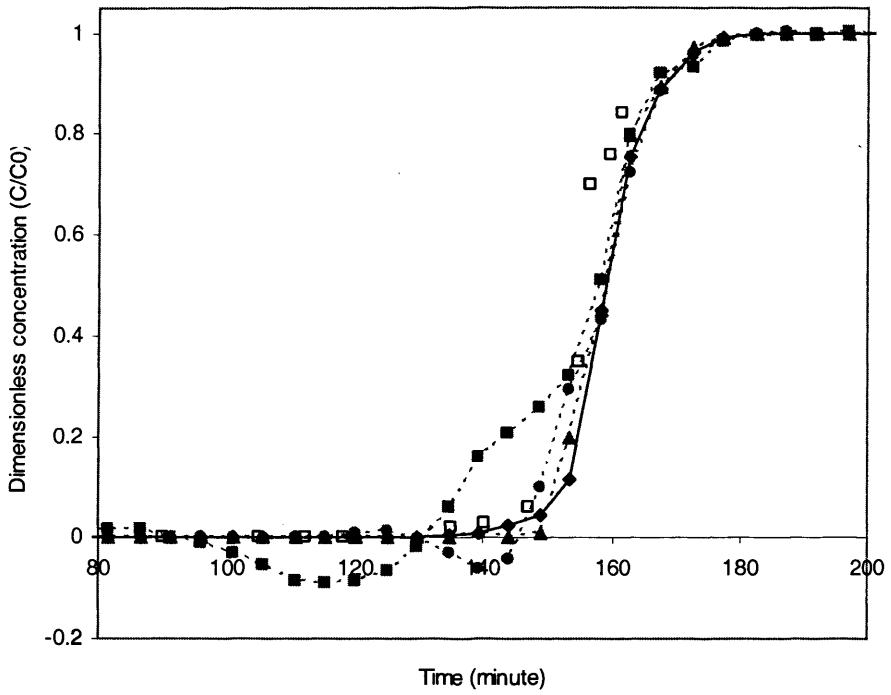

Fig. 7.3 Convergence analysis of breakthrough curves at 40 cm bed height using Mono-sized Bed model. *en* is number of elements used in the simulation. ■, 2 *en*; ●, 4 *en*; ▲, 7 *en*; ♦, 10 *en*; □, experimental data.

7.3.5 Results and Discussion

As in the section 6.5.4, simulations were performed for the Lysozyme-Streamline SP data set of Bruce and Chase (2001) using the Mixed bed particle dispersion model as described above to predict the breakthrough at 10 cm and 40 cm axial positions of the bed. All datasets and associated parameter values were as described in section 6.6.

The breakthrough curve simulated at 40 cm using the MB-particle dispersion (MB-PD) model (Fig. 7.4a) was not significantly different from that using MB-size partition (MB-SP) model. Both of them were close to the experimental data. At 10 cm there was a slight difference in the simulation result of the MB-PD and MB-SP models (Fig. 7.4b). The concentration of component rose slightly more slowly in the MB-PD model.

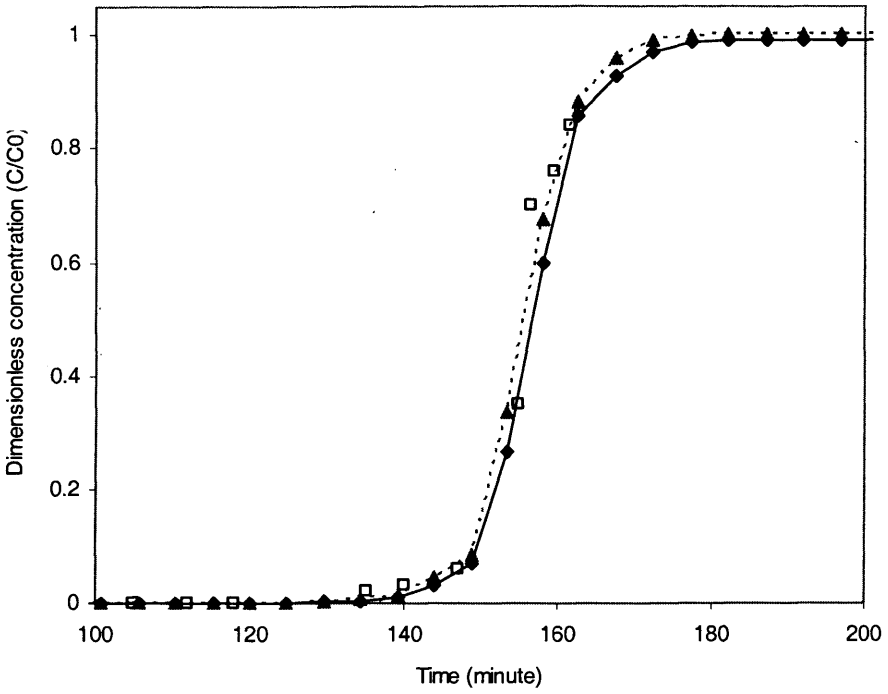

(a)

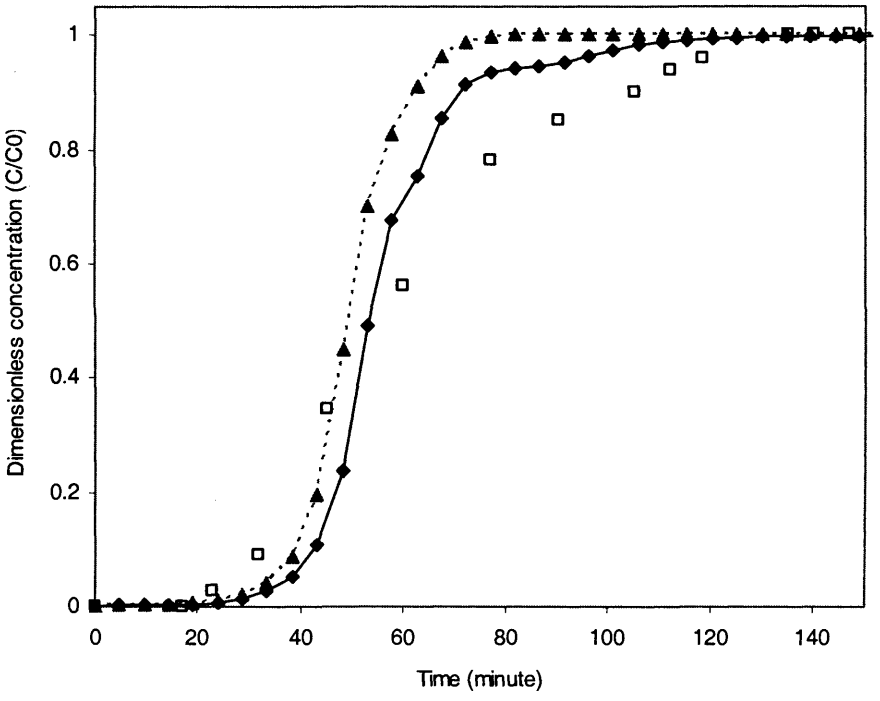

(b)

Fig. 7.4 Breakthrough curves at (a) 40 cm and (b) 10 cm bed heights as simulated by Mixed bed particle dispersion model (MBPD) and Mixed bed size partition model (MBSP). ♦, MBPD; ▲, MBSP; □, experimental data.

Based upon these results, it seems that the inclusion of particle dispersion did not have a significant effect in the adsorption response of EBA under the operating conditions

investigated where analysing breakthrough at the column outlet. This observation agrees with that reported by Wright and Glasser (2001) who also concluded that the effect of particle dispersion is not significant in EBA. In spite of that, failure to achieve an accurate simulation of breakthrough within the lower parts of the bed by the model indicates that it may not be entirely true. The observed slightly earlier rise and slower rate of reaching saturation within the lower parts of the bed does in fact indicate a possible effect of particle dispersion.

Thus to improve the model prediction and the shortcomings of the model, as explained in the introduction (section 7.3.1), an investigation on a new approach to the modelling of particle dispersion in EBA was performed and discussed in the following section.

7.4 Simulated Particle Dispersion Model

7.4.1 Introduction

During loading of EBA, the component concentration in particles at the lower parts of the bed is higher than it is in upper parts. When dispersion exists, particle moves randomly in the bed in all directions. This causes some portion of more densely loaded particles (i.e. having higher component concentration) from the lower section of the bed to reach the upper part of the bed while some portion of lightly loaded particles from the upper bed part will reach the lower part of the bed. These particles try to come to an equilibrium with their new environment in terms of the component concentration inside them and outside in the bulk fluid phase through mass transfer. This will simultaneously cause an increase in the component concentration in bulk fluid phase in the upper parts of the bed and simultaneously a decrease in the lower parts. This means that in all parts of the bed, the component concentration in bulk fluid phase and in the averaged particle phase will rise earlier but reaches the saturation point (or maximum) slowly. This will reduce the sharp concentration gradient in the bed which otherwise would have existed. From an industrial use perspective, this could be problematic, as it will severely limit the separation efficiency of the bed. So knowing the magnitude of particle dispersion and its effect on the adsorption response of EBA becomes important.

The current approach of representing particle dispersion in the expanded bed adsorption (EBA) model, developed by Wright and Glasser (2001), has an important weakness that has been discussed in section 7.3. Here, a new approach to include particle dispersion phenomenon correctly in EBA model will be developed and validated. The projected effect of particle dispersion on the adsorption response of EBA will also be tested using simulation results.

7.4.2 Model Development

The modelling approach is similar to that adopted in the mixed bed-size partition model as discussed in section 6.7 except for the inclusion of the effect of particle dispersion. An independent hydrodynamic part of the model determines the size distribution of particles and bed voidage along the bed axis (z). As in the MBSP or MBPD model, the approach used in hydrodynamic part can be an appropriate steady state hydrodynamic model or rely upon interpolation using experimental data. This gives bed voidage at a given axial position of the bed and the proportion of each size category.

If the particle dispersion is ignored, the EBA system can be represented by the same model as described in section 6.7 (MB-SP model). Dispersion causes the particle of each size partition to migrate between adjacent cells or nodes. As the bed is considered to be at hydrodynamic steady state, the rate of such migration both to and from nodes will be equal so that net change in concentration of particles in each size partition will remain null, i.e., their concentration remains constant as shown in Fig. 7.1 (in section 7.3.2).

Though the bed is considered to be at hydrodynamic equilibrium, from an adsorption perspective, it is in a transient state. The concentration of a component at different parts of the bed both in the bulk liquid phase and particle phase change until it also reaches an equilibrium (i.e. when the bed is fully saturated). When there is no particle dispersion, all the particles are considered fixed in place throughout an operation. Therefore, the mechanism of adsorption is the same as described for the MB-SP model in section 6.7. However, due to particle dispersion, some random portions of particles are continuously moving as described earlier. Though the particle flux is null, the adsorbed component flux will not be. For example during loading a mono-component EBA system, the concentration of a component is likely to be higher of within the lower parts of the bed compared to upper parts. Thus due to particle dispersion, at any given node (or a cell) the amount of component coming in from the upper adjacent node will be lower than the

amount of the component going out to the upper node until they reach to a local equilibrium, i.e., equal concentration at both. Such a mechanism of particle dispersion can be represented as in Fig. 7.5. Dispersion results in an additional dispersive flux of a component along the bed axis.

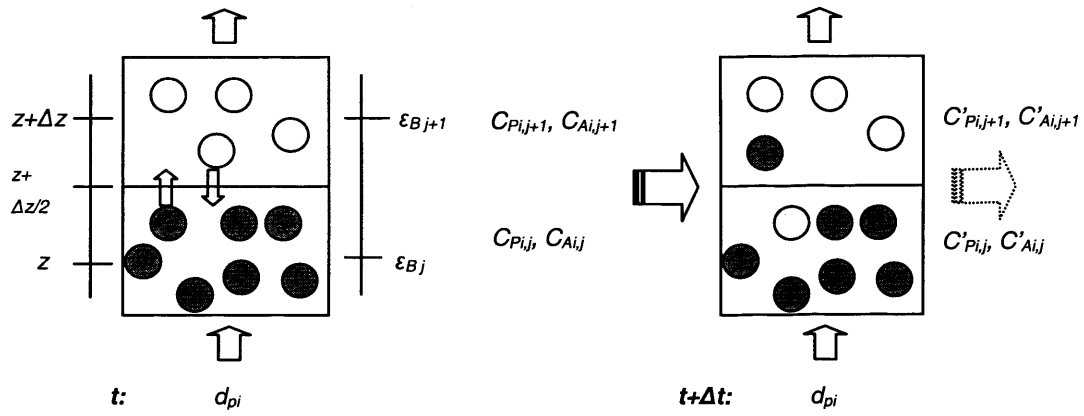

Fig. 7.5 A particle dispersion mechanism in EBA. The darker circles or particles contain different amounts of a component than do lighter ones. Due to particle dispersion, at the next time step ($t+\Delta t$), though the number of particle remain the same in both upper ($z+\Delta z$) and lower (z) cells of the bed as in the previous time step (t), the total amount of the component in the cells will be different as the new composition of particles is different. The voidage (ε_{Bj} and ε_{Bj+1}) of the cells j and $j+1$ will remain the same after the interchange of particles but their average concentration of component i in the particle, pore phase (C_{Pi}) and adsorbent phase (C_{Ai}) will change to new values, C'_{Pi} and C'_{Ai}.

One of the simplest ways to represent this component flux due to particle dispersion is by directly replicating the physical phenomena into a numerical scheme. Due to the enormously increasing computational power and decreasing monetary cost, such an approach becomes increasingly viable for many such simulation works.

In such an approach, the bed is represented as done in MB-SP models but instead of representing the portion of an axial node by one particle, a large number of particles of the same size are used. To make the result statistically significant at least 30 or more particles at each partition of each axial node is preferable. The adsorption mechanism for each particle will be the same as before. The net effect in the bulk liquid phase will be due to the cumulative fractional effect of all particles in that axial node across all partitions.

Similar to the MB-SP model, the mass balance of component i is given by:

$$\frac{\partial u_{Bi}}{\partial t} = -\frac{\partial u_{Bi}}{\partial z} + \frac{1}{Pe_L}\frac{\partial^2 u_{Bi}}{\partial z^2} - \sum_m \phi_m \sum_{q=1}^{q_N} \frac{1}{q_N} \xi_{im}(u_{Bi} - u_{pimq}\big|_{r=1}) \tag{7.42}$$

where ϕ_m is fraction of size partition m and q is the particle number within that partition of total of q_N particles.

The boundary conditions, initial conditions and feed inlet for bulk phase are same as in the earlier model.

$$\left.\frac{\partial u_B}{\partial z}\right|_0 + Pe_L(u_B|_{in} - u_B|_0) = 0 \tag{7.43}$$

$$\left.\frac{\partial u_B}{\partial z}\right|_{z=1} = 0 \tag{7.44}$$

Initial conditions:

$$u_{Bi}|_{t=0} = u_{Bi}^0 \tag{7.45}$$

Feed concentration:

$$u_{0i} = \max\{u_{Bi-feed}(\tau)\} \quad -\infty < \tau + \infty \tag{7.46}$$

The component concentration at particle phase for each particle within a partition is also the same as in the MB-SP model. However, instead of one set of equations at each partition of an axial node, there will be q_N sets of equations, one for each particle. A set of equations for a component i at particle q of partition m at axial position z is as follows.

$$\frac{\partial u_{Kimq}}{\partial \tau} = \eta_{im}\frac{1}{r^2}\frac{\partial}{\partial r}\left(r^2\frac{\partial u_{Pimq}}{\partial r}\right) \tag{7.47}$$

$$u_{Kimq} = \varepsilon_{Pm}u_{Pimq} + (1-\varepsilon_{Pm})u_{Aimq} \tag{7.48}$$

With boundary conditions:

$$\left.\frac{\partial u_{Pimq}}{\partial r}\right|_0 = 0 \tag{7.49}$$

$$\left.\frac{\partial u_{Pimq}}{\partial r}\right|_{r=1} = Bi_{im}(u_{Bi} - u_{Pimq}\big|_{r=1}) \tag{7.50}$$

With initial conditions:

$$u_{Pimq}|_{t=0} = u_{Pimq}^0, \quad u_{Aimq}|_{t=0} = u_{Aimq}^0, \quad u_{Kimq}|_{t=0} = u_{Kimq}^0 \tag{7.51}$$

Isotherm relation:

$$f_k(u_{A1},\ldots,u_{AN},u_{P1},\ldots,u_{PN})|_m = 0 \qquad k = 1,2,\ldots,N \qquad \forall j \tag{7.52}$$

or for a multi-component competitive Langmuir:

$$u_{Aimq} = \frac{b_{0i} u_{Pimq}}{1 + \sum_{k=1}^{N} b_k u_{0i} u_{Pkmq}} \tag{7.53}$$

And constants of the system:

$$Pe_L = \frac{vL}{E}, \qquad \xi_{im} = Bi_{im} \eta_{im} \frac{3(1-\varepsilon_B)}{\varepsilon_B}, \tag{7.54}$$

$$\eta_{im} = \frac{\varepsilon_{Pm} D_i}{R_m^2} \frac{L}{v}, \qquad Bi_{im} = k_{fim} \frac{R_m}{\varepsilon_{Pm} D_i}$$

The additional term in this set of equations is the flux of a component i due to particle dispersion. Here instead of calculating such component flux, particle flux due to dispersion (J_P) will be computed and incorporated into the model. This automatically updates the component flux resulting from it. Molecular diffusion or dispersion is due to the random motion of molecules. Similarly applying the same principle at the particle level, the particle dispersion is due to random motion of particles. In the one-dimensional case, it means movement of particles going away from a position and coming into it. For an equilibrium to exist both going out and coming in will have to be equal. Thus the particle flux will be given by total amount of such transport of particles on both directions.

The amount of particle flux (J_P) due to dispersion will have to be determined using experimental data or estimated using a particle dispersion coefficient. Once established, J_P can be used to determine the fractional amount of particles which will interchange between two adjacent axial positions (or nodes) in a small time step Δt. Let such a fraction be w_{Jp}. Assuming a constant particle dispersion coefficient for all particle sizes, the flux fraction, w_{Jp}, will also remain constant.

To implement this in a numerical scheme, adsorption in the bed at time t was simulated using the equation set as done in MB-SP model. The maximum time step Δt was restricted such that at time step $t+\Delta t$ the flux fraction (w_{Jp}) was calculated based on the axial discretisation size (Δz), time step (Δt) and particle dispersion (E_P) index.

$$w_{jp} = \frac{1}{2} \Delta z \, \Delta t * \text{Particle Dispersion Index} \tag{7.55}$$

Out of the total number of particles selected at each partition, a fraction w_{Jp} was randomly selected at each node. Half of these selected particles were be interchanged with similarly selected particles of the corresponding upper node and the remaining half with the lower node in a similar manner. Simulation was continued from $t+\Delta t$ time step to new $t+2\Delta t$

time step with the new set of interchanged particles. Again at the end of the new time step, calculation of w_{Jp}, random selection and interchange was performed. This sequence of steps was continued until the completion of the physical process.

At this stage, for simplification, particle dispersion index was used instead of particle dispersion coefficient. They will have a bijective relationship. However, the exact relationship between them will have to be established in future. Here, the value used for the index will be hypothetical but it will enable the study of the effect of particle dispersion in the EBA system and demonstration of the proof-of-concept of the modelling approach developed here.

7.4.3 Parameter Estimation

As in the MB-SP model, the parameters (E_i, D_i, K_{fi}, b_{0i} and b_{1i}) for the adsorption part of the model and their estimation in the mixed bed model were the same as described earlier. For the hydrodynamic part, the Richardson-Zaki correlation parameter was determined using a *Ga*-based correlation but the natural terminal velocity was modified using a fitting parameter to match the observed final bed height. For mixed bed model the mean mixing sigma (σ_m) value of 40 and σ_m slope (the linear variation of σ_m w.r.t. particle size) of 0.5 were used assuming these do not to vary much from similar operating conditions as used by Willoughby (2000). A hypothetical particle dispersion index was used for test purposes.

7.4.4 Simulation

The discretisation was same as described in the previous section for the MB-SP model (section 6.7.4). For each particle, there will be a set of particle phase equations. The resulting system of ordinary differential equations was solved using Matlab's ODE-solver. For each simulation 6 elements were assumed for the bulk phase, 2 internal orthogonal collocation points for particle phase, 1 component species, 3 particle size categories and 3 particles per size categories were used. Maximum time step was restricted to 0.2% of total process time. Matlab's in-built ode-solver routine was slightly modified to call a function after each successful time step. Based upon the magnitude of the dispersion flux calculated, selection of a set of random particles and interchange between adjacent axial nodes was made to simulate the effect of dispersion during such

function calls. Due to the large computing time required, only coarse discretisation was possible. Thus, the simulation here was done just for testing the trend and for establishing proof-of-concept.

Simulation in a 1.7 GHz Pentium 4 processor with 500 MB RAM took 5 hours for the discretisation used here. For a reliable estimate, much finer discretisation would be required. As it would take lot of time, it was not performed and recommended as a future.

7.4.5 Results and Discussion

As in the previous section 6.7.4, the simulation was done for the Lysozyme-Streamline SP data set of Bruce and Chase (2001) using the Simulated particle disperison model as described above to predict the breakthrough at 10 cm and 40 cm axial positions of the bed. Except for the particle dispersion, all data set and associated parameter values were as described in section 6.6.

Simulations were performed using a hypothetical value of particle dispersion index. Higher index values correspond to higher rate of particle dispersion. However, the exact magnitude and its relation to particle dispersion coefficient have not been established in this work. Due to the large amount of computational time required, only a very coarse-grid simulation was done. Therefore, the result cannot be reliably compared to the experimental data or with simulation results produced by other models. Nevertheless, it will provide some knowledge on the trends and tentative effects of particle dispersion. It is demonstrated here as a proof-of-concept.

Simulation was performed for a particle dispersion (E_P) index of 20 and 1000. At an E_P index of 20, the predicted breakthrough was close to that predicted using MB-SP model (section 6.7.5) and the result at 40 cm breakthrough was also close to the experimental data. It appears that the index value of 20 essentially does not affect the system. When an E_P index value of 1000 was used, the simulation result for both 40 cm and about 10 cm bed height differed from the MB-SP model result. The results are shown in Fig. 7.6 a,b.

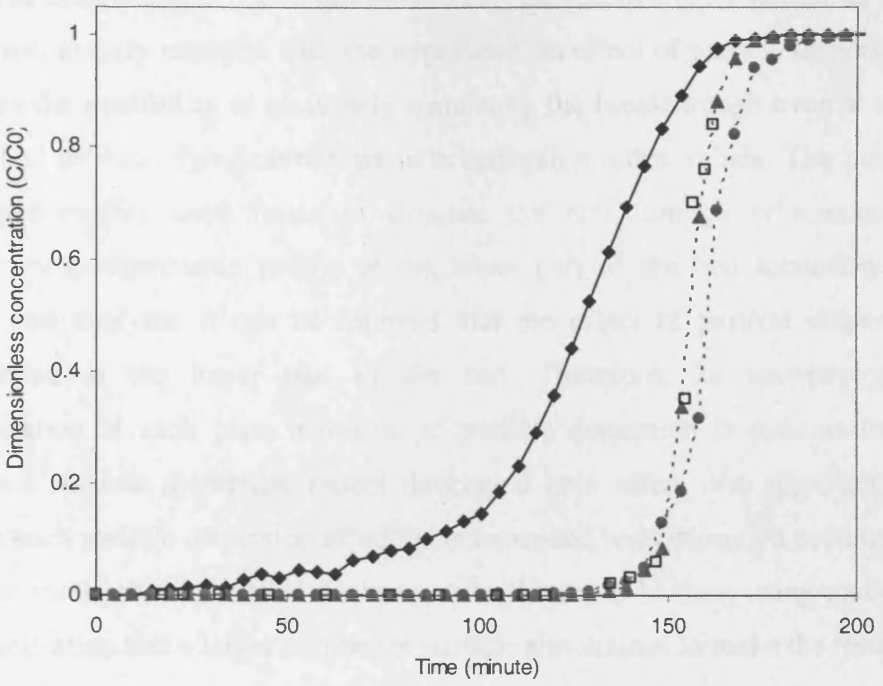

(a)

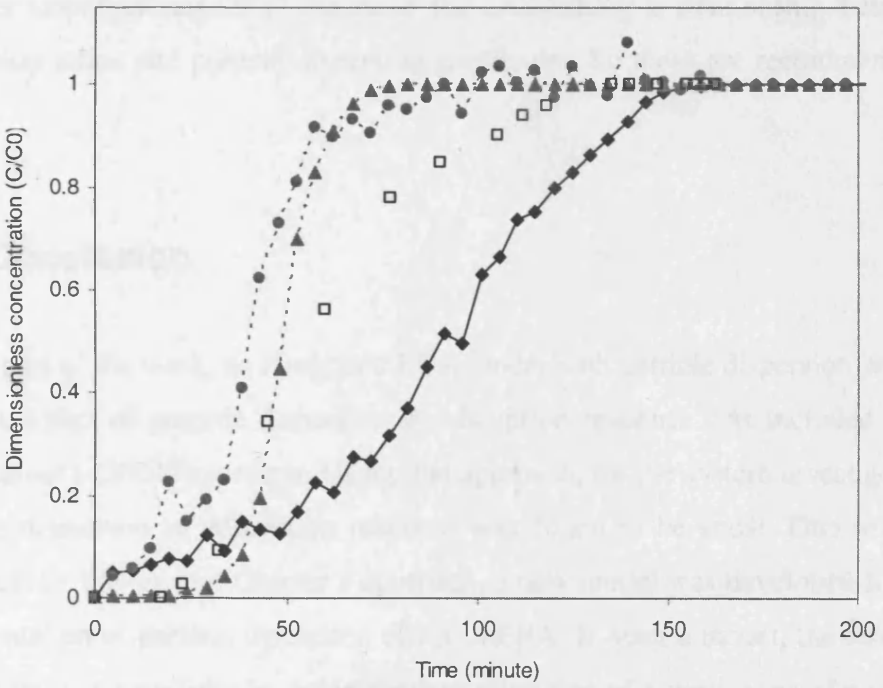

(b)

Fig. 7.6 Breakthrough curves at (a) 40 cm and (b) 9.23 cm bed heights as predicted by Simulated particle dispersion (SPD) model using a hypothetical value of 1000 and 20 for particle dispersion (Ep) index, and by Mixed bed size partition (MBSP) model. ♦, SPD with Ep index of 1000; ●, SPD with Ep index of 20; ▲, MBSP; □, experimental data.

The component concentration rose early and reached to its saturation value, slowly. This result exactly matched with the hypothesis on effect of particle dispersion. This also indicates the possibility of accurately simulating the breakthrough even at the lower part of the bed by identifying correct particle dispersion index values. The previous models developed in this work failed to simulate the breakthrough or temporal change in component concentration profile at the lower part of the bed accurately. From these results and analysis, it can be inferred that the effect of particle dispersion is more pronounced at the lower part of the bed. Therefore, for accurate simulation of concentration at such parts inclusion of particle dispersion is seen as important. The simulated particle dispersion model developed here offers one approach by which to include such particle dispersion effect in an expanded bed adsorption accurately.

To establish this method further tests will have to be done using much higher level of discretisation and a larger number of particle simulations to make the result statistically reliable. Due to large amount of time required for such simulation, this has not been done. Another important aspect is the need for establishing a relationship between particle dispersion index and particle dispersion coefficient. So these are recommended as future work.

7.5 Conclusion

In this part of the work, an integrated EBA model with particle dispersion was developed. At first, effect of particle dispersion in adsorption response was included using Wright and Glasser's (2001) approach. Using that approach, for the system investigated, effect of particle dispersion in adsorption response was found to be small. Due to an important weakness in Wright and Glasser's approach, a new model was developed for an accurate representation of particle dispersion effect in EBA. In such a model, the effect of particle dispersion was simulated by using random migration of a proportion of particles at each axial position at each time step. Using a hypothetical particle dispersion index corresponding to particle dispersion coefficient, the effect of particle dispersion in EBA adsorption response was demonstrated. It was observed that the inclusion of particle dispersion effect would be particularly useful in accurately predicting the breakthrough profile even at lower parts of the bed, which the models developed without particle dispersion were not able to represent accurately. In the next chapter, the steady state

assumption of hydrodynamics will be relaxed and attempt will be made to develop a model that would be capable to predict adsorption response while the bed is at hydrodynamic transient state.

8 Integrated Model: Transient Hydrodynamics

8.1 Introduction

There is as yet no literature with which to predict the adsorption response of EBA when the bed is still under a transient state i.e. during expansion or contraction. At the start up or at the time of loading, changes due to either flow or fluid will bring about changes in EBA hydrodynamics and consequently its adsorption behaviour during that period. Being able to predict EBA response can be advantageous for optimal operation, e.g. during loading and will give more confidence during process validation. To address these needs, a simple integrated EBA model with transient hydrodynamics is developed in this chapter. At this initial stage the model is simplified by assuming homogeneous mono-sized bed. Future work would focus on relaxing this so as to provide for a more realistic bed model where the distribution of particle sizes will be considered.

8.2 Plan and Objectives

The individual independent models for adsorption and hydrodynamics have been developed in chapters 3 and 5 respectively. In this part of the work a complete transient EBA model will be developed by integrating the adsorption and hydrodynamic models developed earlier. For simplification at this initial stage, the bed will be considered mono-sized.

8.3 Model Development

In this work, a simplified approach is followed whereby the hydrodynamic and adsorption parts of the model were partially decoupled so that the hydrodynamic part is independent of the adsorption part. The hydrodynamic element is simulated independently and is progressed in single time steps. The different parameter values at an axial position of the bed are updated from it. These updated parameter values are then used in the adsorption part for that time step. In this way the two parts of the model are simulated sequentially at each time step.

8.3.1 Model Parts

In a simplified approach as mentioned above, the model itself is same as hydrodynamic and adsorption models as described in section 5.4 and 3.4. At any given time the bed properties of an axial segment (Fig. 8.1) will be given by hydrodynamic part of the model and adsorption within it will be given by adsorption part of the model.

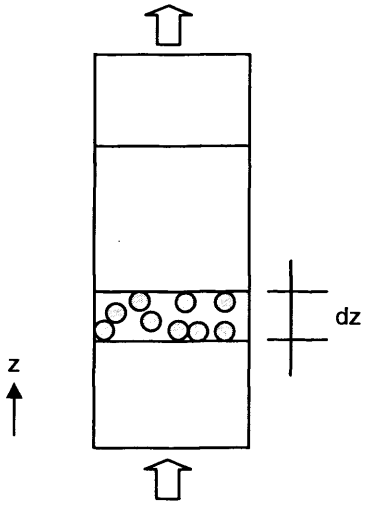

Fig. 8.1 A section or differential volume element of bed shown during transient state of EBA

The details of the model parts are as follows:

i. Hydrodynamic part: The hydrodynamic part of EBA is represented as described in Chapter 5 by Eq. (5.46) with initial conditions Eq. (5.47), boundary conditions Eqs. (5.61)-(5.62), and constants of the system, Eqs (5.41)-(5.44).

ii. Adsorption part: The adsorption part is represented by set of equations (3.83)-(3.97) but with axial variation in parameters and bed properties based on a transient state of the hydrodynamic part.

A crucial step in the integration of the models is the shifting of the particles due to hydrodynamics at each time step and the updating of the component concentrations in both the pore and adsorbent phases of the particle resulting from adsorption. This is achieved by a particle shifting method which is explained in the following section.

8.3.2 Integration Approach: Particle Shifting Method

At time t particles are located at their respective positions along the bed axis. Due to adsorption, they will reach certain values of concentration of component chemical in the pore and adsorbent phases. Now due to transient hydrodynamic state, the bed will expand (or contract if flow rate falls). This means at $t+\Delta t$ time step the particle occupying the space at a given axial position, z comes from a different bed location. If it is an expansion, it comes from below, $z-\Delta z_1$. The particle originally at z at time t will have moved to $z+\Delta z_2$ at $t+\Delta t$. So tracking which particle is the originating particle at t becomes important so that the appropriate initial pore phase and adsorbent phase component concentrations are used during the adsorption process at that time step. Had it been a fully coupled model, it would have been automatically take care of by the model. However since for simplification the hydrodynamic and adsorption parts are partially decoupled, such tracking and updating becomes an integral part of the approach and is achieved by mass balance. The update is done at discrete time steps rather than in a continuous fashion. Providing such time steps are sufficiently small, it can be considered almost a continuous process for practical purposes. The reason for the partial decoupling is valid as for practical purpose it can be considered that due to the adsorption process, the viscosity and density of fluid does not substantially change in a small time step Δt. Here only adsorption element depends on the results of the hydrodynamic part and so there is a one-way update. The step-wise detail of the method is as follows.

Method:

The implementation of the approach is depicted in Fig. 8.2.

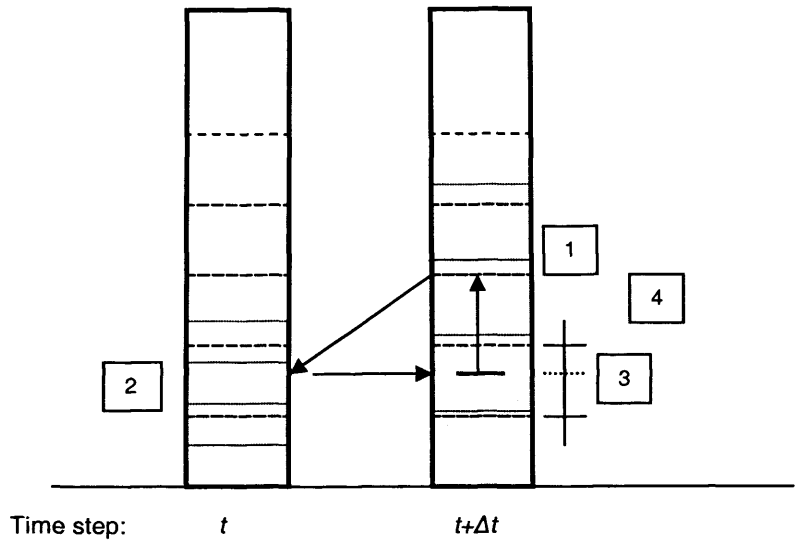

Fig. 8.2 Particle shifting method for integrating hydrodynamic and adsorption parts. (1) Values of adsorption node to be determined at $t+\Delta t$; (2) Mapping it to location at t using mass balance; (3) Interpolation of values at that location at the end of t; (4) Shifting or updating the values to the search-originating adsorption node before start of $t+\Delta t$ for adsorption process. ---, Adsorption nodes; ·····, Hydrodynamic nodes.

1. To update concentrations of component in the particle pore and adsorbent phase at time step $t+\Delta t$ at an axial position z, its concentrations at time step is required. Due to movement of the particle during Δt, the original particle location moves to $z+\Delta z'$ while the particle occupying this former axial position comes from location $z-\Delta z$. So concentrations at the end of time step t from particle of location $z-\Delta z$ should be used as the initial concentration of particle at z at the beginning of time step $t+\Delta t$ for the update due to the adsorption process.
2. Location of particles at time t or the value of axial migration Δz is determined using a mass balance. What it means is that as the bed is uniformly expanding the mass proportion of particle below it or above it remains constant throughout the operation. And so it is true while going to $t+\Delta t$ from t time step and thus the Δz is determined.
3. So original position (or $z-\Delta z$) of particle at z at $t+\Delta t$ is determined. This particle is shifted to new location i.e. at z. Hence the concentration of component in the pore and adsorbent phase of particle at $z-\Delta z$ at the end of time step t will be used as the initial value for update at time step $t+\Delta t$.

4. Since Δz is arbitrary, the location of a particle is rarely at the nodes when discretised for simulation. So as only nodal concentration values are known or computed, such values lying in between nodes (of adsorption discretisation axis) will have to be interpolated.

In the present simplified method, during expansion if the upper surface of bed does not match with the nodes on the adsorption axis (which is more a rule than an exception) while going from t to $t+\Delta t$, the effect of the mass of particles in-between that location and the upper most node on the adsorption axis which is covered, will not be included in the adsorption process update for that time step Δt. Since the hydrodynamic part is independent of the adsorption part the total mass of particles in the bed is always conserved. The loss of a sink term at such upper surface of the adsorption axis is just transient and will soon be covered and used by the next time step when the surface rises above that node. Even after reaching a hydrodynamic equilibrium, it is possible that a tiny fraction of the particle phase may remain excluded from its effects updates. Providing the use of a finer mesh or a larger degree of discretisation is made, the effect can be made very small and negligible. Hence the total error is bound and can be neglected. More accurate remedies could be by applying a moving-mesh approach to match exactly hydrodynamic and adsorption axial nodes, or by using of a weighted sink in the upper node just above the particle phase surface, etc. At this stage only a simple method is adopted.

In this way a simple integration of adsorption and transient hydrodynamics of EBA is achieved.

8.4 Parameter Estimation

There are number of parameters used in both adsorption and hydrodynamic parts of the model. Adsorption part uses parameters bulk liquid phase dispersion (E), diffusivity of component species i (D_i), film mass transfer coefficient (k_{fi}) and isotherm parameters (b_{0i}, b_{1i}). Estimation of their values was the same as described in section 3.5. Similarly the hydrodynamic part uses particle dispersion coefficient (E_p) and Richardson-Zaki correlation (n) parameter values. The method employed to estimate them are same as explained in section 5.5.

8.5 Simulation

The adsorption part of the model was discretised using orthogonal collocation – finite element method (OCFE) as described in section 3.6, and the hydrodynamic part of the model was discretised using finite difference (method of line principle) to yield a set of ordinary differential equations (ODE). Such an ODE-set was solved using Matlab's stiff ODE-solver. The maximum time step (Δt) was specified to keep that small. Integration between the adsorption and hydrodynamic parts of the model was achieved by applying the particle shifting method at the end of each time step progression as explained earlier. For this Matlab's built-in ODE-solver code had to be slightly modified to call an external routine and to pass and update variables after completing each successful time step and before going to the next time step. That routine was developed as an interface between Matlab's ODE-solver code and other user made time step operation codes at each time step. The integration between hydrodynamic and adsorption parts of the model was applied through that interface.

8.6 Convergence Analysis

To validate the numerical scheme employed, convergence analysis was performed for the discretisation size of space related with the adsorption part of the model, the hydrodynamic part and the maximum size of each time step. In each case as the number of discretisation events was increased, the result was found to converge as seen in following Fig. 8.3-Fig. 8.5.

Use of 10 elements in the bulk fluid phase was found to give a result very close to the converged solution (Fig. 8.3) for 40 cm bed height breakthrough. In this work, 30 elements will be used to be able to estimate the component concentration at 10 cm bed height more accurately. Five internal orthogonal collocation points were used for higher accuracy of estimation at lower axial positions. For hydrodynamic nodes, even use of five nodes was found to give very close result to the converged solution (Fig. 8.4). It is probably due to a simple bed voidage profile expected at any time, which could have been represented using a low order polynomial, or even just a quadratic function.

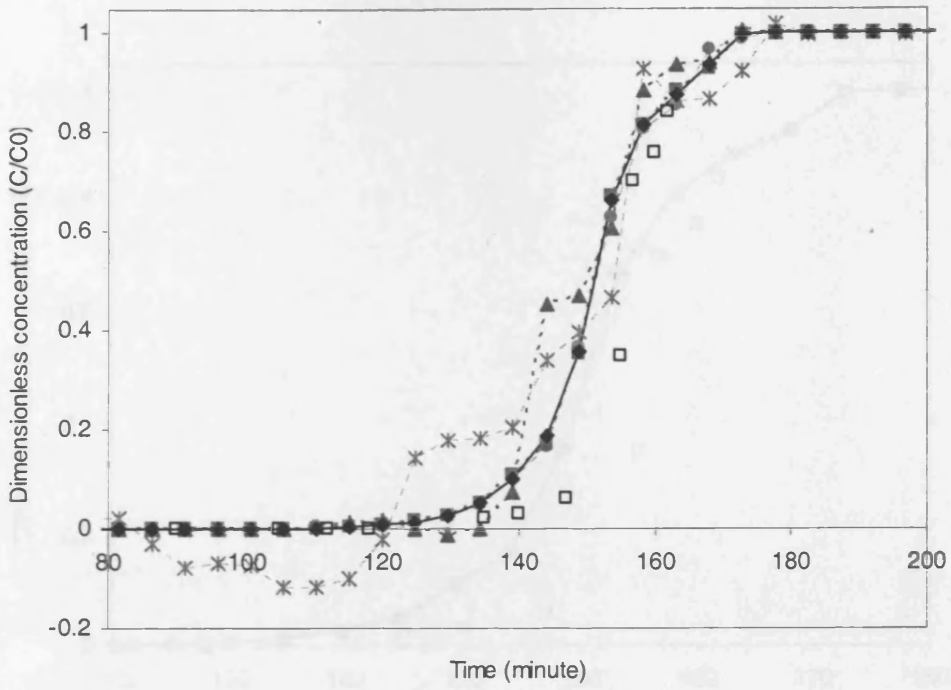

Fig. 8.3 Convergence analysis of Transient-hydrodynamic EBA model with respect to number of elements (*en*) using breakthrough curve at 40 cm bed height. ✳, 2 *en*; ▲, 5 *en*; ●, 10 *en*; ■, 20 *en*; ♦, 30 *en*; □, experimental data.

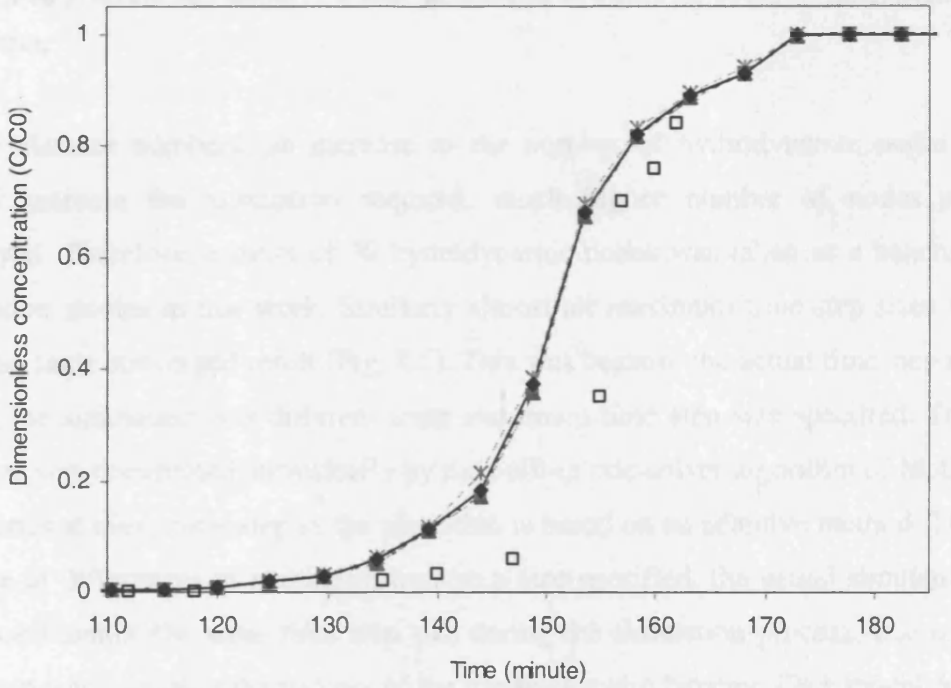

Fig. 8.4 Convergence analysis of Transient-hydrodynamic EBA model with respect to number of hydrodynamic nodes (*Nh*) using breakthrough curve at 40 cm bed height. ✳, 5 *Nh*; ▲, 10 *Nh*; ●, 20 *Nh*; ■, 30 *Nh*; ♦, 50 *Nh*; □, experimental data.

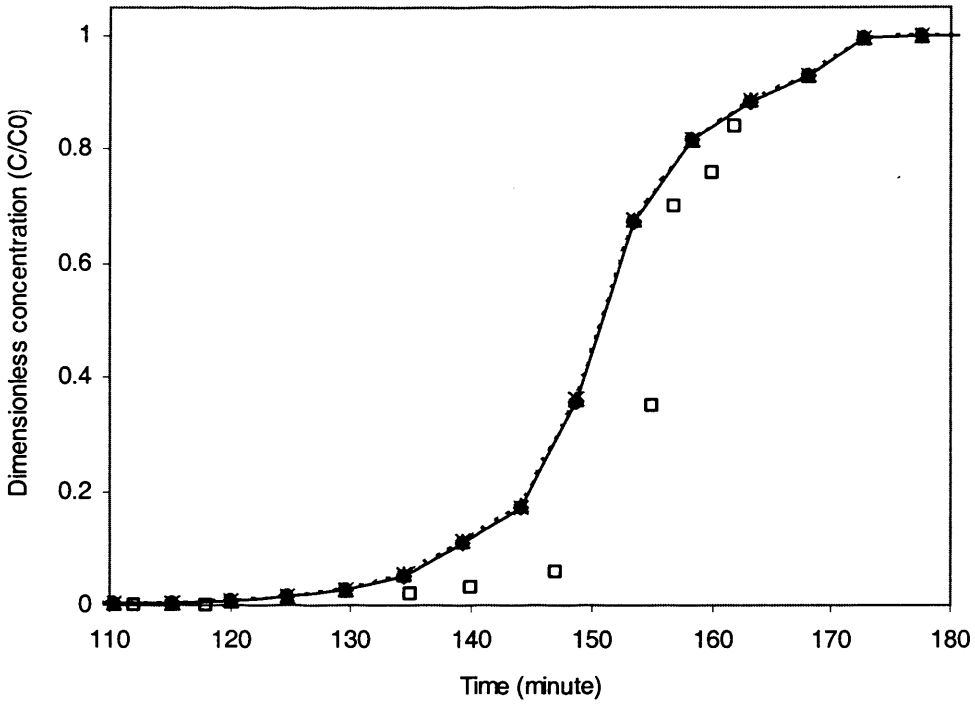

Fig. 8.5 Convergence analysis of Transient-hydrodynamic EBA model with respect to maximum time step size (*dt*) as a percentage of total process time using breakthrough curve at 40 cm bed height. *, 1% *dt*; ▲, 0.1% *dt*; ●, 0.05% *dt*; ♦, 0.01% *dt*; □, experimental data.

Unlike element numbers, an increase in the number of hydrodynamic nodes did not greatly increase the simulation required, much higher number of nodes could be employed. Therefore, a mesh of 30 hydrodynamic nodes was taken as a benchmark for simulation studies in this work. Similarly almost all maximum time step sizes specified gave the same converged result (Fig. 8.5). This was because the actual time step size used during the simulation was different from maximum time step size specified. The actual step size was determined intrinsically by the built-in ode-solver algorithm of Matlab. That also varies at every time step as the algorithm is based on an adaptive method. Therefore, in spite of differences in maximum time step size specified, the actual simulation could have used almost the same time step size during the simulation process. Use of a small time-step was critical to the success of the transient-hydrodynamic EBA model developed in this work due to the need for discrete updates of bed properties. In order to avoid the use of large time steps even if the ode-solver allowed, a maximum time step size of 0.05% of the total process time was taken as a standard for this work.

8.7 Results and Discussions

Due to a lack of time, experimental data could not be generated to verify the model. However, simulation was done using the Lysozyme-Streamline SP data set of Bruce and Chase (2001) to see how different the adsorption response of an expanded bed would have been, had it been loaded simultaneously as the bed expanded instead of after reaching a hydrodynamic equilibrium. In such a mode, adsorption would be taking place while the bed is still at a hydrodynamic transient state. There are a number of circumstances during an EBA operation that adsorption takes place while the bed is at hydrodynamic transient state, e.g. during changing of feedstock, during stabilisation after a non-propagating small shock or disturbance in the bed for example by a lump of feed having tendency to aggregate, during gradient change of fluid velocity, etc. Thus, the simulation done here would be a test for its possible uses and adaptations in other operating scenarios, which would require consideration of the hydrodynamic transient state.

Simulation was done for the Lysozyme-Streamline SP data set of Bruce and Chase (2001) to predict the breakthrough at 10 cm and 40 cm axial positions of the bed. Mean particles size of 192 μm was used as estimated by Bruce and Chase (2001). The density of particle was considered to be 1.184 gm/cc as by Yun et a. (2004) which was close to the manufacturer's specification of 1.2 gm/cc. Fluid density and viscosity of the sample in phosphate buffer were taken to be 0.99 gm/cc and 0.102 gm/cm.s respectively. As before based on the estimate of Coulson (1991), the settled bed voidage was taken to be 0.4. Particle pore voidage was taken to be 0.35 as described by Li et al. (2004).

In the experimental set up, the settled bed height was 21.2 cm and the superficial fluid velocity was 184 cm/h. The use of *Ga* based correlation underestimated the bed height. Thus as done in transient hydrodynamic modelling in chapter 5, experimental fitting of Richardson-Zaki correlation parameter and effective terminal velocity was employed. The particle size and density of Streamline SP is not much different from that of Streamline DEAE used in the hydrodynamic experiment of Thelen and Ramirez (1997). They used water as the mobile phase. Assuming the variation in density and viscosity of mobile phase in lysozyme-Streamline SP system, i.e. phosphate buffer with lysozyme sample, to be not too far from water, the parameter values to define bed

expansion can be reasonably used to predict the transient bed expansion in later systems when the settled bed height and fluid velocity are also similar. The settled bed height here was 21.2 cm and it was 20.5 cm in Thelen and Ramirez experiment. The fluid velocity used here 184 cm/h was also close in the range of fluid velocities used in their experiment, which was 61 cm/h to 169 cm/h. Therefore, the correlation developed based upon their experimental data was used here for the prediction of bed expansion, which was a terminal velocity of 0.139 cm/s and Richardson-Zaki correlation parameter of 2.663. To match the simulated height and the observed experimental bed height for 2 times expansion with about average 0.7 bed voidage (as observed in experiment and reported by Bruce and Chase), the effective terminal velocity had to be reduced by about 5% to 0.132 cm/s.

The simulation results for both 40 cm and 10 cm breakthrough data using the system when loading was done simultaneously with bed expansion from its settled state were found to be almost exactly the same as if the loading was done after the system reached to a steady state and the whole bed had a homogenous equilibrium voidage of 0.7. This can be seen in the following Fig. 8.6 a,b.

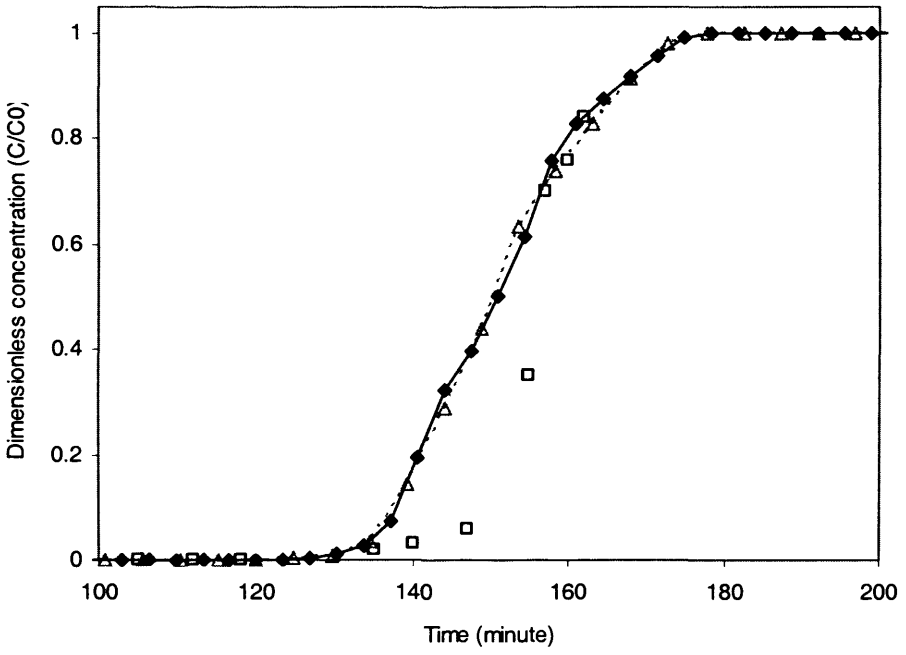

(a)

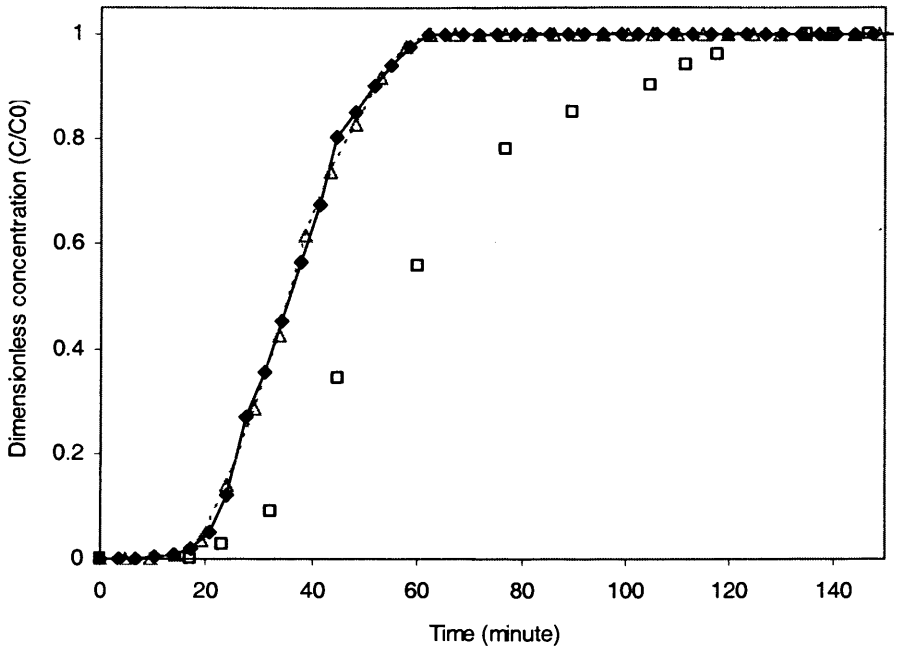

Fig. 8.6 Simulation of breakthrough curves at (a) 40 cm and (b) 10 cm bed heights using Transient-hydrodynamic EBA model and mono-sized steady state hydrodynamic EBA model (developed in chapter 6.4) and using the correlation for the lysozyme-Streamline SP system at investigated operating conditions. ♦, simulation result when hydrodynamic-transient state of the bed is considered i.e. both bed expansion and loading done simultaneously; Δ, simulation by considering the bed to be already at hydrodynamic steady state and so homogeneous in terms of bed voidage and particle size before the start of loading and during it; □, experimental data of EBA operation at hydrodynamic steady state (Bruce and Chase, 2001).

For the lysozyme-Streamline SP system used here, it seems the change in voidage to its equilibrium value was much faster than the change in component concentration in any axial position. If we consider the voidage change as a hydrodynamic front and the component concentration as an adsorption front, it can be said that the hydrodynamic front moved much faster in this system investigated than did the adsorption front. Such a situation is possible when a component is rapidly adsorbed to the matrix. Therefore, effectively, when a component reaches a higher axial position downstream, the local bed voidage at that position might already have been close to an equilibrium voidage. Another way to look at it is that, in this system, most of the adsorption process at a given axial position happens when the local voidage is already at or close to an equilibrium voidage. It is also worth noting that the complete hydrodynamic equilibrium of the bed was reached in about 20 minutes compared to more than 200 minutes in terms of adsorption,

that is, the bed being almost fully saturated with the component of interest. In essence, the adsorption response of an expanding bed of such rate parameters, in effect, will be the same as that of the bed at equilibrium. This is an interesting finding. What it implies is that assuming the bed remains stable in such a hydrodynamic transient operation, loading can be done simultaneously while the bed is expanding without need to reach it to hydrodynamic equilibrium first when the rate of adsorption is fast. This will save about 30-40 minutes of operation time and result in a valuable increase in throughput. Before making any general conclusions here, these simulation results and the hypothesis should be validated with experimental data. Such a validation experiment is recommended as a future work.

In order to verify the above hypothesis that the faster rate of adsorption is the reason, in this system, why the breakthrough result from hydrodynamic-transient bed operation was not different from hydrodynamic-steady state bed operation, the following investigation was conducted.

Hypothesis Testing:

For a simple test of the above mentioned hypothesis, an investigation was conducted such that the rate of adsorption was delayed. Using simulation studies, the film mass transfer from the bulk fluid phase to particle phase was found to be one of the important rate limiting factors for adsorption. So as to reduce the rate of adsorption and observe its effect, the film mass transfer coefficient (k_f) was reduced to 10% and three operating scenarios investigated:

i. Both expansion and loading were done simultaneously resulting into a hydrodynamic-transient state of the bed. (Transient hydrodynamic EBA model developed in this chapter was used for the simulation.)
ii. Bed was taken to be already at hydrodynamic-equilibrium so it was homogeneous in terms of bed voidage and particle size before starting loading. (So simulation for this was conducted using mono-sized steady state hydrodynamic EBA model developed in section 6.4)
iii. Loading was done 30 minutes after the operation started. This meant the bed would expand and possibly equilibrate before loading started. (This was also simulated using transient hydrodynamic EBA model.)

All simulations were done for first 7.5 minutes of loading only as the effect of hydrodynamic-transient bed state would be more pronounced in the beginning of the operation. All other operating conditions and parameters were same like before, i.e. Lysozyme-Streamline SP system investigated earlier.

As can be seen in Fig. 8.7, the breakthrough curves at 10 cm of bed height for scenario (*ii*) and (*iii*) matched exactly while there was a slight delay in concentration rise for scenario (*i*) for the first few minutes or for an early part of the adsorption process.

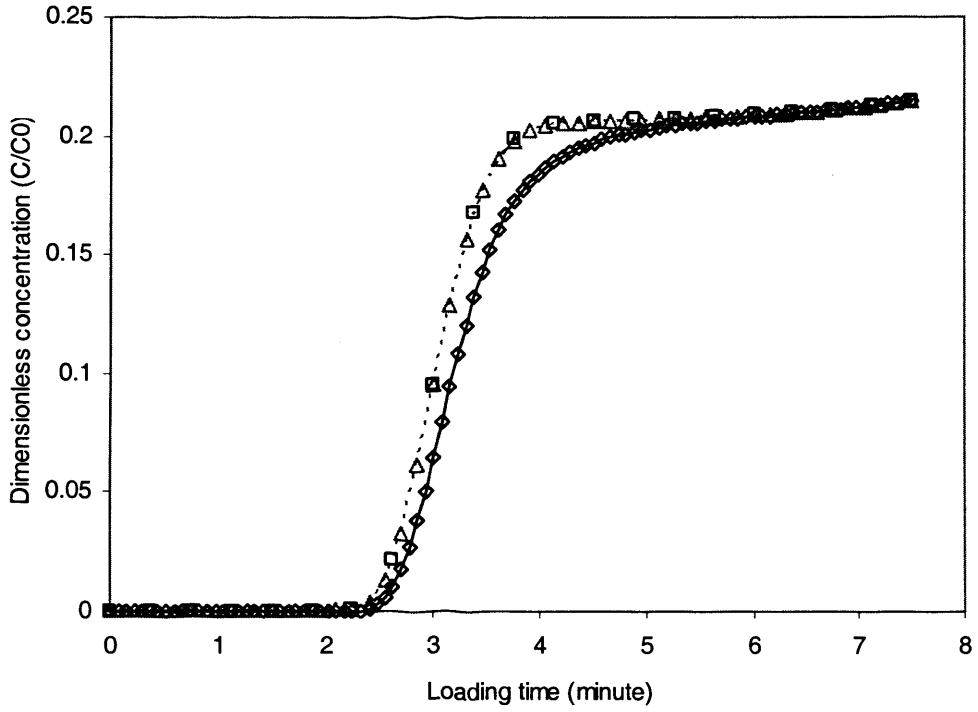

Fig. 8.7 Simulation of breakthrough curves at 10 cm bed height for first 7.5 minutes of loading using Transient-hydrodynamic EBA model. Film mass transfer coefficient (k_f) was reduced to 10% of the original as estimated by correlation for the lysozyme-Streamline SP system at investigated operating conditions. ◊, simulation result when hydrodynamic-transient state of the bed is considered i.e. both bed expansion and loading done simultaneously; △, simulation by considering the bed to be already at hydrodynamic-equilibrium or steady state and so homogeneous in terms of bed voidage and particle size before the start of loading and during it; □, simulation when loading was done 30 minutes after the operation started.

This demonstrated that, at a lower rate of adsorption, the difference in the component concentration rise in a hydrodynamic-transient bed and a hydrodynamic-equilibrium bed would be more pronounced. In a hydrodynamic-transient bed operation, scenario (*i*), the

voidage of the first 10 cm of the bed will be at slightly lower than that it would have been had it been at equilibrium voidage from the beginning as in scenario (*ii*), as there would be more particles to adsorb. Therefore the rise of the component concentration in the bulk fluid phase at such a location will be slightly delayed. This is clearly visible in Fig. 8.7. Further process time would result in an equilibrium voidage being achieved, and the difference would disappear as observed. When the bed was not loaded for the first 30 minutes of operation, as in scenario (*iii*), the bed would expand and would reach its hydrodynamic equilibrium. As it took only about 20 minutes for this system to reach to its hydrodynamic equilibrium, by 30 minutes the bed would have become fully homogeneous with an equilibrium voidage. So when it was loaded after that, its adsorption response would be same as that of a homogenous bed of scenario (*ii*). These results perfectly satisfied the expectation.

When the adsorption rate is sufficiently high, as observed in normal EBA operation here for the Lysozyme-Streamline SP system, the breakthrough curve at both 10 cm and 40 cm bed heights for both hydrodynamic-transient bed operation and hydrodynamic-steady state bed operation were found to match exactly as seen in Fig. 8.6 b,a. This corroborates the hypothesis that when the adsorption rate is fast, such that the hydrodynamic front moves much faster than adsorption front, the adsorption response of the expanded bed in terms of breakthrough curve, or component concentration rise in bulk fluid phase, at the bed exit would be similar.

There are number of assumptions taken in formulating the hydrodynamic model as described in Chapter 5. The validity of such assumptions in addition to the assumptions of the adsorption part of the model is one of the limitations of this model.

8.8 Conclusion

The approach, particle shifting method, developed in this work to integrate transient hydrodynamics and adsorption parts of EBA model seems to be feasible and valid based on: simulation result and the logic. Though due to lack of time, experimental data on hydrodynamic-transient EBA operation could not be generated to validate the model, when compared to hydrodynamic-steady state data, the result was found to be within the bounds of expectation. On the other hand, the assumed independence of hydrodynamics from adsorption for normal EBA operation and the possibility of reducing the time step to

make the two processes (adsorption and hydrodynamics) practically simultaneous makes the approach logically valid. As the hydrodynamic part is practically independent of the adsorption part, any better hydrodynamic model, possibly a theoretical model, when available can be integrated to the adsorption part by the same approach as explained in this chapter so as to describe a complete EBA system.

There are number of areas in which further investigations are recommended in terms of development of a hydrodynamic-transient EBA model from here. One is its applications. It looks like it can have a number of potential applications, some of which are enumerated in the next chapter. The second is to replace the current mono-sized hydrodynamic part of the model by a more advanced model which considers the distribution of particle sizes. Such a model has been described in appendix A.3.4. Along with that then the adsorption part of the model will have to be updated with a model which encompasses such a distribution of particle sizes and which provides more realistic representation of a mixed bed. Such models have been developed and studied in detail in Chapter 6.

Finally a more advanced method of integration is recommended to be developed. One limitation of the current approach is a possible need to limit the maximum time step to a small size. This means that the simulation takes a long time to run. Especially if the model had distribution of particle sizes and when such models used in simulating multi-component scenario, it would require a very long simulation time. Such a problem can be obviated by developing a new integrated model.

9 Model Applications

9.1 Introduction

In this thesis a series of models of expanded bed adsorption (EBA) have been developed commencing with somewhat simplified descriptions to more realistic, comprehensive but complex models. In this part of the thesis some important areas of application where such models can be useful will be explored and studied. It is not always necessary to use very involved models. Depending upon the purpose in many cases a simple model can be sufficient. In some cases a simple model will be more suitable as complex models more likely to require additional parameter values and computational resource. But obviously the more involved models provide some additional details of the system and so will be a pre-requisite when such details become an integral part of any process objective.

9.2 Plan and Objectives

There are a large number of possible applications of models, and a few will be selected here. The specific objectives are as follows.

- Sensitivity analysis
- Determination of Windows of Operation
- Determination of optimal loading time
- Enumeration of some possible applications of transient hydrodynamic EBA model.

9.3 Sensitivity Analysis

9.3.1 Introduction

One of the purposes of a model can be to optimise a process or maximise a performance index within a given set of constraints. The EBA models developed in this work can also be used for such purposes for example finding a superficial fluid velocity at which bed

productivity or throughput is maximum, purity of separated product is highest, etc. To determine these metrics, models will have to be simulated at varying conditions, model parameters estimated and supplied in the model. The methods employed to estimate such parameters have already been explained but such estimates normally will have errors. It is therefore important to know how sensitive the system is to these errors in order to ascertain the reliability of the findings. Thus sensitivity analysis of such parameters becomes an integral part of modelling work. It is also important to know what parameters or variables are the major limiting factors of a system. Such information can be useful in improving the desired performance of the system. Besides these, sensitivity analysis is also an important tool for validation of the model and its implementation. In a way, it provides dissection view of the model for its examination.

In this work the sensitivity of the steady state hydrodynamic EBA models to the following parameters will be performed:

- Bulk liquid phase dispersion coefficient (E)
- Diffusion coefficient of component i (D_i)
- Film mass transfer coefficient of component i (k_{fi})
- Superficial fluid velocity (v_0)
- Particle size (R)
- Adsorption parameter of component i
- Particle porosity (ε_P)

9.3.2 Method

For the purposes of a sensitivity analysis a mixed bed EBA model using the equivalent diameter approach (as discussed in section 6.7) was used. Though this is the simplest mixed bed model of EBA with steady state hydrodynamics developed in this work, it is as accurate as other involved ones like MB-SP model. Most importantly, it takes a fraction of time for simulation compared to other involved model and for these reasons was chosen as the basis for this part of the study. For sensitivity analysis, the magnitude of the objective parameter was both increased and decreased and its result in the breakthrough of a component from the bed was observed. The effect of the observation was then interpreted. The normal settings of all parameters and variables were as described in section 6.6 for lysozyme-Streamline SP system (Bruce and Chase, 2001). For simulation

12 elements, 5 internal orthogonal collocation points and 5 particle size categories were used.

9.3.3 Results and Discussion

The results of the sensitivity analysis of the parameters studied are discussed individually as follows.

9.3.3.1 Bulk liquid phase dispersion coefficient (*E*)

The effect of the bulk liquid phase dispersion coefficient (E) was indirectly tested using a change in Peclet number (Pe). Pe being a ratio of the convective to dispersive term, it is indirectly proportional to the liquid dispersion coefficient (E). For the lysozyme-Streamline SP system investigated at given operating conditions, the mean Pe estimated at an average bed voidage of 0.7 was 623. The actual Pe in the bed at different axial positions will be slightly different around that mean based upon the local bed voidage and interstitial velocity. To see the effect of the change in Pe, the set of Pe values were varied by a factor of 0.1 and 0.01-100. The observed effects can be seen in Fig. 9.1 a,b.

Pe was not found to be a sensitive parameter in affecting the breakthrough results of an expanded bed at both 40 cm and 10 cm bed heights. Decreases of Pe or increases of liquid dispersion by a factor of 10 did not change the result appreciably at either axial position. Only when E was increased 100-fold, was there a clear visible effect. Under such conditions the component (lysozyme) concentration rose early and reached to the maximum, i.e. the saturation point slowly resulting into a reduced axial concentration gradient. This is consistent with a high level of liquid dispersion. The effect was more pronounced at the lower axial position (10 cm bed height) tested.

Increases of Pe or decreases of liquid dispersion even by 100 times did not change the result appreciably at either axial position. This indicates that at its default condition, the magnitude of liquid dispersion as estimated by the correlation is small and thus the bulk liquid phase dispersive flux in the system investigation has been small.

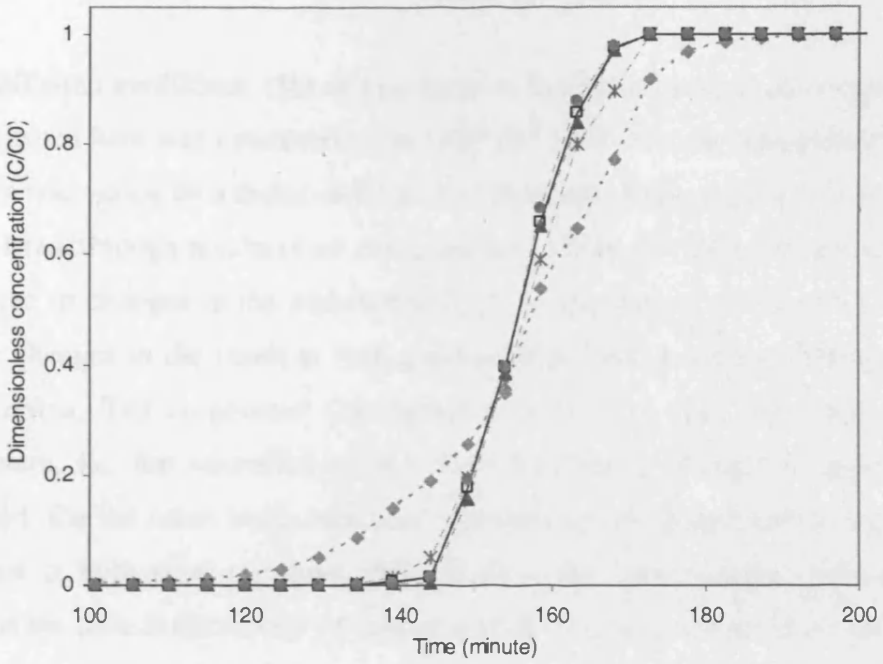

(a)

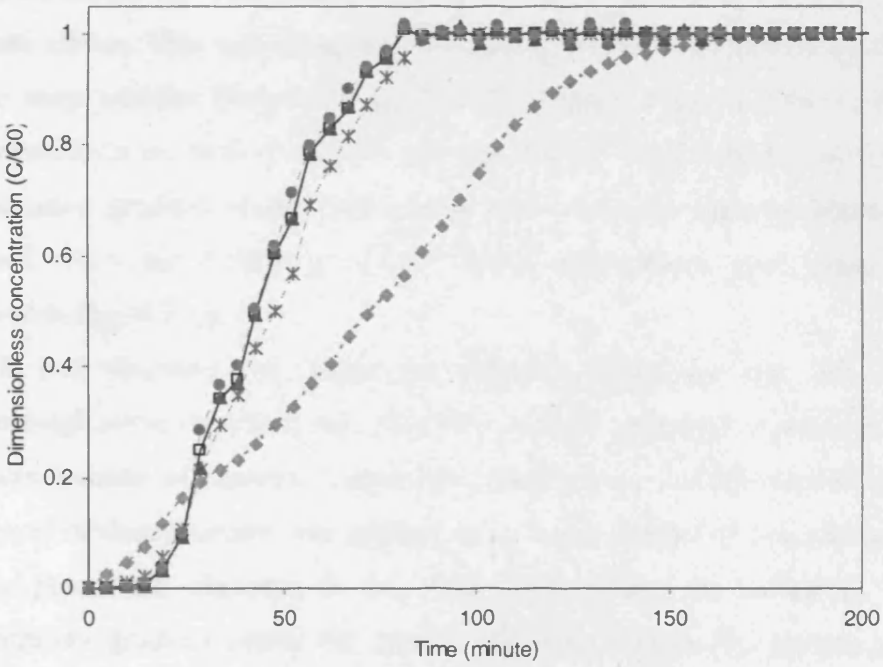

(b)

Fig. 9.1 Effect of bulk liquid phase dispersion by changing associated *Pe* number on breakthrough curves at (a) 40 cm and (b) 10 cm bed heights. Mean *Pe* estimated using correlation for average bed voidage of 0.7 was 623. The correlation estimated values of *Pe* were decreased or increased by a constant proportion for the sensitivity analysis. ♦, x0.01; *, x0.1; □ x1; ▲, x10; ●, x100.

9.3.3.2 Diffusion coefficient of component *i* (D_i)

The diffusion coefficient (D_i) of lysozyme in the buffer used in the experimental set up investigated here was estimated to be $1.08*10^{-6}$ cm^2/s. To see the effect of the change in D_i, this was varied by a factor of 0.5-4. The observed effects can be seen in Fig. 9.2 a,b.

Breakthrough results of an expanded bed at both 40 cm and 10 cm bed heights were sensitive to changes in the assumed diffusivity. Decreasing D_i by a factor of 2 showed minor changes in the result at both axial positions but at 4 times reduction there was a huge effect. The component (lysozyme) concentration rose early and reached to its maximum, i.e. the saturation point slowly resulting in a reduced axial concentration gradient. On the other hand, increases in diffusivity sharpened further the concentration gradient at both axial positions although since the concentration gradient was already steep at the default diffusivity value assumed, the further increases were less serious.

As convective flux is absent in the pore liquid phase inside particles, diffusion is the only mechanism of mass transports there. When diffusivity is low, such transport becomes slower. This will cause the slow saturation rate of a particle by the component. As the mass transfer from the bulk phase to particle phase is limited, the component concentration in the bulk phase will also rise earlier. These effects resulted in a reduced concentration gradient in the bulk liquid phase. Thus an opposite phenomena will be observed when the diffusivity is low. These expectations were satisfied as can be observed in Fig. 9.2 a,b.

It was observed that when the assumed diffusivity was low, the simulated breakthrough curve especially at a 10 cm bed height appeared as series of step changes. This was a result of numerical procedure. Such curves would become smooth when a finer level of discretisation was applied using large number of collocation points in the particle phase and elements in the bulk phase. When the diffusivity is small, the concentration gradient inside the particle becomes steeper. To capture such gradients accurately a much higher number of collocation points become necessary. However in this work in order to keep the simulation time small, such a finer level of discretisation was not applied.

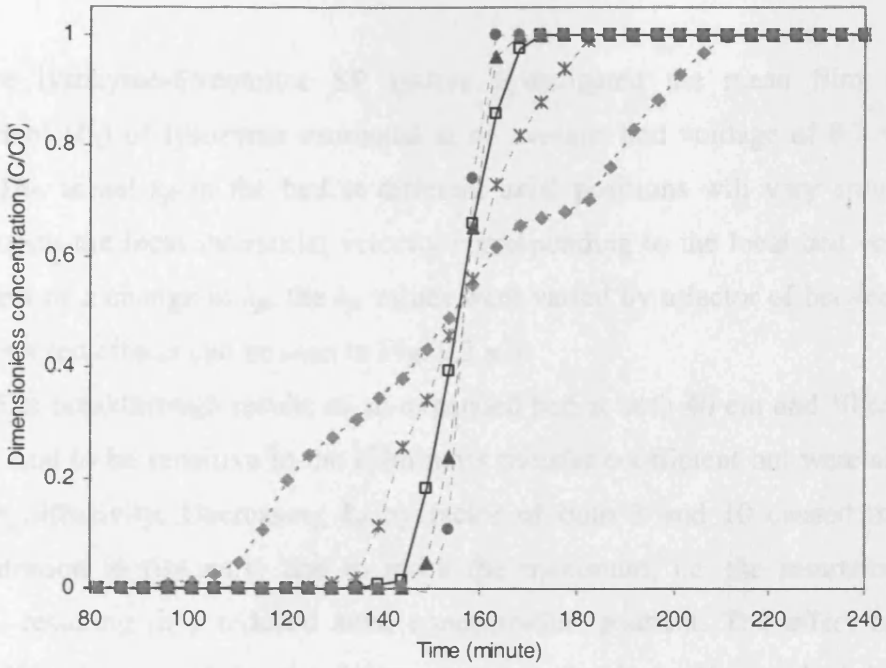

(a)

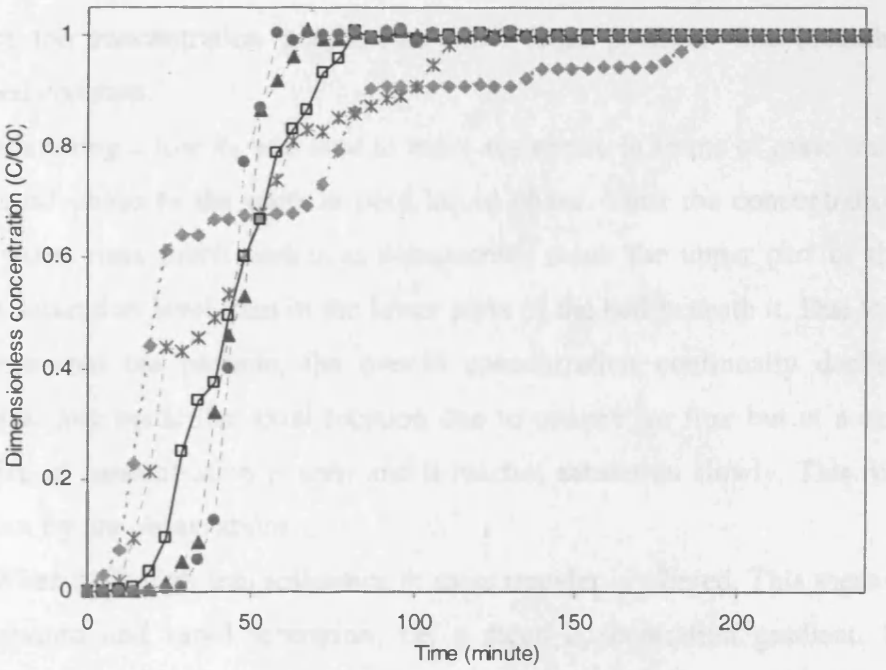

(b)

Fig. 9.2 Effect of a component diffusivity (D_i) on breakthrough curves at (a) 40 cm and (b) 10 cm bed heights. The D_i estimated using correlation was $1.08*10^{-6}$ cm^2/s. This was decreased or increased by a constant proportion for the sensitivity analysis: ♦, x0.25; *, x0.5; □, x1; ▲, x2; ●, x4.

9.3.3.3 Film mass transfer coefficient of component *i* (k_{fi})

For the lysozyme-Streamline SP system investigated the mean film mass transfer coefficient (k_{fi}) of lysozyme estimated at an average bed voidage of 0.7 was $9.74*10^{-4}$ cm/s. The actual k_{fi} in the bed at different axial positions will vary around that mean based upon the local interstitial velocity corresponding to the local bed voidage. To see the effect of a change in k_{fi}, the k_{fi} values were varied by a factor of between 0.3 and 10. The observed effects can be seen in Fig. 9.3 a,b.

The breakthrough results of an expanded bed at both 40 cm and 10 cm bed heights were found to be sensitive to the Film mass transfer coefficient but were slightly less so than to diffusivity. Decreasing k_{fi} by factor of both 3 and 10 caused the component concentration to rise early and to reach the maximum, i.e. the saturation point more slowly, resulting in a reduced axial concentration gradient. The effect of low k_{fi} was especially pronounced in the lower parts of the bed (10 cm bed height) as the concentration rise here is much rapid than at the later stages. Increases in k_{fi} did not increase the concentration gradient at either axial position. The breakthrough curves remained constant.

Assuming a low k_{fi} will lead to more resistance in terms of mass transfer from the bulk liquid phase to the particle pore liquid phase. Thus the concentration in the bulk liquid phase rises much earlier as components reach the upper part of the bed with a smaller saturation level than in the lower parts of the bed beneath it. Due to mass transfer resistance into the particle, the overall concentration continually declines from that reaches at any particular axial location due to convective flux but at a slower rate. An early rise in concentration is seen and it reaches saturation slowly. This result is clearly borne out by the observations.

When k_{fi} is high less resistance to mass transfer is offered. This means a late rise in concentration and rapid saturation, i.e. a steep concentration gradient. However, the breakthrough curves remain constant. This was most likely because beyond the default k_{fi} value as estimated by correlation other factors become rate limiting. Component diffusivity is the most likely rate limiting process. Therefore even if large k_{fi} is assumed which allows a high amount of transfer into the particle phase, due to the diffusion process, material cannot transport inside the particle so rapidly. Hence overall the rate of transport remains constant, and hence the breakthrough curves remain unaffected.

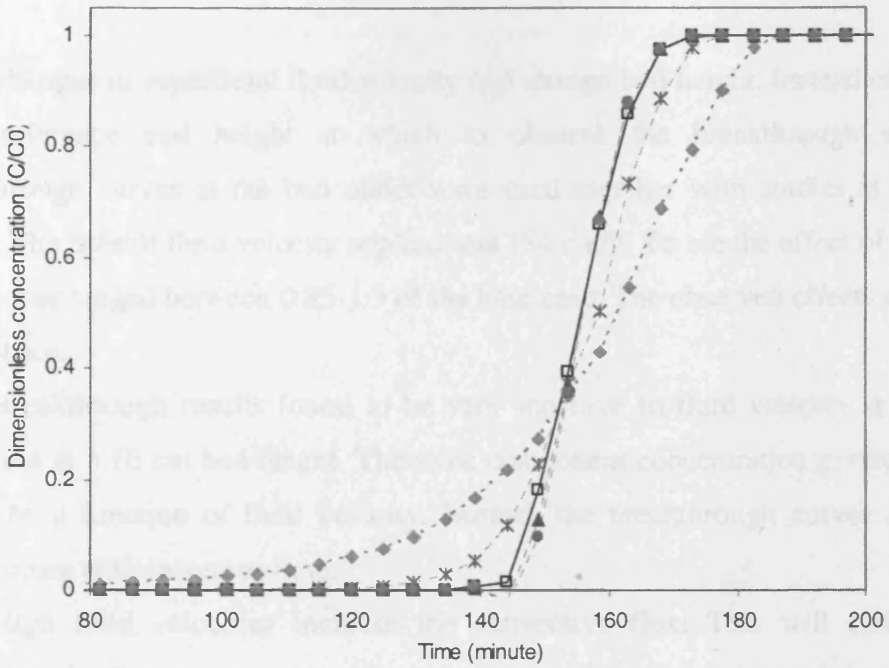

(a)

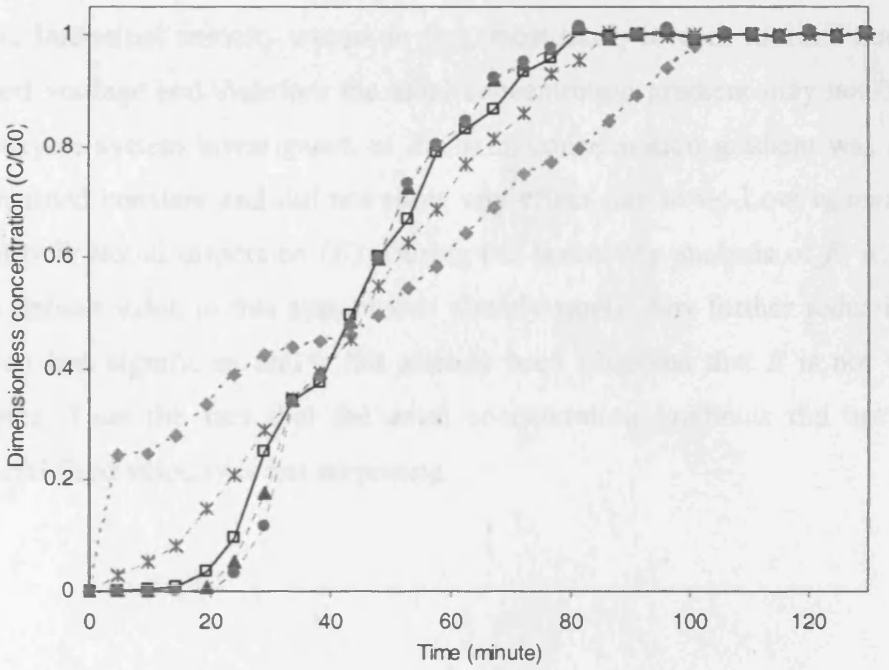

(b)

Fig. 9.3 Effect of film mass transfer coefficient (k_f) on breakthrough curves at (a) 40 cm and (b) 10 cm bed heights. Mean k_f estimated using correlation for average bed voidage of 0.7 was $9.74*10^{-4}$ cm/s. The correlation estimated values of k_f were decreased or increased by a constant proportion for the sensitivity analysis: ♦, x0.1; *, x0.3; □, x1; ▲, x3; ●, x10.

9.3.3.4 Superficial fluid velocity (v_0)

Since changes in superficial fluid velocity (v_0) change bed height, instead of using 40 cm as a reference bed height at which to observe the breakthrough concentration, breakthrough curves at the bed outlet were used together with studies at a 10 cm bed height. The default fluid velocity applied was 184 cm/h. To see the effect of the change in v_0, this was ranged between 0.85-1.3 of the base case. The observed effects can be seen in Fig. 9.4 a,b.

Breakthrough results found to be very sensitive to fluid velocity at both the bed outlet and at a 10 cm bed height. The axial component concentration gradient was found not to be a function of fluid velocity. Instead, the breakthrough curves are shifted to earlier times with increases in v_0.

High fluid velocities increase the convective flux. This will cause an earlier breakthrough. Contrary to packed bed chromatography, in an expanded bed, the rise in fluid velocity does not necessarily increase the bulk liquid phase dispersion as the effective interstitial velocity would, in fact, most likely it leads to a fall due to increased local bed voidage and therefore the axial concentration gradient may not be reduced. In the lysozyme system investigated, as the axial concentration gradient was already steep, this remained constant and did not show any effect due to v_0. Low v_0 means a reduced level of bulk liquid dispersion (E). During the sensitivity analysis of E, it was observed that its default value in this system was already small. Any further reduction will make this even less significant and it has already been observed that E is not very sensitive parameter. Thus the fact that the axial concentration gradients did not change with superficial fluid velocity is not surprising.

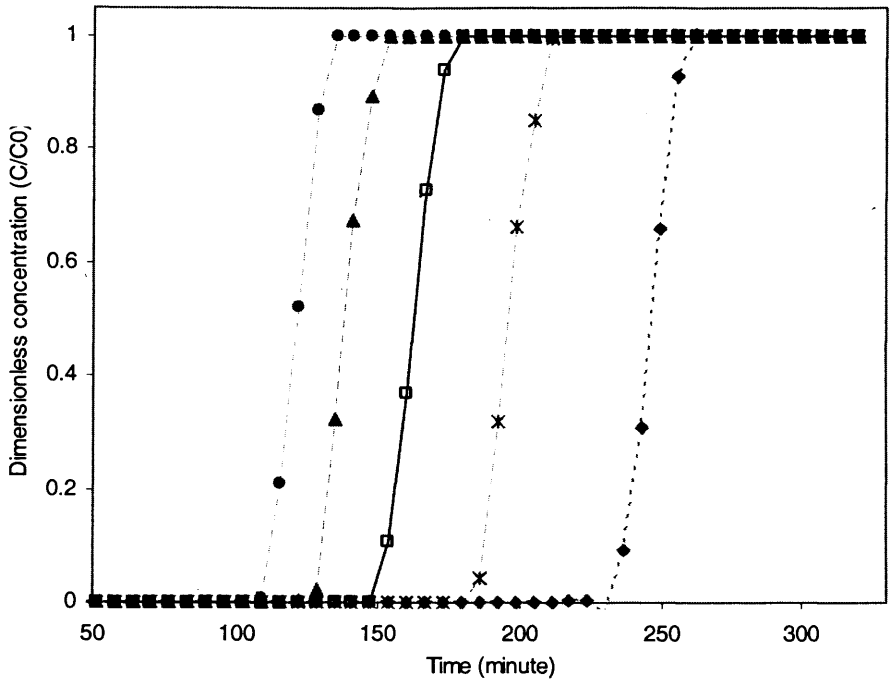

(a)

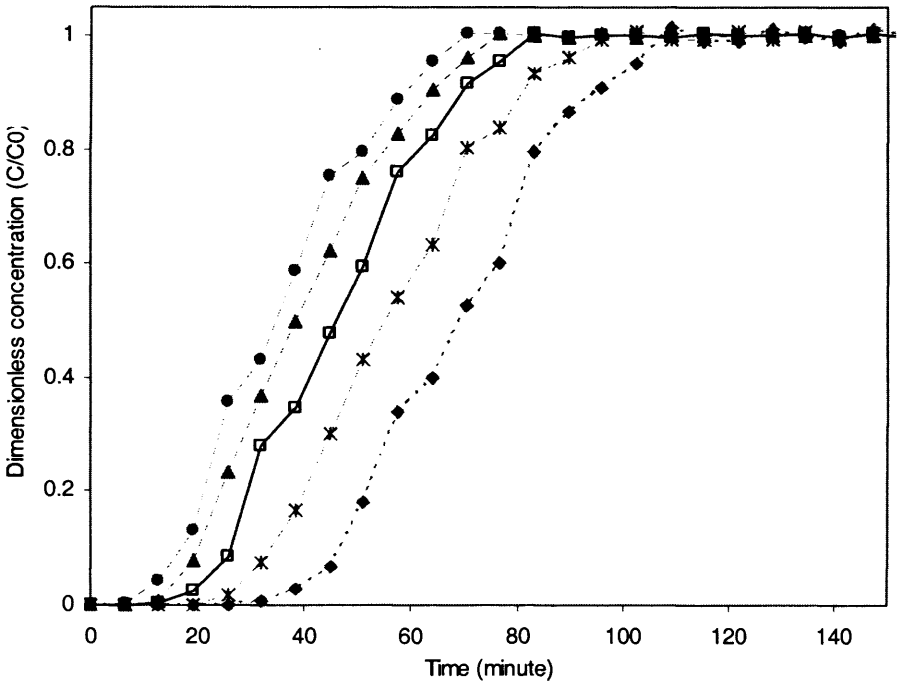

(b)

Fig. 9.4 Effect of superficial fluid velocity (v_0) on breakthrough curves at (a) bed outlet and (b) 10 cm bed height. The default v_0 applied was 184 cm/h. This was decreased or increased by a constant proportion for the sensitivity analysis: ♦, x0.7; *, x0.85; □, x1; ▲, x1.15; ●, x1.3.

9.3.3.5 Particle size (d_p)

As with superficial fluid velocity (v_0), changes in mean particle size (R) also changes the bed height. Larger particles will have higher terminal velocities leading to lower bed heights and vice versa. Again breakthrough curves at the bed outlet were used. As before for v_0, studies at a 10 cm bed height was used for observing the effect in the lower part of the bed. The default average particle size (diameter) of the bulk of adsorbent was 192 μm. To see the effect of changes in d_p, this was ranged by a factor of 0.7-1.3. The observed effects can be seen in Fig. 9.5 a,b.

Breakthrough results were found to be sensitive to particle size at both the bed outlet and 10 cm bed height. Axial component concentration gradient decreased with an increase in particle size. This effect was found to be more pronounced in the lower parts of the bed (Fig. 9.5b). The breakthrough at the bed outlet was also delayed with increase in particle size as seen in Fig. 9.5a.

Small particles have a large surface area per unit volume so providing for greater rate of mass transfer to the particle from the bulk phase. The concentration rise in the bulk liquid will be delayed. However due to the small size, it also rapidly exhausts its adsorptive capacity. In the larger particle the opposite holds. The net film mass transfer slows. Besides due to longer diffusion path the mass transfer within the particle will also be slow. Overall this causes earlier rise and slow saturation resulting in a reduced concentration gradient. As the proportion of large particles is much higher in the lower part of the bed, the effect would be more pronounced at that location compared to the overall average adsorption response of the bed. Similarly larger particles have a higher net adsorptive capacity. So the breakthrough curve at the bed outlet would be delayed. The observations clearly satisfy these expectations.

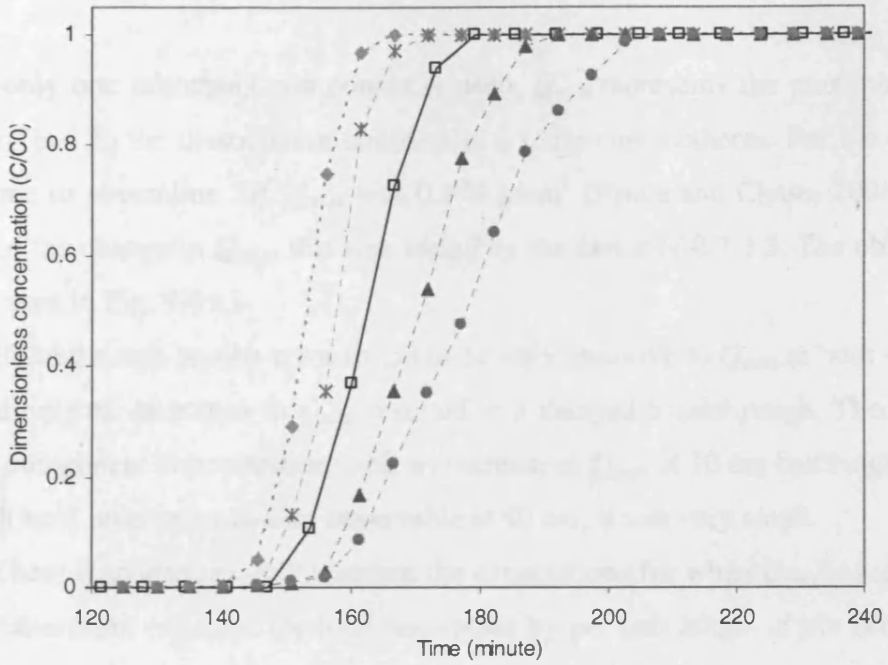

(a)

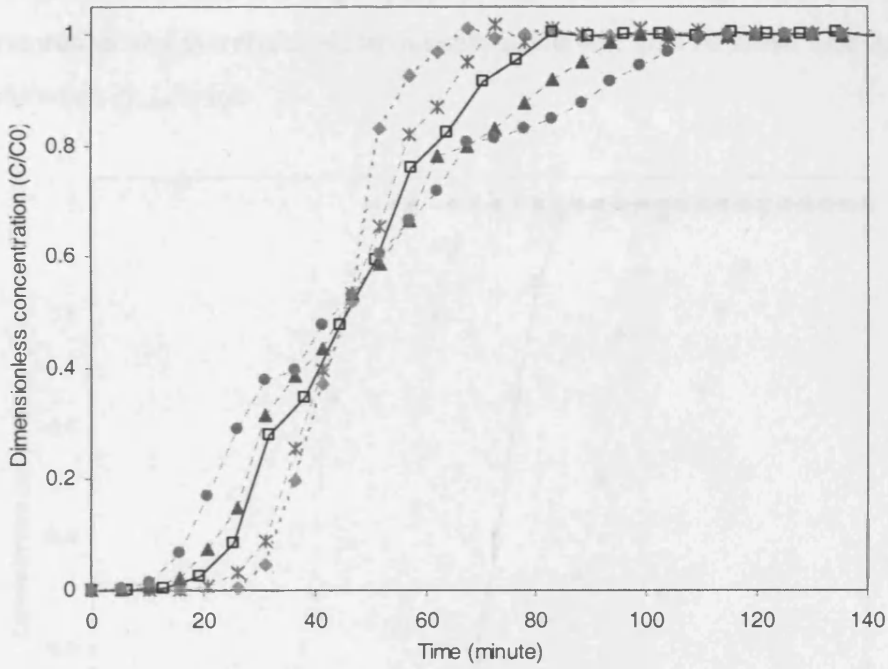

(b)

Fig. 9.5 Effect of bulk mean particle diameter (d_p) on breakthrough curves at (a) bed outlet and (b) 10 cm bed height. The default d_p was 192 μm. This was decreased or increased by a constant proportion for the sensitivity analysis: ♦, x0.7; *, x0.85; □, x1; ▲, x1.15; ●, x1.3.

9.3.3.6 Adsorption parameter of component *i*

When only one adsorbing component is used, Q_{max} represents the maximum adsorptive capacity and k_d the dissociation constant in a Langmuir isotherm. For the adsorption of lysozyme to streamline SP, Q_{max} was 0.178 g/cm^3 (Bruce and Chase, 2001). To see the effect of the change in Q_{max}, this was varied by the factor of 0.7-1.3. The observed effects can be seen in Fig. 9.6 a,b.

Breakthrough results were found to be very sensitive to Q_{max} at both 40 cm and 10 cm bed heights. Increases in Q_{max} resulted in a delayed breakthrough. There was a slow rise of component concentration with an increase in Q_{max} at 10 cm bed height (Fig. 9.6b). Though such an effect was also observable at 40 cm, it was very small.

These responses exactly matched the expectations for when Q_{max} is high. Due to the larger adsorption capacity, the total adsorption by per unit length of the bed will be high and hence. So breakthrough will be delayed at all axial positions and especially so at the 40 cm region of the bed. At large Q_{max}, it will also take longer time for the particle to reach saturation and therefore rise in concentration will also be slow. The opposite of this will hold when Q_{max} is low.

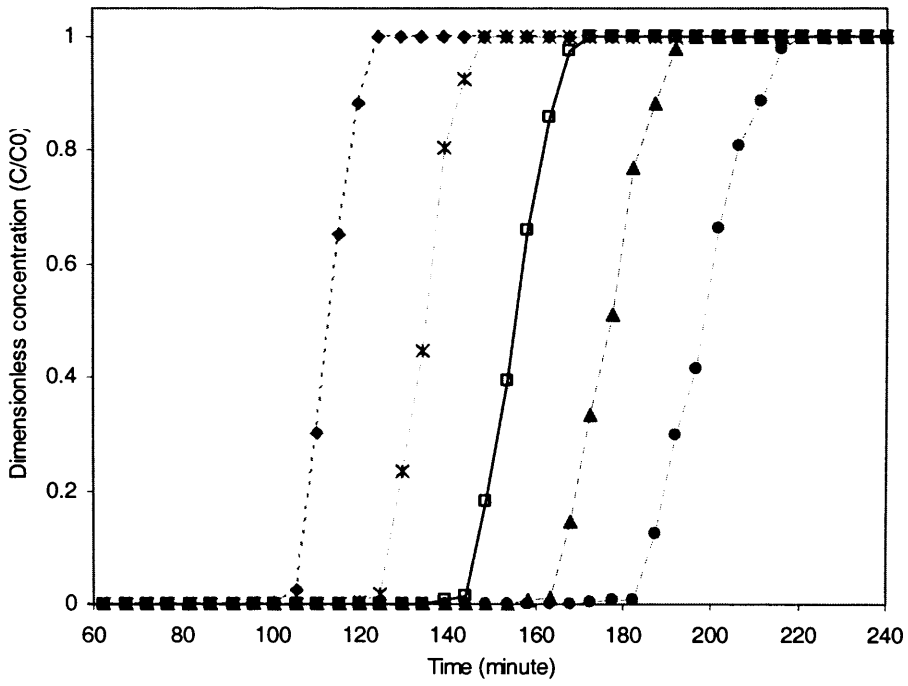

(a)

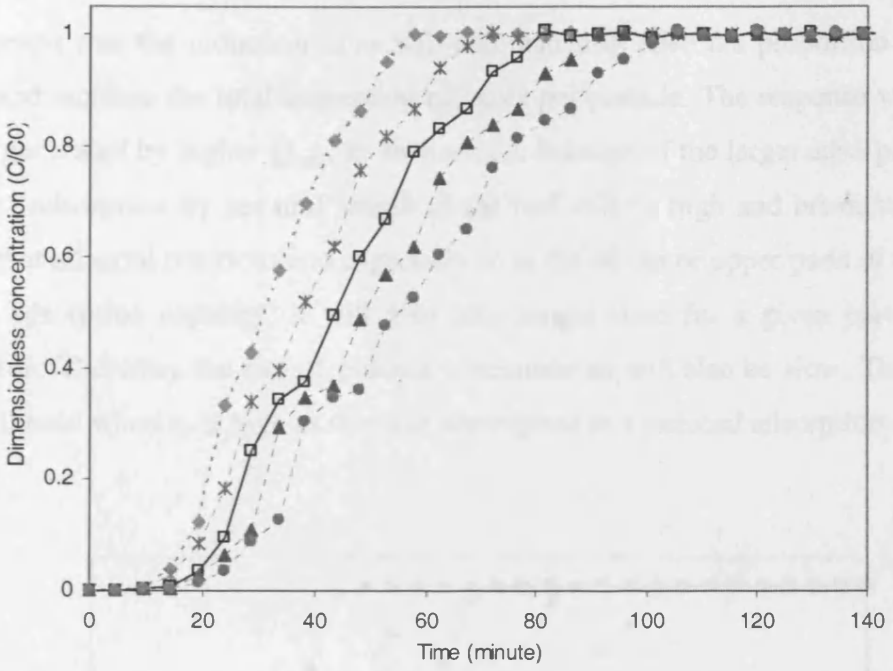

(b)

Fig. 9.6 Effect of an isotherm parameter, Q_{max}, on breakthrough curves at (a) 40 cm and (b) 10 cm bed heights. The default Q_{max} was 0.178 g/cm^3. This was decreased or increased by a constant proportion for the sensitivity analysis: ♦, x0.7; *, x0.85; □, x1; ▲, x1.15; ●, x1.3.

9.3.3.7 Particle porosity (ε_P)

The default particle porosity (ε_P) of adsorbent Streamline SP was 0.35 as discussed in Chapter 6. To see the effect of the change in ε_P, this was altered by a factor in the range of 0.7-1.3. The observed effects can be seen in Fig. 9.7 a,b.

Breakthrough results were found to be very sensitive to the particle porosity. The observed result of a decrease of ε_P was found to be similar to that generated by an increase in Q_{max}. The decrease in ε_P resulted in a delayed breakthrough. There was a slow rise of the component concentration with a decrease in ε_P at a 10 cm bed height (Fig. 9.7b). Though such an effect was also observable at 40 cm, it was very small.

The similarity of response between fall in ε_P and rise in Q_{max}, or vice versa, is due to the nature of the mass balance represented for both the pore liquid phase (u_{Pi}) and adsorbent phase (u_{Ai}) of particle. That is from Eq. (3.85) for a combined aggregate (u_{Ki}) phase of these two:

$$u_{Ki} = \varepsilon_P u_{Pi} + (1-\varepsilon_P) u_{Ai} \tag{9.1}$$

This means that the reduction in ε_P will automatically raise the proportion of adsorbent phase and increase the total adsorption capacity per particle. The response will be similar to that generated by higher Q_{max}. In such a case, because of the larger adsorption capacity, the total adsorption by per unit length of the bed will be high and breakthrough will be delayed at all axial positions and especially so at the 40 cm or upper parts of a bed. Due to higher adsorption capacity, it will also take longer time for a given particle to reach saturation. Therefore the rise of product concentration will also be slow. The opposite of this will hold when ε_P is high as this will correspond to a reduced adsorption capacity.

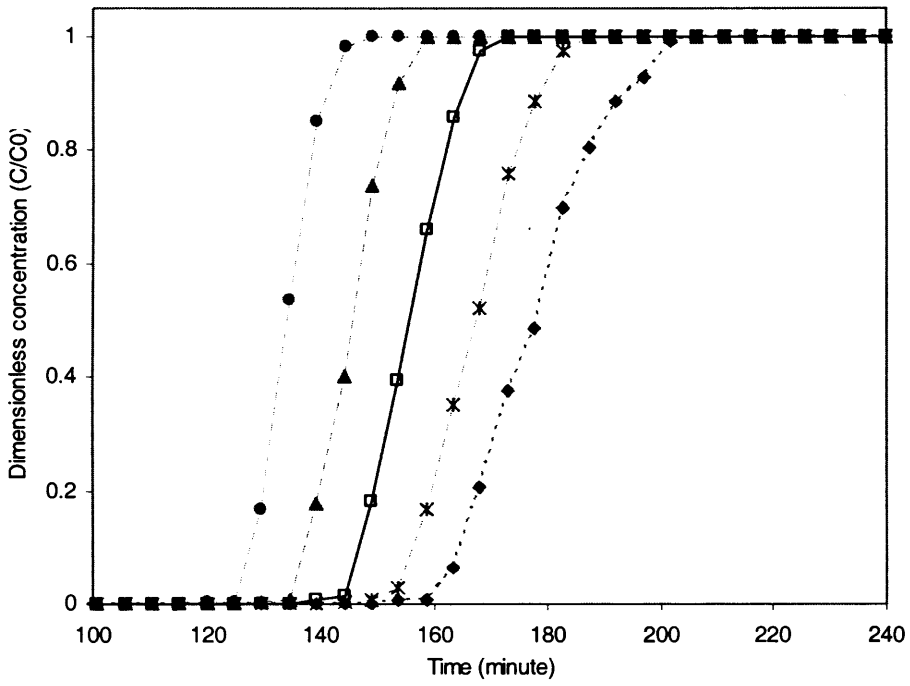

(a)

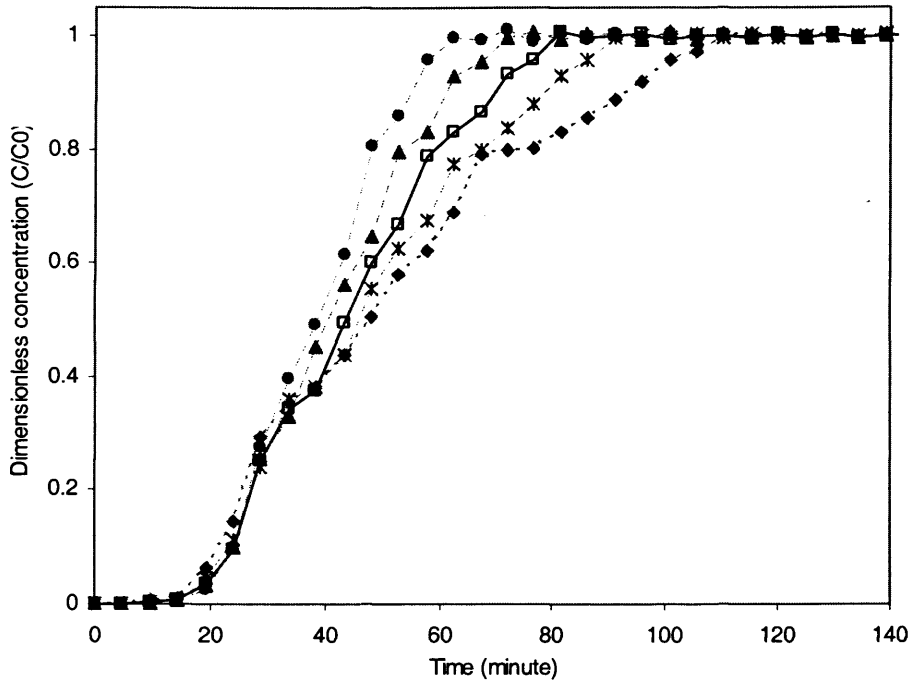

(b)

Fig. 9.7 Effect of particle porosity (ε_P) on breakthrough curves at (a) 40 cm and (b) 10 cm bed heights. The default ε_P was 0.35. This was decreased or increased by a constant proportion for the sensitivity analysis: ♦, x0.7; *, x0.85; □, x1; ▲, x1.15; ●, x1.3.

In this section a detailed sensitivity analysis of different parameters was performed using an EBA model developed in Chapter 6. The purpose was to observe the effects on the adsorption response of an expanded bed. In the next section use of such a model to determine Windows of Operation will be performed.

9.4 Determination of Windows of Operation

9.4.1 Introduction

While running a process, it will be desired to maximise the values of one or more target parameters while satisfying the system constraints. This is achieved by controlling one or more operation variables. The need to satisfy constraints leads to the generation of Windows of Operation (WO) only within which the process can be operated. One of the important uses of EBA model can be to determine such windows for expanded bed

operation. The use of simulation obviates the need to conduct huge numbers of experiments to find out such permissible windows.

Depending upon the specified constraints and control variables, there can be different windows of operation. One of the important WOs in the EBA context is the superficial fluid velocity (v_0) and the load volume which satisfies constraints of minimal yield and throughput. Naturally both high yield and high throughput are desirable. However, often, maximising one will compromise the other. Thus control variables have to be set such that both yield and throughput satisfies minimal requirements. In this work such windows of operation will be determined for EBA.

9.4.2 Method

A simple mixed bed EBA model with steady state hydrodynamics using the equivalent diameter approach (as derived in section 6.6) was used for generating windows of operation due to its simplicity and accuracy.

Specified process constraints were yield (g/g) and throughput (g/hour) while control variable were superficial fluid velocity (cm/min) and load volume (litres). The definition of yield and throughput are:

$$\text{Yield} = \frac{\text{Amount of product recovered after adsorption and elution (g)}}{\text{Amount of product loaded (g)}} \quad (9.2)$$

$$\text{Throughput} = \frac{\text{Amount of product recovered after adsorption and elution (g)}}{\text{Total time of operation (hour)}} \quad (9.3)$$

where,

Total time of operation = equilibrium expansion time + loading time + washing time + elution time + washing time + regeneration time (9.4)

In a simple approximation it can be represented by

Total time of operation = loading time + overhead time (9.5)

Load volume is the amount of product containing fluid passed through the column for adsorption which can be calculated by

Load volume (cm^3) = Superficial fluid velocity (cm/s) * Cross-sectional area of the column (cm^2) * Time loaded (s) (9.6)

And amount of product loaded is given by

Amount of product loaded (g) = Load volume (cm^3) * Feed concentration (g/cm^3)

(9.7)

The method of computing amount of product recovered (g) is as follows:

Amount of product captured in the column (g) = Amount of product loaded (g) - Amount of product exited from column during loading (g) - Amount of product contained in bed voidage when the loading was stopped (g)

(9.8)

Amount of product recovered (g) = Amount of product captured (g) * Recovery rate (%)

(9.9)

For simplicity it was assumed that the entire product that existed in the voidage at the time when loading was stopped will exit out of the bed without adsorption. This is not likely to be true. However, as the earliest time when loading was stopped was at least after the onset of breakthrough at bed exit, in the system investigated, as shown by the a steep breakthrough curve, there would be only small adsorption capacity left. Therefore for an approximate purpose, neglect of a further adsorption after loading and during the start of washing by such remaining capacity is likely not be critical.

The following algorithm was followed to generate windows of operation:

- Range of superficial fluid velocity (v_0) and load volume were specified.
- Discrete v_0 values were chosen within the range
- Maximum loading time was calculated using maximum load volume.
- EBA simulation was done for each v_0 until it reaches a maximum loading time. The concentration of a component in the column was recorded at frequent time intervals.
- Total product loaded was calculated by integrating the concentration over the entire column at particular time intervals corresponding to load volumes for each v_0 applied.
- Using a recovery rate and an overhead time, yield and throughputs were calculated specific to a particular v_0 and load volume.
- Contour plots of yield and throughput in relation to v_0 and load volume were made and superimposed one above the other.

- The overlap of v_0 and load volume which satisfied the minimum yield and throughput required was the windows of operation.

9.4.3 Results and Discussion

A mixed bed model equivalent diameter approach was used for this investigation. The lysozyme-Streamline SP data set of Bruce and Chase (2001), as used and discussed during development and validation of that model in section 6.6, was used. Particles size distribution (PSD) of the Streamline SP matrix was taken to be of 192 μm mean and 51 μm std. deviation as estimated by Bruce and Chase (2001). The range of particle size was taken to be 90-450 μm as estimated by Yun et al. (2004). The density of particle was considered to be 1.184 gm/cc as by Yun et a. (2004). Fluid density and viscosity of the sample in phosphate buffer were taken to be 0.99 gm/cc and 0.102 gm/cm.s respectively. Based on the study of Coulson (1991) for packed bed, the settled bed voidage was taken as 0.4. Particle pore voidage was taken to be 0.35 as described by Li et al. (2004).

For using the mixing approach to define mixed bed hydrodynamics, a mixed bed mean mixing sigma value of 40 μm and slope (with respect to particle diameter) of 0.5 were used based on similar experiment data available from Willoughby et al. (2000) in terms of size column of 50 mm, flow rate and density of matrix. As the use of *Ga* based correlation underestimated the bed height, a parameter (a_1) with value 0.80 was fitted to accommodate for the observed terminal velocity (v_t) in the multi-particle environment. This matched the simulated height and the observed experimental bed height for 2 times expansion with about average 0.7 bed voidage (as observed in experiment and reported by Bruce and Chase (2001)).

Simulation was done for five sets of superficial fluid velocity (v_0): 55, 92, 184, 276 and 368 cm/h. Mixing parameter values, mixing sigma and its slope, were based on mean fluid velocity (v_0) applied, i.e. 184 cm/hour. For simplicity, at this stage, it was assumed that though the expansion would be different based upon the fluid velocity applied, the proportion of mixing of different size categories would remain same. This assumption is not likely to be true. However, it is envisaged that the variation from this would not be too high and it would be within the limit of tolerance in terms of overall adsorption behaviour of the bed. Maximum load volume was calculated based on the amount of fluid that would need to be passed through the bed to get the breakthrough concentration of 100%, which would mean the bed would be fully saturated. For this study 95% recovery

and 8 hours of overhead time were assumed arbitrarily for the simulation. Simulations were performed for each fluid velocity to its corresponding maximum load volume and windows of operation were generated as shown in Fig. 9.8. For simulation, 20 elements, 5 internal orthogonal collocation points and 5 particle size categories were used.

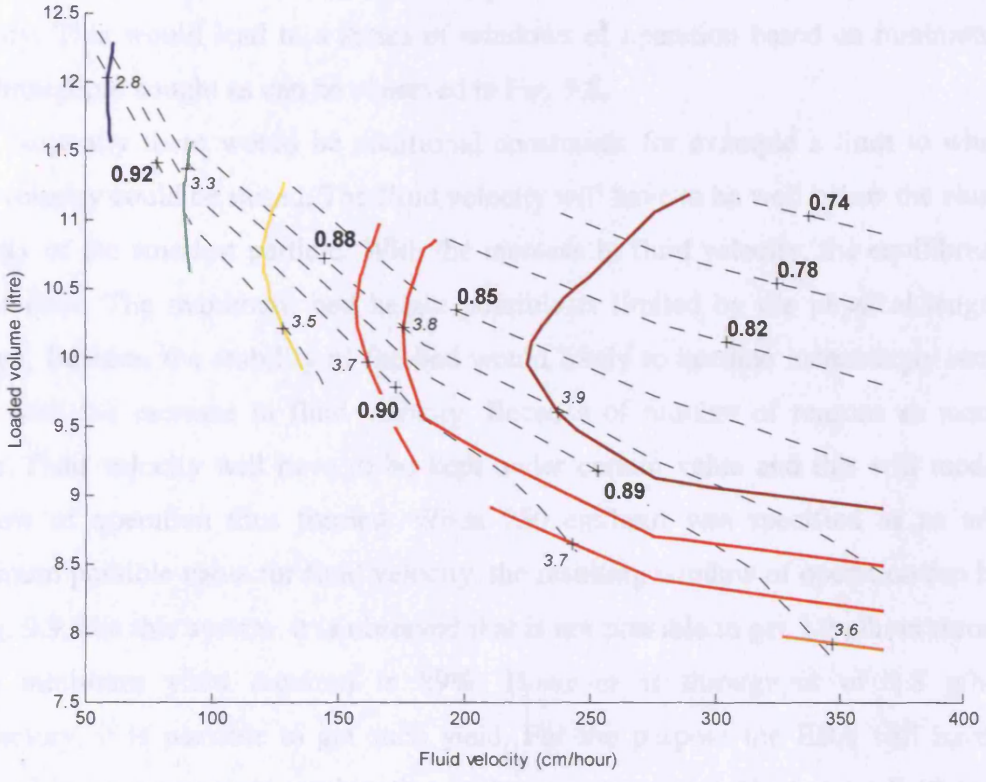

Fig. 9.8 Windows of Operation generated based upon overlapping contour plots of yield and throughput with respect to Fluid velocity (cm/hour) and Loaded volume (litre). The basic parameter values were based on lysozyme-Streamline SP data set of Bruce and Chase (2001). Recovery rate of 95% and overhead time of 8 hours assumed. (----) Yield (Amount recovered/Amount loaded, g/g); (——) Throughput (Amount recovered/Time, g/hour).

As seen in Fig. 9.8, throughput increased with increase in fluid velocity for same loaded volume whereas yield decreased. Similarly, for a given fluid velocity, yield decreased with increasing loaded volume. This satisfies the trend that would be normally expected in an expanded bed adsorption (EBA). Increase in fluid velocity means less time required for operation for those same volumes of loading so throughput will increase. Whereas with increased fluid velocity the convective transfer becomes large, so the amount of component exiting from the bed before the bed is fully saturated also can rise.

This means increasing loss of product and yield decreases. One additional aspect of EBA is the increase in bed voidage with increase in fluid velocity. Therefore, when length of bed is long due to increased fluid velocity, much large amount of component residing in the bed voidage would be wasted in cases where loading was continued at least until the onset of breakthrough. This means the yield will fall with increasing rate with rise in fluid velocity. This would lead to a series of windows of operation based on minimum yield and throughput sought as can be observed in Fig. 9.8.

Normally there would be additional constraints for example a limit to which the fluid velocity could be raised. The fluid velocity will have to be well below the elutriation velocity of the smallest particle. With the increase in fluid velocity, the equilibrium bed height rises. The maximum bed height possible is limited by the physical length of a column. Besides, the stability of the bed would likely to become increasingly important issue with the increase in fluid velocity. Because of number of reasons as mentioned above, fluid velocity will have to be kept under certain value and this will modify the window of operation thus formed. When 250 cm/hour was specified as an arbitrary maximum possible value for fluid velocity, the resulting window of operation can be seen in Fig. 9.9. For this system, it is observed that is not possible to get 3.9 g/hour throughput when minimum yield required is 89%. However if throughput of 3.8 g/hour is satisfactory, it is possible to get such yield. For the purpose the EBA will have to be operated in an appropriate combination within a narrow interval of about 9-10 litre load volume and about 175-250 cm/hour fluid velocity.

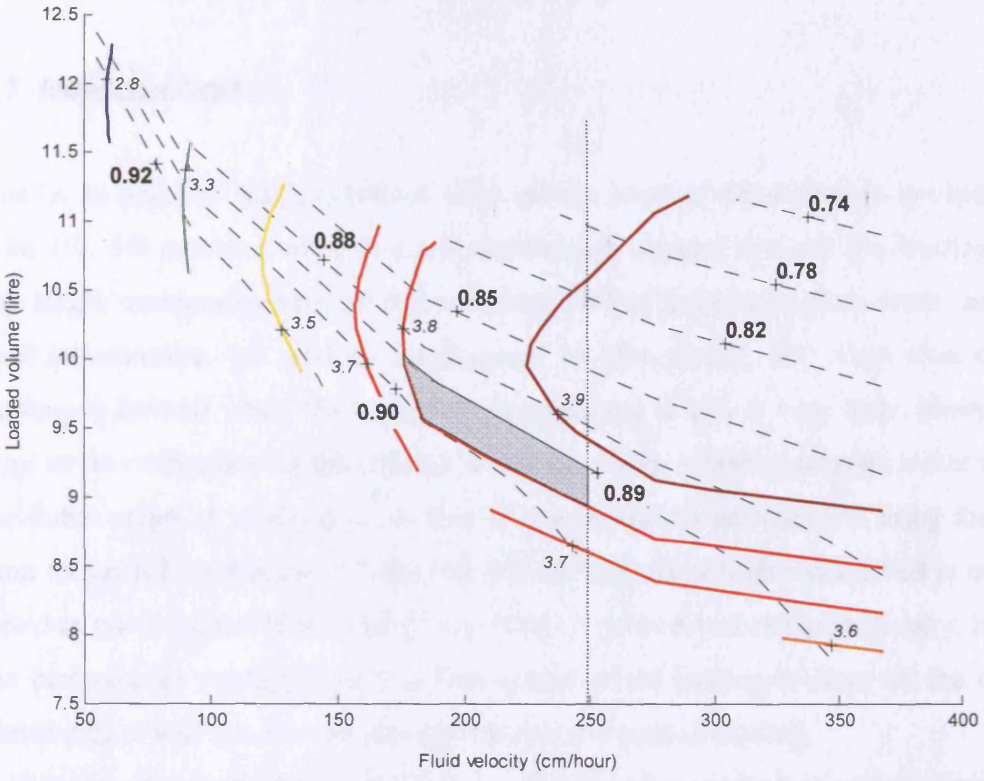

Fig. 9.9 Windows of Operation generated based upon overlapping contour plots of yield and throughput with respect to Fluid velocity (cm/hour) and Loaded volume (litre) when maximum possible fluid velocity was fixed to be 250 cm/h. The basic parameter values were based on lysozyme-Streamline SP data set of Bruce and Chase (2001). Recovery rate of 95% and overhead time of 8 hours assumed. (----) Yield (Amount recovered/Amount loaded, g/g); (——) Throughput (Amount recovered/Time, g/hour); (·····) Constraint due to maximum fluid velocity; Shaded area: a window of operation for 3.8 g/hour minimum throughput, 89% minimum yield and 250 cm/hour maximum fluid velocity.

9.4.4 Conclusion

Hence in this section the use of a model developed in earlier chapters to develop windows of operation of expanded bed has been demonstrated. Use of such windows of operation method to determine the optimal operating condition for a lysozyme-Streamline SP system has been shown and explained. Due to its utility in maximising yield and throughput of the operation, a windows-of-operation method can be considered as a valuable tool in analysis and design of an expanded bed process.

9.5 Determination of Optimal Loading Time

9.5.1 Introduction

Normally, in practice, EBA is loaded till a certain level of breakthrough is observed. It may be 1%, 5% or some other percent breakthrough depending upon the binding nature of the target component and adsorbent matrix. When breakthrough is steep, as in the lysozyme-Streamline SP system investigated in this thesis, the adsorption capacity remaining in the bed when the loading is stopped, say at 1%, is very little. However the amount of the component in the column which is still un-adsorbed is large. After loading, in the initial stage of washing, a fraction of this would be sufficient to bring the whole column to the full saturation and the rest will be washed out. Expanded bed is normally operated at much higher bulk voidage than that of packed bed chromatography. Here the whole bed average voidage was 0.7. This means when loading is done till the onset of breakthrough, it will incur a considerable loss due to wasted loading.

To minimise such loss, it might be possible to stop loading at an appropriate time which is sometime before the onset of breakthrough. The product loss is minimised because the unbound product in the voidage space will be adsorbed into the upper part of bed which is still not saturated when it is conveyed to such parts during the initial stage of washing immediately after the loading. The optimal time to stop loading is the timing which would minimise product loss and maximising bed utilisation. Such loading time appropriate for the system which would maximise yield and throughput of the operation can be determined using a model. Thus following investigation was carried out to determine the optimal loading time and see what happens when loading is stopped only after the onset of breakthrough.

9.5.2 Method

Yield and throughput of the system were defined as in the previous section of windows of operation. The simulation was done for the lysozyme-Streamline SP system data set of Bruce and Chase (2001) described in earlier sections using MB-EQD model developed in section 6.6 for its simplicity. The fluid velocity applied was 184 cm/h. For simulation 12 elements, 5 internal orthogonal collocation points and 5 particle size categories were used. For the system, as the onset of breakthrough starts as about 145 minute, simulation

was done with 90-180 minute range of loading time. As in WO section, arbitrary 95% recovery rate and 8 hours of overhead time were assumed. Optimal loading time is defined as the range of time which would maximise both yield and throughput.

9.5.3 Results and Discussion

The yield and throughput of the system for different loading time can be seen in the Fig. 9.10. As the loading time increased, the yield continually decreased due to increasing loss of the product existed in the bed voidage. As can be observed in the figure, if loading is stopped only after the onset of breakthrough, i.e. after about 145 minutes, there would have been a considerable loss with maximum yield to be near 0.75. This compares very badly to the yield of almost 0.95 had the loading been stopped at 100 minutes or earlier. This is because almost no product is lost as any product that was in the voidage of lower part of the bed would be adsorbed in the upper part of the bed during initial stage of washing. The caveat, however is throughput will sharply fall as the bed will be increasingly under-utilised when the loading time is decreased. Hence it will lead to an optimal loading time which would maximise yield while satisfying minimum throughput requirement or vice versa. As can be seen in the figure, the range of optimal loading time for the system investigated was found to be between 100 to 130 minutes which would satisfy minimum yield of about 0.85 g/g and minimum throughput of 2.8 g/hour. This is about 10-30% time earlier than the onset of breakthrough. Such timing can be determined by either use of a model or by a series of experiments. Experimental approach has a drawback that the finding will be valid only to a particular operating condition in which it was investigated besides the requirement of large amount time and resources. This clearly demonstrates the importance of a model.

Furthermore, the loss of product with respect to application of different loading strategies is shown in Fig. 9.11. Using optimal loading the loss can be minimised to maximum possible, i.e. 5%, as the recovery rate was assumed to be 95%. On the other hand, stopping loading at 1% breakthrough incurred 26% loss. Higher breakthroughs will incur even larger losses. The throughput achieved at 1% breakthrough was about 2.95 g/h. This was not significantly higher than 2.8 g/h throughput achieved while applying optimal loading with 5% loss. This demonstrates the importance of applying model based optimal loading strategy in minimising product loss.

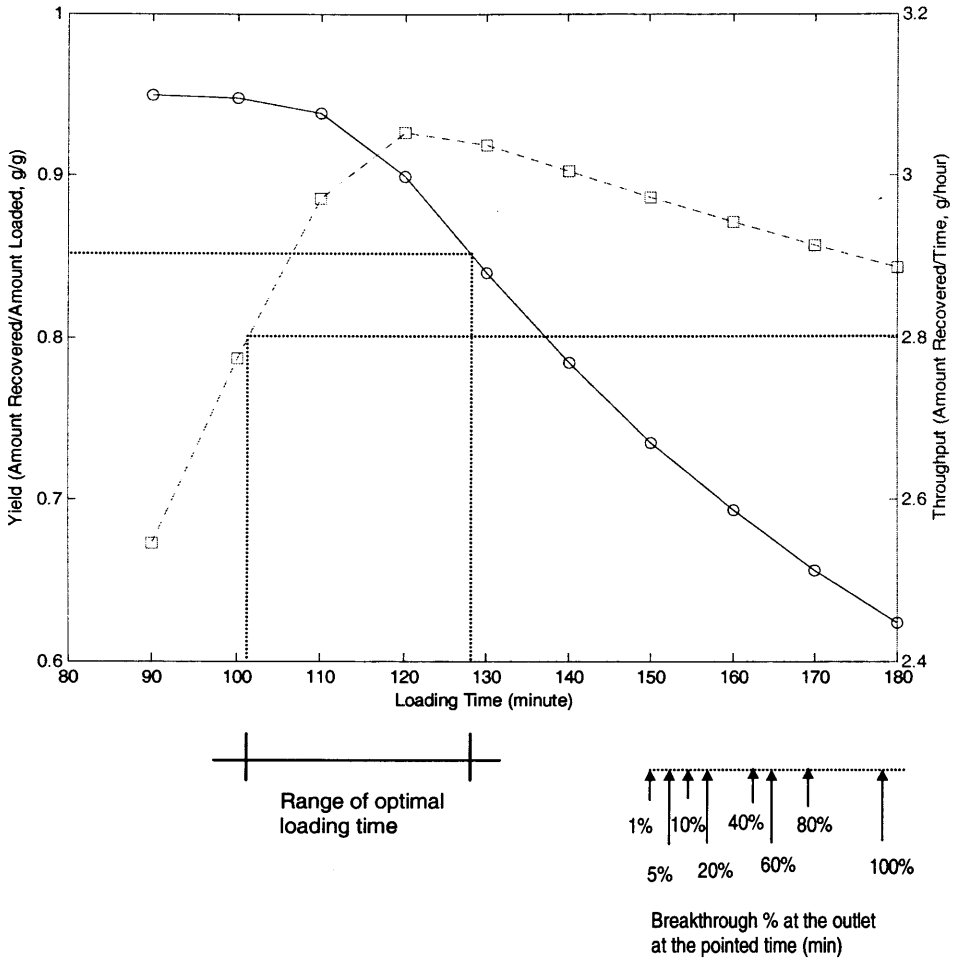

Fig. 9.10 Yield (Amount recovered/Amount loaded, g/g) and throughput (Amount recovered/Time, g/hour) for different loading time (minute). The basic parameter values were based on lysozyme-Streamline SP data set of Bruce and Chase (2001). The fluid velocity applied was 184 cm/h. Recovery rate of 95% and overhead time of 8 hours assumed. •, Yield; □, Throughput. Optimal loading time was found to be between 100 and 130 minutes which satisfied the minimum yield of about 0.85 g/g and throughput of 2.8 g/hour. Arrows points to the time (min) at which specific breakthrough % were observed at the outlet. The onset of breakthrough starts at about 150 min. The range of optimal loading time is much earlier than this as can be seen in the figure.

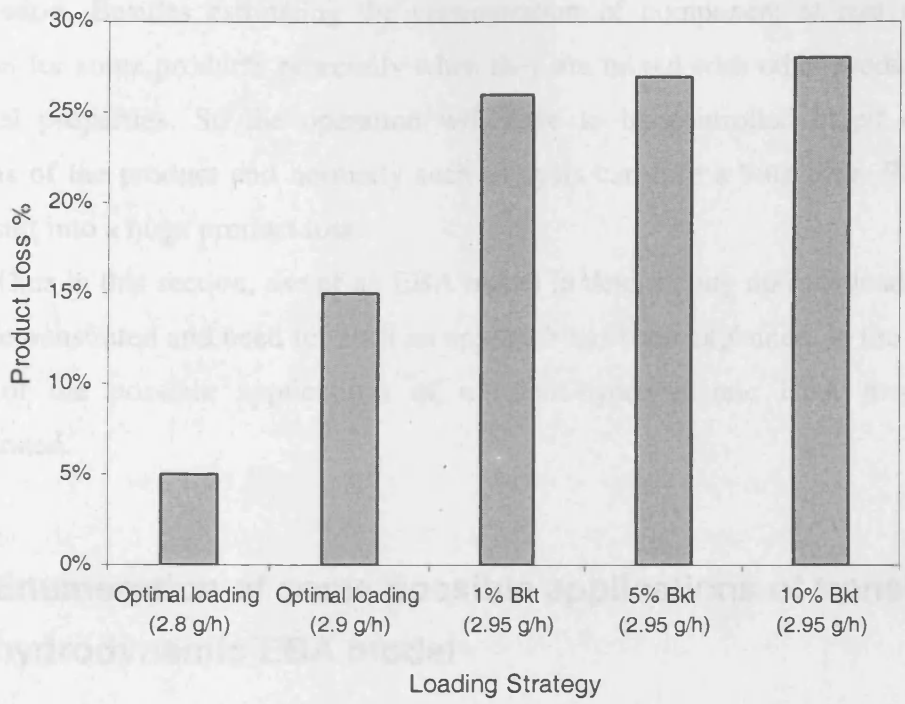

Fig. 9.11 Product loss (%) with respect to loading strategies applied. *Bkt* is abbreviation for breakthrough %. Figures in parenthesis are throughputs (g/h). Recovery rate of 95% and overhead time of 8 hours are arbitrarily assumed. Simulation was done for Bruce and Chase (2001) data set at 184 cm/h fluid velocity. The figure clearly demonstrates the importance of applying optimal loading strategy to minimise product loss.

It is also worth to note that the operating condition of an EBA is much harsh due to use of crude feedstock, existence of particle dispersion, etc. Due to this it is possible that there can be some minor intermittent breakthroughs at bed outlet before the real onset of breakthrough. If the onset of breakthrough is taken as a condition to stop loading, a false signal of breakthrough can lead to a stop in loading before it is actually intended. This can particularly happen if the system is automated and the prior knowledge in approximate time required is either not available or not applied. A model based specification could solve such problems.

A component breakthrough at the bed outlet as a signal to stop loading has one additional weakness. Normally there exists a dead volume for example the volume between the upper bed particle surface and adapter, and the volume in rig before it reaches to the monitor. So the real breakthrough at the end of the bed will be earlier than when it is observed. When such dead volume is large, it will be desirable to minimise loss by stopping the operation based on model prediction than waiting for the experimental

observation. Besides estimating the concentration of component at real time can be difficult for some products especially when they are mixed with other product of similar physical properties. So the operation will have to be controlled based on chemical analysis of the product and normally such analysis can take a long time. Such time lag can result into a huge product loss.

Thus in this section, use of an EBA model in determining optimal loading time has been demonstrated and need for such an approach has been explained. In the next section some of the possible applications of transient-hydrodynamic EBA model will be enumerated.

9.6 Enumeration of some possible applications of transient hydrodynamic EBA model

Out of many possible applications, some of the uses of the transient hydrodynamic EBA model can be as follows. Due to lack of time, they have just been mentioned here as possibilities, and detail analysis and validations were not performed.

9.6.1 Modelling the Effect of Feedstock Changes

Expanded bed is normally operated after it reaches to a hydrodynamic equilibrium, and final expanded bed height becomes constant. But while changing feedstock for loading or elution, the fluid properties will change, thus bed will be in a hydrodynamic transient state till it reaches to a new equilibrium. Transient EBA model being able to capture such an event and their effect in the system and its adsorption response, it can be a valuable predictive tool. Such prediction can be very useful for both analysis and control purposes.

9.6.2 Study of Gradient Change of Fluid Velocity

Keeping the bed stable is one of the important concerns during an EBA operation. Step change of fluid velocity is more likely to cause the bed to become unstable especially when size of such change is large. To avoid this, fluid velocity can be applied either in a gradient or small increment over time. This can result the bed to be in a hydrodynamic transient state for a long time causing reduction in throughput. To avoid such fall in

throughput, when such operation is overlapped with adsorption, hydrodynamic-transient EBA model becomes an important tool to predict the bed behaviour.

9.7 Conclusion

Besides some of the application described in this chapter, models developed in this thesis can be used for numerous other applications. They can be used for analysis, validation, control, etc. They can estimate detail and specific information about the system which would be very difficult or expensive to determine using experimental procedures. For example: particle size specific information can be useful in designing new series of matrices, etc. Finally it is recommended to explore more applications of models to make the EBA operation even more useful, robust and productive.

10 Conclusions and Future Work

10.1 Conclusions

Expanded bed adsorption (EBA) chromatography is an important technique for the purification of macromolecules from solids-containing feedstock. The process naturally exhibits mixed particle sizes along the bed axis along with particle dispersion. To date models have not accounted for this simultaneously and accurately. Besides, there has not been any work to predict the adsorptive response when the bed is operating under a hydrodynamic-transient state; which occurs for example while changing feedstock. In order to address this, developing appropriate EBA models have been the major objective to this thesis work. For this, two categories of EBA models were developed. The first relies upon the integration of an adsorption model with steady state hydrodynamics and the second is with transient hydrodynamics. Some of the applications of such models have been demonstrated.

At first a comprehensive general rate model of chromatography as developed by Gu (1995) was established. The model and its implementation was validated using literature data. This model provides the basis for representing the adsorption behaviour of an EBA when bed properties are constant and known. To develop an integrated model, hydrodynamic aspects of expanded bed behaviour was established next.

The steady state expansion of a liquid fluidised bed or an expanded bed is normally represented by the Richardson-Zaki relation. But there are a number of methods available in literature to estimate its correlation parameter. As this expansion relation is the basis for determining particle velocity in all hydrodynamic model of EBA, establishing this was important. Three main approaches for estimating expansion of the bed are: correlation parameter estimated using *Ga*-based correlation or *Re*-based correlation, or fitting both effective terminal velocity and correlation parameter using experimental data. It was found that the Ga-based correlation to represent bed expansion was found to be better than Re-based original correlation of Richardson-Zaki. In some circumstances, experimental fitting was found be necessary as the error in prediction using such correlations could be high.

Steady state hydrodynamic model was studied using a simple mono-sized bed (MSB) and Perfectly Classified Bed (PCB) approaches for their suitability in representing

the bed. The PCB model did not significantly improve the accuracy of the model prediction for steady state bed height. However, as PCB considers the distribution of particle size, it provides a better representation axial variation of particle size and voidage in expanded bed. PCB, though an improvement over MSB, does not represent reality as the bed is in fact mixed and there exists different particle sizes in each axial position. Hence the development of an approximate method to represent the mixed bed state which takes into account axial variations of particle size distribution of an expanded bed was attempted. It was partially completed providing the number of particle size categories used is not high (preferably within 5). It represented the axial variation of particle size distribution and bed voidage better than either MSB or PCB models. The further improvement in the developed approach was required but was not completed in this thesis due to lack of time. In spite of this, this mixed bed approach to represent hydrodynamics was employed when integrated EBA models with steady state hydrodynamics were developed. For this reason those models were also tested using interpolated experimental data of bed properties. Such an approach being independent from hydrodynamic model, the EBA models developed would be self-standing and could be evaluated based on their own merits.

Steady state hydrodynamic EBA model development was performed in a series of steps by representing the hydrodynamics progressively by: mono-sized bed (MSB), perfectly classified bed (PCB) and mixed bed (MB) approaches. The adsorption part of the model was also made increasingly representative of the reality by progressively considering: an equivalent particle size per axial position (EQD), distribution of particle size per axial position by using size-partition (SP) approach and inclusion of an additional component flux due to particle dispersion. Each model was assessed by comparing with literature data for lysozyme-Streamline SP system. Use of a mixed bed approach for hydrodynamics of EBA gave more accurate breakthrough prediction compared to MSB and PCB approaches clearly demonstrating the importance of including size distributions in axial positions. The result of mixed bed EBA model matched very close to the experimental data for 40 cm bed height breakthrough when EQD approach for adsorption part was used. The use of an SP approach for adsorption gave almost exactly the same result as that of EQD approach but provided additional information of the system for example the individual adsorption response of different particle size categories at different axial position of the bed, etc. However as MB-EQD model takes much less computational time and resource for a simulation, it is expected that it would be useful for

a number of applications for example real time model based evaluation and control of the process, etc.

When particle dispersion was considered, its effect in adsorption response was included at first using Wright and Glasser's (2001) approach. Using that approach, for the system investigated, the effect of particle dispersion in adsorption response was found to be small. Due to an important weakness in Wright and Glasser's approach, a new model was developed for an accurate representation of particle dispersion effect in EBA. In such a model the effect of particle dispersion was simulated by using random migration of a proportion of particles at each axial position at each time step. Using a hypothetical particle dispersion index corresponding to particle dispersion coefficient, the effect of particle dispersion in EBA adsorption response was demonstrated. It was observed that the inclusion of particle dispersion effect would be particularly useful in increasing the accuracy of the breakthrough profile prediction even at lower parts of the bed which was lacking in the models developed without particle dispersion.

As a first step towards developing an integrated transient EBA model, a literature available transient hydrodynamic model with mono sized particle was implemented with modification in boundary conditions. The predicted results were found to match experimental data. This transient hydrodynamic model was then integrated with an adsorption model to formulate an integrated transient hydrodynamic EBA model. Using the simulation study of the integrated model, it was found that the adsorption response of the bed when it was expanded and loaded simultaneously was not different from the response when the bed was loaded only after it reached to a hydrodynamic equilibrium. This is most likely due to fast adsorption rate in the system investigated. Providing bed remains stable for such an operation, it would mean a possibility of high throughput due to possible reduction of operation time. However, due to lack of time, an experimental verification could not be performed.

The effects of various physical parameters on the performance of EBA were investigated using simulation. At its default operating condition investigated for the system, the liquid dispersion estimated by correlation was found to be small and its effect little. Thus it was not found to be very sensitive at that level either by increase or decrease by the factor of 10. On the other hand, component diffusivity (D_i) and film mass transfer coefficient (k_{fi}) were found to be sensitive parameters. Lower D_i and k_{fi} decreased the axial concentration gradient. Superficial fluid velocity (v_0) which directly determines the convective flux besides bed height and voidage profile was found to be very sensitive to

the adsorption response. Higher v_0 resulted into faster breakthrough. Particle size was found to be sensitive. Increase in size delayed breakthrough and decreased concentration gradient. Adsorption capacity, Q_{max}, was found to be naturally very sensitive. Increase in this delayed the breakthrough. Particle porosity (ε_P) was also found to be a very sensitive parameter due to the fact that the complementary portion of this was automatically taken as the proportion of adsorbent phase in the model. So any change in ε_P was reflected as the change in adsorption capacity of the bed.

As an example of application of models developed in this work, a window of operation in relation to fluid velocity and load volume was determined, using steady state hydrodynamic EBA model (EQD), which would satisfy minimum yield and throughput. The model was also used to determine optimal loading time. For the system investigated, it was found that the loading should be stopped at least 15-40 minutes before the start of breakthrough at bed outlet for higher yield and throughput. Such timing can not be determined without use of a model and thus clearly demonstrates the importance of modelling in EBA operation for product yield and economy. Some of the possible applications of transient hydrodynamic EBA model were also enumerated.

Finally, two important areas in hydrodynamics which need to be addressed for further development of EBA modelling were identified. The first is a steady state hydrodynamics representation of EBA by considering mixed bed state as done Kennedy and Bretton (1966) and the other is transient hydrodynamics representation of EBA by considering distribution of particle size as done by Asif et al. (1995). Their models were derived and included as an appendix. However, it was found difficult to implement them at this stage due to numerical problems. Possibly use of a PDE software tool might be a simple solution for this problem. Hence they are recommended as a future work.

10.2 Future work

One of the key future areas which need immediate attention in modelling EBA is the use of hydrodynamic model which takes into account the particle size and density distribution and existence of mixed bed. This applies to both steady state and transient hydrodynamics of EBA. As these affects bed height and voidage distribution which are critical parameters for adsorption response of EBA, their accurate representation is important and make the model more robust and useful. Moreover such models already exist for liquid

fluidised bed whose physical and operating parameters are not much different from those of expanded bed used in downstream processing of proteins. However as observed in this thesis, implementing those models, Kennedy and Bretton (1966) and Asif et al. (1995) was found to be not easy due to some numerical problems. So solving these problems is recommended as one of the first priorities. To circumvent the problem an approximate mixed bed approach was developed in this work to represent mixed bed state of steady state hydrodynamics of expanded bed. However, the approach needs additional work for its refinement and make it more robust and useful.

It was observed that transient hydrodynamics of EBA can be useful for many purposes. Here a simple model assuming a mono-sized bed was developed. To have more confidence in the result, an experimental verification is recommended. Besides, its use and verification for several important operating scenarios of EBA is recommended. When transient hydrodynamic model with PSD is working, its integration with adsorption would provide more complete description of an EBA system.

In this study, the data set of a model protein in a clean system was used. As the objective of the model is for its use in a real system having crude feedstock and a target protein in the mixture of many other proteins and bio-molecules, such experimental result should be used for the test of the models developed here. It is possible that further improvements in the models might be required to predict adsorption response in such systems accurately.

An appropriate method to include effect of particle dispersion in EBA has been developed in this work. However, the simulation was done based on a hypothetical value for particle dispersion index. For practical applications of the model, there is a need to develop a method to estimate particle dispersion index, or to establish a relationship between particle dispersion index and particle dispersion coefficient so as to make use of the correlations already available for the latter.

Another crucial area of study in expanded bed modelling would be the bed stability. As crude feedstock is applied in expanded, the operating environment of an EBA is much more complex and extreme compared to packed bed chromatography. Besides, dispersion of particles and the possibility of not considerable difference in density of particle from fluid phase, etc. can result into existence of certain degree of uncertainties in the system. A small disturbance may get damped or in some circumstances can propagate. For example there can be flocking of particles, channelling of fluid, etc. So knowing the

conditions when a minor disturbance can propagate and make the system unstable become important. Hence it is recommended as another important future work.

A Appendix

A.1 Conservation in a Control Volume having internal moving Interface

When the interior of control volume contains a moving interface (Fig. A. 1) at which the concentration is discontinuous, Eq. 2.2 becomes (Deen, 1998):

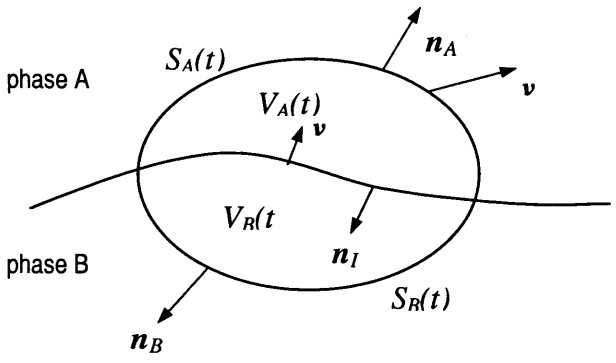

Fig. A. 1 A control volume at the interface between two phases. (Figure adapted from Deen, 1998.)

Applying Liebnitz integral formula to phase A and B:

$$\frac{d}{dt}\int_{A(t)} u dV = \int_{A(t)} \frac{\partial u}{\partial t} dV + \int_{S_A(t)} u\boldsymbol{v}_s \cdot \boldsymbol{n}_A dS + \int_{S_I(t)} u_A \boldsymbol{v}_I \cdot \boldsymbol{n}_I dS \qquad \text{(A. 1)}$$

$$\frac{d}{dt}\int_{B(t)} u dV = \int_{B(t)} \frac{\partial u}{\partial t} dV + \int_{S_B(t)} u\boldsymbol{v}_s \cdot \boldsymbol{n}_B dS - \int_{S_I(t)} u_B \boldsymbol{v}_I \cdot \boldsymbol{n}_I dS \qquad \text{(A. 2)}$$

where $\boldsymbol{v}_I(\boldsymbol{r},t)$ = interface velocity.

Adding Eqs (A. 1) and (A. 2)

$$\frac{d}{dt}\int_{V(t)} u dV = \int_{V(t)} \frac{\partial u}{\partial t} dV + \int_{S(t)} u\boldsymbol{v}_s \cdot \boldsymbol{n} dS + \int_{S_I(t)} (u_A - u_B)(\boldsymbol{v}_I \cdot \boldsymbol{n}_I) dS \qquad \text{(A. 3)}$$

Substituting into Eq. 2.3

$$\int_{V(t)} \frac{\partial u}{\partial t} dV + \int_{S_I(t)} (u_A - u_B)(\boldsymbol{v}_I \cdot \boldsymbol{n}_I) dS = -\int_{S(t)} \boldsymbol{F} \cdot \boldsymbol{n} dS + \int_{V(t)} R_V dV + \int_{S_I(t)} R_S dS \qquad \text{(A. 4)}$$

If there is a source/sink term at the interface:

$$\int_{V(t)} \frac{\partial u}{\partial t} dV + \int_{S_{I(t)}} (u_A - u_B) \boldsymbol{v}_I \cdot \boldsymbol{n}_I dS = -\int_{S(t)} \boldsymbol{F} \cdot \boldsymbol{n} dS + \int_{V(t)} R_V dV + \int_{S_{I(t)}} R_S dS \quad \text{(A. 5)}$$

where

I refers to interface between phases A and B, n_I is normal to the interface and v_I is velocity of the interface. Eq. (A. 5) represents the mass balance of u in the control volume having a moving interface inside it.

A.2 Conservation Equation at a Point on an Interface

Applying mass balance of u at interface (Fig. A. 2), from Eq. (A. 5), denoting volume by $\Omega(t)$ and surface by $\Gamma(t)$:

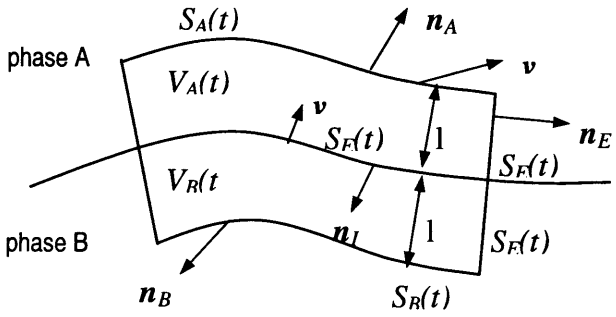

Fig. A. 2 A control volume at interface. (Figure adapted from Deen, 1998.)

$$\int_{\Omega(t)} \frac{\partial u}{\partial t} dV + \int_{\Gamma_I(t)} (u_A - u_B) \boldsymbol{v}_I \cdot \boldsymbol{n}_I dS = -\int_{\Gamma(t)} \boldsymbol{F} \cdot \boldsymbol{n} dS + \int_{\Omega(t)} R_V dV + \int_{\Gamma_I(t)} R_S dS \quad \text{(A. 6)}$$

$$\int_{\Gamma(t)} \boldsymbol{F} \cdot \boldsymbol{n} dS = \int_{\Gamma_A(t)} (\boldsymbol{F} \cdot \boldsymbol{n})_A dS + \int_{\Gamma_B(t)} (\boldsymbol{F} \cdot \boldsymbol{n})_B dS + \int_{\Gamma_E(t)} (\boldsymbol{F} \cdot \boldsymbol{n}_E) dS \quad \text{(A. 7)}$$

$$\lim_{l \to 0} V = 0 \Rightarrow \int_{\Omega_{(t)}} f dV = 0 \quad \text{(A. 8)}$$

Thus

$$\int_{\Gamma_I(t)} (u_A - u_B) \boldsymbol{v}_I \cdot \boldsymbol{n}_I dS + \int_{\Gamma(t)} \boldsymbol{F} \cdot \boldsymbol{n} dS = \int_{\Gamma_I(t)} R_S dS \quad \text{(A. 9)}$$

As it is valid for any arbitrary small surface ΔS_I as $l \to 0$,

$$\Gamma_A(t) = \Gamma_B(t) = \Gamma_I(t) \quad \text{and} \quad -n_A \to n_B \to n_I \quad \text{(A. 10)}$$

$$\int_{\Gamma_I(t)} \left[(\boldsymbol{F} \cdot \boldsymbol{n}_I)_A + (\boldsymbol{F} \cdot \boldsymbol{n}_I)_B + u_A \boldsymbol{v}_I \cdot \boldsymbol{n}_I - u_B \boldsymbol{v}_I \cdot \boldsymbol{n}_I - R_S \right] dS = 0 \quad \text{(A. 11)}$$

$$[(\boldsymbol{F}\cdot\boldsymbol{n}_I)_A+(\boldsymbol{F}\cdot\boldsymbol{n}_I)_B+u_A\boldsymbol{v}_I\cdot\boldsymbol{n}_I-u_B\boldsymbol{v}_I\cdot\boldsymbol{n}_I-R_S]\Delta S_I=0 \quad \text{(A. 12)}$$

$$[(\boldsymbol{F}-u\boldsymbol{v}_I)_B-(\boldsymbol{F}-u\boldsymbol{v}_I)_A]\cdot\boldsymbol{n}_I=R_S \quad \text{(A. 13)}$$

where $(\boldsymbol{F}-u\boldsymbol{v}_I)$ is flux in relation to the interface, I refers to interface between phases A and B, and n_I is normal to the interface. Here accumulation and transport within the interfaces are neglected. Eq. (A. 13) represents the mass balance of u at a point on interface between two phases.

A.3 Further Hydrodynamic Models of Expanded Bed

A.3.1 Introduction

Adsorption part of the EBA model developed in this thesis will be sufficient for wide varieties of needs and uses. But hydrodynamic part has been relatively not that robust due number of assumptions taken for both steady state and transient models. Though they are sufficient for many practical applications, there are opportunities of improving them. One of the immediate improvements possible for steady state hydrodynamic model is adoption of Kennedy and Bretton (1966) model. Similarly, consideration of particle size distribution instead of mono-sized bed by adopting Asif et al. (1995) model would be immediate an improvement in transient hydrodynamic model. As a part of future work these two additional models will be established here. Instead of direct adoptions, these models will be established using first principle for ease in their adaptation in the context of EBA.

A.3.2 Plan and Objectives

In this work, two additional models of expanded bed, one for steady state and the other for transient state as available in literature, will be established. The specific objectives are:

- To establish steady state hydrodynamic model of expanded bed which considers the bed to be mixed as developed by Kennedy and Bretton (1966)
- To establish transient hydrodynamic model of expanded bed which considers the distribution of particle size as developed by Asif et al. (1995)

A.3.3 Steady State Hydrodynamic Mixed Bed Model

A.3.3.1 Introduction

In the section 4.7, an approximate method was devised to represent EBA as a mixed bed. In this part of the work, the model developed by Kennedy and Bretton (1966) to represent segregation and mixing in a liquid fluidised bed consisting of two particle categories will be tried to be adopted in the context of EBA having a wide particle sized distribution.

A.3.3.2 Model Establishment

In the mixed bed model, the existence of different particle sizes at each axial position or strata is taken into account (Fig 4.5). For a given flow rate, it is assumed that the bed expands such that there exists a characteristic PSD and voidage at each axial position.

Kennedy and Bretton (1966) developed a model to represent simultaneous dispersion and segregation occurring in a fluidized bed with more than one particle size and demonstrated the result using mixtures of two particle sizes. Assuming the validity of self-diffusion of small particles (<300 μm diameter) as shown by Brotz (1952) is correct for practical purposes, Fick's law will be applied to model dispersion in expanded bed as done by Kennedy and Bretton for fluidized glass beads.

From Eq. (2.8), the mass balance for a particle size species i is:

$$\frac{\partial c_i}{\partial t} = -\nabla \cdot \boldsymbol{n}_i + R_{Vi} \qquad \text{(A. 14)}$$

where c_i = concentration of particle species i

(Density, ρ_s for all species is considered constant.)

and n_i = mass flux of species i

$$\boldsymbol{n}_i = \boldsymbol{n}_{vi} + \boldsymbol{n}_{ei} \qquad \text{(A. 15)}$$

where n_{vi} and n_{ei} are convective and dispersive flux of species *i* respectively.

As there is no source term, at steady state Eq. (A. 14) becomes

$$\nabla \cdot \boldsymbol{n}_i = \nabla \cdot \boldsymbol{n}_{vi} + \nabla \cdot \boldsymbol{n}_{ei} = 0 \qquad \text{(A. 16)}$$

Convective and dispersive fluxes are given by

$$\boldsymbol{n}_{vi} = c_i v_i \tag{A. 17}$$

$$\boldsymbol{n}_{ei} = -E_i \frac{dc_i}{dz} \quad \text{(a simplified form as used by Kennedy-Bretton)} \tag{A. 18}$$

E_i is the diffusivity of particle species i and v_i its velocity. Velocity has been taken as the inclination of particles to reach an equilibrium concentration in relation to an applied superficial velocity (v_0) and its magnitude is given by the Richardson-Zaki correlation. As v_i will be different for different sizes, it will result in segregation, and is thus called a classification velocity.

For equilibrium to occur for a given particle size i at a given concentration, the required effective v_{0i} is given by:

$$v_{0i} = v_{ti}\varepsilon^{n_i} \tag{A. 19}$$

As this is different from the real applied v_{0i}, the particle species i will move so that the concentration at that location will reach equilibrium. The velocity of such movement is given by:

$$v_i = \frac{v_0 - v_{0i}}{\varepsilon} = \frac{v_0 - v_{ti}\varepsilon^{n_i}}{\varepsilon} \tag{A. 20}$$

Voidage (ε) is given by

$$\varepsilon = 1 - \frac{\sum c_i}{\rho_s} \tag{A. 21}$$

Terminal velocity (v_{ti}) and Richardson-Zaki correlation parameter (n_i) are given as in section 4.4.

Thus from Eq. (A. 16)-(A. 18):

$$c_i v_i - E_i \frac{dc_i}{dz} = 0 \tag{A. 22}$$

$$E_i \frac{dc_i}{dz} - \frac{c_i}{\varepsilon}\left(v_0 - v_{ti}\varepsilon^{n_i}\right) = 0 \tag{A. 23}$$

The total mass of each species i will remain constant which provides an additional constraint to the system as follows:

$$\int_0^L c_i dz = m_i \tag{A. 24}$$

where m_i = total mass of species i in the bed

A.3.3.3 Simulation and Result

The model of Kennedy-Bretton results in a non-linear first order differential equation, a boundary value problem, with Eq. (A. 24) as a constraint. As it is not an initial value problem, it can start from any concentration combination of particle i at z=0 and proceed up along z satisfying the total mass constraint (Eq. (A. 24)). Due to the nonlinearity of Eq. (A. 23) and a single constraint, different initial values can result in different solutions. It is likely this is the reason for model being difficult to solve though it has been successfully implemented in the literature for the bed with two-particle categories. For the more complex PSD problem set in this work it appears that additional constraints are needed to solve it. It is recommended as a topic for future work as the generation of mixed bed model is an important part of EBA modelling. In the next section, transient hydrodynamic model which considers distribution of particle size will be developed.

A.3.4 Transient Hydrodynamic PSD Model

A.3.4.1 Introduction

As particle size distribution (PSD) is a reality and also an intrinsic necessity of expanded bed operation, its inclusion in any model is important for the accuracy of the model and making it robust in its prediction. Asif et al. (1994) and Kaufmann et al. (1995) each developed models for liquid fluidized bed of coal particles considering the distribution of particle sizes. This model should be valid in the context of EBA. As in mono-sized bed model in the previous section, the following assumptions are taken.

- Assuming the validity of self-diffusion of small particles (<300 μm diameter), Fick's Law will be applied to account for particle dispersion in the expanded bed as done by Kennedy and Bretton.
- Only one axial dimension will be taken as Willoughby et al. (2000) has demonstrated that there is no radial variation in particle phase concentration
- Bed is stable.
- Convective flux is the result of particles movement to bring the local solid phase concentration to equilibrium with respect to applied superficial velocity. It is assumed that it can be represented by the Richardson-Zaki correlation as

developed for mono-sized bed in spite of the bed in reality having a PSD. Irrespective of the particular composition of size sp., only the total solid phase concentration is considered to be a factor which is important for determining the equilibrium state.

A.3.4.2 Model Establishment

The model follows closely that developed by Asif et al. (1994). The detail derivation is as follows. From Eq. (2.8), a mass balance for particle size species i, with no source term yields:

$$\frac{\partial \rho_i}{\partial t} + \nabla \cdot \boldsymbol{n}_i = 0 \tag{A. 25}$$

where ρ_i is concentration of particle and n_i mass flux which is given by

$$\boldsymbol{n}_i = -\rho E_i \nabla w_i + \rho_i v_i \tag{A. 26}$$

where ρ is bulk density, E_i dispersivity of particle size species i, w_i is mass fraction and v_i is velocity of particle size species i w.r.t. to bed (that is Eularian).

$$\frac{\partial \rho_i}{\partial t} - \nabla \cdot (\rho E_i \nabla w_i) + \nabla \cdot (\rho_i v_i) = 0 \tag{A. 27}$$

Taking only one axial dimension (z),

$$\frac{\partial \rho_i}{\partial t} - \frac{d}{dz}(\rho E_i \nabla w_i) + \frac{d}{dz}(\rho_i v_i) = 0 \tag{A. 28}$$

Representing in terms of a fractional volumetric concentration, c_i

$$\rho_i = \rho w_i \tag{A. 29}$$

$$\rho_i = \overline{\rho}_{si} c_i \tag{A. 30}$$

Equating Eqs (A. 29) and (A. 30),

$$\rho w_i = \overline{\rho}_{si} c_i \tag{A. 31}$$

where ρ_{si} is density of particle size species i.

$$w_i = \frac{\overline{\rho}_{si}}{\rho} c_i \tag{A. 32}$$

Substituting the value of w_i into ∇w_i,

$$\frac{\partial w_i}{\partial z} = \overline{\rho}_{si} \frac{\partial}{\partial z}\left(\frac{c_i}{\rho}\right) = \frac{\overline{\rho}_{si}}{\rho^2}\left(\rho \frac{\partial c_i}{\partial z} - c_i \frac{\partial \rho}{\partial z}\right) \tag{A. 33}$$

Substituting the value of w_i and ∇w_i into Eq. (A. 28),

$$\bar{\rho}_{si}\frac{\partial c_i}{\partial t}-\frac{\partial}{\partial z}\left[E_i\rho\frac{\bar{\rho}_{si}}{\rho^2}\left(\rho\frac{\partial c_i}{\partial z}-c_i\frac{\partial \rho}{\partial z}\right)\right]+\bar{\rho}_{si}\frac{\partial}{\partial z}(c_i v_i)=0 \qquad \text{(A. 34)}$$

$$\frac{\partial c_i}{\partial t}-\frac{\partial}{\partial z}\left[E_i\left(\frac{\partial c_i}{\partial z}-\frac{c_i}{\rho}\frac{\partial \rho}{\partial z}\right)\right]+\frac{\partial}{\partial z}(c_i v_i)=0 \qquad \text{(A. 35)}$$

$$\frac{\partial c_i}{\partial t}-E_i\frac{\partial^2 c_i}{\partial z^2}+E_i\frac{\partial}{\partial z}\left(\frac{c_i}{\rho}\frac{\partial \rho}{\partial z}\right)+v_i\frac{\partial c_i}{\partial z}+c_i\frac{\partial v_i}{\partial z}=0 \qquad \text{(A. 36)}$$

Eq. (A. 36) represents the transient hydrodynamic model of expand bed behaviour for a distribution of particle sizes. The crucial part of this is the ability to determine the particle size species velocity. For this the same approach as used by Kennedy-Bretton (1966) was adopted as described in the section A.3.3.

Particle size species velocity (v_i):

The particle size species velocity (v_i) is determined as follows. The particle interstitial relative velocity with respect to fluid (v_{ri}), as a result of bed expansion to reach the equilibrium as given by Richardson-Zaki (RZ) correlation, is:

$$v_{ri}=v_f-v_i=\frac{v_{ti}\varepsilon^{n_i}}{\varepsilon}=v_{ti}\varepsilon^{n_i-1} \qquad \text{(A. 37)}$$

where v_{ti} is terminal velocity of particle species i, n_i is its Richardson-Zaki correlation parameter and ε is the voidage at that axial position z. Fluid velocity (v_f) is given by:

$$v_f=v_0+\sum_i c_i v_{ri} \qquad \text{(A. 38)}$$

$$v_f=v_0+\sum_i c_i v_{ti}\varepsilon^{n_i-1} \qquad \text{(A. 39)}$$

From Eq. (A. 37)

$$v_i=v_f-v_{ti}\varepsilon^{n_i-1} \qquad \text{(A. 40)}$$

Substituting the value of v_f

$$v_i=v_0+\sum_i c_i v_{ti}\varepsilon^{n_i-1}-v_{ti}\varepsilon^{n_i-1} \qquad \text{(A. 41)}$$

Voidage (ε) and bulk density (ρ):

Voidage is given by

$$\varepsilon=1-\sum_i c_i \qquad \text{(A. 42)}$$

And bulk density is given by

$$\rho = \sum_i c_i \overline{\rho}_{si} + \varepsilon \rho_f \tag{A. 43}$$

where ρ_f is density of fluid.

From Eqs (A. 40) and (A. 41), ρ can be represented as

$$\rho = \sum_i \left(\overline{\rho}_{si} - \rho_f\right) c_i + \rho_f \tag{A. 44}$$

Boundary conditions:

Due to the operating conditions of an expanded bed, with the lower adapter forming the bottom of the bed and provided the fluid velocity is below elutriation velocity of the smallest particle, the total mass of all particle species in the bed is conserved and remains constant.

Thus integrating the Eq. (A. 25) in the whole system domain (Ω)

$$\int_\Omega \left(\frac{\partial \rho_i}{\partial t} + \nabla \cdot \boldsymbol{n}_i \right) dV = 0 \tag{A. 45}$$

$$\int_\Omega \frac{\partial \rho_i}{\partial t} dV + \int_\Omega \nabla \cdot \boldsymbol{n}_i dV = 0 \tag{A. 46}$$

As the total mass of each particle species in the system remains unaltered, the first term in Eq. (A. 46) becomes zero. Converting the volume integral to a surface integral using Gauss' divergence theorem yields:

$$\int_\Gamma \overline{\boldsymbol{n}} \cdot \boldsymbol{n}_i dS = 0 \tag{A. 47}$$

where $\overline{\boldsymbol{n}}$ is a unit normal vector at the boundary surfaces (Γ).

From Eqs (A. 47) and (A. 26),

$$\int_\Gamma \overline{\boldsymbol{n}} \cdot \left(-\rho E_i \nabla w_i + \rho_i v_i \right) dS = 0 \tag{A. 48}$$

Using Eq. (A. 31) and expanding Eq. (A. 48) and taking only one axial dimension

$$\int_\Gamma \overline{\boldsymbol{n}} \cdot \left[-E_i \left(\frac{\partial c_i}{\partial z} - \frac{c_i}{\rho} \frac{\partial \rho}{\partial z} \right) + c_i v_i \right] dS = 0 \tag{A. 49}$$

Thus at $z=0$ (inlet):

$$-E_i \left(\frac{\partial c_i}{\partial z} - \frac{c_i}{\rho} \frac{\partial \rho}{\partial z} \right) + c_i v_i = 0 \tag{A. 50}$$

and at $z=L$ (outlet):

$$-E_i\left(\frac{\partial c_i}{\partial z}-\frac{c_i}{\rho}\frac{\partial \rho}{\partial z}\right)+c_i v_i=0 \qquad \text{(A. 51)}$$

Some simplification of terms in terms of c_i:

The term $\frac{\partial}{\partial z}\left(\frac{c_i}{\rho}\frac{\partial \rho}{\partial z}\right)$ can be expanded to yield:

$$=\frac{\partial \rho}{\partial z}\frac{\partial}{\partial z}\left(\frac{c_i}{\rho}\right)+\frac{c_i}{\rho}\frac{\partial^2 \rho}{\partial z^2}$$

$$=\frac{\partial \rho}{\partial z}\left(\rho\frac{\partial c_i}{\partial z}-c_i\frac{\partial \rho}{\partial z}\right)\frac{1}{\rho^2}+\frac{c_i}{\rho}\frac{\partial^2 \rho}{\partial z^2}$$

$$=\frac{1}{\rho}\frac{\partial \rho}{\partial z}\frac{\partial c_i}{\partial z}-\frac{c_i}{\rho^2}\left(\frac{\partial \rho}{\partial z}\right)^2+\frac{c_i}{\rho}\frac{\partial^2 \rho}{\partial z^2} \qquad \text{(A. 52)}$$

Substituting the value of ρ from Eq. (A. 44),

$$=\frac{1}{\sum_j(\bar{\rho}_{sj}-\rho_f)c_j+\rho_f}\left(\sum_j(\bar{\rho}_{sj}-\rho_f)\frac{\partial c_j}{\partial z}\right)\frac{\partial c_i}{\partial z}$$

$$-\frac{c_i}{\left(\sum_j(\bar{\rho}_{sj}-\rho_f)c_j+\rho_f\right)^2}\left(\sum_j(\bar{\rho}_{sj}-\rho_f)\frac{\partial c_j}{\partial z}\right)^2 \qquad \text{(A. 53)}$$

$$+\frac{c_i}{\sum_j(\bar{\rho}_{sj}-\rho_f)c_j+\rho_f}\left(\sum_j(\bar{\rho}_{sj}-\rho_f)\frac{\partial^2 c_j}{\partial z^2}\right)$$

Furthermore the term v_i can be replaced by:

$$=v_0+\sum_j c_j v_{tj}\varepsilon^{n_j-1}-v_{ti}\varepsilon^{n_i-1}$$

$$=v_0+\sum_j c_j v_{tj}\left(1-\sum_k c_k\right)^{n_j-1}-v_{ti}\left(1-\sum_k c_k\right)^{n_i-1} \qquad \text{(A. 54)}$$

The term $\frac{\partial v_i}{\partial z}$ becomes:

$$=\frac{\partial}{\partial z}\left(\sum_j c_j v_{tj}\left(1-\sum_k c_k\right)^{n_j-1}\right)-v_{ti}\frac{\partial}{\partial z}\left(1-\sum_k c_k\right)^{n_i-1}$$

$$=\sum_j\left[v_{tj}\left(1-\sum_k c_k\right)^{n_j-1}\frac{\partial c_j}{\partial z}-c_j(n_j-1)\left(1-\sum_k c_k\right)^{n_j-2}\frac{\partial\sum_k c_k}{\partial z}\right] \qquad \text{(A. 55)}$$

$$+v_{ti}(n_i-1)\left(1-\sum_k c_k\right)^{n_i-2}\frac{\partial\sum_k c_k}{\partial z}$$

(with the assumption of uniform convergence of c_i)

In summary the model can be expressed by 3 simultaneous equations:

$$\frac{\partial c_i}{\partial t} - E_i \frac{\partial^2 c_i}{\partial z^2} + E_i \frac{\partial}{\partial z}\left(\frac{c_i}{\rho}\frac{\partial \rho}{\partial z}\right) + v_i \frac{\partial c_i}{\partial z} + c_i \frac{\partial v_i}{\partial z} = 0 \qquad \text{(A. 56)}$$

$$v_i = v_0 + \sum_i c_i v_{ti} \varepsilon^{n_i - 1} - v_{ti} \varepsilon^{n_i - 1} \qquad \text{(A. 57)}$$

$$\rho = \sum_i (\bar{\rho}_{si} - \rho_f) c_i + \rho_f \qquad \text{(A. 58)}$$

And with boundary conditions:

At z =0:

$$-E_i\left(\frac{\partial c_i}{\partial z} - \frac{c_i}{\rho}\frac{\partial \rho}{\partial z}\right) + c_i v_i = 0 \qquad \text{(A. 59)}$$

and at z =L:

$$-E_i\left(\frac{\partial c_i}{\partial z} - \frac{c_i}{\rho}\frac{\partial \rho}{\partial z}\right) + c_i v_i = 0 \qquad \text{(A. 60)}$$

A.3.4.3 Simulation and Result

Equations (A. 36), (A. 41), (A. 44), (A. 50) and (A. 51) describe the complete transient EBA hydrodynamics. This is a differential-algebraic equation system. It was found difficult to implement this model at this stage in spite of already available published works in its successful implementation. It looks like it will need a special method to simulate. Due to lack of time, detail study on its solution was not performed. One possible simple approach could be implementing the model using a PDE software tool. Such a tool is likely to have an automatic provision to handle certain numerical difficulties that may arise in a differential-algebraic equation system of this type. Hence it is recommended as future work.

A.3.5 Conclusion

Two additional models of hydrodynamics of expanded bed, one for steady state and the other for transient state as developed by Kennedy and Bretton (1966) and Asif et al. (1995) were established. Both considers the distribution of particle size and mixed bed and thus are more realistic representation of the bed. The model equations derived here are same as that of those authors. However due to numerical difficulties, they could not

be implemented here at this stage. As both of these are important areas for the further improvement in EBA model, they are recommended as future work.

References

Al-Dibouni, MR, Garside, J. 1979. Particle mixing and classification in liquid fluidised beds. Trans IChemE 57: 94-103.

Amersham Pharmacia Biotech. Expanded bed adsorption: principles and methods. 18-1124-26 Edition AB.

Anderson, DA, Tannehill, JC, Pletcher, RH. 1984. Computational fluid mechanics and heat transfer. Series in computational method in mechanics and thermal sciences. McGraw-Hill Book Company.

Asif, M, Petersen, JN. 1994. A dynamic model of the hydrodynamics of liquid fluidized bed. Ind. Eng. Chem. Res. 33: 2151-2156.

Bathe, KJ. 1996. Finite element procedures. Prentice-Hall, Inc.

Bruce, LJ, Chase, HA. 2001. Hydrodynamics and adsorption behaviour within an expanded bed adsorption column studied using in-bed sampling. Chemical Engineering Science 56: 3149-3162.

Bruce, LJ, Chase, HA. 2002. The combined use of in-bed monitoring and an adsorption model to anticipate breakthrough during expanded bed adsorption. Chemical Engineering Science 57: 3085-3093.

Chen, WD, Dong, XY, Sun, Y. 2003. Modeling of the whole expanded-bed protein adsorption process with yeast cell suspensions as feedstock. Journal of Chromatography A 1012: 1-10.

Deen, WM. 1998. Analysis of transport phenomena. Oxford University Press.

Fenneteau, F, Aomari, H, Chahal, P, Legros, R. 2002. Modeling of scale down effects on the hydrodynamics of expanded bed adsorption columns. Biotechnology and Bioengineering 81: 790-799.

Finlayson, BA. 1972. The method of weighted residuals and variational principles: with applications in fluid mechanics, heat and mass transfer. Mathematics in science and engineering: vol. 87. Academic Press. New York.

Guichon, G, Golshan-Shirazi, S, Katti, AM. 1994. Fundamentals of preparative and nonlinear chromatography. Academic Press Inc. USA.

Gu, T. 1995. Mathematical modeling and scale-up of liquid chromatography. Springer-Verlag. Berlin Heidelberg.

Hassan, S, Titchener-Hooker, NJ, Willoughby, N. 2005. Determining particle density distribution of expanded bed adsorbents. Biotechnology and Bioengineering 92: 659-663.

Hjorth, R. 1997. Expanded-bed adsorption in industrial bioprocessing: recent developments. Trends in Biotechnology 15: 230-235.

Kaczmarski, K, Bellot, JC. 2005. Influence of particle diameter distribution on protein recovery in the expanded bed adsorption process. Journal of Chromatography A 1069: 91-97.

Kreyszig, E. 1999. Advanced engineering mathematics. 8th ed. Johny Wiley, Inc. New York.

Kaufman, EN, Petersen, JN, Wang, Y, Little, MH. 1995. Experimental and numerical characterization of liquid fluidized beds of coal particles. Chemical Engineering Science 50: 3703-3714.

Kennedy, SC, Bretton, RH. 1966. Axial dispersion of spheres fluidized with liquids. A.I.Ch.E. Journal 12: 24-30.

Lazo, C. 1999. Simulation of liquid chromatography and simulated moving bed (SMB) systems. Technische Universitat Hamburg-Harburg.

Li, P, Xiu, G, Rodrigues, AE. 2004. A 3-zone model for protein adsorption kinetics in expanded beds. Chemical Engineering Science 59: 3837-3847.

Li, P, Xiu, G, Rodrigues, AE. 2005. Experimental and modeling study of protein adsorption in expanded bed. AIChE Journal 51: 2965-2977.

Li, Z, Gu, Y, Gu, T. 1998. Mathematical modeling and scale-up of size-exclusion chromatography. Biochemical Engineering Journal 2: 145-155.

Michel, M, Epping, A, Jupke, A. 2005. Modeling and determination of model parameters. In Preparative chromatography of fine chemicals and pharmaceutical agents. Edited by Schmidt-Traub, H. Wiley-VCH Verlag GmbH & Co. Weinheim.

Reddy, JN. 1993. An introduction to the finite element method. 2nd ed. McGraw Hill series in mechanical engineering. McGraw-Hill, Inc. New York.

Reddy, JN. 1986. Applied functional analysis and variational methods in engineering. McGraw-Hill, Inc. New York.

Richardson, JF, Zaki, WN. 1954. Sedimentation and fluidisation: part I. Trans. Instn. Chem. Engrs. 32: 35-53.

Schmidt-Traub, H. 2005. Preparative chromatography of fine chemicals and pharmaceutical agents. Wiley-VCH Verlag GmbH & Co.

Schulte, M, Epping, A. 2005. Fundamentals and general terminology. In Preparative chromatography of fine chemicals and pharmaceutical agents. Edited by Schmidt-Traub, H. Wiley-VCH Verlag GmbH & Co. Weinheim.

Spieker, A, Kloppenburg, E, Gilles ED. 1998. Computer modeling of chromatographic bioseparation. In Bioseparation and bioprocessing: a handbook. Edited by Subramanian, G. Vol. 1. Wiley-VCH. Cambridge.

Subramanian, G. 1995. Process scale liquid chromatography. VCH Verlagsgesellschaft. Weinheim.

Thomasset, F. 1981. Implementation of finite element method for Navier-Stokes equations. Springer series in computational physics. Springer Verlag. New York.

Thelen, TV, Ramirez, WF. 1997. Bed-height dynamics of expanded beds. Chemical Engineering Science 52: 3333-3344.

Tong, XD, Dong, XY, Sun, Y. 2002. Lysozyme adsorption and purification by expanded bed chromatography with a small-sized dense adsorbent. Biochemical Engineering Journal 12: 117-124.

Versteege, HK, Malalasekera, W. 1995. An introduction to computational fluid dynamics: the finite volume method. Prentice Hall. Pearson Education Ltd. England.

Welty, JR, Wicks, CE, Wilson, RE, Rorrer, G. 2001. Fundamentals of momentum, heat, and mass transfer. John Wiley & Sons, Inc.

Wiblin, DJ, Roe, SD, Myhill, RG. 1995. Computer aided desk-top scale up and optimisation of chromatographic processes. Journal of Chromatography A 702: 81-87.

Willoughby, N, Hjorth, R, Titchener-Hooker, NJ. 2000. Experimental measurement of particle size distribution and voidage in an expanded bed adsorption system. Biotechnology and Bioengineering 69: 648-653.

Willoughby, N, Martin P, Titchener-Hooker, N. 2004. Extreme scale-down of expanded bed adsorption: purification of an antibody fragment directly from recombinant E.coli culture. Biotechnology and Bioengineering 87: 641-647.

Wistrand, M, Lacki, K. 2002. Modelling the effect of particle size distribution on expanded bed adsorption process. Amersham Biosciences UK Limited.

Wright, PR, Glasser, BJ. 2001. Modeling mass transfer and hydrodynamics in fluidized-bed adsorption of proteins. AIChE Journal 47: 474-448.

Wright, PR. 2000. The effect of mass transfer and hydrodynamics on fluidized bed adsorption of proteins. PhD Thesis. Rutgers University, New Brunswick, NJ.

Yun, J, Lin, DQ, Yao, SJ. 2005. Predictive modeling of protein adsorption along the bed height by taking into account the axial nonuniform liquid dispersion and particle classification in expanded beds. Journal of Chromatography A 1095: 16-26.

Yun, J, Yao, SJ, Lin, DQ, Lu, MH, Zhao, WT. 2004. Modeling axial distributions of adsorbent particle size and local voidage in expanded bed. Chemical Engineering Science 59: 449-457.

Zienkiewicz, OC, Taylor, RL. 2000a. The finite element method. Volume 1: The basis. 5th Ed. Butterworth-Heinemann.

Zienkiewicz, OC, Taylor, RL. 2000b. The finite element method. Volume 3: Fluid dynamics. 5th Ed. Butterworth-Heinemann.

UNIVERSITY OF LONDON

SENATE HOUSE. MALET STREET, LONDON, WCIE 7HU

REPRODUCTION OF THESES

A thesis which is accepted by the University for the award of a Research Degree is placed in the Library of the College and in the University of London Library. The copyright of the thesis is retained by the author.

As you are about to submit a thesis for a Research Degree, you are required to sign the declaration below. This declaration is separate from any which may be made under arrangements with the College at which you have *pursued* your course (for internal candidates only). The declaration will be destroyed if your thesis is not approved by the examiners, being either rejected or referred for revision.

Academic Registrar

To be completed by the candidate

NAME IN FULL (please type surname in BLOCK CAPITALS)

Sabin Raj MASKEY

THESIS TITLE

An integrated hydrodynamic and adsorption model of expanded bed operation: its development and application

DEGREE FOR WHICH THESIS IS PRESENTED Doctor of Philosophy (Ph.D.)

DATE OF AWARD OF DEGREE *(To be completed by the University):* _____

DECLARATION

1. I authorise that the thesis presented by me in *[2007] for examination for the MPhil/PhD Degree of the University of London shall, if a degree is awarded, be deposited in the library of the appropriate College and in the University of London Library and that, subject to the conditions set out below, my thesis be made available for public reference, inter-library loan and copying.

2. I authorise the College or University authorities as appropriate to supply a copy of the abstract of my thesis for inclusion in any published list of theses offered for higher degrees in British universities or in any supplement thereto, or for consultation in any central file of abstracts of such theses.

3. I authorise the College and the University of London Libraries, or their designated agents, to make a microform or digital copy of my thesis for the purposes of inter-library loan and the supply of copies.

4. I understand that before my thesis is made available for public reference, inter-library loan and copying, the following statement will have been included at the beginning of my thesis: The copyright of this thesis rests with the author and no quotation from it or information derived from it may be published without the prior written consent of the author.

5. I authorise the College and/or the University of London to make a microform or digital copy of my thesis in due course as the archival copy for permanent retention in substitution for the original copy.

6. I warrant that this authorisation does not, to the best of my belief, infringe the rights of any third party.

7. I understand that in the event of my thesis being not approved by the examiners, this declaration would become void.

***Please state year by hand, using a pen.**

DATE July 5th, 2007 SIGNATURE Sabin R. Maskey

Note: The University's Ordinances make provision for restriction of access to an MPhil/PhD thesis and/or the abstrac but only in certain specified circumstances and for a maxiumum period of two years. If you wish to apply fo such restriction, please enquire at your College about the conditions and procedures. External Students sho enquire at the Research Degree Examinations Office, Room 261, Senate House.

THIS DECLARATION MUST BE COMPLETED AND RETURNED WITH THE EXAMINATION ENTRY FORM